

Scientific Journal

**PACIFIC
OCEANOGRAPHY**

Volume 1, Number 2

2003



FAR EASTERN REGIONAL

HYDROMETEOROLOGICAL RESEARCH INSTITUTE

Russian Federal Service For Hydrometeorology and Environmental Monitoring

(ROSHYDROMET)

<http://po.hydromet.com>

Editor-in-Chief

Dr. Yuriy N. Volkov
FERHRI, Vladivostok, Russia / Email: hydromet@online.ru

Editor

Dr. Igor E. Kochergin
FERHRI, Vladivostok, Russia / Email: ikochergin@hydromet.com

Editor

Dr. Mikhail A. Danchenkov
FERHRI, Vladivostok, Russia / Email: danchenk@vladivostok.ru

Executive Secretary

Mrs. Elena S. Borozdinova
FERHRI, Vladivostok, Russia / Email: eborozdinova@hydromet.com

Editorial Board

D.G. Aubrey (Woods Hole Group, Falmouth, USA)	Yu.A. Mikishin (FESU, Vladivostok, Russia)
T.A. Belan (FERHRI, Vladivostok, Russia)	J.E. O'Reilly (Exxon/Mobil, Houston, USA)
G.H. Hong (KORDI, Ansan, Republic of Korea)	Y.D. Resnyansky (Hydrometcenter of RF, Moscow, Russia)
J.H. Yoon (RIAM, Kyushu University, Fukuoka, Japan)	S.C. Riser (University of Washington, Seattle, USA)
E.V. Karasev (FERHRI, Vladivostok, Russia)	M. Takematsu (RIAM, Kyushu University (retired), Fukuoka, Japan)
K. Kim (Seoul National University, Seoul, Republic of Korea)	A.V. Tkalin (FERHRI, Vladivostok, Russia)
V.B. Lobanov (POI FEBRAS, Vladivostok, Russia)	S.M. Varlamov (RIAM, Kyushu University, Fukuoka, Japan)

Secretariat contact:

Elena Borozdinova, Pacific Oceanography, FERHRI,
24, Fontannaya Street, Vladivostok 690990, Russia

Email: po@hydromet.com

Home page: <http://po.hydromet.com>

Tel: +7 (4232) 267352

Fax: +7 (4232) 269281

**“Pacific Oceanography” registered with the Russian Ministry of Mass Media,
Reg. No. 77–12296, 2 April 2002**

PUBLISHED BY:

Far Eastern Regional Hydrometeorological Research Institute (FERHRI),
24, Fontannaya Street, Vladivostok 690990, Russia
Email: hydromet@online.ru
Home page: <http://www.hydromet.com>



PRINTED AND BOUND IN:

Dalnauka Press, Far Eastern Branch of Russian Academy of Science,
7, Radio Street, Vladivostok 690041, Russia



(Order no. 55, Print run 240, Rel. sheets 7,3)

TABLE OF CONTENTS

89 FROM THE EDITORS

PAPERS

Physical Oceanography

90 SST FRONTS OF THE PACIFIC COASTAL AND MARGINAL SEAS

I. Belkin, P. Cornillon

114 HEAT EXCHANGE BETWEEN THE NORTHERN PACIFIC AND THE ATMOSPHERE

A.D. Nelezin, A.N. Man'ko, V.A. Petrova

120 ON SOME FEATURES OF THE WATER CIRCULATION IN THE NW PACIFIC UNDER DIFFERENT SYNOPTIC CONDITIONS

G.A. Vlasova, S.S. Sugak

Marine Meteorology

125 MULTISCALE CLIMATE VARIABILITY IN THE ASIAN PACIFIC

V.I. Ponomarev, V.V. Krokhin, D.D. Kaplunenko, A.S. Salomatin

138 MULTIYEAR VARIABILITY OF NORTH PACIFIC HIGH AND ALEUTIAN LOW

T.V. Bogdanovskaya, N.S. Kupera

144 INTRA-ANNUAL BUNDLES OF CLIMATIC PARAMETERS

V.A. Svyatuha, G.Sh. Tsitsiashvili, T.A. Shatilina, A.A. Goryainov

Marine Environment

149 FLUXES AND BALANCE OF ²¹⁰Pb IN THE NORTHWESTERN JAPAN SEA

S. Otsuka, M. Baba, O. Togawa, E.V. Karasev

158 THE PRESENT STATUS OF BOTTOM ECOSYSTEMS OF PETER THE GREAT BAY (THE SEA OF JAPAN)

T.A. Belan, A.V. Tkalin, T.S. Lishavskaya

Applied Oceanography

168 SEASONAL AND SPATIAL VARIABILITY OF SEA CURRENTS ON THE SAKHALIN NORTHEASTERN SHELF (BY INSTRUMENTAL DATA)

S.I. Rybalko, G.V. Shevchenko

179 SEAWATER DENSITY DISTRIBUTION IN PETER THE GREAT BAY

M.A. Danchenkov

INFORMATION

- 185 TRACE METALS IN BOTTOM SEDIMENTS NEAR VLADIVOSTOK, RUSSIA

A.V. Tkalin, B.J. Presley

- 188 ARSENIC CONTENT IN WATERS OF AMURSKY BAY (THE SEA OF JAPAN) IN NOVEMBER 2001

E.A. Grebenyuk

ARGO News

- 192 PROFILING FLOATS LOST AND CAUGHT IN THE JAPAN SEA

M.A. Danchenkov, S.C. Riser

FERHRI News

- 194 ON-LINE OIL SPILL MODELING WITHIN NAVY EXERCISES IN THE NW PACIFIC MARGINAL SEAS IN AUGUST 2003

I.E. Kochergin, A.A. Bogdanovsky, I.A. Arshinov, V.D. Budaeva, N.S. Kupera, V.G. Makarov, S.I. Rybalko, P.A. Fayman

History

- 198 BEGINNING OF HYDROMETEOROLOGICAL OBSERVATIONS IN VLADIVOSTOK

L.V. Kobylinsky

FROM THE EDITORS

Dear colleagues,

This is the second issue of the new international and peer-reviewed journal "Pacific Oceanography". This is a specialized publication devoted to advances in oceanography of the Northwestern Pacific and its marginal seas and related topics.

"Pacific Oceanography" is published by the Far Eastern Regional Hydrometeorological Research Institute (FERHRI, Vladivostok, Russia) but it does not mean that the scientists from Russian Far East have higher priority. Results of joint marine expeditions and research published in "Pacific Oceanography" will be a good proof of establishing international data exchange.

The first two issues of the journal are distributed free of charge. We would be very pleased and grateful to receive, in exchange, any periodical publication or conference proceedings related to oceanography, meteorology and marine ecology. Starting from the 3rd issue, you will be able to subscribe to "Pacific Oceanography" journal or to continue getting it in exchange for other publications.

We invite all Russian and foreign scientists dealing with oceanography and related topics to contribute their results to our journal. The main criteria for publishing a manuscript or a short note in "Pacific Oceanography" are high quality and urgency. We

hope our journal will contribute to the progress in oceanography and cooperation between the scientists all over the world.

Starting from this issue, we will open our journal with a review paper. We invite you to submit reviews on oceanographic and meteorological conditions of the seas of the Pacific Ocean or about leading oceanographic institutions working in the Pacific Ocean basin.

We invite advertisers to place their information in "Pacific Oceanography" too. By placing your advertisement in "Pacific Oceanography" you will not only have a chance to find new partners in the Russian Far East, but also help the new Russian journal to grow up and become known worldwide.

Abstracts and contact information of editorial office can be found at <http://po.hydromet.com>.

We understand that many people may perceive our journal skeptically, but we have started it and are going to continue issuing it twice a year and improving its quality.

Editors of "Pacific Oceanography"

SST FRONTS OF THE PACIFIC COASTAL AND MARGINAL SEAS

I. Belkin, P. Cornillon

Graduate School of Oceanography, University of Rhode Island (URI), USA

Email: ibelkin@gso.uri.edu

The Pathfinder AVHRR SST data from 1985–1996 are used to survey thermal fronts of the Pacific coastal and marginal seas. The SST fields are declouded and fronts are detected with the Cayula-Cornillon algorithms developed at the URI. In this work we describe newly found, persistent frontal features and their seasonal variability as well as interannual variability. Major climatic fronts are identified and compared with literature data. The ocean-wide frontal pattern consists of several types of fronts. Western boundary currents (Kuroshio, Oyashio, and the East Australian Current) are associated with well-defined fronts. Eastern boundary fronts are also prominent, especially in the North Pacific (California Current System). In the Tasman Sea, a quasi-stationary bifurcation of the Tasman Front is identified at 35°S, 165°E; the Subtropical Front has been traced from south of Tasmania eastward up to the Southland Current off New Zealand. A well-defined double Subtropical Frontal Zone is confirmed east of New Zealand. A new front is observed in the tropical-subtropical Southeast Pacific. Shelf-slope fronts are observed over the shelf break/upper slope almost everywhere. Being strictly controlled by topography, these fronts are quasi-stationary and therefore readily located from satellite data. Inner shelf fronts are observed in the Bering Sea, Eastern China Seas, and South China Sea. Coastal upwelling fronts are observed west of the American continent. These fronts are seasonally dependent, being best seen in winter. Vast frontal zones, apparently associated with coastal upwelling, extend much farther offshore than anticipated, up to O(1000km) into the open ocean.

INTRODUCTION

Ocean fronts are relatively narrow zones that separate broader zones with different stratification types and/or different water masses; the fronts are almost always accompanied by enhanced horizontal gradients of temperature, salinity, density, nutrients and other properties (Fedorov, 1986; Belkin, 2003). Fronts and the associated currents are critically important in heat and salt transport, ocean-atmosphere interaction and ecosystem functioning.

Satellite-retrieved sea surface temperature (SST) data have been used to study the Pacific Ocean fronts since the 1970s (*e.g.* Legeckis, 1978). Earlier studies have been focused mainly on fronts associated with western boundary currents such as Kuroshio (Qiu *et al.*, 1990) and East Australian Current (Nilsson and Cresswell, 1980). Fronts associated with eastern boundary currents and coastal upwellings have been studied in such areas as the California Current (Strub *et al.*, 1991; Strub and James, 1995) and Peru-Chile Current (Brink *et al.*, 1983; Fonseca, 1989).

The above studies, being very important in elucidating physics and geography of regional features, have utilized different methods; most studies were based on data sets of relatively limited duration. The present work is based on a unifying approach developed at the URI, consistently applied to a global data set of thoroughly calibrated measurements. We took advantage of and greatly benefited from availability of (1) advanced algorithms for front detection and cloud screening developed earlier at the URI, and (2) the Pathfinder data set, both briefly described in Section “Data and Method”. A general outline of the Pacific coastal/marginal seas’ frontal pattern is given in “General pattern of surface thermal fronts”, followed

by “Western and eastern boundary currents” that details boundary currents of the Northwest Pacific, Northeast Pacific, Southwest Pacific, and Southeast Pacific. Fronts of the Pacific marginal seas are described in “Marginal Seas”. Principal results and conclusions are summarized in the last Section. The References section contains an extensive bibliography; the space limitations, however, forced us to provide only the minimum number of references for each front and region to serve as starting points for the interested reader. Detailed regional studies of fronts will be published elsewhere, complete with exhaustive bibliographies (*e.g.* Hickox *et al.*, 2000; Belkin and Cornillon, 2003; Belkin *et al.*, 2004).

DATA AND METHOD

Fronts are high-gradient zones; therefore most objective computer-based approaches to front identification are based on gradient computations (Kazmin and Rienecker, 1996; Yuan and Talley, 1996; Nakamura and Kazmin, 2003). Our approach is based on histogram analysis. Since every front separates two relatively uniform water bodies, frequency histograms of any oceanographic characteristic, *e.g.* SST, in the vicinity of the front should have two frequency modes that correspond to the water masses separated by the front, while the latter corresponds to the frequency minimum between the modes. The front detection and tracking is performed at three levels: window, image and a sequence of overlapping images. An optimum window size determined experimentally is 32 by 32 pixels (Cayula and Cornillon, 1992). The edge (front) detection algorithm uses all pixel-based SST values within each window to compute a SST frequency histogram for the given window. For each window

that contains a front, the corresponding SST histogram would have a frequency minimum identified with the front.

This basic idea has been implemented by Cayula *et al.* (1991), Cayula and Cornillon (1992, 1995, 1996) and Ullman and Cornillon (1999, 2000, 2001); the reader is referred to these works for pertinent details. The fronts were derived from the NOAA/NASA Pathfinder SST fields (Vazquez *et al.*, 1998) for the period 1985–1996. These fields were obtained from the Advance Very High Resolution Radiometer (AVHRR) Global Area Coverage data stream (two 9.28 km resolution fields per day) and are available from the Jet Propulsion Laboratory. SST fronts were obtained from the cloud-masked SST fields with the multi-image edge detection algorithm (Cayula and Cornillon, 1996; Ullman and Cornillon, 1999, 2000, 2001). The cloud masking and front detection algorithms were applied to each of the 8364 SST images in the 12 year data set. The frontal data were aggregated monthly (*e.g.* 12 Januaries taken together) and seasonally (*e.g.*, the winter climatology is obtained from all Januaries, Februaries, and Marches taken together). Two basic types of frontal maps are used in the analysis: long-term frequency maps and quasi-synoptic composite maps. The long-term frequency maps show the pixel-based frequency F of fronts normalized on cloudiness: For each pixel, $F = N/C$, where N is the number of times the given pixel contained a front, and C is the number of times the pixel was cloud-free. Thus, the frequency maps are best suited for displaying most stable fronts. At the same time, frontal frequency maps understate some fronts associated with time-varying meandering currents. In such cases quasi-synoptic composite maps are most useful since they present synoptic snapshots of “instant” fronts detected in individual SST images within a given time frame (*e.g.* week, month, or season), without any averaging or smoothing. The frontal composite maps thus allow one to detect most unstable fronts that are not conspicuous in the frontal frequency maps.

GENERAL PATTERN OF SURFACE THERMAL FRONTS

General pattern of surface thermal fronts of the Pacific Ocean is illustrated by two long-term frontal frequency maps, for boreal winter and summer (Figures 1–2, p. 101). The color scale emphasizes stable fronts shown in hot colors (red, orange and yellow). Except for a few open oceans fronts – Kuroshio Extension, subtropical frontal zones, equatorial fronts, and the Antarctic Circumpolar Current fronts – a great majority of stable fronts is situated in coastal and marginal seas. These fronts could be broadly categorized as follows:

- **Western boundary fronts.** These fronts are associated with the Kuroshio Current and Oyashio Current in the North Pacific, and with the East Australian Current in the South Pacific. The Kuroshio front south of Japan is best seen in winter. The Oyashio front is prominent NNE of Japan year-round. The East Australian Current front is better seen in the austral winter and spring.
- **Eastern boundary fronts.** These fronts are related to the wind-induced coastal upwelling; they are best defined off Washington–Oregon–California coasts, off Central America gulfs (Tehuantepec, Papagayo, and Panama), and off Peru–Chile coasts.
- **Marginal seas fronts.** The semi-enclosed seas east of Asia (Bering, Okhotsk, Japan, Bohai, Yellow, East China, and South China seas) feature numerous well-defined fronts located either over the shelf break or within the shelf area. The shelf break and inner shelf fronts are strongly seasonal. The Sea of Japan is also crossed by the westernmost extension of the trans-ocean North Pacific Polar Front.

WESTERN AND EASTERN BOUNDARY CURRENTS

Northwest Pacific. The northernmost western boundary current of the NW Pacific originates in the western Bering Sea off the Koryak Coast of Siberia. After exiting the Bering Sea, the current continues east of Kamchatka Peninsula as the East Kamchatka Current with the associated East Kamchatka Front (EKF). The EKF (and the associated current) is likely a major source of the Polar Front; the latter has recently been tracked across the entire North Pacific (Belkin *et al.*, 2002). Farther downstream, off Kuril Islands, the Polar Front is associated with the Kuril Current, termed the Kuril Front (KurF). Off the southern Kuril Islands and Hokkaido, the Kuril Current is alternatively called the Oyashio Current, so the Polar Front there is often called the Oyashio Front (OF).

The East Kamchatka Front (EKF) is observed along the east coast of the Kamchatka Peninsula, south of 55°N. The front is best defined in late winter–early spring (March–April). The EKF was observed each March and each April from 1985–1996 except for April 1992. From June through August, the EKF visibility is poor mainly because of the maize of SST fronts typical of the summertime. In late summer–early fall (September–November), the front is again visible most of the time. The multi-annual variability of the EKF is noticeable in late fall–winter (December–February). From 1985–1989, the front was only visible 20% of the time, whereas from 1990–1996, the front was present 70% of the time. The timing of the above-noted transition from one regime to another (1989–1990) is close to the timing of the basin-wide relaxation (1988) after the ocean climate regime shift of 1976–1977. It should be stressed that the year of 1990 was especially good for the EKF observations because the front was prominent even in winter, from January–April, and then again in fall, from September–December. It seems quite remarkable that sometimes the EKF has been clearly seen to

originate in the westernmost part of the Bering Sea, over the Commander Basin.

The Kuril Front (KurF) is the southward extension of the East Kamchatka Front described above. The front extends along the Kuril Islands, east of the island chain, and is best seen in late summer–early fall (September–October), sometimes persisting through November; this season seems to be the best for the front's observations. From December through February, the KurF is rarely seen (~10% of the time); it has never been observed in January. In late winter–early spring (March–April), the front is seen again, especially in the south, where it is called the Oyashio Front. From June through August, the KurF cannot be discerned in frontal composite maps amid the multitude of detected SST fronts.

The Kuroshio Current, the second strongest western boundary current in the World Ocean, is a North Pacific counterpart of the Gulf Stream. Therefore it would be natural to expect the Kuroshio Front (KF) and Kuroshio Extension Front (KEF), associated with the Kuroshio Current and its extension downstream of the Izu Ridge (or Cape Inubo) (*e.g.* Qiu, 2002), to be analogous to the Gulf Stream Front (GSF) and its extension, the Gulf Stream Extension Front (GSEF).

From our data, however, the KF/KEF appears different from the GSF/GSEF. First of all, the KF/KEF is much less distinct compared with the GSF/GSEF. In fact, the KF/KEF is well defined only locally and temporarily (*e.g.* a quasi-stationary meander south of Honshú or a quasi-zonal meandering frontal path east of Honshú). Second, as a rule, only one front associated with the Kuroshio Current can be seen, namely the cold-side front (the “left” front looking downstream), whereas two fronts associated with cold and warm sides of the Gulf Stream are typically distinct in the NW Atlantic. It is noteworthy that other strong western boundary currents, *e.g.* Falkland Current, Agulhas Current and East Australian Current manifest as a two-front structure as well (Belkin *et al.*, 1998, 2000, 2001).

The KF can be traced from east of Luzon past Taiwan, into the East China Sea and Sea of Japan, and south of Japan where the Kuroshio forms a well-known quasi-stationary meander (“Kuroshio Large Meander”), clearly seen as a SST front. Downstream of Cape Inubo, the KEF forms one or two quasi-stationary meanders (“First” and “Second” meanders of the Kuroshio Extension). Farther east, the KEF extends along ~35°N. In the middle of the ocean, the KEF is getting close to the Subtropical Front because the latter is gradually making its way ENE (see below).

The Kuroshio Front (KF) southwest of Japan can be seen any time of year, albeit somewhat sporadically. During the 12-year study period, there was no year with an interrupted time series of the KF observations. It is difficult to pinpoint the best seasons of the KF visibility. The worst season is certainly late summer

(August–September) when the front is barely seen. Hickox *et al.* (2000) have determined the seasonal variability of the SST step across the KF in the East China Sea. They obtained the maximum step of about 4°C (warm water offshore) from February through April and the minimum step of 0.3–0.6°C from July through September. The interannual variability of the KF detectability is notable: the best years have been from 1990 (more exactly, from December 1989 through 1993). During that period, the KF was prominent during at least five months each year, up to seven months in 1992. During the same period, a seasonal shift was noticeable of the onset of the best detection season: from December, in 1989–1990, to October, in 1992–1993. The longest uninterrupted period of good detectability of the KF (ten months) occurred later, from October 1995 through July 1996.

The Kuroshio Front (KF) south of Japan is seen year-around. Those rare occasions when the front was not detected were apparently associated with extreme cloudiness. The famous Kuroshio Large Meander or simply Meander is easily detected in frontal composite maps and can be recognized in frontal frequency maps (Figure 1, p. 101). A profound change of the Kuroshio regime has occurred abruptly in late 1992. Our monthly frontal composite maps allow an even more precise dating of the transition: it took place from September to October 1992. Before this regime shift, the Meander mode dominated, as observed in 1985, 1987–1988, and 1990–1991, with shorter (one year) periods of the no-Meander mode in 1986 and 1989 (*cf.* Qiu and Miao, 2000). Since the transition, the no-Meander mode persisted through the rest of the observation period (December 1996), punctuated by short (one to three months) appearances of the Meander.

Northeast Pacific Fronts in the Gulf of Alaska vary strongly with season and year. In late fall–winter, the Shelf-Slope Front (SSF) is observed in the northern and northwestern Gulf that peaks in February–April between 140°W and 165°W, extending from Queen Charlotte Islands in the east up to Shumagin Islands in the west. This front is associated with the Alaskan Stream (*e.g.* Reed and Schumacher, 1987). In winter, the Alaskan Stream seems to be bounded by two parallel fronts. Such situations were clearly recorded in March 1987, April and December 1992, January and March 1995, and March 1996; less clearly, in February 1986 and March–April 1990. The SSF seems to sporadically form a large meander off Kodiak Island at 148–150°W, first described by Musgrave *et al.* (1992) who correctly, albeit tentatively, mapped it from a single hydrographic section in April 1988 augmented by drifter observations. Our frontal composite maps for April and May 1988 revealed the same meander and confirmed the mapping by Musgrave *et al.* (1992). Moreover, we have identified similar meanders in February 1989, December 1992, and March 1993.

From May through July, the Gulf is full of short frontal segments that do not form any pattern (Figure 3, p. 102). This is the season when the new upper mixed layer is thin and the density difference across the new seasonal thermocline is small, hence the upper layer and seasonal thermocline could be easily mixed by a storm. Thus, any fronts that appear in the new upper mixed layer are found to be short-lived.

In August–September, a newly found “horseshoe” front east of Kodiak Island is prominent that persists through November (Figure 3, p. 102). This front consists of two parts, (1) zonal front along $\sim 59^\circ\text{N}$, east of Barren Islands and north of Portlock Bank, and (2) outer shelf-slope front along the shelf break/upper slope (SSF). The zonal front is apparently associated with the Alaska Coastal Current, which flows westward into Cook Inlet. Indeed, a CTD section in October 1991 along a quasi-meridional 151°W line has revealed a westward geostrophic jet at 59°N (Stabeno *et al.*, 1995); our frontal SST map from the same month has shown a very stable zonal front at 59°N , collocated with the concurrent hydrography. The front bounds the relatively warm inshore waters diluted by the Kenai Peninsula runoff, hence the old term the “Kenai Current” (Schumacher and Reed, 1980), later replaced by the “Alaska Coastal Current” (Royer, 1981; Reed and Schumacher, 1987). The front is distinct from May through November and is best defined in late summer and fall. The front maintenance/intensification might be partially accounted for by the tides that are known to completely mix the water column over Portlock Bank, south of the front (Reed and Schumacher, 1986: fig. 3–10). The outer shelf-slope front (SSF) is apparently associated with the Alaskan Stream. This front is prominent from August through October when, together with the above zonal front, it dominates the Gulf’s frontal pattern (Figure 3, p. 102).

A shelf front SW of Kodiak Island was sporadically observed from February through May (in 1985, 1986, 1990, 1991, and 1996) when it extended from Trinity Islands (154°W) up to 158°W where it joined the Alaska Coastal Current. Another front in the lee of Kodiak Island, NE of Chirikof Island was observed for one or two months in late summer, between July and October. Both features have not been described before. It is not clear at this point if there is any relation between these fronts. Both fronts might have some relevance to the southwestward outflow from the Shelikof Strait observed from drifters (Schumacher and Kendall, 1991) and reproduced in a model (Hermann and Stabeno, 1996; Stabeno and Hermann, 1996). Since these fronts are neither seasonally persistent nor spatially stable, they do not show up in long-term frontal frequency maps but are distinct in quasi-synoptic frontal composite maps for individual months. Both fronts might play an important role in the life cycle of walleye pollock

because the adult migration to the spawning ground in the lower Shelikof Strait and the subsequent larvae drift out of Shelikof Strait (as shown by Schumacher and Kendall (1995: fig. 1)) take place in the immediate vicinity of these fronts.

Thomson and Gower (1998) reported a “train” of six eddies in March 1995 between Queen Charlotte Islands and Kayak Island. Our front detection algorithm correctly identified the offshore rims of these eddies as fronts connected to each other in a way reminiscent of Thomson and Gower (1998: fig. 1). Moreover, we found evidence of similar wave/eddy train patterns in February 1989, March–April 1990, April–May 1992, and March and May 1996. Thus, the instability events that cause the observed eddy/wave trains might be quite typical of the wintertime regime of the Gulf of Alaska.

Using a limited data base of nine clear AVHRR images, all from 1983, Thomson and Emery (1986) have observed a narrow along-shore poleward current off British Columbia, termed the Haida Current, between October and April. From cloud-free 1 km resolution AVHRR images between July 1987 and September 1991, Jardine *et al.* (1993) noticed the Haida Current in summer too, albeit rarely. Our declouding algorithm allowed even partly cloudy images to be used in front detection and tracking. As a result, the Haida Front was distinguished from September through March. Alternative explanations of the improved visibility of the front implicate a regime shift after 1983 or a strong interannual variability of the front, with the year of 1983 being the poor visibility year. Note that our front tracking algorithm consistently detected the Haida Front despite its relatively weak SST signal, up to 1°C in the Haida Current core (Thomson and Emery, 1986).

A well-defined front was observed in Hekate Strait ($\sim 131^\circ\text{W}$) from July through March (Figure 3, p. 102). The front is best defined in September, when it extends along the eastern coasts of the Queen Charlotte Islands between $52.5\text{--}54^\circ\text{N}$. The front’s northern part is the Dogfish Banks Front (east of the islands), interpreted by Jardine *et al.* (1993) as a tidal mixing front. They observed this front to reverse seasonally, with the on-bank water being $1\text{--}2^\circ\text{C}$ colder in winter and $2\text{--}3^\circ\text{C}$ warmer in summer than the off-bank water. The seasonal reversal is explained by the Banks’ shallowness, with the front located over the 20–30 m depths (Jardine *et al.*, 1993). This front has the maximum near-surface concentrations of Chl-a, nutrients, diatoms and copepods relative to ambient waters (Perry *et al.*, 1983). Other local fronts reported by Jardine *et al.* (1993) and Crawford *et al.* (1995) have also been sporadically observed, including the mainland coastal upwelling front in eastern Hekate Strait, a semi-circular front associated with the Moresby Eddy in southern Hekate Strait/Queen Charlotte Sound and the Cape Scott upwelling front NW of Vancouver Island.

The main front of the California Current System (CCS) is the front between the cold waters of the southward California Current and the warmer ambient waters. This front, called the California Current Front (CCF) is a typical eastern boundary equatorward current front, similar to the Canary Current Front in the North Atlantic. The front is best developed in late summer (August–September) when it extends from Washington coast to Baja California.

Thermal contrast between the warm offshore waters and cold waters of the CCF is enhanced due to the coastal upwelling, which is best developed off the coasts of Washington and Oregon. Upwelling fronts often produce offshoots (“filaments”) that carry the cold upwelled waters offshore, sometimes as far as 100 to 300 km from the coast (*e.g.* Rienecker and Mooers, 1989).

While the coastal upwelling off North America is distinct year-round, the upwelling intensity attains its absolute maximum in winter, whereas the offshore extent of the CCS climatic and upwelling frontal zone attains its maximum in summer, when the associated fronts can be seen as far west as 130–135°W.

The annual variability of the upwelling location is very substantial. In summer, the upwelling extends from off British Columbia (where persistent local fronts are observed off Vancouver Island and in Hecate Strait) to off Baja California. Few fronts are observed farther south, from off Mexico to Panama Bight (Golfo de Panama). In fall, the upwelling zone spreads southward up to Costa Rica, while retreating along British Columbia. Also in fall, quasi-zonal offshoots form a regular pattern off the entire U.S. coast and Baja California, with offshoots spaced 3–4° of latitude. The origin of the regular pattern remains a mystery. The pattern itself is reminiscent of a “wave train” observed farther north, mainly in the Gulf of Alaska (Thomson and Gower, 1998). In winter, the continuous North American upwelling zone extends from off Washington and Oregon (where the upwelling is still poorly developed) to Panama (the western Panama shelf is however front-free), still separated from the Panama Bight frontal zone, while the latter seems to be connected to the North Equatorial frontal zone. Another seasonal front emerges in late spring–early summer near the Gulf of California entrance, off the Baja California's southern tip. The front is best developed in May–June.

Three frontal areas, Gulf of Tehuantepec (GT), Gulf of Papagayo (GP), and Panama Bight (PB) appear to be separated from each other (Figure 1, p. 101). These are the areas where ageostrophic upwelling develops owing to the orographic channeling of easterlies caused by the intermittent arrival of atmospheric highs from Canada to the Caribbean (Legeckis, 1988). The first two areas (GT and GP) are also of special interest because it is there that large rings form and migrate westward (Stumpf and Legeckis, 1977). The GT

Front, a quasi-zonal feature that seemingly emanates from Gulf of Tehuantepec to WSW, is evident only in winter. In spring, the GT Front is no longer visible. In contrast, the GP Front stands out as a remarkable quasi-stationary double front regularly observed off GP. This front appears as a nearly circular, or double-convex (lens-like) feature. The front development begins in October and culminates in January–April. Then, in May the front disappears without a trace.

Strong seasonal signal is evident in the Panama Bight. This area is completely void of any fronts in summer. Few fronts emerge there in fall. However in winter the Bight is full of fronts, most of which are apparently of the upwelling origin (*e.g.*, Rodriguez-Rubio *et al.*, 2003). The most conspicuous feature is a front (or two) connected to the equatorial front(s). These fronts are best developed from January–February through March–April. A sequence of maps from March through May 1989 (not shown) clearly reveals two Panama Bight fronts in March, a single (northern) front in April, and none in May.

Generally, in spring, most fronts in the Bight degenerate and only those fronts persist that are located south of the Peninsula de Azuero (80–81°W). Obviously, their origin is related to the upwelling-favorable winds whose direction is controlled by the Peninsula.

Our results fully confirm and significantly extend the earlier observations of Legeckis (1988) who described the upwelling plumes off GT, GP, and PB as a “unique ocean response” (*ibid.*, p. 15485), based on a unique data set from March 1985. Our algorithms have identified exactly the same fronts in the same area in March 1985 and also in winters of 1986 and 1989. Therefore we conclude that the upwellings off GT, GP, and PB are rather regular phenomena. Their seasonal and interannual variability will be reported elsewhere.

Southwest Pacific. Due south from the equator, one first encounters the westward South Equatorial Current (SEC) between 10°S and 30°S associated with a very broad, diffuse, quasi-zonal Tropical-Subtropical Frontal Zone (TSFZ) that consists of numerous mesoscale fronts that do not form a continuous, coherent, large-scale front. The average width of this zone is 10–15° of latitude and it can be located anywhere between 15°S and 35°S, subject to the strong seasonal and interannual variability. Within this zone tropical and subtropical currents and fronts are found and “there is no clear separation between subtropical and tropical currents in the velocity field” (Morris *et al.*, 1996). Modeling results also indicate that the SEC is “broken up into a series of zonal jets by the extensive shallow topography associated with islands and reefs... some of the jets advect cores of high or low salinity water, which may be used experimentally to identify the jets and their pathways” (Webb, 2000). All of the above helps explain the

TSFZ's poor definition in the long-term frontal probability maps (Figures 1–2, p. 101). The maps also reveal the TSFZ's seasonal shift due north/south in austral winter/summer respectively in accordance with the seasonal shift of the atmospheric Trade Wind Belt. In the northern SW Pacific, the Trade Wind Belt is the strongest and the most persistent in winter–spring (May–November), between 0–25°S (Wyrski, 1960; Maxwell, 1968). During this time, the TSFZ's northern edge shifts northward to 15°S and remains stable for several months (Figures 1–2, p. 101). In summer (December–April), the Trade Wind Belt moves south to 10–30°S (Wyrski, 1960); accordingly, the TSFZ in January–March shifts southward (Figure 1, p. 101). The magnitude of the seasonal shift is about 5° of latitude. The TSFZ latitude varies considerably on the interannual time scale and might be subject to the ENSO influence.

The TSFZ is a seasonally-intensified feature: it is prominent in fall, winter and spring (May–June through December) and is often completely absent in summer (January through April–May). During its peak time (May–December), the TSFZ develops a well-defined meso-to-large-scale filamentous structure; otherwise, the TSFZ consists of patchy, small-scale frontal segments. Moreover, during its development, the TSFZ changes not only its internal structure (from chaotic to filamentous) but also its morphology, from band-like to fan-like, fanning out toward Australia. This fan-like TSFZ in the Coral Sea off northeastern Australia is usually best defined in October. The interannual variability of the filamentous pattern is notable: the pattern persisted from 2–4 months in 1985–1988 up to 6–7 months in 1989–1996. At this point, it is unclear what might have caused such a fundamental change of the frontal regime. The velocity/transport field has also become more fragmented albeit later, starting with “a rapid transition to an intensified eddy field state in mid-1991” (Morris *et al.*, 1996).

Our results have confirmed the existence of two fronts suggested by Heath (1985) and detected by Roemmich and Cornuelle (1990) from XBT sections between New Zealand and Fiji, namely, the 32°S front NW of North Cape (which continues as the East Auckland Current) and the 29°S front, a likely extension of the Tasman Front (described below). The 32°S front is prominent year round, whereas the 29°S front is only distinct from April through August; both results corroborate observations of Roemmich and Cornuelle (1990). The 32°S is relatively deep: it is distinct at the 400 m depth, with the axial isotherms of 11.0–11.5°C (Roemmich and Sutton, 1998, Plate 1). The 29°S front appears fuzzy in the seasonal frequency maps because of vigorous meandering but is clearly distinct in the monthly probability maps. The 22°S front, the Tropical Convergence (Heath, 1985), is visible in June–July, consistent with findings of Roemmich and Cornuelle (1990).

In western Coral Sea, we found two distinct fronts along the Great Barrier Reef, GBR (Figure 4, p. 102), the world's largest reef system extending ~2600 km off Queensland, Australia, from 25°S to 9°S (Maxwell, 1968; Wolanski, 1994). Both fronts have not been systematically studied yet, even though the presence of thermal fronts in this area was noted in the literature (*e.g.* Burrage *et al.*, 1996). The Queensland Coastal Front (QCF) is located over shallow (20–40 m), reef-free, inner shelf waters of the southern GBR area, fairly close to the coast (30–50 km). The QCF forms in early fall (April) and is most robust in late fall and winter (June–October). The front is best defined between 19–25°S and extends southward past Frazer Island up to 27–28°S. Interestingly, the QCF consists of three collinear but disconnected fragments, with gaps at 20°S (Cumberland Islands) and 23.5–24°S (Capricorn Group reefs). The front's origin is apparently related to tidal mixing, evident from the global map of M2 tidal energy dissipation that clearly portrays a localized maximum in this area (Ray, 2000). The Queensland Shelf Break Front (QSBF) extends along the outer GBR, over a very sharp shelf break, immediately offshore of a very steep GBR slope. The front consists of two major fragments separated by the Swain complex of small patch reefs at 21–22°S. The QSBF emerges approximately two months later than its inshore counterpart (QCF), in late fall (June), peaks in winter (July–September) and persists through the fall, till January. The origin of this front is likely related to the water mass contrast between the southward East Australian Current and the northward shelf current. Tidal energy dissipation should also play a significant role.

Approaching the Australian continent, the SEC bifurcates. The lesser branch turns north to form the West Queensland Current, while the main branch turns south to form the East Australian Current (EAC) (Hamon, 1965; Pickard *et al.*, 1977; Church, 1987; Cresswell, 1995, personal communication, cited by Church and Craig, 1998: p. 935, fig. 33.2).

The EAC spawns large warm-core rings (Nilsson and Cresswell, 1980), therefore some fronts observed in the SW Tasman Sea are associated with these rings. The EAC leaves the coast at ~35°S and continues eastward as the Tasman Current associated with the Tasman Front (TasF) (Andrews *et al.*, 1980; Stanton, 1981; Mulhearn, 1987). From our frontal composite maps and earlier *in situ* data, the TasF forms numerous meanders, especially in the western and central Tasman Sea, known to be derived from both the EAC variability and topographic effects of quasi-meridional ridges in the northern Tasman Sea (Andrews *et al.*, 1980; Stanton, 1981; Mulhearn, 1987). Notwithstanding the vigorous meandering, the long-term frontal probability maps (Figure 4, p. 102) have revealed a double structure of the TasF in the eastern Tasman Sea caused by a quasi-stationary bifurcation of the TasF at ~35°S, 165°E. The double

structure is distinct year round, best defined in summer (December–May). It consists of the Northern TasF (NTasF) extending toward North Cape and the Southern TasF (STasF) heading toward Cook Strait. Thus the NTasF feeds the North Cape Current while the STasF emerges as a newly identified source of the Subtropical Frontal Zone that forms east of Cook Strait (Belkin, 1988).

In the southern Tasman Sea, the Subtropical Front (STF) extends eastward from off southern Tasmania, passing south off New Zealand, where it is known as the Southland Front (SLF) and where it is distinct year round. The continuous STF–SLF is more common in summer (January–March) and has never been observed in winter (July–August), therefore the emergence of a continuous front across the southern Tasman Sea might be a seasonal phenomenon. Moreover, as evidenced by frontal composite maps and *in situ* data (Stanton and Ridgway, 1988; Szymanska and Tomczak, 1994), the STF meanders vigorously as it crosses the southern Tasman Sea in the absence of any topographic control, therefore the long-term frontal probability maps barely show any dominant path of the STF. The CTD sections of Szymanska and Tomczak (1994) clearly reveal the front, which is best defined in the salinity field and much less conspicuous in the temperature field; moreover, these data “give the impression that there are two regimes, a relatively stable one in the lower part of the front and a highly variable one close to the surface” (Szymanska and Tomczak, 1994). Our analysis corroborates this conclusion.

In the SW Tasman Sea, off the eastern entrance to Bass Strait, a quasi-permanent shelf break front is observed, termed the Bass Front, BF (Figure 4, p. 102). The BF was previously believed to be largely a wintertime front (Godfrey *et al.*, 1980; Tomczak, 1985, 1987; Gibbs *et al.*, 1991). Our analysis, however, has shown the BF to be a year-round feature, best defined in winter and spring (July–November) (Figure 4, p. 102). From *in situ* data, the cross-front gradient decreases from 2.5°C in June–July to 1.5°C in November, with Bass Strait water being always colder than Tasman Sea surface water; the corresponding salinity contrast $S_{Bass}-S_{Tasman}$ reverses from +0.6 to -0.3, so the density contrast becomes insignificant (Tomczak, 1985, 1987). Despite the very small thermal contrast across the BF in winter (~1°C), our front detection algorithm reliably detected the front. We have also observed the front's seasonal cycle of wintertime southward expansion – summertime northward retreat, along the eastern coast of Tasmania, not reported before.

In the SW Pacific, the South STF (SSTF) continuity south of New Zealand was debatable for decades. Indeed, most SST maps show a bunch of isotherms, presumably corresponding to the SSTF, approaching South Island from the west near Foveaux Strait and then apparently being interrupted by South Island. The

broken isotherms reappear on the other side of the island, much farther north, off Otago Peninsula. This pattern, repeatedly reproduced in numerous sources, suggests that the SSTF might not be a continuous feature off New Zealand. Our data show, however, that at least at times, if not most of the time, the SSTF is continuous all the way around South Island (*e.g.* in June–October 1985). The front passes around the continental shelf of South Island, approximately following the 200 m isobath, immediately south of the Snares, then follows the shelf break southeast and east of South Island up to Otago Peninsula where the front turns east and continues along the Chatham Rise. Sometimes (*e.g.* winter 1989) the SSTF splits upstream of the Snares, with the inshore branch crossing the shelf via Snares Strait (between Stewart Island and the Snares) and the offshore branch following the shelf break south of the Snares as described above. The spring frontal composite maps show that either mode can dominate. For example, in spring of 1985 and 1986 the SSTF was passing entirely through Snares Strait, whereas in spring of 1989 the SSTF was passing south of the Snares.

A newly found front has been observed between South Island and the eastern end of the Campbell Plateau, termed the Bounty Front (BF), for the front always comes very close to the Bounty Islands. The BF exhibits strong seasonal variability. It is pronounced in summer, degenerates in fall (remaining however clearly identifiable), and is noticeable at times through the rest of the year (*e.g.* in winter of 1985 and in spring of 1989). The BF location is undoubtedly controlled by the bottom relief, first of all by the northern flank of the Campbell Plateau and especially by the steep northern flank of the Bounty Rise, the easternmost part of the Campbell Plateau. The front's origin might be related to the Subantarctic Front (SAF), described below, in that the BF might represent the northernmost branch of the SAF that splits from the SAF probably between Antipodes Islands and Bollons Seamount, and veers anticyclonically around the Bounty Rise.

A front that crosses the Campbell Plateau, from Campbell Island to Antipodes Islands has been noticed just once, in summer of 1989. Seemingly free from any topographic control, this is an unusual feature. More data are required to study this front in any detail.

Another surprising feature has been observed over the Chatham Rise, west of the Chatham Islands, namely an apparent confluence of two well-defined fronts, the SSTF (Southland Front) and the Auckland Front (North STF), with a possible contribution of the Cook Strait water. The confluence's location exhibits strong seasonal variability. In summer and fall, the fronts confluence close to the Cook Strait, over Hikurangi Trough. In winter and spring, however, the two fronts do not confluence before the dateline. The winter of 1985 (June–October) map provides an excellent

example showing both fronts extended eastward and clearly separated. These observations confirm that the STF is indeed a double front zone, consisting of the North and South STF, as found by Belkin (1988) from hydrographic data. In the full agreement with the frontal schematic by Belkin (1988), the NSTF and SSTF continue along the opposite flanks of the Chatham Rise as far east as the Chatham Islands (Figure 4, p. 102). Farther east, however, the double STFZ cannot be reliably traced from our data. The NSTF seems to pass north of Chatham Island and extend eastward, while the SSTF path south of Chatham Island appears more convoluted (or more variable).

Even though the Subantarctic Front (SAF) is known to be a continuous circumpolar front (Patterson and Whitworth, 1990; Orsi *et al.*, 1995; Belkin and Gordon, 1996), it is poorly manifested in our data. The front is better developed in the central South Pacific, SE of New Zealand. In the SE Pacific (east of $\sim 120^\circ\text{W}$) the SAF has not been observed at all although this front is known to extend there. The SAF is better defined in spring and summer, whereas in fall and winter the front is barely noticeable.

The Antarctic Polar Front (APF) is known to follow the northern flank of the Pacific-Antarctic Rise up to the Urdintsev Fracture Zone at 145°W , where it crosses the Rise and extends quasi-zonally up to the Drake Passage (Gordon, 1971; Belkin, 1988; Patterson and Whitworth, 1990; Orsi *et al.*, 1995; Moore *et al.*, 1999). Our observations confirm this pattern. The PF is always pronounced in spring and summer and sometimes also distinct in fall and winter (*e.g.* in 1986). The front is almost invariably best defined near the Urdintsev Fracture Zone, apparently because of the topographic control. Seasonally, the front is best defined in winter. It is also noticeable that one or two fronts, which are located north of the PF in the Ross Sea sector, join the PF immediately upstream of the Urdintsev Fracture Zone.

Southeast Pacific. The seasonal ocean-wide frontal frequency maps (Figures 1–2, p. 101) reveal major frontal zones of the SE Pacific: the Peru-Chile upwelling, with two centers, off Peru and off central Chile; Tropical-Subtropical Frontal Zone between ~ 20 – 45°S ; and the ACC fronts south of 60°S . A newly found ocean front west of Peru and northern Chile, between 10 – 25°S , is well defined in the austral summer and fall.

Coastal upwelling is a seasonal phenomenon, and so are the coastal upwelling fronts (CUF). In spring, summer and fall, the CUF are developed relatively poorly and confined mostly to off Ecuador and Peru. In winter, however, the CUF extend alongshore from the equator southward up to central Chile ($\sim 35^\circ\text{S}$) to form the Peru-Chile upwelling zone. The offshore extent of the CUF is also at maximum in winter when the CUF reach westward beyond 90°W . A newly

found, seasonally intensified front has been observed in austral summer only, extending from off Antofagasta (23°S , northern Chile) to the northwest (Figure 1, p. 101). Because the front crosses the Nazca Ridge, it was tentatively termed the Nazca Front (NF).

The newly identified Nazca Front (NF) is a seasonally persistent feature that only develops in late spring and summer, typically from December through March, sometimes through May. The front extends from off northern Chile (23 – 25°S) to the northwest into the open ocean, gradually shifting away from the coast, crossing the Nazca Ridge, reaching 10°S at 90°W and continuing far beyond, in the general WNW direction, albeit much weakened. The above coordinates are crude estimates of the long-term average path of the front, which is rather a relatively diffuse frontal zone that consists of multiple loosely connected or unconnected filaments extended in the same SE–NW or ESE–WNW direction.

The Nazca Front separates warm, less saline waters of the Peru-Chile Countercurrent flowing southeastward from relative cold, salty waters of the Peru Oceanic (or Offshore) Current flowing northwestward. The latter is better regarded as the eastern limb of the subtropical gyre (Wyrski, 1977). The nomenclature of currents, countercurrents and undercurrents in the Peru-Chile region is complicated and somewhat confusing, with some countercurrents being referred to as undercurrents (Tomczak, 1981; Fonseca, 1989; Strub *et al.*, 1995). Nonetheless, main water masses and currents seem well established (Wyrski, 1964, 1965; Strub *et al.*, 1998). The departure from the coast near 25°S of cool surface waters to the northwest has been recognized by Gunther (1936), who termed this flow the Peru offshore current. The seasonal variability of the ensuing equatorward cold tongue has been described by Wyrski (1977), who has also noted its striking interannual changes in 1975–1976 and related these changes to El Niño 1976.

The long-term monthly SST maps by Wyrski (1964) have revealed two adjacent, oppositely directed tongues from November through April: a narrow poleward warm tongue offshore of Peru and northern Chile and a broad equatorward cold tongue farther west. The emergence of the poleward warm tongue was earlier interpreted as a southeastward countercurrent (Gunther, 1936). However, as argued by Strub *et al.* (1995), the appearance of the poleward warm tongue may largely result from seasonal surface heating combined with continued coastal upwelling off Peru. Indeed, the Peru-Chile countercurrent derived by Strub *et al.* (1995) from satellite altimetry lies over the inshore side of the climatological warm tongue, not inside the tongue, suggestive of a rather coincidental, not dynamical, relation (*i.e.* the countercurrent is not dragging the tongue). The presence of the Nazca Front between the poleward warm tongue and the equatorward cold tongue, however, is suggestive of surface convergence caused

by differential advection of two different water masses flowing in opposite directions. The apparent contradiction between the above inferences might be resolved with the help of surface drifter data; moored current meter data from the warm tongue area are absent.

Although the surface water masses separated by the Nasca Front are well known (Wyrski, 1964), the front itself has not been recognized before. This could be partly explained by the data scarcity in this offshore area since most field studies were focused on the coastal upwelling off Peru and Chile. Another reason for the front's obscurity is its seasonal nature and relatively small SST gradients at the front that complicate its detection from SST data alone. For example, the WOCE P19 line along $\sim 86\text{--}88^\circ\text{W}$ has crossed the eastern limb of the subtropical gyre between 10°S and $30\text{--}34^\circ\text{S}$ in February–March 1994 (Tsuchiya and Talley, 1998); in both cases the gyre's boundaries at the sea surface were marked by strong salinity fronts. Across the Nazca Front at 10°S , the SSS dropped from 35.6 to 34.6 due north, whereas the corresponding SST front was weak and fuzzy (Tsuchiya and Talley, 1998).

FRONTS OF MARGINAL SEAS

Bering Sea. The fronts' importance in the Bering Sea is well documented, especially in its southeastern part that features three prominent fronts, inner, middle, and outer, that correspond roughly to the 50, 100, and 170 m (shelf break) isobaths respectively (Kinder and Coachman, 1978; Schumacher *et al.*, 1979; Coachman *et al.*, 1980; Kinder and Schumacher, 1981a; Coachman, 1986; Schumacher and Stabeno, 1998). Tides are important, especially over the Bering Sea shelf (Kowalik, 1999), where strong tidal mixing fronts (TMF) are observed to completely surround main islands of the Pribilof Archipelago (Schumacher *et al.*, 1979; Kinder *et al.*, 1983; Brodeur *et al.*, 1997, 2000). The fronts play a key role as principal biogeographical boundaries. They separate distinct biotopes (Iverson *et al.*, 1979; Vidal and Smith, 1986) and at the same time they are biotopes *per se* (Kinder *et al.*, 1983; Hansell *et al.*, 1989; Russell *et al.*, 1999). The primary and secondary biological productivity is enhanced at fronts that attract fish, birds, and mammals, including whales (Schneider, 1982; Schneider *et al.*, 1987; Moore *et al.*, 1995; Springer *et al.*, 1996; Russell *et al.*, 1999).

Our knowledge of these fronts is, however, rudimentary, except for, perhaps, the SE Bering Sea. Much less is known, however, about fronts of the northern Bering Sea (*e.g.* Gawarkiewicz *et al.*, 1994). The northern Bering Sea fronts are intimately related to the SE Bering Sea fronts since the mean along-front flows are northwestward (Kinder and Schumacher, 1981b) so that northern fronts are essentially downstream extensions of the southern fronts (*e.g.* Coachman, 1986). In the same time, the northern

Bering Sea frontal pattern continues to the Chukchi Sea via the Bering Strait. This connection is highly important: a large amount of nutrients and phytoplankton is brought by the Bering Slope Current associated with the shelf break front to the Gulf of Anadyr, from where it is transported by the Anadyr Current to the Chirikov Basin and eventually to the Chukchi Sea (Hansell *et al.*, 1989; Walsh *et al.*, 1997).

Notwithstanding the overwhelming importance of fronts in physical and biological processes that evolve in the Bering Sea, a reliable climatology of fronts is absent. The fronts' association with bottom topography and relations to principal ocean-atmosphere variables (ice, air temperature, wind, runoff, and Bering Strait exchange) have not been studied. The seasonal, interannual and decadal variability of the fronts are expected to correlate with the above-mentioned environmental parameters. For example, some of the fronts are located near the maximum extent of the sea ice cover, which fluctuates widely on the interannual time scale, between “warm” and “cold” years, with minimum and maximum development of the sea ice cover respectively (Niebauer, 1998; Wyllie-Echeverria and Ohtani, 1999). Consequently, parameters of such fronts are expected to be different during “warm” and “cold” years. Possible “regime shifts” in the study area's frontal pattern and its characteristics might be linked to the known regime shifts in the North Pacific (Graham, 1994; Polovina *et al.*, 1994; Niebauer, 1998; Brodeur *et al.*, 1999).

Satellite observations of surface fronts in high-latitude seas are hampered by seasonal ice cover and persistent cloudiness. Nonetheless, several studies have demonstrated the great potential of remote sensing, including infrared imagery, in observing surface manifestations of oceanic phenomena (fronts, eddies, upwelling *etc.*) such as the Warm Coastal Current in the Chukchi Sea (Ahlнас and Garrison, 1984), coastal upwelling off St. Lawrence and St. Matthew islands in the Bering Sea (Saitoh *et al.*, 1998), the St. Lawrence Island Polynya (SLIP; Lynch *et al.*, 1997), and spring blooming in the Bering Sea (Maynard and Clark, 1987; Walsh *et al.*, 1997).

The Bering Sea frontal pattern changes dramatically as the season progresses. The frontal pattern in May (Figure 5 top, p. 103) features a well-defined ridge of elevated frontal frequencies extended from Bristol Bay westward to Cape Navarin. The ridge is not isobathic, so the corresponding front is located over shallow depths (~ 50 m) in Bristol Bay but continues over the outer shelf (100–200 m depth) in the northwestern part of the sea. Hence the front location does not correspond to any of the major known fronts (inner, middle, or outer) since these fronts are believed to be isobathic (*e.g.* Coachman, 1986). The front configuration is however remarkably similar to the sea ice cover's edge in May; the edge is located about 1° of latitude to the north of the front (Gloersen *et al.*,

1992; NASA, 1998). The front thus appears to be related to the marginal ice zone processes (Muench and Schumacher, 1985) and represents an imprint left in the ocean by the receding sea ice cover.

In November, the frontal pattern is different (Figure 5 bottom, p. 103). Instead of one major front, several fronts extend essentially in the same SE–NW direction over the shelf break, outer shelf and inner shelf. Some inner shelf fronts are observed well inshore of the 50 m isobath, so they are not necessarily related to the tidal mixed front believed to be associated with the 50 m isobath (*e.g.* Coachman, 1986). Two fronts are distinct in the northwest that correspond to the northward Anadyr Current and southward Kamchatka Current, branches of the Bering Slope Current.

Sea of Okhotsk. The Sea of Okhotsk fronts are described in detail by Belkin and Cornillon (2003). Here we present a summary of the most important results obtained in the above study, which *inter alia* contains an extensive bibliography, therefore references are omitted here for brevity.

Four principal mechanisms generate fronts in the Sea of Okhotsk: (1) tidal mixing along the sea's coasts, on top of banks, in the Kuril Straits and along the Kuril Islands; (2) water mass advection from the Pacific Ocean and Sea of Japan that is accountable for the West Kamchatka front, Soya Warm Current front, and some fronts off the Kuril Islands; (3) Amur River runoff that contributes to the formation of the Amur River plume front and eventually the East Sakhalin front; and (4) wind-induced upwelling, mainly off eastern Sakhalin. Fronts are also known to form near the ice edge; it is unclear, however, if this mechanism plays a significant role in the Sea of Okhotsk. Coastal polynyas and Kashevarov Bank Polynya are important in water mass formation and hence could contribute to front genesis.

Figure 6 (p. 104) is a new schematic of the Sea of Okhotsk frontal pattern (after Belkin and Cornillon, 2003) that significantly improves and supercedes the provisional frontal schematic by Belkin (2001). Most of the portrayed fronts are strongly seasonal: they wax and wane in different months, so at any given moment just a few fronts have been seen. The following 11 fronts were distinguished: West Kamchatka, TINRO Basin, North and South Shelikhov Bay, North, West, Shantar, East Sakhalin, Central, Kashevarov Bank and Soya fronts. The large-scale pattern of these fronts is consistent with the dominant cyclonic circulation of the Okhotsk Sea. The West Front, TINRO Basin Front, Central Front and Shelikhov Bay Fronts have not been previously identified. The West Kamchatka and TINRO Basin fronts form a double front observed in winter only. The North Front continues farther west than it was known, up to 146°E, where it likely connects to the West Front, which often joins the Shantar Front. The latter extends from Shantar Islands to Sakhalin Bay where the Amur River Plume

interrupts a nearly continuous line of fronts around the northern and western Sea of Okhotsk. The Amur discharge feeds the East Sakhalin Front that follows the shelf break, branches eastward at 48°N and 46°N, and eventually merges with Soya Front, which exits the sea via Vries Strait. The 48°N branch of the East Sakhalin Front seems to join the Central Front, which in turn merges with the TINRO Basin Front, thus forming the southern limb of the sea-wide frontal pattern. The Kashevarov Bank Front likely consists of three separate fronts around the namesake bank, St. Iona Island and Iona Bank.

The Sea of Okhotsk frontal pattern was found to be seasonally variable but inter-annually persistent. The fronts rapidly form and degenerate during the ice-free period (May–November). Unlike many other seas, the Sea of Okhotsk fronts are best defined in late summer.

Sea of Japan. The Sea of Japan/East Sea fronts have been studied since 1930s, where the Polar Front (PF) is a major biogeographical and climatic boundary that separates the Sea of Japan in two parts, northern and southern (Isoda *et al.*, 1991; Isoda, 1994; Preller and Hogan, 1998; Zuenko, 1996, 1999). The Tsushima Current Front, associated with the easternmost Kuroshio branch in the Sea of Japan, enjoyed attention since this current significantly moderates Japan's climate; notwithstanding the long history of the front's investigation, its branching pattern and structure is being debated (Moriyasu, 1972; Katoh, 1994; Katoh *et al.*, 1996; Preller and Hogan, 1998; Hase *et al.*, 1999).

The Sea of Japan fronts are robust, especially the Polar Front (Figure 7, p. 105). This front is well defined along 40°N, from off Korea up to off Japan where it sharply turns north. The front dominates the Japan Sea regime. Its vigorous meandering and eddy shedding (Chu *et al.*, 1999; Takematsu *et al.*, 1999) are accountable for the bulk of meridional cross-frontal heat and salt transport. The front separates two regions with different modes of long-term SST variability (Isoda, 1994). The front is a boundary between regions with different vertical structures and different regimes of ocean-atmosphere interaction; the subduction processes at the front and the sporadic, localized deep convection north of the front are critically important for the formation of the Sea of Japan intermediate and deep waters (Seung and Yoon, 1995; Senjyu, 1999). Other fronts are studied relatively poorly, compared to the Polar Front; a notable exception is the shelf front in the Tsushima/Korea Strait (Lee *et al.*, 1984; Huh and Shim, 1987).

This marginal sea features a rich frontal pattern, including several well-defined fronts. Unquestionably, the Polar Front (PF) is the principal boundary that separates the northern and southern parts of the sea. This front is the westernmost extension of the ocean-scale North Pacific Polar Front described above. A

remarkably robust Shelf-Slope Front (SSF) extends along the coast of Primorskiy Krai, Russia, from south of Vladivostok all the way up to Tatar Strait. This front seems to be best defined from October through December. The Tsushima Current Front (TCF) can be distinguished most of the time in the southern part of the sea. This front is associated with the westernmost branch of the Kuroshio that penetrates the East China Sea and Japan Sea. The TCF seems to substantially vary inter-annually. For example, the TCF was well defined in winter of 1986, whereas in winters 1985 and 1989 the front was much less distinct.

The PF usually extends zonally along $\sim 40^\circ\text{N}$ across most of the sea. In the eastern part of the sea, the PF extends meridionally from $\sim 40^\circ\text{N}$ northward, toward Tatar Strait. The seasonal variability of the PF is very strong. The PF is best developed in winter, from January through April, and sometimes can persist through June. In fall, the frontal pattern in the Japan Sea becomes so complicated that the PF cannot be reliably distinguished. The PF can also be seen in spring and summer, although less distinct. The interannual variability of the PF seasonal evolution is substantial.

Our results confirm and significantly extend the analysis of Isoda *et al.* (1991) based on the NOAA-9 AVHRR SST monthly composites for 1987. In particular, we were able to identify the PF almost year around except fall, whereas Isoda *et al.* (1991) could not identify the PF in summer, apparently because of the smoothing nature of the monthly SST composites they used. We also confirm that the Yamato Rise (located at $39\text{--}40^\circ\text{N}$, $134\text{--}136^\circ\text{E}$) plays a significant role in the PF dynamics, noted first by Isoda *et al.* (1991) who found that east of the Yamato Rise the PF is stronger and more stable in all seasons than west of the Rise. Also a quasi-stationary meander of the PF around the Yamato Rise is likely topographically controlled and associated with a warm eddy trapped over the Rise; therefore this meander can be clearly seen in all seasons.

Eastern China Seas (East China, Yellow, and Bohai Seas). The Eastern China Seas have been chosen for a detailed investigation based on the observed richness and robustness of their frontal pattern. This research has already resulted in the most complete regional frontal climatology: ten SST fronts have been distinguished in the Bohai, Yellow and East China Seas (Figure 8, p. 106) and their seasonal variability was quantified (Hickox *et al.*, 2000). From previous studies (*e.g.*, Huh and Shim, 1987; He *et al.*, 1995; Tseng *et al.*, 2000), these fronts are of different nature, associated with one of the following mechanisms: tidal mixing, wind-induced coastal upwelling, topographic upwelling, water mass convergence, and river discharge. Fronts of the Bohai, Yellow, and East China Seas are located over the vast Eastern China Seas shelf or along the shelf break and

are associated with rich fishery grounds (He *et al.*, 1995; Ning *et al.*, 1998).

Three main persistent fronts have been observed there, the Coastal Front (CF), Kuroshio Front (KF) and Central Gyre Front (CGF). The CF ("Yellow Sea coast water front" according to Ning *et al.*, 1998) generally closely follows the coastline (except of off the Hangzhou Bay, where the CF veers offshore), offshore of numerous islands in the southern part of the sea. The CF is prominent in fall and winter, from October through March, being best developed in December. It remains distinct, although less coherent, in spring, and becomes poorly defined in summer.

The Kuroshio Front (KF) extends along the shelf break from Taiwan to Kyushu. The KF is pronounced in fall, winter and spring, and becomes virtually indistinct in summer. The KF is associated with the westernmost branch of the Kuroshio that penetrates the East China Sea and continues along the shelf break/upper slope toward the Japan Sea (*e.g.* Ichikawa and Beardsley, 2002). A remarkable newly identified circular front has been observed off the Changjiang (Yangtze) River estuary. This front might have been a manifestation of a gyre formed by the river runoff, hence the term "Central Gyre Front". The front can be noticed from October through March, being best developed in December. Finally, a front in the Bohai Sea is observed most of the time, being better developed in winter.

Our frontal maps portray a robust frontal pattern that significantly differs from the most recent frontal schematic of Ning *et al.* (1998: fig. 4). These newly found discrepancies, as well as comparison with historical data, are discussed elsewhere (Belkin I.M., Z. Shan, and P. Cornillon, Fronts of the Eastern China Seas, in preparation).

South China Sea. The South China Sea features numerous fronts, most of them aligned with the shelf break, while at least one front (west of Luzon) extends over deep waters (Figure 9, p. 107). The West Luzon Front in the SST field is co-located with winter phytoplankton blooms observed from the CZCS data; the blooms appeared to be related to upwelling (Tang *et al.*, 1999), which might be associated with a quasi-stationary cyclonic eddy off northwest Luzon (Qu, 2000). This front and a quasi-zonal offshore front east of Vietnam (Figure 9, p. 107) coincide with three dynamically active areas observed from the TOPEX/Poseidon altimetry (Ho *et al.*, 2000). The inshore Vietnam front in Figure 3 (p. 102) is close to the narrow band of significant mesoscale variability found by Wang *et al.* (2000) from the TOPEX/Poseidon data, the strongest variability maximum in the South China Sea. Main wintertime SST fronts (Figure 9, p. 107) coincide with winter pigment fronts (Kester and Fox, 1993), *e.g.* along the shelf break off southern China, across the Gulf of Thailand entrance, and NW of Luzon.

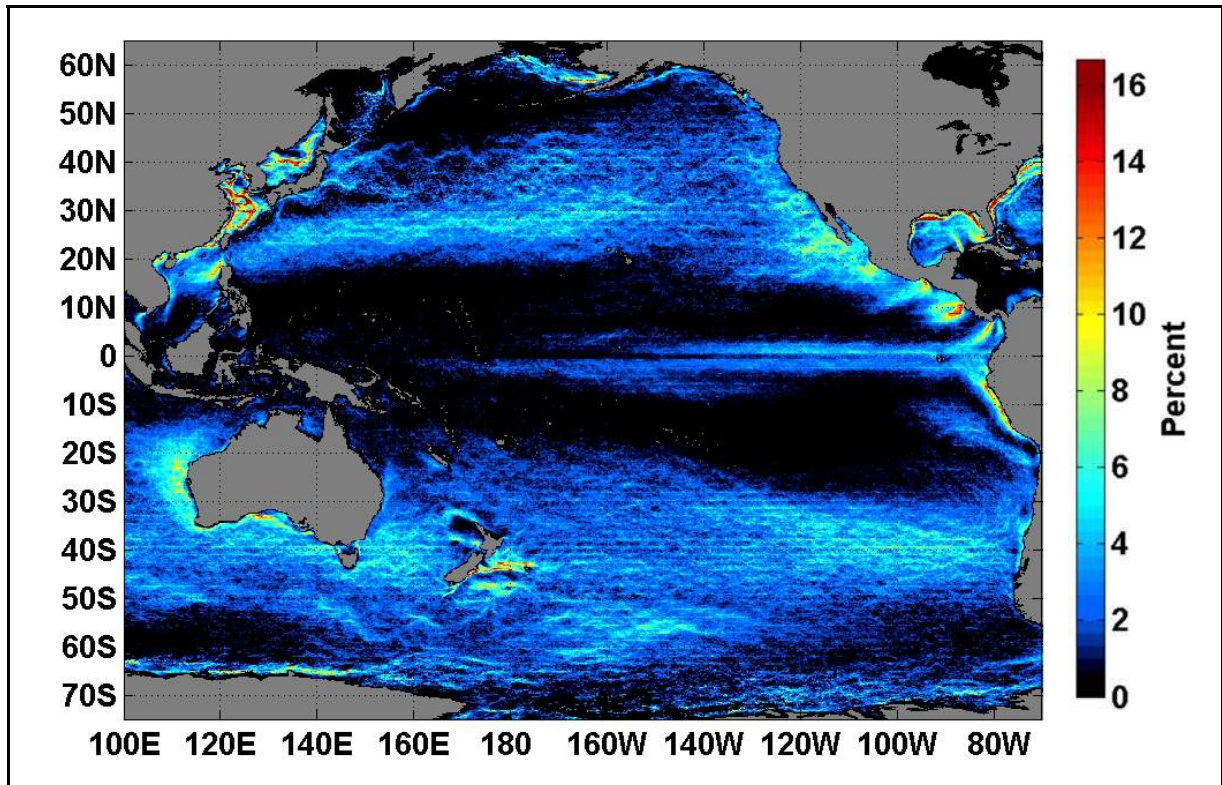


Figure 1. Long-term frequency of SST fronts, 1985–1996, boreal winter (January, February, March)

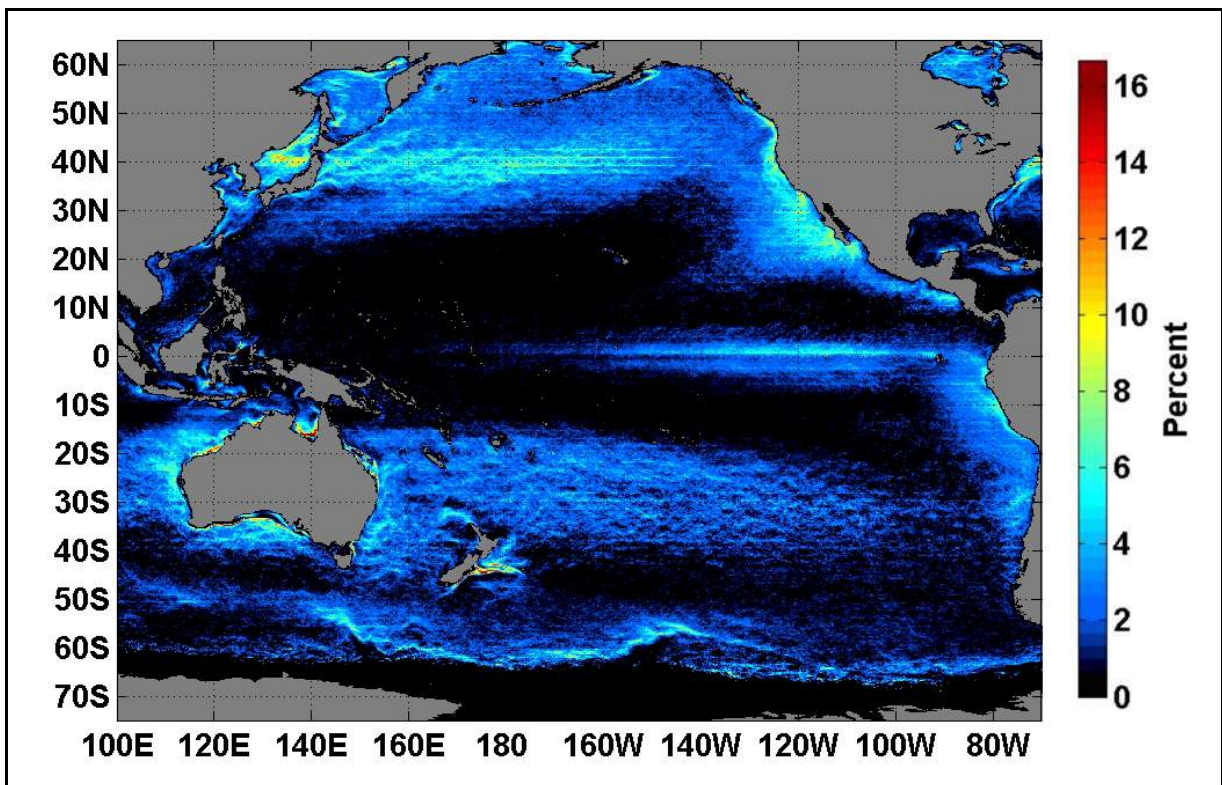


Figure 2. Long-term frequency of SST fronts, 1985–1996, boreal summer (July, August, September)

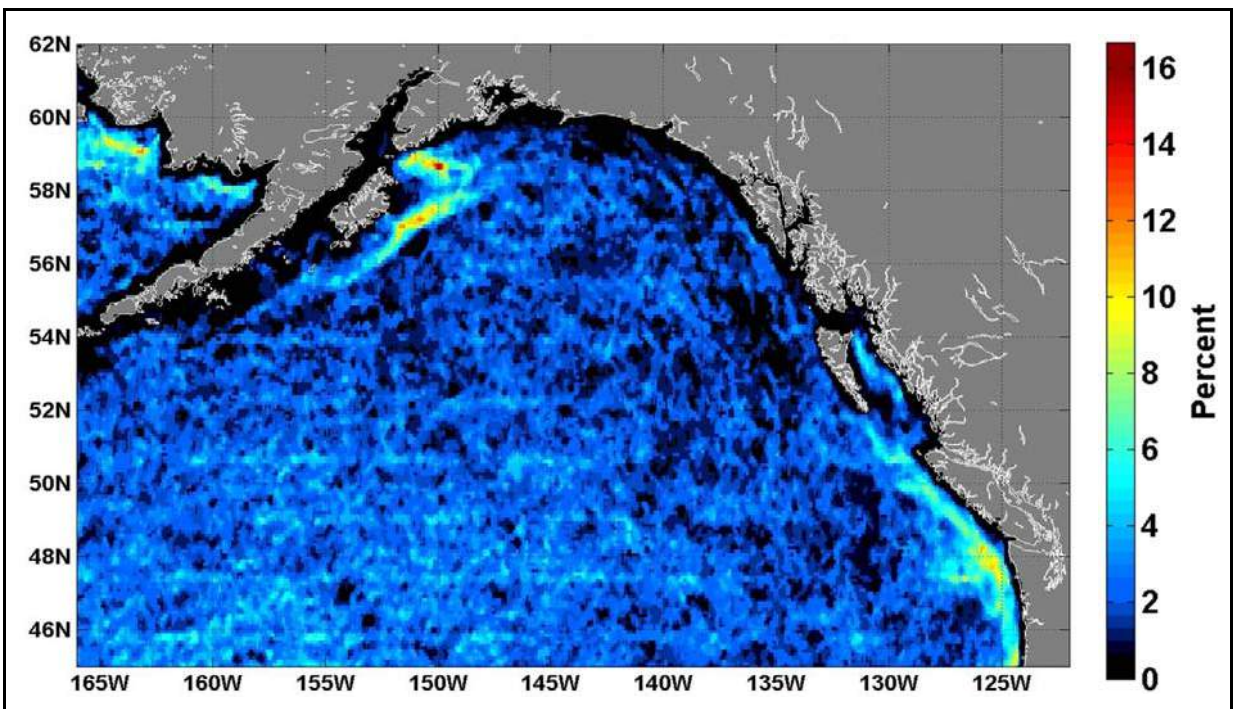


Figure 3. Long-term frequency of SST fronts in the Gulf of Alaska, August 1985–1996

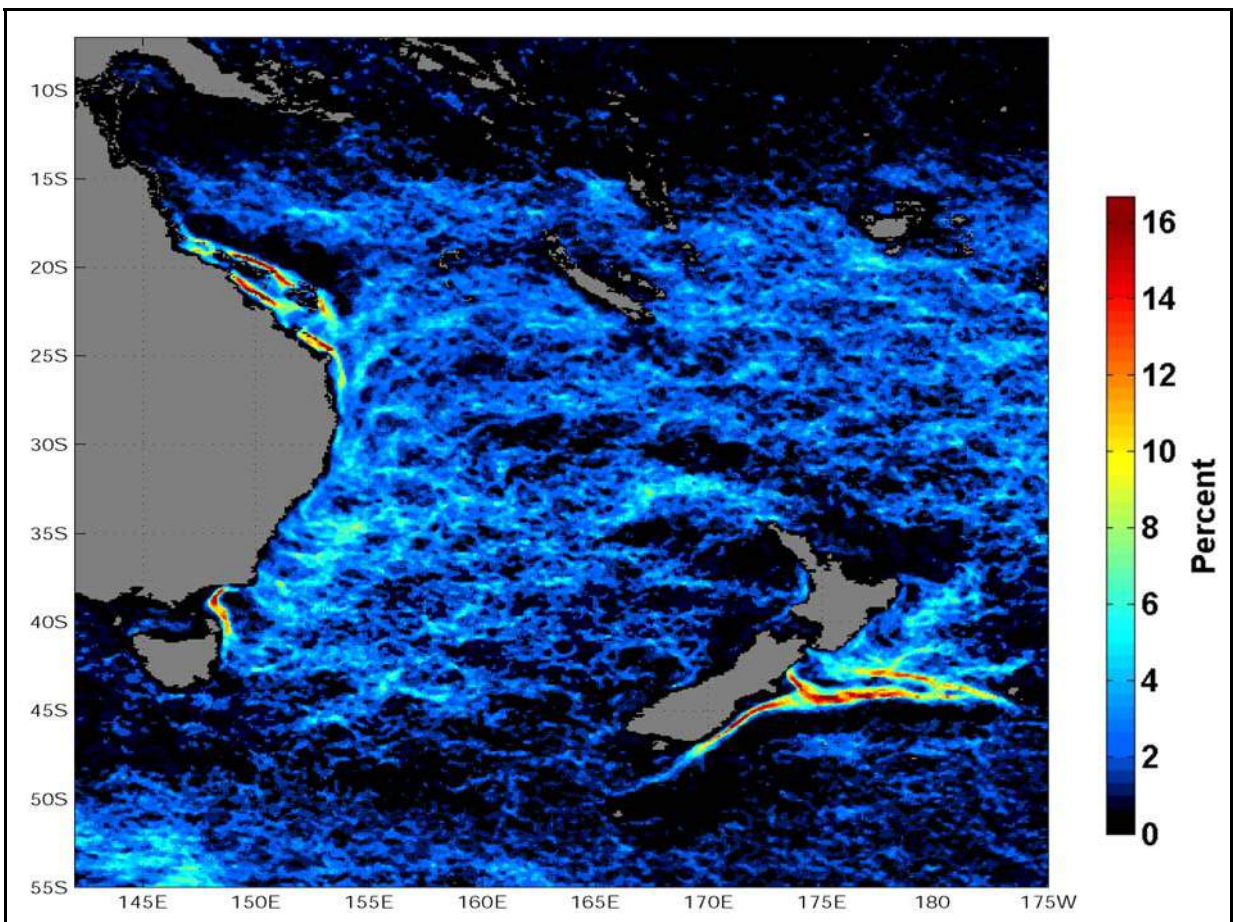


Figure 4. Long-term frequency of SST fronts in the Southwest Pacific, August 1985–1996

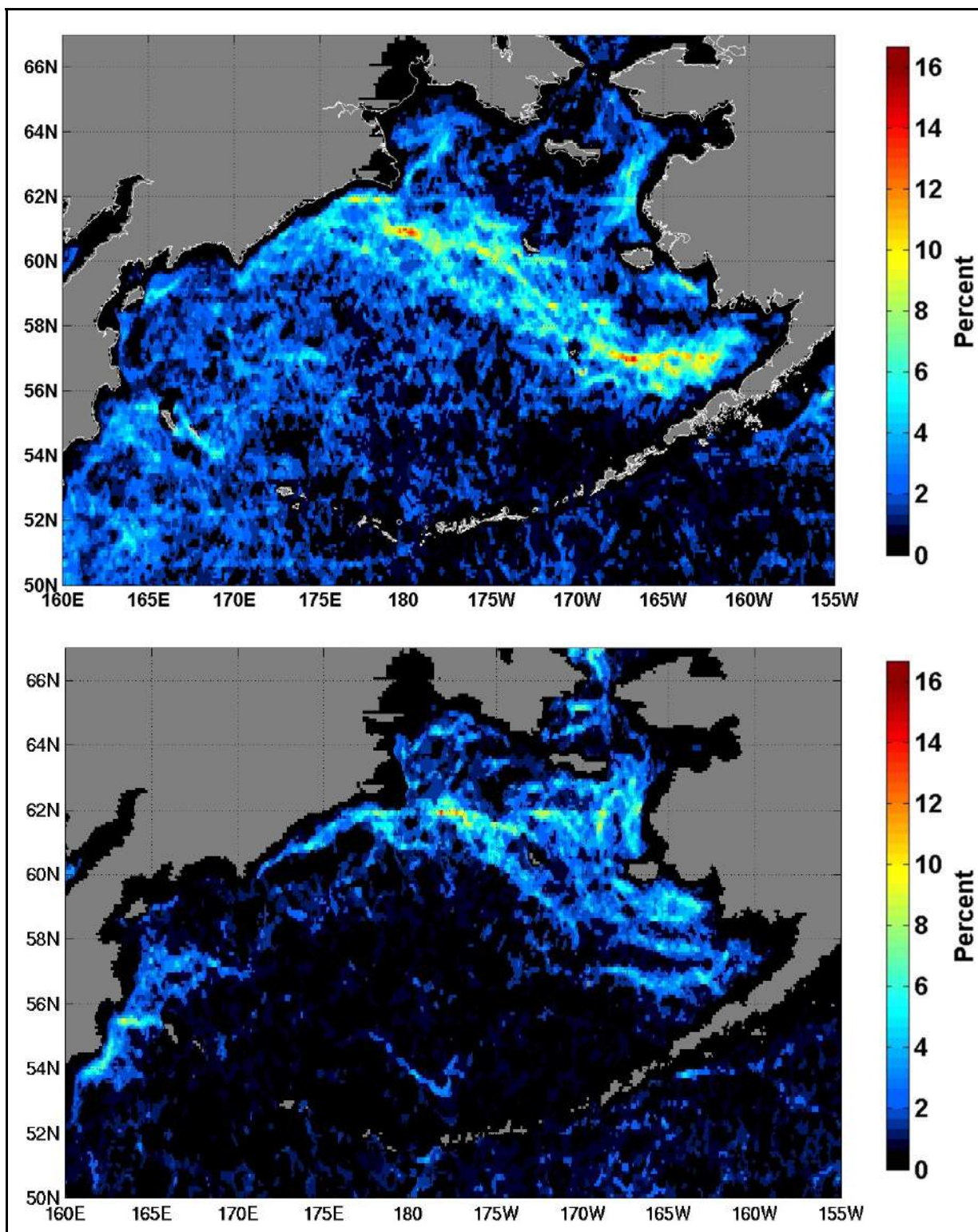


Figure 5. Long-term (1985–1996) frequency of SST fronts in the Bering Sea, May (top) and November (bottom)

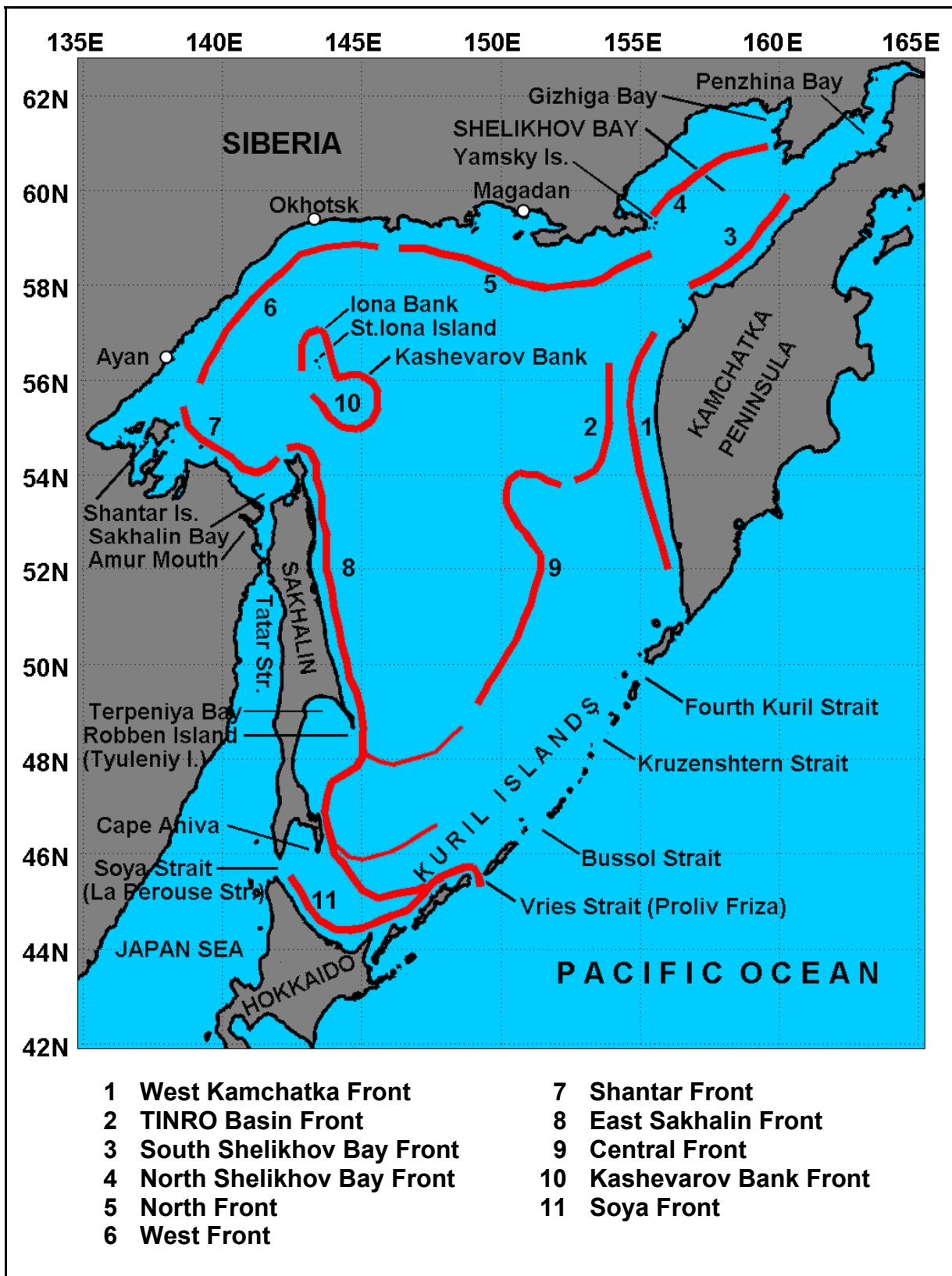


Figure 6. Long-term annual mean pattern of SST fronts of the Okhotsk Sea, 1985–1986 (schematically). After Belkin and Cornillon (2003)

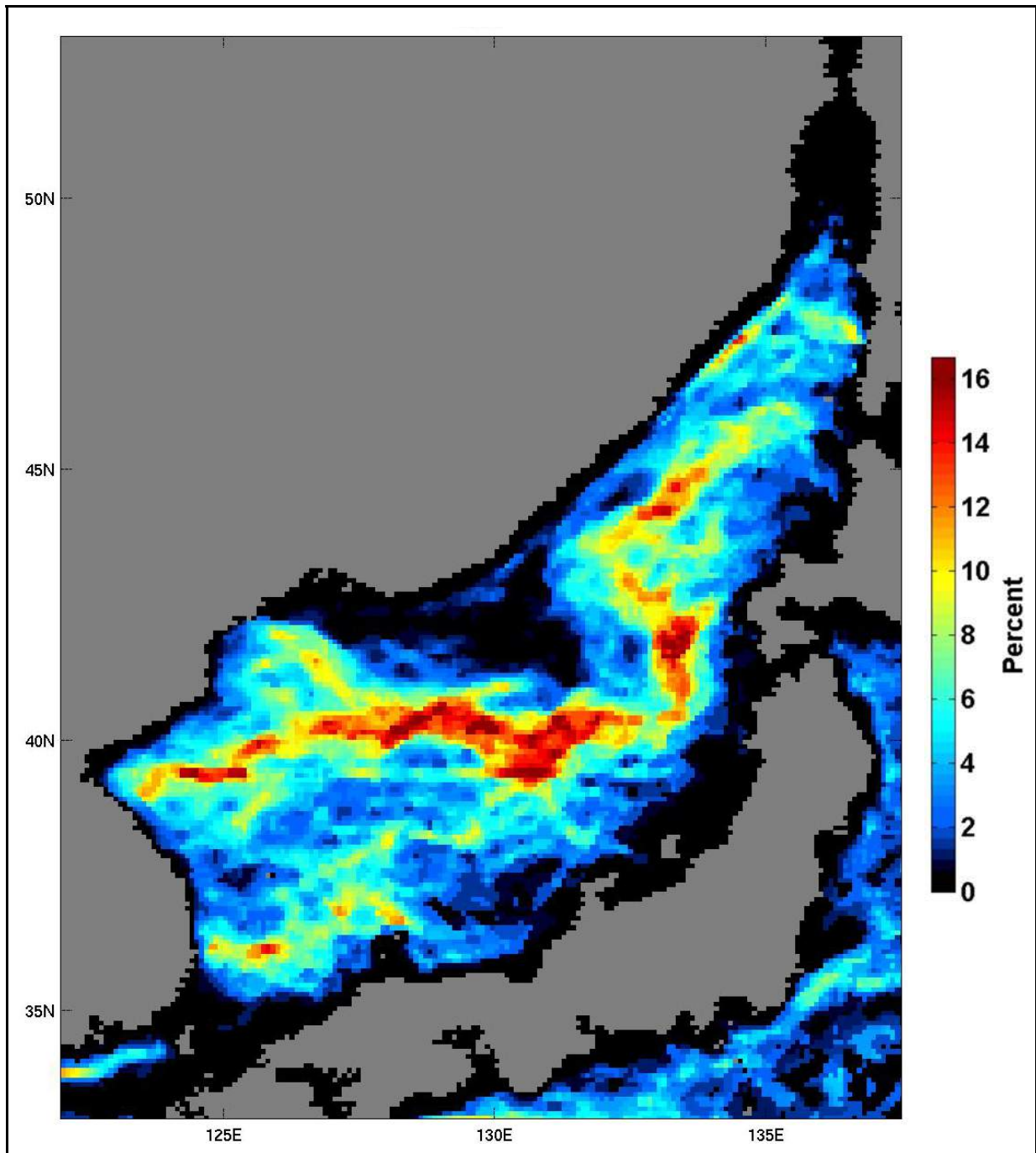


Figure 7. Long-term SST fronts of the Japan Sea, March 1985–1996

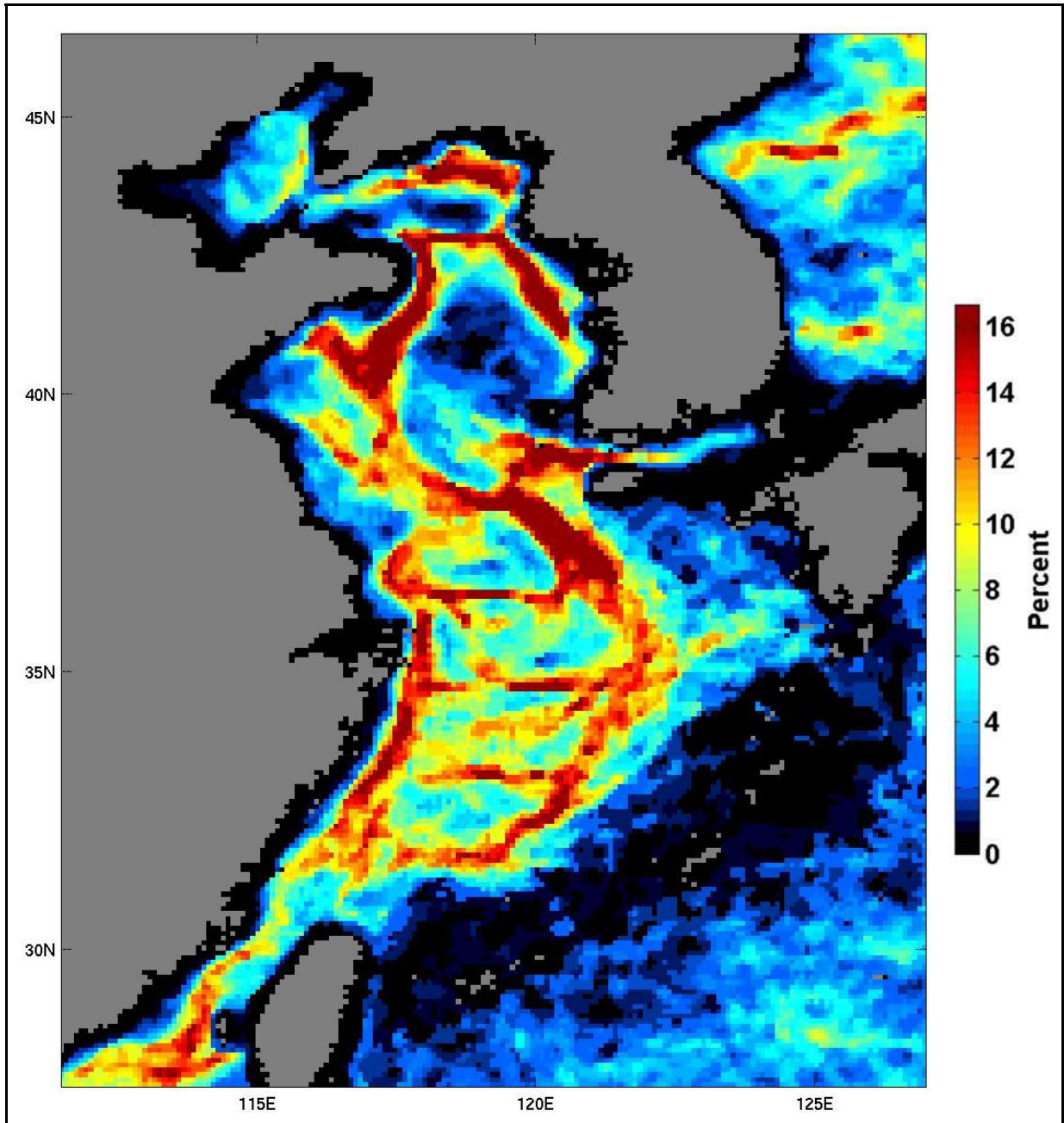


Figure 8. Long-term SST fronts of the East China Seas, March 1985–1996

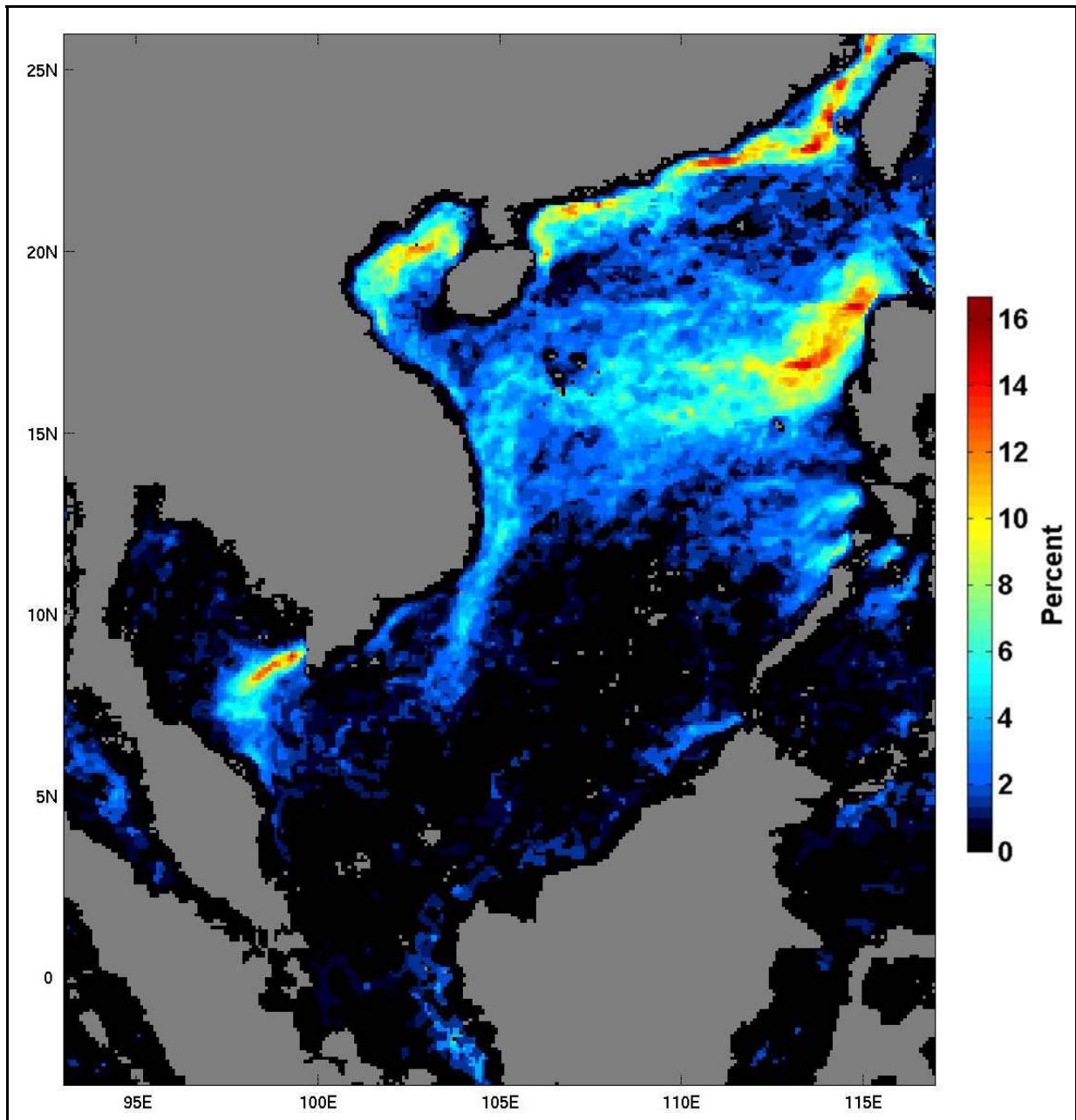


Figure 9. Long-term SST fronts of the South China Sea, February 1985–1996

This sea exhibits very strong seasonal variability of its fronts, which is monsoon-related. The patterns of the seasonal variability are strikingly different across the sea, owing likely to its extremely complex physiography. The following fronts are distinguished here: South China Coastal Front (SCCF) in the northern part of the sea, Bakbo Bay Front (BBF) between Vietnam and Hainan Island; Gulf of Thailand Front (GTF), and a front west of Luzon (WLF).

The SCCF is distinct in winter (from October–November through April–May) and disappears in summer (from June–July through September–November). Like the SCCF, the BBF is prominent in winter (from November–December through April–May) and completely disappears in summer (from May–June through October–November). Fronts are ubiquitous in winter in the northern part of the sea, while almost completely absent in the southern part. The only exception is the Gulf of Thailand's entrance, where a seasonal shelf front (GTF) develops in January–February (described in the next section).

The WLF is observed west of Luzon (over deep waters) in winter (from October–November through April–May). The WLF expands northward as the seasons progress, finally reaching the Bashi Strait, and then disappears in summer (from May–June through September–October). A coastal front off northwestern Borneo exists in spring, summer and fall, and dissipates in winter. An upwelling front off Vietnam is rather weak and can be seen only in spring.

Compared with the above seas, the South China Sea fronts are poorly studied, however their relation to wind-induced upwelling, tidal mixing, and river discharge seem established (Kwan, 1978; Kester and Fox, 1993; Huang *et al.*, 1994; Li, 1996; Tang and Ni, 1996; Su, 1998; Tang *et al.*, 1999).

Gulf of Thailand. The Gulf of Thailand is a shallow (maximum depth <80 m) marine embayment of ~350,000 km² which receives a large amount of brackish water (primarily from the Mekong River, whose runoff peaks at >30,000 m³s⁻¹ in September–December), so the density distribution is mainly governed by the salinity distribution and therefore the Gulf is essentially an estuary (Wattayakorn *et al.*, 1998; Yanagi and Takao, 1998). A strong salinity front at the Gulf's entrance develops in winter (December–January), with the surface salinity range $dS=32.0\text{--}33.8$ (Yanagi and Takao, 1998; Yanagi *et al.*, 2001). A thermal front, associated with the salinity front (termed the Gulf of Thailand Front, GTF), develops in December–February (Figure 9, p. 107), when it's clearly visible in our data and also from hydrographic data for March–April, when the surface temperature range across the front (dT) is at maximum, $dT = 28.5\text{--}30.5^\circ\text{C}$, with the relatively fresh Gulf waters being warmer than the South China Sea waters across the GTF, so the surface density range (dD) across the GTF is substantial, $dD = 19.4\text{--}21.4$

(Yanagi and Takao, 1998). From our data, the thermal GTF completely dissipates by May. Hydrographic data show no trace of the thermal GTF in June, while the salinity GTF still exists, although the surface salinity range is reduced to $dS = 32.8\text{--}33.2$ (Yanagi and Takao, 1998).

The Gulf's tidal currents are generally shore-parallel, with the monthly mean currents being weak, $<0.07\text{ ms}^{-1}$ (Wattayakorn *et al.*, 1998), so the tides apparently do not play a significant role in the GTF formation and maintenance. The wind field over the Gulf is non-uniform and variable (Yanagi and Takao, 1998), therefore the wind stress seems to be of minor importance to the GTF genesis. The Mekong River water import is thus the primary cause of the GTF formation. Accordingly, one can expect a significant interannual variability of the GTF characteristics (including its location, because the GTF is not topographically controlled) related to the interannual variability of precipitation and runoff in the Mekong River basin. To some extent, the South China Sea circulation, that brings the Mekong River water to the Gulf, is also accountable for the GTF genesis and variability.

Indonesian Seas. Waters of the Indonesian Archipelago are completely front-free in austral summer and almost completely front-free in spring, except for a front in the southern Banda Sea. In fall and winter, numerous fronts form in various seas of the Archipelago, including: (1) shelf front north of Java, in the Java Sea; (2) deep-water fronts off Celebes, in the Flores Sea and Banda Sea; and (3) shelf front west of Dolak Island, New Guinea, in the northern Arafura Sea. None of these fronts has been studied *in situ*. Tidal mixing (Ffield and Gordon, 1996) and upwelling (Hughes, 1982; Susanto *et al.*, 2001) are expected to be important in regional front genesis.

SUMMARY AND CONCLUSIONS

Using Pathfinder 9 km resolution SST data from 1985–1996, we were able to identify virtually all of the previously known surface fronts of the Pacific coastal and marginal seas and detect a number of new fronts, or new, important features of known fronts. Below we summarize the findings as follows:

Shelf areas feature rich frontal structures. These shelf fronts are typically tidal mixing fronts or thermal fronts associated with salinity fronts created by river outflows.

Monsoon-driven seasonal circulation changes in the East Asian marginal seas of the Western North Pacific profoundly influence their respective frontal patterns. At the same time, the interannual variability in these regions seems to be less important than the seasonal variability. Thus the same fronts regularly emerge and disappear in the same locales as the season progresses.

Topographically-constrained, hence relatively stable fronts were readily identified even in those high-latitude regions where persistent cloudiness was expected to hinder the study, such as the Bering Sea and others.

Vast frontal zones, associated with coastal upwelling, were found to extend far offshore, up to $O(1000\text{ km})$ into the open ocean. The seasonal development (and relaxation) of coastal upwelling fronts was observed in each of the upwelling areas studied.

The results obtained in this work provide ample validation of the algorithms for edge detection and clouds screening that form the backbone of this

research. This, in turn, allows us to move from the general global frontal survey to in-depth studies of regional frontal patterns and their temporal variability, on variety of scales, from seasonal to decadal.

ACKNOWLEDGMENTS

Principal funding for this research was provided by NASA through grants NAG 53736 and NAG 512741. The Bering Sea study was also supported by the Cooperative Institute for Arctic Research, under NOAA Cooperative Agreement No. NA17RJ1224. The support of both agencies is greatly appreciated. Edge detection and declouding algorithms were run by Zhengqiang Shan.

REFERENCES

- Ahlnäs K., Garrison G.R. 1984. Satellite and oceanographic observations of the warm coastal current in the Chukchi Sea, Arctic, 37(3), pp. 244–254.
- Andrews J.C., Lawrence M.W., Nilsson C.S. 1980. Observations of the Tasman Front, J. Phys. Oceanogr., 10(11), pp. 1854–1869.
- Belkin I.M. 1988. Main hydrological features of the Central South Pacific, in: Ecosystems of the Subantarctic Zone of the Pacific Ocean, edited by M.E. Vinogradov and M.V. Flint, Nauka, Moscow, pp. 21–28; English translation published in: Pacific Subantarctic Ecosystems, pp.12–17, New Zealand Translation Centre Ltd., Wellington, 1997.
- Belkin I.M., Gordon A.L. 1996. Southern Ocean fronts from the Greenwich meridian to Tasmania, J. Geophys. Res., 101(C2), pp. 3675–3696.
- Belkin I.M., Shan Z., Cornillon P. 1998. Global survey of oceanic fronts from Pathfinder SST and in-situ data, AGU 1998 Fall Meeting Abstracts, Eos, 79 (45, Suppl.), F475.
- Belkin I.M., Cornillon P., Shan Z., Hickox R. 2000. Fronts of the Western Pacific marginal seas from the Pathfinder SST data, Abstracts of the AGU Fall 2000 Meeting, Eos, 81 (48, suppl.), F722–F723.
- Belkin I.M. 2001. Okhotsk Sea SST fronts from Pathfinder 1985–1996 satellite data, Proc. 16th International Symposium on Okhotsk Sea and Sea Ice, 4–8 February 2001, Mombetsu, Hokkaido, Japan, pp. 391–400.
- Belkin I.M., Cornillon P., Shan Z. 2001. Global survey of ocean fronts from Pathfinder SST data, presented at The Oceanography Society Meeting, April 2–5, 2001, Miami Beach, FL, Oceanography, 14(1), 10.
- Belkin I.M., Krishfield R., Honjo S. 2002. Decadal variability of the North Pacific Polar Front: Subsurface warming versus surface cooling, Geophys. Res. Lett., 29(9), doi: 10.1029/2001GL013806.
- Belkin I.M. 2003. Front, in: Interdisciplinary Encyclopedia of Marine Sciences, edited by Nybakken J.W., Broenkow W.W., Vallier T.L., pp. 433–436, Grolier Academic Reference, Danbury, Conn.
- Belkin I.M., Cornillon P. 2003. Surface thermal fronts of the Okhotsk Sea, Pacific Oceanography, submitted.
- Belkin I.M., Cornillon P., Ullman D. 2003. Ocean fronts around Alaska from satellite SST data, Proceedings of the American Meteorological Society 7th Conference on the Polar Meteorology and Oceanography, Hyannis, MA, Paper 12.7, 15 p.
- Belkin I.M., Shan Z., Cornillon P. 2004. Global pattern of ocean fronts from Pathfinder SST data: II. Pacific Ocean, in preparation.
- Brink K.H., Halpern D., Huyer A., Smith R.L. 1983. The physical environment of the Peruvian upwelling system. Progr. Oceanogr., 12(3), pp. 285–305.
- Brodeur R.D., Wilson M.T., Napp J.M. 1997. Distribution of juvenile pollock relative to frontal structure near the Pribilof Islands, Bering Sea, in: Forage Fishes in Marine Ecosystems, pp. 573–589, Proc. Int'l Symp. on the Role of Forage Fishes in Marine Ecosystems, Alaska Sea Grant College Program Rep. No. 97-01, University of Alaska Fairbanks.
- Brodeur R.D., Mills C.E., Overland J.E., Walters G.E., Schumacher J.D. 1999. Evidence for a substantial increase in gelatinous zooplankton in the Bering Sea, with possible link to climate change, Fish. Oceanogr., 8(4), pp. 296–306.
- Brodeur R.D., Wilson M.T., Ciannelli L. 2000. Spatial and temporal variability in feeding and condition of age-0 walleye pollock (*Theragra chalcogramma*) in frontal regions of the Bering Sea, ICES J. Mar. Sci., 57(2), pp. 256–264.
- Burrage D.M., Steinberg C.R., Skirving W.J., Kleypas J.A. 1996. Mesoscale circulation features of the Great Barrier Reef region inferred from NOAA satellite imagery, Remote Sens. Environ., 56(1), pp. 21–41.
- Cayula J.-F., Cornillon P., Holyer R., Peckinpaugh S. 1991. Comparative study of two recent edge-detection algorithms designed to process sea-surface temperature fields. IEEE Trans. Geosci. Rem. Sens., 29(1), pp. 175–177.
- Cayula J.-F., Cornillon P. 1992. Edge detection algorithm for SST images. J. Atmos. Oceanic Tech., 9(1), pp. 67–80.
- Cayula J.-F., Cornillon P. 1995. Multi-image edge detection for SST images. J. Atmos. Oceanic Tech., 12(4), pp. 821–829.
- Cayula J.-F., Cornillon P. 1996. Cloud detection from a sequence of SST images. Remote Sensing of Environment, 55(1), pp. 80–88.
- Chu P.C., Chen Y., Lu S. 1999. Japan/East Sea (JES) Polar Front meandering and eddy shedding in May 1995, in: Proceedings of the CREAMS'99 International Symposium,

- 26–28 January 1999, Fukuoka, Japan, pp. 11–14, CREAMS Secretariat, Kyushu University.
- Church J.A. 1987.** The East Australian Current adjacent to the Great Barrier Reef, *Aust. J. Mar. Freshwater Res.*, 38(6), pp. 671–683.
- Church J.A., Craig P.D. 1998.** Australia's shelf seas: Diversity and complexity, in: *The Sea*, vol. 11, edited by Robinson A.R. and Brink K.H. John Wiley and Sons, New York etc. pp. 933–964.
- Coachman L.K., Kinder T.H., Schumacher J.D., Tripp R.B. 1980.** Frontal systems of the southeastern Bering Sea shelf, in: *Second International Symposium on Stratified Flows*, vol. 2, edited by T. Carstens and T. McClimans, pp. 917–933, Tapir, Trondheim.
- Coachman L.K. 1986.** Circulation, water masses, and fluxes on the southeastern Bering Sea shelf, *Cont. Shelf Res.*, 5(1/2), pp. 23–108.
- Crawford W.R., Woodward M.J., Foreman M.G.G., Thomson R.E. 1995.** Oceanographic features of Hecate Strait and Queen Charlotte Sound in summer, *Atmosphere-Ocean*, 33(4), pp. 639–681.
- Fedorov K.N. 1986.** *The Physical Nature and Structure of Oceanic Fronts*. Springer-Verlag, Berlin etc., viii+333 pp.
- Ffield A., Gordon A.L. 1996.** Tidal mixing signatures in the Indonesian Seas, *J. Phys. Oceanogr.*, 26(9), pp. 1924–1937.
- Fonseca T. 1989.** An overview of the poleward undercurrent and upwelling along the Chilean coast, in: *Poleward Flows Along Eastern Ocean Boundaries*, edited by Neshyba S.J., Mooers C.N.K., Smith R.L., Barber R.T. Springer-Verlag, New York etc. pp. 203–228.
- Gawarkiewicz G., Haney J.C., Caruso M.J. 1994.** Summertime synoptic variability of frontal systems in the northern Bering Sea, *J. Geophys. Res.*, 99(C4), pp. 7617–7625.
- Gibbs C.F., Arnott G.H., Longmore A.R., Marchant J.W. 1991.** Nutrient and plankton distribution near a shelf break front in the region of the Bass Strait Cascade. *Aus. J. Mar. Freshwater Res.*, 42(2), pp. 201–217.
- Gloersen P., Campbell W.J., Cavalieri D.J., Comiso J.C., Parkinson C.L., Zwally H.J. 1992.** *Arctic and Antarctic Sea Ice, 1978–1987: Satellite Passive-Microwave Observations and Analysis*, NASA SP-511, Washington, D.C., 290 p.
- Godfrey J.S., Jones I.S.F., Maxwell J.G.H., Scott B.D. 1980.** On the winter cascade from Bass Strait into the Tasman Sea, *Aust. J. Mar. Freshwat. Res.*, 31(3), pp. 275–286.
- Gordon A.L. 1971.** Antarctic Polar Front Zone, in: *Antarctic Oceanology I*, edited by J.L. Reid, pp. 205–221, AGU, Washington, D.C.
- Graham N.E. 1994.** Decadal-scale climate variability in the Tropical and North Pacific during the 1970s and 1980s: Observations and model results, *Climate Dynamics*, 10(3), pp. 135–162.
- Gunther E.R. 1936.** A report on oceanographical investigations in the Peru coastal current, *Discovery Rep.*, 13, pp. 107–236.
- Hamon B.V. 1965.** The East Australian Current, 1960–1964. *Deep-Sea Res.*, 12(6), pp. 899–921.
- Hansell D.A., Goering J.J., Walsh J.J., McRoy C.P., Coachman L.K., Whitedge T.E. 1989.** Summer phytoplankton production and transport along the shelf break in the Bering Sea, *Cont. Shelf Res.*, 9(12), pp. 1085–1104.
- Hase H., Yoon J.-H., Koterayama W. 1999.** The current structure of the Tsushima Warm Current along the Japanese coast, *J. Oceanography*, 55(2), pp. 217–235.
- He M.X., Chen G., Sugimori Y. 1995.** Investigation of mesoscale fronts, eddies and upwelling in the China Seas with satellite data. *The Global Atmosphere and Ocean System*, 3(4), pp. 273–288. Delcroix, T., Henin, C., Porte, V., Arkin, P. 1996. Precipitation and sea-surface salinity in the tropical Pacific Ocean. *Deep-Sea Res. I*, 43(7), pp. 1123–1141.
- Heath R. 1985.** A review of the physical oceanography of the seas around New Zealand – 1982. *N. Z. J. Mar. Freshwat. Res.*, 19(1), pp. 79–124.
- Hermann A.J., Stabeno P.J. 1996.** An eddy resolving model of circulation on the western Gulf of Alaska shelf: 1. Model development and sensitivity analyses, *J. Geophys. Res.*, 101(C1), pp. 1129–1149.
- Hickox R., Belkin I.M., Cornillon P., Shan Z. 2000.** Climatology and seasonal variability of ocean fronts in the East China, Yellow and Bohai Seas from satellite SST data, *Geophys. Res. Lett.*, 27(18), pp. 2495–2498.
- Ho C.-R., Kuo N.-J., Zheng Q., Soong Y.S. 2000.** Dynamically active areas in the South China Sea detected from TOPEX/POSEIDON satellite altimeter data, *Remote Sens. Environ.*, 71(3), pp. 320–328.
- Huang Q.-Z., Wang W.-Z., Li Y.S., Li C.W. 1994.** Current characteristics of the South China Sea, in: *Oceanology of China Seas*, edited by D. Zhou, Y.-B. Liang, and C.-K. Zeng (C.K. Tseng), Volume 1, pp. 49–47, Kluwer Academic Publishers, Boston.
- Hughes R. 1982.** On a front between two rotating flows with application to the Flores Sea, *Dyn. Atmos. Oceans*, 6(4), pp. 153–176.
- Huh O.K., Shim T. 1987.** Satellite observations of surface temperatures and flow patterns, Sea of Japan and East China Sea, late March 1979, *Remote Sens. Environ.*, 22(3), pp. 379–393.
- Ichikawa H., Beardsley R.C. 2002.** The Current System in the Yellow and East China Seas, *J. Oceanography*, 58(1), pp. 77–92.
- Isoda Y., Saitoh S., Mihara M. 1991.** SST structure of the Polar Front in the Japan Sea, in: *Oceanography of Asian Marginal Seas*, edited by Takano K. Elsevier, Amsterdam etc. pp. 103–112.
- Isoda Y. 1994.** Interannual SST variations to the north and south of the polar front in the Japan Sea, *La Mer*, 32(4), pp. 285–293.
- Iverson R.L., Coachman L.K., Cooney R.T., English T.S., Goering J.J., Hunt G.L., Jr., Macauley M.C., McRoy C.P., Reeburg W.S., Whitedge T.E., Livingston R.J. 1979.** Ecological significance of fronts in the southeastern Bering Sea, in: *Ecological Processes in Coastal and Marine Systems*, edited by Livingston R.J. pp. 437–468, Plenum Press, London.
- Jardine I.D., Thomson K.A., Foreman M.G., LeBlond P.H. 1993.** Remote sensing of coastal sea-surface features off northern British Columbia, *Remote Sens. Environ.*, 45(1), pp. 73–84.
- Katoh O. 1994.** Structure of the Tsushima Current in the Southwestern Japan Sea, *J. Oceanography*, 50(3), pp. 317–338.

- Katoh O., Morinaga K., Miyaji K., Teshima K. 1996.** Branching and joining of the Tsushima Current around the Oki Islands, *J. Oceanography*, 52(6), pp. 747–761.
- Kazmin A.S., Rienecker M.M. 1996.** Variability and frontogenesis in the large-scale oceanic frontal zones. *J. Geophys. Res.*, 101(C1), pp. 907–921.
- Kester D.R., Fox M. 1993.** Chemical and biological remote sensing of the South China Sea: satellite and *in situ* observations, in: *Symposium on Remote Sensing in Environmental Research and Global Change*, edited by M. Fang and A. Liu, pp. 60–72 and pp. 135–139, The Commercial Press (H.K.) Ltd, Hong Kong.
- Kinder T.H., Coachman L.K. 1978.** The front overlaying the continental slope in the eastern Bering Sea, *J. Geophys. Res.*, 83(C9), pp. 4551–4559.
- Kinder T.H., Schumacher J.D. 1981a.** Hydrographic structure over the continental shelf of the southeastern Bering Sea, in: *The Eastern Bering Sea Shelf: Oceanography and Resources, Volume 1*, edited by D.W. Hood and J.A. Calder, pp. 31–52, NOAA, University of Washington Press, Seattle.
- Kinder T.H., Schumacher J.D. 1981b.** Circulation over the continental shelf of the southeastern Bering Sea, in: *The Eastern Bering Sea Shelf: Oceanography and Resources, Volume 1*, edited by D.W. Hood and J.A. Calder, pp. 53–75, NOAA, University of Washington Press, Seattle.
- Kinder T.H., Hunt G.L., Jr., Schneider D., Schumacher J.D. 1983.** Correlations between seabirds and oceanic fronts around the Pribilof Islands, Alaska, *Estuarine, Coastal and Shelf Science*, 16(3), pp. 303–319.
- Kowalik Z. 1999.** Bering Sea tides, in: *Dynamics of the Bering Sea*, edited by T.R. Loughlin and K. Ohtani, pp. 93–127, University of Alaska Sea Grant, AK-SG-99-03, Fairbanks.
- Kwan P.-H. 1978.** The warm current in the South China Sea - a current flowing against the wind in winter in the open sea off Guangdong Province, *Oceanol. Limnol. Sin.*, 9(2), pp. 117–127.
- Lee J.C., Na J.Y., Chang S.-D. 1984.** Thermohaline structure of the shelf front in the Korea Strait in early winter, *J. Oceanogr. Soc. Korea*, 19(1), pp. 56–67.
- Legeckis R. 1978.** A survey of worldwide sea surface temperature fronts detected by environmental satellites. *J. Geophys. Res.*, 83(C9), pp. 4501–4522.
- Legeckis R. 1988.** Upwelling off the Gulfs of Panama and Papagayo in the Tropical Pacific during March 1985. *J. Geophys. Res.*, 93(C12), pp. 15485–15489.
- Li L. 1996.** An oceanic front at the shelf-slope region of the northeastern South China Sea, March 1992, *Studies on the circulation of the northeastern South China Sea*, No. 6, pp. 33–41, China Ocean Press, Beijing.
- Lynch A.H., Glueck M.F., Chapman W.L., Bailey D.A., Walsh J.E. 1997.** Satellite observation and climate system model simulation of the St. Lawrence Island polynya, *Tellus*, 49A(2), pp. 277–297.
- Maxwell W.G.H. 1968.** *Atlas of the Great Barrier Reef*, Elsevier, New York, 258 p.
- Maynard N.G., Clark D.K. 1987.** Satellite color observations of spring blooming in Bering Sea shelf waters during the ice edge retreat in 1980, *J. Geophys. Res.*, 92(C7), pp. 7127–7139.
- Moore J.K., Abbott M.R., Richman J.G. 1999.** Location and dynamics of the Antarctic Polar Front from satellite sea surface temperature data, *J. Geophys. Res.*, 104(C2), pp. 3059–3073.
- Moore S.E., George J.C., Coyle K.O., Weingartner T.J. 1995.** Bowhead whales along the Chukotka coast in autumn, *Arctic*, 48(2), pp. 155–160.
- Moriyasu S. 1972.** The Tsushima Current, in: *The Kuroshio: Physical Aspects of the Japan Current*, edited by H. Stommel and K. Yoshida, pp. 353–369, University of Washington Press, Seattle and London.
- Morris M., Roemmich D., Cornuelle B. 1996.** Observations of variability in the South Pacific Subtropical Gyre, *J. Phys. Oceanogr.*, 26(11), pp. 2359–2380.
- Muench R.D., Schumacher J.D. 1985.** On the Bering Sea ice edge front, *J. Geophys. Res.*, 90(C2), pp. 3185–3197.
- Mulhearn P.J. 1987.** The Tasman Front: A study using infrared imagery. *J. Phys. Oceanogr.*, 17(8), pp. 1148–1155.
- Musgrave D.L., Weingartner T.J., Royer T.C. 1992.** Circulation and hydrography in the northwestern Gulf of Alaska, *Deep-Sea Res.*, 39(9), pp. 1499–1519.
- Nakamura H., Kazmin A.S. 2003.** Decadal changes in the North Pacific oceanic frontal zones as revealed in ship and satellite observations, *J. Geophys. Res.*, 108(C3), doi:10.1029/1999JC000085.
- NASA 1998.** Sea ice concentrations from Nimbus-7 SMMR and DMSP SSM/I passive microwave data, 1978–1996, Volumes 1–3 (on CD-ROMs; USA_NASA_971_0001, 0002, 0003), Goddard Space Flight Center, Laboratory for Hydrospheric Processes. Archived and distributed by NSIDC, CIRES, University of Colorado Boulder.
- Niebauer H.J. 1998.** Variability in Bering Sea ice cover as affected by a regime shift in the North Pacific in the period 1947–1996, *J. Geophys. Res.*, 103(C12), pp. 27717–27737.
- Nilsson C.S., Cresswell G.R. 1980.** The formation and evolution of East Australian Current warm-core eddies. *Prog. Oceanogr.*, 9(3), pp. 133–183.
- Ning X., Liu Z., Cai Y., Fang M., Chai F. 1998.** Physicobiological oceanographic remote sensing of the East China Sea: Satellite and *in situ* observations. *J. Geophys. Res.*, 103(C10), pp. 21623–21635.
- Orsi A.H., Whitworth T., III, Nowlin W.D., Jr. 1995.** On the meridional extent and fronts of the Antarctic Circumpolar Current, *Deep-Sea Res. I*, 42(5), pp. 641–673.
- Patterson S.L., Whitworth T., III. 1990.** Physical oceanography, in: *Antarctic Sector of the Pacific*, edited by G.P. Glasby, pp. 55–93, Elsevier, Amsterdam etc.
- Perry R.I., Dilke B.R., Parsons T.R. 1983.** Tidal mixing and summer plankton distributions in Hecate Strait, British Columbia, *Can. J. Fish. Aquat. Sci.*, 40(7), pp. 871–887.
- Pickard G.L., Donguy J.R., Henin C., Rougerie F. 1977.** A review of the physical oceanography of the Great Barrier Reef and western Coral Sea, *Austral. Inst. Mar. Science, Monograph Series*, 2, Canberra, 135 p.
- Polovina J.J., Mitchum G.T., Graham N.E., Craig M.P., Demartini E.E., Flint E.N. 1994.** Physical and biological consequences of a climate event in the central North Pacific, *Fish. Oceanogr.*, 3(1), pp. 15–21.
- Preller R.H., Hogan P.J. 1998.** Oceanography of the Sea of Okhotsk and the Japan/East Sea, in: *The Sea*, vol. 11, edited by Robinson A.R. and Brink K.H., pp. 429–481, John Wiley & Sons, New York.

- Qiu B., Toda T., Imasato N. 1990.** On Kuroshio Front fluctuations in the East China Sea using satellite and *in situ* observational data. *J. Geophys. Res.*, 95(10), pp. 18191–18204.
- Qiu B., Miao W. 2000.** Kuroshio path variations south of Japan: Bimodality as a self-sustained internal oscillation, *J. Phys. Oceanogr.*, 30(8), pp. 2124–2137.
- Qiu B. 2002.** The Kuroshio Extension System: Its large-scale variability and role in the midlatitude ocean-atmosphere interaction, *J. Oceanogr.*, 58(1), pp. 51–75.
- Qu T. 2000.** Upper-layer circulation in the South China Sea, *J. Phys. Oceanogr.*, 30(6), pp. 1450–1460.
- Reed R.K., Schumacher J.D. 1987.** Physical oceanography, in: *The Gulf of Alaska, physical environment and biological resources*, edited by D.W. Hood and S.T. Zimmerman, pp. 57–75, U.S. Department of Commerce and U.S. Department of the Interior, U.S. Gov. Printing Office, NTIS #PB87-103230.
- Rienecker M.M., Mooers C.N.K. 1989.** Mesoscale eddies, jets and fronts off Point Arena, California, July 1986. *J. Geophys. Res.*, 94(C9), pp. 12555–12569.
- Rodriguez-Rubio E., Schneider W., Rio R.A. 2003.** On the seasonal circulation within the Panama Bight derived from satellite observations of wind, altimetry and sea surface temperature, *Geophys. Res. Lett.*, 30(7), doi: 10.1029/2002GL016794.
- Roemmich D., Cornuelle B. 1990.** Observing the fluctuations of gyre-scale ocean circulation: A study of the subtropical South Pacific, *J. Phys. Oceanogr.*, 20(12), pp. 1919–1934.
- Roemmich D., Sutton P. 1998.** The mean and variability of ocean circulation past northern New Zealand: Determining the representativeness of hydrographic climatologies, *J. Geophys. Res.*, 103(C6), pp. 13041–13054.
- Royer T.C. 1981.** Baroclinic transport in the Gulf of Alaska, II. Freshwater-driven coastal current, *J. Mar. Res.*, 39(2), pp. 251–266.
- Russell R.W., Harrison N.M., Hunt G.L., Jr. 1999.** Foraging at a front: Hydrography, zooplankton, and avian planktivory in the northern Bering Sea, *Mar. Ecol. Prog. Ser.*, 182, pp. 77–93.
- Saitoh S.-I., Eslinger D., Sasaki H., Shiga N., Odate T., Miyoi T. 1998.** Satellite and ship observations of coastal upwelling in the St. Lawrence Island Polynya (SLIP) area in summer, 1994 and 1995, *Mem. Fac. Fish. Hokkaido Univ.*, 45(1), pp. 18–23.
- Schneider D. 1982.** Fronts and seabird aggregations in the southeast Bering Sea, *Mar. Ecol. Prog. Ser.*, 10(1), pp. 101–103.
- Schneider D., Harrison N.M., Hunt G.L., Jr. 1987.** Variation in the occurrence of marine birds at fronts in the Bering Sea, *Estuarine, Coastal and Shelf Science*, 25(1), pp. 135–141.
- Schumacher J.D., Kinder T.H., Pashinski D.J., Charnell R.L. 1979.** A structural front over the continental shelf of the eastern Bering Sea, *J. Phys. Oceanogr.*, 9(1), pp. 79–87.
- Schumacher J.D., Reed R.K. 1980.** Coastal flow in the northwest Gulf of Alaska: the Kenai Current, *J. Geophys. Res.*, 85(C11), pp. 6680–6688.
- Schumacher J.D., Kendall A.W., Jr. 1991.** Some interactions between young walleye pollock and their environment in the western Gulf of Alaska, *CalCOFI Rep.*, 32, pp. 22–40.
- Schumacher J.D., Kendall A.W., Jr. 1995.** An example of fisheries oceanography: Walleye pollock in Alaskan waters, *Rev. Geophys.*, 33(suppl.), pp. 1153–1163.
- Schumacher J.D., Stabeno P.J. 1998.** Continental shelf of the Bering Sea, in: *The Sea*, vol. 11, edited by A.R. Robinson and K.H. Brink, pp. 789–822, John Wiley and Sons, New York.
- Senjyu T. 1999.** The Japan Sea intermediate water: Its characteristics and circulation, *J. Oceanography*, 55(2), pp. 111–122.
- Seung Y.-H., Yoon J.-H. 1995.** Some features of winter convection in the Japan Sea, *J. Oceanography*, 51(1), pp. 61–73.
- Springer A.M., McRoy C.P., Flint M.V. 1996.** The Bering Sea Green Belt: shelf-edge processes and ecosystem production, *Fish. Oceanogr.*, 5(3/4), pp. 205–223.
- Stabeno P.J., Reed R.K., Schumacher J.D. 1995.** The Alaska Coastal Current: Continuity of transport and forcing, *J. Geophys. Res.*, 100(C2), pp. 2477–2485.
- Stabeno P.J., Hermann A.J. 1996.** An eddy resolving model of circulation on the western Gulf of Alaska shelf: 2. Comparison of results to oceanographic observations, *J. Geophys. Res.*, 101(C1), pp. 1151–1161.
- Stanton B.R. 1981.** An oceanographic survey of the Tasman Front, *N. Z. J. Mar. Freshwat. Res.*, 15(3), pp. 289–297.
- Stanton B.R., Ridgway N.M. 1988.** An oceanographic survey of the Subtropical Convergence zone in the Tasman Sea, *N.Z. J. Mar. Freshwat. Res.*, 22(4), pp. 583–593.
- Strub P.T., Kosro P.M., Huyer A., and CTZ collaborators 1991.** The nature of the cold filaments in the California Current System. *J. Geophys. Res.*, 96(C8), pp. 14743–14768.
- Strub P.T., James C. 1995.** The large-scale summer circulation of the California Current. *Geophys. Res. Lett.*, 22(3), pp. 207–210.
- Strub P.T., Mesias J.M., James C. 1995.** Altimeter observations of the Peru-Chile Countercurrent, *Geophys. Res. Lett.*, 22(3), pp. 211–214.
- Strub P.T., Mesias J.M., Montecino V., Rutllant J., Salinas S. 1998.** Coastal ocean circulation off western South America, in: *The Sea*, vol. 11, edited by Robinson A.R. and Brink K.H., pp. 273–313, John Wiley & Sons, Inc., New York.
- Stumpf H.G., Legeckis R.V. 1977.** Satellite observations of mesoscale dynamics in the Eastern Tropical Pacific Ocean. *J. Phys. Oceanogr.*, 7(5), pp. 648–658.
- Su J. 1998.** Circulation dynamics of the China Seas north of 18°N, in: *The Sea*, volume 11, edited by Robinson A.R. and Brink K.H., pp. 483–505, John Wiley & Sons, New York.
- Susanto R.D., Gordon A.L., Zheng Q. 2001.** Upwelling along the coasts of Java and Sumatra and its relation to ENSO, *Geophys. Res. Lett.*, 28(8), pp. 1599–1602.
- Szymanska K., Tomczak M. 1994.** Subduction of central water near the subtropical front in the southern Tasman Sea, *Deep-Sea Res.*, 41(9), pp. 1373–1386.
- Takematsu M., Ostrovskii A.G., Nagano Z. 1999.** Observations of eddies in the Japan Basin interior, *J. Oceanography*, 55(2), pp. 237–246.
- Tang D.-L., Ni I.-H. 1996.** Remote sensing of Hong Kong waters: spatial and temporal changes of sea surface temperature, *Acta Oceanogr. Taiw.*, 35(2), pp. 173–186.
- Tang D.-L., Ni I.-H., Kester D.R., Müller-Karger F.E. 1999.** Remote sensing observations of winter phytoplankton

- blooms southwest of the Luzon Strait in the South China Sea, *Mar. Ecol. Prog. Ser.*, 191, pp. 43–51.
- Thomson R.E., Emery W.J. 1986.** The Haida Current, *J. Geophys. Res.*, 91(C1), pp. 845–861.
- Thomson R.E., Gower J.F.R. 1998.** A basin-scale oceanic instability event in the Gulf of Alaska, *J. Geophys. Res.*, 103(C2), pp. 3033–3040.
- Tomczak M., Jr. 1981.** Coastal upwelling systems and eastern boundary currents: A review of terminology, *Geoforum*, 12(2), pp. 179–191.
- Tomczak M., Jr. 1985.** The Bass Strait water cascade during winter 1981, *Cont. Shelf Res.*, 4(3), pp. 255–278.
- Tomczak M., Jr. 1987.** The Bass Strait water cascade during summer 1981–1982, *Cont. Shelf Res.*, 7(6), pp. 561–572.
- Tseng C., Lin C., Chen S., Shyu C. 2000.** Temporal and spatial variations of sea surface temperature in the East China Sea, *Cont. Shelf Res.*, 20(4–5), pp. 373–387.
- Tsuchiya M., Talley L.D. 1998.** A Pacific hydrographic section at 88W: Water-property distribution, *J. Geophys. Res.*, 103(C6), pp. 12899–12918.
- Ullman D.S., Cornillon P.C. 1999.** Surface temperature fronts off the East Coast of North America from AVHRR imagery, *J. Geophys. Res.*, 104(C10), pp. 23459–23478.
- Ullman D.S., Cornillon P.C. 2000.** Evaluation of front detection methods for satellite-derived SST data using *in situ* observations, *J. Atmos. Oceanic Tech.*, 17(12), pp. 1667–1675.
- Ullman D.S., Cornillon P.C. 2001.** Continental shelf surface thermal fronts in winter off the northeast US coast, *Cont. Shelf Res.*, 21(11–12), pp. 1139–1156.
- Vazquez J., Perry K., Kilpatrick K. 1998.** NOAA/NASA AVHRR Oceans Pathfinder sea surface temperature data set user's reference manual, Version 4.0. JPL Technical Report, D-14070; URL: http://podaac.jpl.nasa.gov/pub/sea_surface_temperature/avhrr/pathfinder/doc/usr_gde4_0.html.
- Vidal J., Smith S.L. 1986.** Biomass, growth and development of populations of herbivorous zooplankton in the southeastern Bering Sea during spring, *Deep-Sea Res.*, 33(4), pp. 523–556.
- Walsh J.E., Dieterle D.A., Muller-Karger F.E., Aagaard K., Roach A.T., Whitledge T.E., Stockwell D. 1997.** CO₂ cycling in the coastal ocean. II. Seasonal organic loading of the Arctic Ocean from source waters in the Bering Sea, *Cont. Shelf Res.*, 17(1), pp. 1–36.
- Wang L., Koblinsky C.J., Howden S. 2000.** Mesoscale variability in the South China Sea from the TOPEX/Poseidon altimetry data, *Deep-Sea Res. I*, 47(4), pp. 681–708.
- Wattayakorn G., King B., Wolanski E., Suthanaruk P. 1998.** Seasonal dispersion of petroleum contaminants in the Gulf of Thailand, *Cont. Shelf Res.*, 18(6), pp. 641–659.
- Webb D.J. 2000.** Evidence for shallow zonal jets in the South Equatorial Current region of the Southwest Pacific, *J. Phys. Oceanogr.*, 30(4), pp. 706–720.
- Wolanski E. 1994.** *Physical Oceanographic Processes of the Great Barrier Reef*, CRC Press, Boca Raton etc., 194 p.
- Wyllie-Echeverria T., Ohtani K. 1999.** Seasonal sea ice variability and the Bering Sea ecosystem, in: *Dynamics of the Bering Sea*, edited by T.R. Loughlin and K. Ohtani, pp. 435–451, University of Alaska Sea Grant, AK-SG-99-03, Fairbanks.
- Wyrtki K. 1960.** The surface circulation in the Coral and Tasman Seas, *CSIRO Div. Fish. Oceanog. Tech. Papers*, 8, pp. 1–44.
- Wyrtki K. 1964.** The thermal structure of the eastern Pacific Ocean, *Deut. Hydrogr. Z., Ergänzungsheft Reihe A (8°)*, No. 6, 84 p.
- Wyrtki K. 1977.** Advection in the Peru Current as observed by satellite, *J. Geophys. Res.*, 82(27), pp. 3939–3043.
- Yanagi T., Takao T. 1998.** Seasonal variation of three-dimensional circulations in the Gulf of Thailand, *La Mer*, 36(2), pp. 43–55.
- Yanagi T., Sachoemar S.I., Takao T., Fujiwara S. 2001.** Seasonal variation of stratification in the Gulf of Thailand, *J. Oceanogr.*, 57(4), pp. 461–470.
- Yuan X., Talley L.D. 1996.** The subarctic frontal zone in the North Pacific: Characteristics of frontal structure from climatological data and synoptic surveys, *J. Geophys. Res.*, 101(C7), pp. 16491–16508.
- Zuenko Yu.I. 1996.** Seasonal shift of Polar Front in the western part of the Japan Sea and its year-to-year variations, in: *Proceeding of CREAMS'96 Workshop*, 12–13 February 1996, Vladivostok, pp. 89–93, Far-Eastern Regional Hydrometeorological Research Institute, Vladivostok, and Research Institute of Oceanography, Seoul National University.
- Zuenko Yu.I. 1999.** Two decades of Polar Front large-scale meandering in the north-western Japan Sea, in: *Proceedings of the CREAMS'99 International Symposium*, 26–28 January 1999, Fukuoka, Japan, pp. 11–14, CREAMS Secretariat, Kyushu University.

HEAT EXCHANGE BETWEEN THE NORTHERN PACIFIC AND THE ATMOSPHERE

A.D. Nelezin^{1,2}, A.N. Man'ko^{1,2}, V.A. Petrova²

¹ Far Eastern Regional Hydrometeorological Research Institute (FERHRI), Russia
Email: hydromet@online.ru

² V.I. Il'ichev Pacific Oceanological Institute, Far Eastern Branch of Russian Academy of Sciences, (POI FEBRAS), Russia

The components of the surface heat budget are calculated by the data of the on-way observations in the Northern Pacific and using the Methodical Instructions and Recommendations of the Main Hydrometeorological Observatory. Long-time average structure of the surface heat budget, radiation balance, turbulent heat exchange and latent heat are analyzed. Zoning of the Northern Pacific is carried out and the annual motion of the components is studied. The periods of the heat accumulation and heat transfer by the ocean surface are determined.

INTRODUCTION

Investigation of the physical mechanisms for the formation of the anomalies of the thermal state of waters in the active layer of the ocean on the time scale from a month to several years is one of the main problems in studying the hydrometeorological regime of the ocean. Variations of the water heat state are most evident in the energy-active zones of the ocean, which are formed at the participation of the inter-water heat exchange and the external heat balance on the ocean-atmosphere boundary. The main part of two media interaction is the heat one, as it follows from estimating the global energy potentials of the Earth's climatic system (Lappo *et al.*, 1990). Two components of the heat flow between the ocean and atmosphere are distinguished: a climatic flow related to the heat contrast of two media, which is averaged for a year, and a seasonal one that is conditioned by the phase differences of the heat variations in these media.

The Earth's climate changes are related to a number of the most important unsolved problems of the fundamental scientific and great practical meaning. A sign of the global changes in the climate system is the observed non-stability of its thermodynamic regime. The main features predetermining this regime are the turbulent heat fluxes from the ocean, cloudiness, and the heat content of the upper layer of the ocean (Byshev *et al.*, 2001). Diagnostic studies in the North Western Pacific show that the area of the Subarctic Front is characterized by the intensive heat exchange with the atmosphere in the autumn–winter period (Rassadnikov *et al.*, 1986). Variations of the heat state of waters in the NW Pacific are determined both by conditions of the local interaction with the atmosphere, and by the large-scale processes. These circumstances provide an opportunity to study the mechanisms of the oceanic signals formation, and their influence on the climatic system. Spatial-temporal variability of the fields of turbulent flows of heat and heat budget of the ocean surface is an important aspect in the problem of the ocean and

atmosphere interaction. The heat fluxes on the ocean-atmosphere boundary predetermine the temperature changes at various time scales in the active layer of the ocean. The sensible and latent heat fluxes are the main source of the atmosphere heat energy. At the expense of great heat storage of waters the ocean is able to maintain continuously the energy supply of the atmosphere on a local and regional scale. Muzychenko (1987) studied the heat exchange of the Northern Pacific with the atmosphere in the points of the 5° squares from 20° to 55°N by the data for the period of 1948–1978. He calculated the mean monthly and average annual values of the heat budget on the ocean surface and its components, but for the calculations he used the data obtained from different sources. The studies performed in the NW Pacific before ascertained that the temporal variations of the net sea surface heat flux played a great part in the changes of the heat content in the upper layer (Aquad, 1998; Nelezin *et al.*, 1986; Pyatin, 1987).

For the last years, the ocean-atmosphere heat exchange processes have been studied in the bounds of investigating the heat budget in the active layer or the upper quasi-homogeneous layer (Aquad *et al.*, 1998; Qiu, 2002; Cayan, 1992; Hanawa *et al.*, 1995; Huang, 2001). The authors consider the heat fluxes through the sea surface, heat content of the waters, the net sea surface heat flux and their variability, as well as the anomalies of the ocean surface temperature, peculiarities of the large-scale circulation of the ocean and atmosphere. It is determined that in the central part of the Pacific Ocean the heat budget is conditioned by the heat exchange through the surface and the vertical transport of heat in the upper layer of the ocean.

The objective of the given paper is investigating the long-time average spatial structure and the annual variability of the components of the resulting heat exchange between the sea surface of the Northern Pacific and the atmosphere.

Table 1

Number of observation data by months (thousand)

Month	1	2	3	4	5	6	7	8	9	10	11	12
Number	104.5	98.7	113.4	118.6	115.8	113.8	115.4	105.8	105.6	114.0	112.3	110.8

DATA AND METHOD

Investigation of the heat exchange between the Northern Pacific and the atmosphere has been carried out on the basis of calculating the quantitative characteristics of the net sea surface heat flux and its components:

$$B = R \pm H \pm LE,$$

where:

B – is a net sea surface heat flux;

R – is a radiation balance;

H – is a sensible heat flux;

LE – is a latent heat flux.

The net sea surface heat flux components were calculated according to the Methodical Instructions and Recommendations of the Main Hydrometeorological Observatory (Methodical Instructions, 1981; Recommendations for calculating..., 1982). Information support of the studies is based on the available data on the ocean surface and the state of the near-water layer of the atmosphere. Reconstruction of the spatial distribution of the net sea surface heat flux components was carried out on the basis of the earlier developed calculation scheme (Pyatin *et al.*, 1986). Software for calculating the net sea surface heat flux components is based on the widely applied method, which is a quite reliable diagnostic system. Spatial data were averaged within the radius of a circle around a point of the given grid using the linear weight function. A grid area with the mesh width of $2 \times 2^\circ$ was distinguished on the basis of previous estimations on the scale of the spatial variability of the net sea surface heat flux components, the influence of the atmospheric synoptic processes on the formation of heat exchange, and the limited volume of the available information. As the data volume for calculating the mean monthly value of the net sea surface heat flux is minimum, 30 measurements are accepted in each point of the regular grid. At their less number, the circle radius around a point of the grid is automatically increased. In the grid nodes, simultaneously, the temporal averaging of characteristics was carried out, as for each of them an average of all values for the month was calculated. Radiation balance was calculated by the measurement data averaged for a month interval, and the sensible and latent heat fluxes – by the hour observations at their subsequent averaging. Such approach to determining the mean monthly values of the latent heat allows applying correctly the coefficients of the turbulent exchange for the instant values of the latent heat flux and keeps from the necessity to introduce the

corrections for the storm conditions, which make a significant input (up to 30%) into the mean monthly heat exchange of the ocean and atmosphere. The examination of the latent heat calculations, while comparing them with the results obtained in the fixed points of the water area, has shown that the error in determining the latent heat fluxes in the cold period of a year makes about 15%. Preliminary data averaging at calculating the radiation balance allows to a significant degree smoothing its large intra-diurnal variations. Then, the calculated mean monthly values of the net sea surface heat flux components were averaged for determining their long-time average values for each month of a year and the long-time mean annual values.

To calculate the components of the heat exchange between the Northern Pacific and the atmosphere we used data of the ship observations from 1982 to 1997 obtained by the communication channels, the total amount of observations being about 1330 thousand. The data on the number of measurements for each month of the mentioned years are given in Table 1.

The Table shows that the data are relatively regularly distributed during a year: their minimum quantity 98.7 thousand – is for February, and the maximum one – 118.6 thousand is obtained in April. Spatial data distribution for each month of the given years is characterized by the relative irregularity, the data are better provided for the vessel route areas. For calculations of the long-term average values of the net sea surface heat flux components the quantity of the data in the squares makes about a thousand.

RESULTS

A long-term average structure of the spatial distribution of the sea surface heat budget components in the Northern Pacific, as well as the annual variability of the resulting heat exchange and its components on the time scale of the monthly averaging are analyzed by results of calculations. The energy activity of the upper layer in the Northern Pacific is the most vivid in the mean annual field of the resulting heat exchange at the boundary of two media division as an area of the negative values of net sea surface heat flux (Figure 1). Maximum values of the heat loss in average for a year (-100 W/m^2 and more) are observed in a narrow zone ($32\text{--}35^\circ\text{N}$) located in the area of $135\text{--}155^\circ\text{E}$.

Spatial distribution of the radiation balance (Figure 2) in the Northern Pacific (to the north of 25°N) in average for a year varies from 60 W/m^2 along the Aleutian Islands and in the Bay of Alaska up to

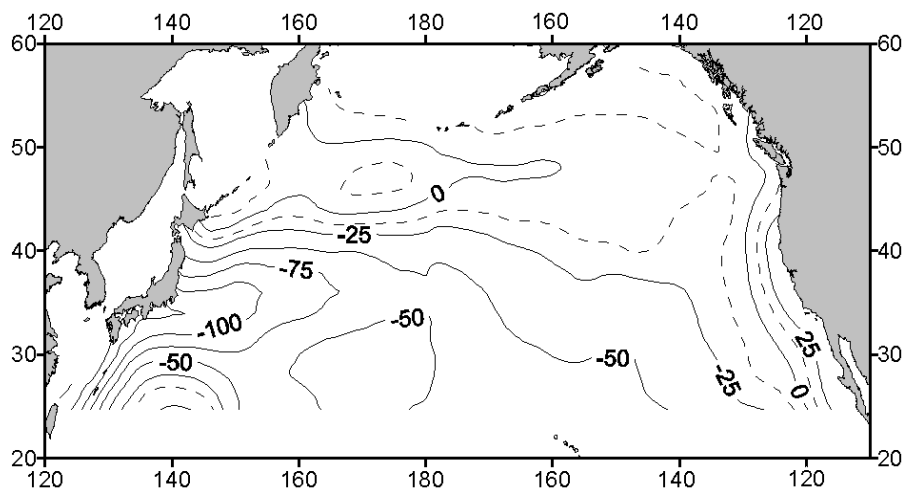


Figure 1. Mean annual net sea surface heat flux (W/m^2)

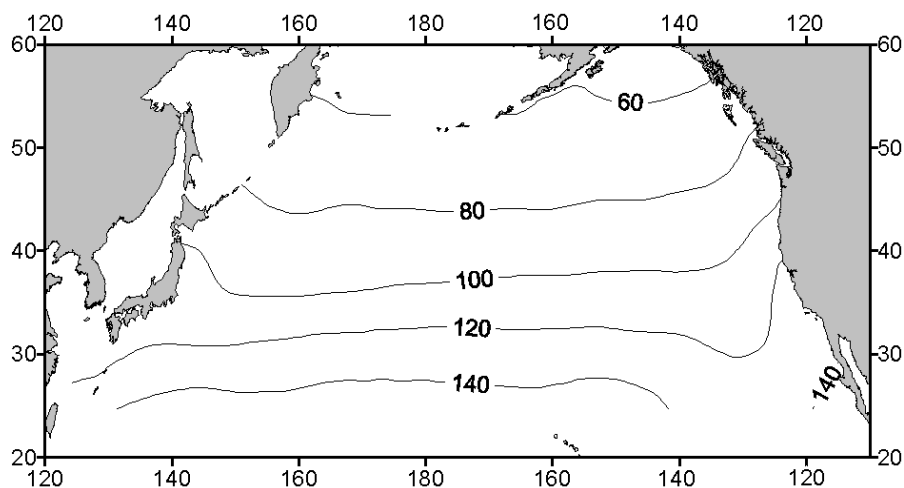


Figure 2. Mean annual radiation balance (W/m^2)

140 W/m^2 in the south of the studied area. This distribution is generally zonal, and it is mainly determined by the structure of the radiation balance in summer. Distribution of the mean monthly and mean annual values of the radiation balance is characterized mainly by a zonal character, near the coast it is violated by the cloudiness, flows of the sensible and latent heat, and makes the conditions for the spatially differentiated energy supply of the atmosphere (Lappo *et al.*, 1990). In the Northern Pacific the radiation balance during a whole year is positive. A characteristic feature of the annual distribution of the radiation balance is diverse variability during various seasons: minimum variability is determined for the summer months (Strokina, 1989).

In the area located to the east of the Japan Islands loss of heat by the ocean at the expense of the turbulent heat exchange is ascertained to be maximum (-40 W/m^2) (Figure 3). In its spatial distribution the influence of the warm Kuroshio Current is seen. We should note the increase of the sensible heat flow through the ocean surface from the North America to the southern termination of the Kamchatka Peninsula (up to

-20 W/m^2). To the north of the Peninsula of California the value of the sensible heat flow is positive and does not exceed 5 W/m^2 . Structure of fields and values of the mean annual flows of the sensible and latent heat are determined mainly by its distribution in the autumn–winter periods. Values of the latent heat flow, as well as the radiation balance, decrease from south to north (from -200 to -60 W/m^2). Maximum values of latent heat (-260 W/m^2) are found in the area of Ryukyu Islands (Figure 4). At small exception, turbulent flows of heat in average for a year are directed from the ocean surface to the atmosphere. Turbulent flows of heat directed from the atmosphere to the ocean may be observed in a zone of cold currents in the Northern Pacific within the California Current zone (Cayan, 1992; Strokina, 1989).

As a result of the performed calculations, the maps of the long-term average values of the total heat budget are done for the surface of the Northern Pacific for each month of a year, which are given in papers (Man'ko and Nelezin, 2002). Earlier the results of calculations were presented (Pokudov *et al.*, 1980) by the data of observations in February and August, as it

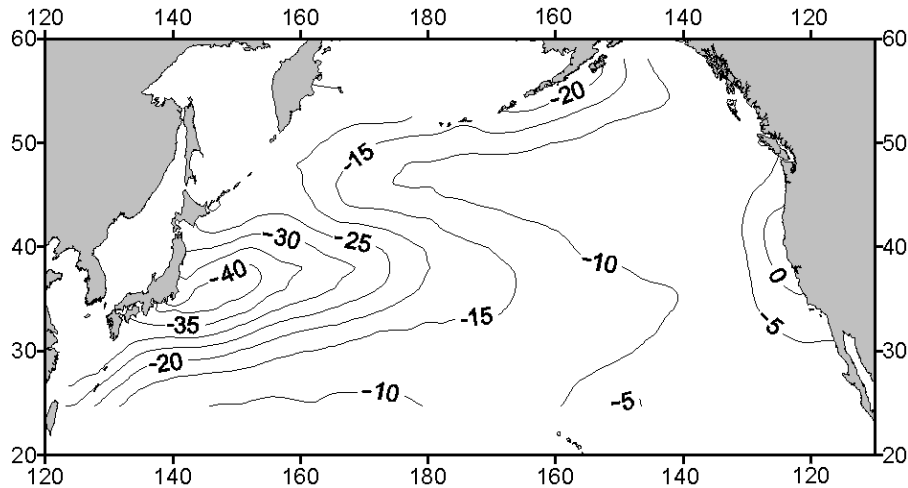


Figure 3. Mean annual sensible heat flux (W/m^2)

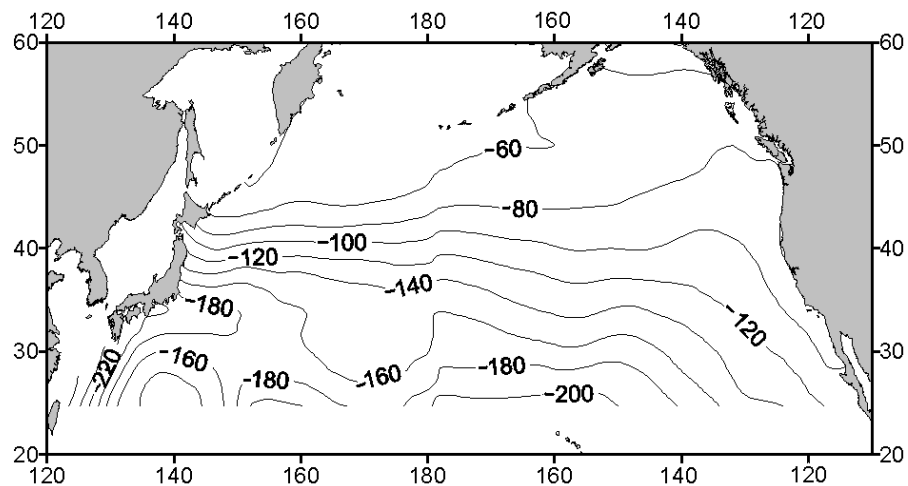


Figure 4. Mean annual latent heat flux (W/m^2)

was accepted – central months of the cold and warm periods. By our calculations heat exchange through the surface of the Northern Pacific in February is characterized by the ocean heat loss, except for a narrow area of the ocean adjacent to the coast of California. The largest values of the heat transfer (more than -300 W/m^2) are obtained for the Kuroshio zone. In March the intensity of heat transfer in the North Western Pacific decreases to -150 W/m^2 . Due to the radiation warm up in April in all places the heat inflow to the surface takes place, which maximum values (100 W/m^2) are formed in the area of the Kuril Islands. In May the isolines acquire mainly a latitudinal direction, except for a narrow zone near the coast of the North America. In June the maximum values of the resulting heat exchange (more than 100 W/m^2) occupy the largest area that is somewhat decreasing in July. In August the largest values of the heat inflow to the surface (more than 100 W/m^2) are observed in the northwestern part of the ocean. In September in the western and central areas of the Northern Pacific a resulting heat exchange is changing a sign in a latitudinal band of $30\text{--}40^\circ\text{N}$. In October the heat transfer is observed within the whole water area

of the Northern Pacific, the maximum values (up to -200 W/m^2) being observed near the coast of the Islands of Japan. Heat exchange through the surface of the predominant part of the Northern Pacific is characterized by the considerable ocean heat loss from November to January. The most intensive heat transfer occurs in December to the east of 180° and to the west of 180° – in January, but these differences are insignificant.

Analysis of maps of the resulting heat exchange done for each month of a year has shown that February and August are not the central months that characterize the maximum heat accumulation and the largest heat transfer from the surface of the Northern Pacific. Extreme values of the resulting heat exchange are typical for December–January and June–July.

Zoning of the Northern Pacific was carried out on the basis of the long-term mean annual map of the net sea surface heat flux and taking account of the continuation of heat accumulation periods and the time of its extreme values (Figure 5). Four areas were distinguished: to the west of 180° – the northern (IN) and southern (IS) areas; to the east of 180° – the

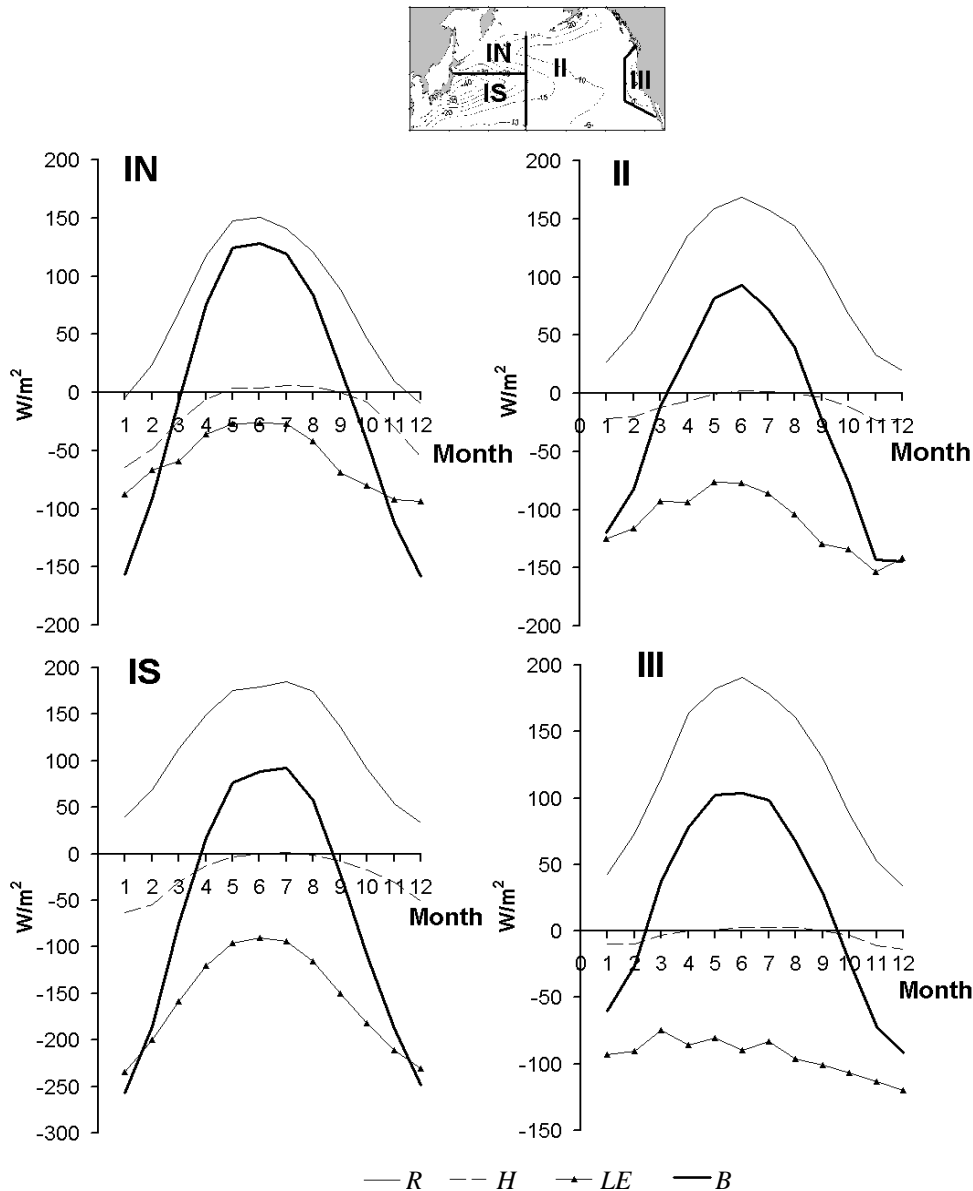


Figure 5. Annual motion of the sea surface heat fluxes averaged for the distinguished areas

eastern area (II), and the Californian one (III). The boundary between the northern and southern areas was determined by the long-term mean annual distribution of the resulting heat exchange ($45^{\circ}N$). The Californian area is stretching along the western coast of the North America from 26° to $50^{\circ}N$.

In the IN area the heat accumulation period lasts for six months (from April to September) with the maximum in June ($130 W/m^2$). The period of the heat loss lasts from October to March, the maximum heat loss being revealed in December ($-143 W/m^2$). Extreme values of the radiation balance and latent heat flow are determined in June and December, and the values of the sensible heat flow – in July and January. From November to February the net sea surface heat flux is mainly predetermined by the latent and sensible heat fluxes, and from April to October it is mainly conditioned by the radiation balance.

In the IS area the heat accumulation period lasts for five months from April to August, the heat accumulation maximum being observed in July ($97 W/m^2$). The heat loss period makes seven months – from September to March, the maximum heat transfer occurs in January ($-244 W/m^2$). The extreme values of the radiation balance are ascertained in July and December, and those of the sensible and latent heat fluxes – in June–July and January. In this area for a year the ocean surface provides $-642 W/m^2$. In December and January the net sea surface heat flux is predetermined by the flows of the sensible and latent heat, and from March to October it is conditioned mainly by the radiation balance and latent heat.

In area II (as well as in the IS area) the heat accumulation period makes 5 months – from April till August, when the ocean surface gets $323 W/m^2$. The sea surface provides the heat to the atmosphere during

7 months – from September to March (-601 W/m^2), the heat transfer maximum (-144 W/m^2) is observed in December. Maximum heat gain by the sea surface due to the radiation balance (168 W/m^2) takes place in June.

The period of heat accumulation in the III (Californian) area lasts for seven months, from March to September, when the heat accumulation at the expense of the radiation balance exceeds the latent heat flux. Maximum radiation inflow of heat (191 W/m^2) is observed in June, when the largest heat accumulation takes place (104 W/m^2). The ocean surface losses the maximum of heat in December due to the latent heat (-112 W/m^2) and sensible (-14 W/m^2) heat fluxes.

Thus, the performed calculations allow estimating the components input to the net sea surface heat flux of the Northern Pacific and studying their seasonal variability. The ocean role in the studied area is determined by the heat transport of the Kuroshio Current system and the active heat transfer to the atmosphere in a cold period of time. On the other part,

the large-scale influence of the atmosphere is significantly conditioning the heat regime of the ocean waters.

CONCLUSION

As a result of the performed calculations and analysis of the net sea surface heat flux components, zoning of the Northern Pacific water area, new quantitative characteristics of their annual variability are obtained. Maximum annual variability of the radiation balance and turbulent heat exchange are found in the IN area, and the latent heat – in the IS area. In the IS area the variability of the resulting heat exchange is conditioned by the radiation balance and latent heat. Sensible heat exchange is the most manifested in the net sea surface heat flux variability in the IN area, and in the III area the net sea surface heat flux variability is conditioned mainly by the radiation balance. As a whole, by our data, the Northern Pacific surface, provides the heat to the atmosphere in average for a year. These losses are evidently compensated by the intra-water advective-turbulent heat exchange.

REFERENCES

- Auad G.**, Miller A.J., White W.B. **1998**. Simulation of heat storages and associated heat budgets in the Pacific Ocean. 1. El Nino southern oscillation timescale. 2. Interdecadal timescale. *J. Geophys. Res.*, v. 103, C12, pp. 27603–27635.
- Byshev V.I.**, Neiman V.G., Pozdnyakova T.G., Romanov Yu.A. **2001**. New data on the thermodynamic regime of the climate system in the northern hemisphere. Report of Academy of Sciences, v. 381, 4, pp. 539–544. (In Russian).
- Cayan D.R.** **1992**. Latent and sensible heat flux anomalies over the northern ocean. Driving the surface temperature. *J. Phys. Oceanogr.*, v. 22, 8, pp. 859–881.
- Hanawa et al.** **1995**. Statistic relationship between anomalies SST and air-sea heat fluxes in the north Pacific. *J. Meteorol. Soc. Jap.*, v. 73, 3, pp. 757–763.
- Huang B.Y.** **2001**. Temperature trend of the last 40 years in the upper Pacific Ocean. *J. Climate*, v. 14, 17, pp. 3738–3750.
- Lappo S.S.**, Gulev S.K., Rozhdestvenskii A.E. **1990**. Large-scale heat interaction in the ocean-atmosphere system and the energy-active areas of the ocean. Leningrad, Gidrometeoizdat, 336 p. (In Russian).
- Man'ko A.N.**, Nelezin A.D. **2002**. Annual variability of the heat budget of the North Pacific surface. *Trudy FERHRI*. Issue 150, pp. 48–58. (In Russian).
- Methodical Instructions**. Calculation of turbulent fluxes of heat, moisture, and the volume of motion over the sea. **1981**. Leningrad, Gidrometeoizdat, 56 p. (In Russian).
- Muzychenko A.G.** **1987**. Heat exchange between the ocean and atmosphere in the North Pacific. *Itogi Nauki I Tekhniki*. **Atmosphere, ocean, space**. Program “Razrezy”. Moscow, v.8, pp. 319–326. (In Russian).
- Pokudov V.V.**, Tunegolovets V.P., Vel'yaots K.O., Kondrat'eva N.F. **1980**. Heat regime of the surface waters in the Subarctic zone of the Pacific Ocean. *Trudy FERHRI*, Issue 90, 165 p. (In Russian).
- Pyatin O.G.** **1987**. Formation of the mean monthly fields of the heat budget of the ocean surface in the Kuroshio energy-active zone, and their variability in 1981–1985. *Itogi Nauki I Tekhniki*. **Atmosphere, ocean, space**. Program “Razrezy”, Moscow, v. 8, pp. 278–288. (In Russian).
- Pyatin O.G.**, Rassadnikov Yu.A., Nelezin A.D., Vanin N.S. **1986**. Informational provision of studies in the Kuroshio energy-active zone. *Meteorologiya I gidrologiya*. N 9, pp. 72–78. (In Russian).
- Qiu B.** **2002**. The Kuroshio Extension system: its large scale variation and role in the midlatitude ocean-atmosphere interaction. *J. of Oceanogr.*, v. 58, pp. 57–75.
- Rassadnikov Yu.A.**, Nelezin A.D., Pyatin O.G. **1986**. Heat balance of the ocean surface in a zone of the energy-active study area of Kuroshio. *Trudy FERHRI*, Issue 106, pp. 83–96. (In Russian).
- Recommendations on calculating** the components of the radiation balance on the ocean surface. **1982**, Leningrad, Gidrometeoizdat. 92 p. (In Russian).
- Strokina L.A.** **1989**. Heat balance of the ocean surface. Reference book. Leningrad, Gidrometeoizdat. 448 p. (In Russian).

ON SOME FEATURES OF THE WATER CIRCULATION IN THE NW PACIFIC UNDER DIFFERENT SYNOPTIC CONDITIONS

G.A. Vlasova, S.S. Sugak

V.I. Il'ichev Pacific Oceanological Institute, Far Eastern Branch of Russian Academy of Sciences
(POI FEBRAS), Russia
Email: sugak@poi.dvo.ru

The North Western Pacific is characterized by the extremely complex hydrological conditions: the presence of two largest water structures and two major water mass gyres, the transformed waters of the Far Eastern Seas, *etc.* All these conditions make the given region to be a powerful zone of the Pacific Ocean, and a unique natural base for investigating a complex of hydrophysical and meteorological processes, which understanding is necessary for the solution of many fundamental and applied problems in oceanography.

In the given paper the integral functions of the flow from the surface to the bottom are calculated for the NW Pacific (20–50°N, 146–180°E) to estimate the water circulation basing on a hydrodynamic model and taking into account the influence of various types of the atmospheric circulation: “north-western”, “okhotsk-aleutian” and “cyclones over the ocean”. The given model considers a real spatial distribution of the water density, interaction with the atmosphere, variable coefficients of the vertical and horizontal turbulent exchange, β -effect, bottom topography and the coast outline.

As a result the hydrodynamic structures are distinguished for the water area being studied, both non-depending and depending on the type of the atmospheric circulation. The non-depending structures are found in three areas of the evident anticyclonic activity, and in two ones – of the cyclonic activity. Hydrodynamic structures depending on the atmospheric circulation types have their peculiarities in the spatial-temporal distribution. So, in conditions of the “okhotsk-aleutian” type of the atmospheric circulation the anticyclonic motion of waters prevails. Under the influence of the atmospheric circulation “cyclones over the ocean” the cyclonic motion of the water masses prevails.

INTRODUCTION

The North Western Pacific is characterized by the extremely complex hydrological conditions:

- Presence of two major water mass gyres: a cyclonic subpolar one and an anticyclonic subtropical one.
- Occurrence of two largest water structures: a subarctic and a subtropical ones separated by a zone of the subarctic front.
- Powerful marginal Kuroshio Current.
- Influence of the transformed waters of the Far Eastern Seas through the straits of the island arcs.

All these factors make the given region to be a unique natural area for investigating a complex of hydrodynamic processes, which understanding is necessary to solve many fundamental and applied problems in oceanography.

In the studied region a great number of hydrodynamic studies has been carried out, mainly, in the areas of the largest currents, among which the Kuroshio is specially distinguished (Kawabe, 1995; Kuroshio, 1972; Nelepo *et al.*, 1984; Nelezin and Man'ko, 1999; Novozhilov, 1978; Pokudov and Vel'yaots, 1974; Subarctic Front..., 1972; and others). Internal dynamics of the studied currents is very complicated, as in their bounds numerous dynamic structures of various spatial-temporal scales are formed.

While estimating the currents structure and their spatial-temporal variability at the end of XX century, the investigators generally were attracted by the

methods of numerical modeling of the currents. Fundamentals of such modeling were initiated in the papers by Shtockman, Sarkisyan, Bryen, Marchuk, Kamenkovich, Lineikin, Kochergin, Kuzin, Fel'zenbaum, Kozlov, *etc.* Still, for many practical applications in solving such difficult problems, it is necessary to have complex models allowing to involve a wide circle of hydrometeorological characteristics. At present time such models are not available. There are some models that at least partially help the investigators to fill in the given gap by different approaches, such as the models by Sarkisyan, Shapiro, Vasiliev, and others.

The objective of the given paper is investigation of seasonal changes of the currents system in the studied water area. A proposed approach consists in numerical modeling of the waters circulation under the influence of various types of atmospheric circulation (Polyakova, 1999). To solve the given problem a hydrodynamic model was used (Fel'zenbaum, 1968; Polyakova, 2002), in the bounds of which the integral flow functions were calculated. A study area is bounded by 20–50°N, 146–180°E.

METHOD

The given quasi-stationary baroclinic model (Fel'zenbaum, 1968; Polyakova, 2002) based on solving complete non-linear equations of the ocean hydrothermodynamics and turbulent diffusion of the conservatives admixtures is related to a class of modern multi-layer models. It presupposes a

principle of self-similarity of the second order (a similarity of the vertical distribution) and considers a real spatial distribution of the water density, interaction with the atmosphere, β -effect, water exchange through the straits, bottom topography, and the coast outline. A peculiar feature of the given model is that it uses some class of functions allowing to separate the variables by spatial coordinates and to pass to the dependence on the function of self-similarity. To determine these functions the problem of calculating the spatial-temporal distribution of the sea system parameters is solved. In oceanography we know the functions possessing the natural self-similarity, *i.e.* the similarity of the vertical distribution. First of all, it is temperature and density of the water. The density can be described by the model determined by the data of *in situ* observations carried out in the ocean at some characteristic station. In this case, while using the models of temperature and density, the problem of determining the main physical fields in the four-dimensional space is reduced to solving a plain system of equations. The given problem is solved by a method of minimum errors of Academician Marchuk, which is applied for each equation in the general iteration process. As a result of solving this problem, at each step of iteration, by the explicit ratios obtained as a result of integrating the initial equations by the vertical coordinate, we calculate the components of the current velocity, the sea level, temperature distribution, the depth of the homogeneous layer, and the sea water density. Salinity distribution is calculated from the state equation.

To estimate its adequacy, the given model has been used in various areas of the World Ocean. In a majority of cases, it is describing the physical processes known from observations. That has given us an opportunity to pass to a wider analysis of hydrodynamic characteristics.

INITIAL DATA

The input information to calculate the integral waters circulation are:

- Average monthly fields of the atmospheric pressure for the period of 1949–2000 (average monthly near-land synoptic maps of the Northern Pacific compiled at the Weather Forecast Bureau of Primorsky Hydromet office), corresponding to certain types of the atmospheric processes.
- The GDEM archive (Generalized Digital Environmental Model) – a global massive of the monthly averaged climatic data on the surface temperature and salinity in the points of a regular grid $1 \times 1^\circ$.
- A bank of the research cruise data “Ocean-2” of the POI FEBRAS for the period of 1970–1990 (temperature and salinity), that served the basis for calculating the real vertical density distribution.

The depth values were taken from the navigational chart (1:5,000,000). To conduct calculations a regular grid $1 \times 1^\circ$ was used. To form the given grid, all input information was processed with the help of the interpolation method in the mode of Surfer (Kriging).

ANALYSIS

By results of calculations, the maps of the integral waters circulation were built for the following types of atmospheric circulation: the “north-western”, the “okhotsk-aleutian”, and “cyclones over the ocean”, that are mostly active over the studied water area (Polyakova, 1999).

The “north-western” type of the atmospheric circulation is distinguished according to the following features: the main trajectories of cyclones are located in the north-western part of the Pacific Ocean, cyclones move to the north-east from the Japan Islands towards the Aleutian Island Arc. Periodicity of single cyclones or their series moving at different depth or intensity makes 1–3 days and occurs during the whole year. The given type is characterized by the distinctly expressed seasonal motion: in winter and autumn its intensity is maximum, in spring and especially in summer – it is weak (Figure 1a).

The “okhotsk-aleutian” type is distinguished as a system of two baric depressions: the Okhotsk Depression and the Aleutian one. The Okhotsk Depression is a system of cyclones rotating around some quasi-stationary center over the Okhotsk Sea water area. The Aleutian Depression is located above the water area of the Alaska Bay, the trajectories of some particular cyclones of this depression are characterized by complexity and variability in time, they often acquire a helicoids form. In its intensity, the Aleutian Depression yields to the Okhotsk Depression. For the given type of the atmospheric circulation a seasonal motion is also typical: its maximum activity is observed in winter, the minimum one – in summer. In autumn and winter the given process is characterized by low activity (Figure 1b).

The type of the atmospheric circulation “cyclones over the ocean” is characterized by the predominance of low baric formations formed over the northern part of the Pacific Ocean. This type is notable for a complex set of trajectories of numerous cyclones, which cannot be classified and do not obey to any regularity in the spatial position. Here, several processes may develop simultaneously and their combination may be very diverse. Vortex diversity leads to the intensive mixing of the air masses till their quasi-homogenous composition (Figure 1c).

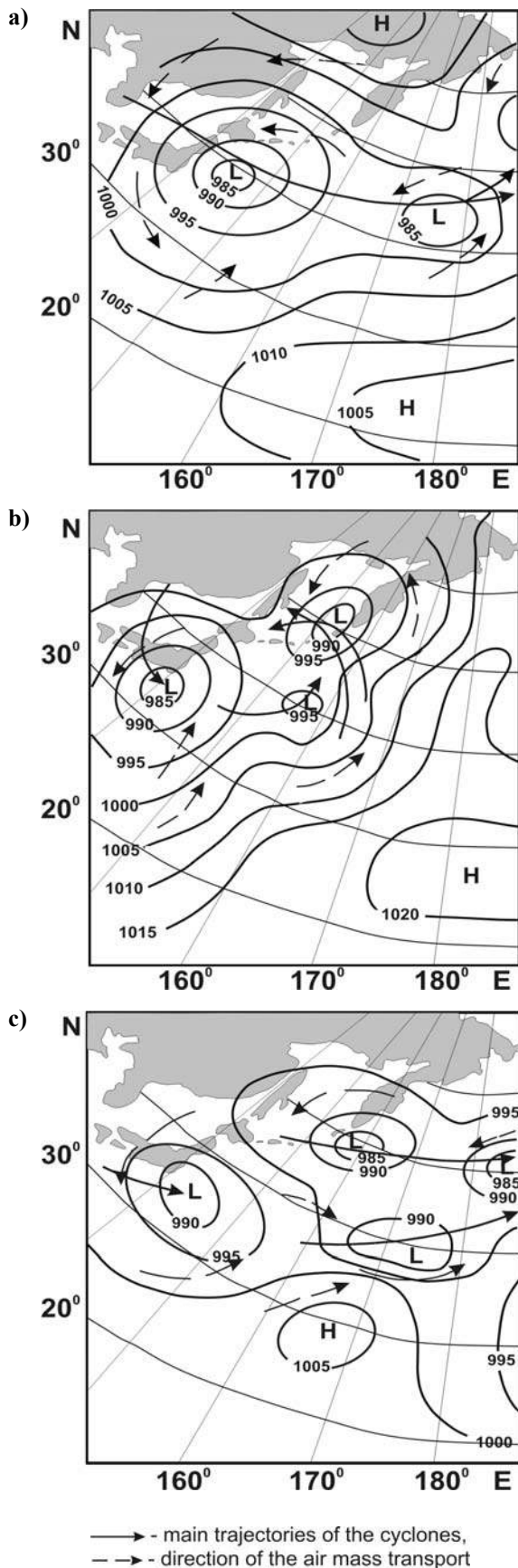


Figure 1. Types of the atmospheric circulation:
a – “north-western” type; b – “okhotsk-aleutian”
type; c – type of “cyclones over the ocean”

All calculations of the integral flow function were done taking into account the peculiarities of the atmospheric circulation types. Table 1 presents a scheme of calculations by the given types considering the time of their manifestation.

In accordance with the performed calculations for the water area being studied, the hydrodynamic structures are distinguished both non-depending and depending on the type of the atmospheric circulation.

The non-depending structures are found in three areas of the evident anticyclonic activity, and in two ones – of the cyclonic activity (Figures 2, 3).

An area, where the first anticyclonic vortex is found, is bounded by 36–42°N and 145–154°E. It coincides with the area distinguished before (Novozhilov, 1978; Pokudov and Vel’yaots, 1974; Subarctic Front..., 1972). It is located in a zone of the subarctic front in the bounds of the main meander of Kuroshio, which top is situated at 38°N, and its eastern boundary passes approximately along the meridian of 146°E. The second similar vortex is bounded by 27–33°N and 157–163°E, it is also located in the Kuroshio zone, in the area where the previous studies (Kuroshio, 1972) ascertained a similar hydrodynamic structure. The third anticyclonic vortex bounded by 40–42°N and 176–180°E, as it is evident, is situated beyond the limits of the Kuroshio and confined to the warm Northern-Pacific Current.

The first of the distinguished cyclonic vortices is located in the area of 33–36°N and 148–156°E. It turns out that it spatially coincides with the similar, earlier known, vortex, which center has the coordinates of 36°N, 143–154°E (Pokudov and Vel’yaots, 1974). The given structure was formed on the northern periphery of Kuroshio, where the cold waters of the subarctic origin prevail. The second cyclonic vortex is bounded by 22–27°N and 158–166°E and it also coincides with the similar, earlier distinguished, hydrodynamic structure (Kuroshio, 1972; Nelepo *et al.*, 1984). The last one is located in the area of the Kuroshio meander bend to the south of 30°N, in the area of 160°E.

To our opinion, the formation of hydrodynamic structures not depending on the atmospheric processes state is conditioned by the constant and intensive influence of the warm and cold water masses, which are generated by the stationary currents of the studied area.

So, the performed calculations allowed confirming the existence of a series of the earlier unknown cyclonic and anticyclonic vortices. On this basis, the peculiarities distinguished by us within the studied water area may be considered as the probably existing objects.

Hydrodynamic structures depending on the atmospheric circulation types have their peculiarities in the spatial-temporal distribution.

Table 1

Manifestation of different types of atmospheric circulation

Type of atmospheric circulation	Calculation period (months)											
	I	II	III	IV	V	VI	VII	VIII	IX	X	XI	XII
north-western	X	X	X	X	X	X	X	X	X	X	X	X
okhotsk-aleutian			X	X	X	X	X	X	X	X		
cyclones over the ocean	X	X								X	X	X

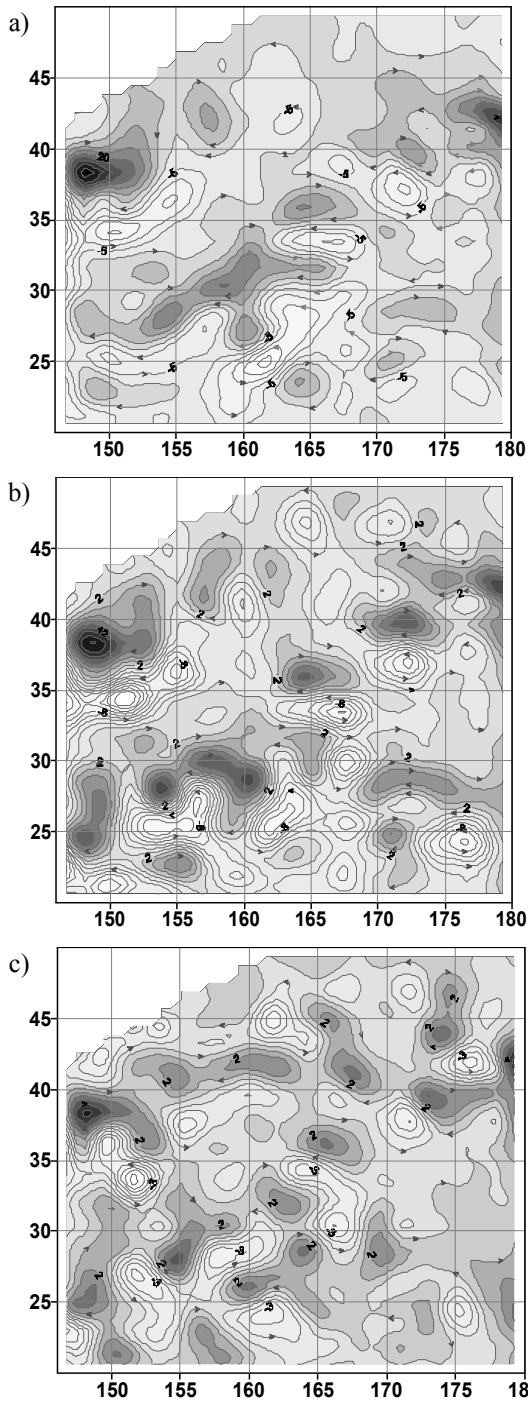


Figure 2. Integral function of the stream (Sv) for northwest Pacific. “North-western” type of atmospheric circulation in January (a), April (b) and July (c)

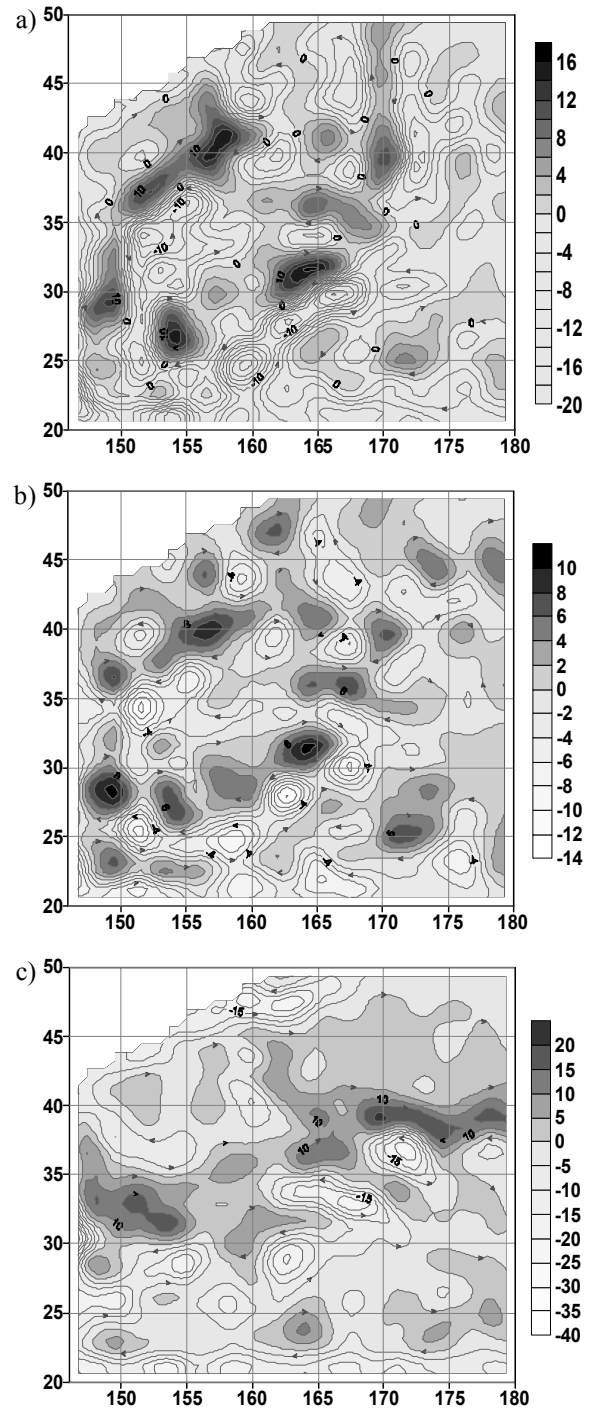


Figure 3. Integral function of the stream (Sv) for northwest Pacific. “Okhotsk-aleutian” type of the atmospheric circulation in March (a) and June (b) and “cyclones over the ocean” type in January (c)

Under the influence of the atmospheric circulation of the “north-western” type, a mosaic of the vortex formations of different scale and sign originates in the water environment. In autumn–winter period, practically the whole southern part and partially the western part of the studied area are covered by cyclonic vortex formations (Figure 2a). In spring, the cyclonic vortices are stretching as a local chain in the meridional direction approximately between 165–170°E (Figure 2b). In summer, on the background of the anticyclonic water motion the cyclonic vortices are distributed throughout the whole water area (Figure 2c).

In conditions of the “okhotsk-aleutian” type of the atmospheric circulation the general picture, as compared to the preceding type, is on the whole preserved, but the increase of the area of the anticyclonic water motion takes place. For instance, in spring, a chain of local cyclonic vortices, stretching meridionally higher than 30°N, is moving to 180°E while broadening the spatial distribution of the warm waters (Figure 3a). In summer, the number of anticyclonic vortices considerably increases (Figure 3b).

Under the influence of the atmospheric circulation “cyclones over the ocean” in winter, the cyclonic activity predominates. Still, on this background the warm Kuroshio Current and the Northern Pacific Current are distinctly traced (Figure 3c).

The comparison of the obtained data with the paper conclusions (Nelezin and Man'ko, 1999) shows that they are overestimated approximately 2 times.

Considering the available results of particular measurements of currents (the Data Base “Ocean-2” of the POI FEB RAS), the authors consider that the obtained results are similar to the real ones.

CONCLUSIONS

In the studied water area the quasi-stationary hydrodynamic structures are found, which do not depend on the character of the atmospheric circulation: three anticyclonic vortices and two cyclonic ones.

Dependence of hydrodynamic characteristics of the studied region on the type of the atmospheric baric formations originating over the ocean surface is revealed.

Under the influence of the atmospheric circulation of the “north-western” type in the water thickness a system of the vortex formation originates, which acquires either mainly cyclonic or anticyclonic character of the waters motion depending on the season.

In conditions of the “okhotsk-aleutian” type of the atmospheric circulation in the spring–summer period, the anticyclonic motion of waters prevails and the largest number of anticyclonic vortices of different scale occurs.

Under the influence of the atmospheric circulation “cyclones over the ocean” in winter, cyclonic motion of the water masses prevails.

REFERENCES

- Fel'zenbaum A.I. 1968.** Dynamics of the sea currents // “Hydrodynamics” Itogi Nauki. Series “Mechanics”. VINITI, Moscow, 1970. pp. 99–338. (In Russian).
- Kawabe M. 1995.** Variations of current path, velocity, and volume transport of the Kuroshio in relation with the large meander // *J. Phys. Oceanogr.* V.25. N 12. pp. 3103–3117.
- Kuroshio and the adjacent areas of the Pacific Ocean. 1972** // *Trudy Gos.okeanogr.in-ta.* Issue 106, 210 p. (In Russian).
- Nelepo B.A., Bulgakov N.P., Blatov A.S., Ivanov V.A., Kosarev A.N., Tuzhilkin V.S. 1984.** Classification and distribution of synoptic eddy formations in the World Ocean // preprint BYa N 09556, Marine Hydrophysical Institute of the Ukrainian AS, Sebastopol, 40 p. (In Russian).
- Nelezin A.D., Man'ko A.N. 1999.** Variability of a thermodynamic structure of waters in the NW Pacific // Vladivostok. DVGU Publishing House, 127 p. (In Russian).
- Novozhilov V.N. 1978.** Location and structure of the southern subarctic front of the NW Pacific in autumn of 1976 // Paper Collection “Gidrofizicheskiye issledovaniya v severo-zapadnoi chasti Tikhogo okeana”. Vladivostok, pp. 6–12. (In Russian).
- Pokudov V.V., Vel'yaots K.O. 1974.** Transport of waters and heat by the Kuroshio Current in winter period // *Trudy DVNIGMI.* Issue 45. pp. 87–96. (In Russian).
- Polyakova A.M. 1999.** Calendar of atmospheric circulation types with regard to non-stationarity over the Northern Pacific, and their brief characteristics // Vladivostok, DVGU, 116 p. (In Russian).
- Polyakova A.M., Vlasova G.A., Vasiliev A.S. 2002.** The Atmosphere effect on the underlying surface and hydrodynamic processes of the Bering Sea // Vladivostok. Dal'nauka. 203 p. (In Russian).
- Subarctic Front of the NW Pacific. 1972** // Monograph, Ed. N.P.Bulgakov. Vladivostok. 133 p. (In Russian).

MULTISCALE CLIMATE VARIABILITY IN THE ASIAN PACIFIC

V.I. Ponomarev¹, V.V. Krokhin², D.D. Kaplunenko¹, A.S. Salomatin¹

¹ V.I. Il'ichev Pacific Oceanological Institute, Far Eastern Branch of Russian Academy of Sciences
(POI FEBRAS), Russia
Email: ponomarev@poi.dvo.ru

² Far Eastern Regional Hydrometeorological Research Institute (FERHRI), Russia

The paper describes major patterns of centennial/semi-centennial climatic tendencies and oscillations in the surface air temperature and precipitation for the Northeast Asia in the 20th century, as well as, in the sea surface temperature (SST) for the Northwest Pacific in the second half of the century. Linear trend of monthly mean precipitation and air/water temperature is estimated by two statistical methods. The first one is the least squares method with the Fisher's test for a significance level. The second method is a nonparametric robust method based on the Theil's rank regression and the Kendall's test for a significance level applicable to the dataset with the abnormal distribution function typical for the precipitation time series. Differences of the trend in precipitation estimated by two methods are shown. Regional features of climate change and dominating oscillations associated with cooling or warming, positive or negative precipitation anomalies in different seasons and large-scale areas are found. High seasonality of both climatic trends and the low frequency variability in the studied area are revealed. It is shown that the semi-centennial summer cooling in a central continental area of Asia accompanies the semi-centennial negative SST anomaly in the offshore region of the western subarctic pacific gyre. At the same time, warming at Kamchatka Peninsula and marginal subtropical area of the Northeast Asia accompanies the positive SST trend in the Kuroshio and Aleutian current systems. Similar alternation and seasonality of positive and negative temperature anomalies are also typical for the El Niño signal in the Northwest Pacific SST.

INTRODUCTION

Recent examination of global and hemisphere changes in the annual mean surface air temperature, precipitation (Bradley *et al.*, 1986; Vinnikov *et al.*, 1990) and SST (Folland *et al.*, 2001; Casey and Cornillon, 2001) in the 20th century has shown the statistically significant global warming (Vinnikov *et al.*, 1990; Folland *et al.*, 2001; Izrael *et al.*, 2001) and precipitation increase in the latitude band of 35–70°N over land areas (Bradley *et al.*, 1986; Vinnikov *et al.*, 1990). It is increasing in the late 20th century and dominating in moderate latitudes and subarctic zone (Folland *et al.*, 2001; Kondratiev and Demirchan, 2001).

Regional climatic tendencies in annual/seasonal mean air temperature in Russia (Rankova and Gruza, 1998; Varlamov *et al.*, 1998) and countries situated in the East Asia (Tyson *et al.*, 2002) are in agreement with major conclusions on climate change in the northern hemisphere mentioned above. At the same time, it was shown that precipitation tendencies estimated by the least squares method for Russia and Far East in the 20th century and second half of the century are unstable and insignificant (Rankova and Gruza, 1998; Dashko *et al.*, 1997). Precipitation decrease in Japan from 1948 to 1985 (Matsumoto and Yanagimachi, 1991) was not also confirmed later by using extended dataset for the next decade (Tase and Nakagawa, 1990), and confidence probability of trend in precipitation is not high in comparison with that in the air temperature trend.

At the same time, distribution function of precipitation time series is usually abnormal, unlike the distribution function of the air temperature samples. Therefore, in case of precipitation it is more accurate to use the nonparametric robust method for estimation of trend and its statistical significance (Gan, 1995; Krokhin, 1997, 2001). The aim of our study is to estimate centennial/semi-centennial climatic tendencies in the monthly mean surface air temperature and precipitation over Northeast Asia in the 20th century, as well as the trend in the Northwest Pacific SST for the second half of the century. Moreover, dominating low frequency variability of the surface air temperature and precipitation in the Northeast Asia is estimated for the 20th century using wavelet techniques.

OBSERVATION DATA AND STATISTICAL METHODS

The linear trends of surface air temperature and precipitation in the 20th century and the second half of the century are estimated for each month of a year in the wide continental area of the extratropical Asia east of 55°E, from the Ural Ridge to the coastal areas of the Northwest Pacific and Alaska Peninsula. Semi-centennial tendency in the monthly mean SST in the Northwest Pacific region extended to the west of 180°E is examined for the second half of the 20th century. Dataset of monthly mean grid SST also covers East China, Japan, Okhotsk and Bering Seas. Thus, the climate change in the wide latitude band from the North Tropic to the coast of Arctic Ocean is estimated. Monthly mean time series of air temperature and precipitation at the meteorological

stations were selected for the area studied from data bases of NOAA Global History Climatic Network (USA), RIHMI-WDC (Russia) and JMA (Japan) for the period of instrumental observations since late 19th century to 2000. To outline the details of climate change associated with extreme cooling or warming in winter and summer, we also used the daily time series of surface air temperature at some meteorological stations. Two monthly datasets of the Northwest Pacific SST on different grids were selected from: (1) WMU/COADS World Atlas of Surface Marine Data NOAA/NESDIS/NCDC CD-ROM, 1994 of time series since 1945 to 1989 with horizontal resolution $1 \times 1^\circ$; (2) JMA data base of time series since 1946 to 2000 with horizontal resolution $2 \times 2^\circ$ for the ocean area $15\text{--}65^\circ\text{N}$, $110\text{--}180^\circ\text{E}$. Initial time series of air temperature, precipitation and JMA SST have missing data. To use complete datasets, missing data of the time series in each month were recovered by the statistical method of incomplete multivariate data analysis (Schafer, 1997) using EM and AM algorithms.

Two methods of the linear trend estimation are applied. The first one is based on the least square (LS) method, Pearson's regression and the Fisher's test for statistical significance level. The second one is the nonparametric robust (NR) method (Holander and Wolfe, 1973; Hettmansperger, 1984), based on Theil's rank regression and the Kendall's test for statistical significance level (Bendat and Piersol, 1986). The NR method should be applied to time series with abnormal distribution function typical mainly for precipitation time series. It does not demand the assumption that function of distribution is Gaussian. In this case the rank statistics is used to determine both linear regression and its significance. The NR method was earlier applied to examine trends of precipitation in Canada and northeastern USA (Gan, 1995), as well as, in Russian Far East for a warm season (Krokhin, 1997, 2001). To estimate trends of surface air temperature, precipitation and SST we have applied both LS and NR methods to all time series independently on distribution function of datasets.

We also use wavelet techniques (Grossman, 1988) to reveal seasonality of dominating climate oscillation in monthly surface air temperature and precipitation over Northeast Asia. The method and its possible applications in physics are explained in details by Astafieva (1996). Application of wavelet analysis in geophysics, meteorology and oceanography is also explained in (Salomatin *et al.*, 2000). Using MATHLAB software and "sombbrero" wavelet, we estimate the amplitude and phase of climate oscillation of ENSO, decadal and interdecadal time scales.

CLIMATIC TENDENCY IN SURFACE AIR TEMPERATURE

Large-scale areas of warming and cooling in the Northeast Asia and their seasonality are revealed for both the whole period of instrumental meteorological observations and the second half of the 20th century by using two statistical methods of linear trend estimation. The sign and confidence probability of semi-centennial air temperature trend for the second half of the 20th century are shown in Figure 1 for winter and summer months. The area studied is mostly covered by observation data for this period.

A semi-centennial warming ($0.02^\circ\text{C}/\text{year}$) of high confidence probability of 99% (Figure 1) in the second half of the 20th century is clearly recorded over subtropic Pacific marginal zone (Korean Peninsula, Japanese Islands) all the year round, over Kamchatka Peninsula in summer, spring, and fall, and at the Pacific side of Alaska Peninsula in most months. Weak semi-centennial warming is also found over Chukotka Peninsula, but only in summer months. Significant semi-centennial cooling (from 1946 to 2000) in the Northwest Pacific marginal area is found in southeast subtropic continental area adjacent to the East China Sea in the latitude band of $25\text{--}35^\circ\text{N}$ (Figure 1a, c, d). Negative air temperature trend with confidence probability of 95–99% occurs in the latitude band of $25\text{--}35^\circ\text{N}$ in June and July ($-0.04^\circ\text{C}/\text{year}$), and in $25\text{--}30^\circ\text{N}$ band it occurs in August, September ($-0.02^\circ\text{C}/\text{year}$), October, December, March and April ($-0.01^\circ\text{C}/\text{year}$). Significant centennial cooling in other months is also typical for this latitude band but mainly in the offshore continental area. The most substantial seasonality of semi-centennial air temperature trends is found in the continental area of $35\text{--}55^\circ\text{N}$, $90\text{--}110^\circ\text{E}$. As shown in Figure 1, seasonality of climatic trend in this large-scale area is characterized by warming in winter and cooling in summer. Positive temperature trend in this area is the most significant and expanded in December–March, whereas negative one expands in June–September with maximum significance in June–July. Correspondingly, differences between monthly mean air temperature in June and December, July and January, August and February substantially decrease in this continental area both in the 20th century and the second half of the century. Substantial difference of the air temperature tendencies in the offshore continental area and marginal zone of the Northwest Pacific is also manifested. It seems to be due to amplification of ocean impact to the mid-latitude Asian continental areas, as well as to long-term anomaly of the Asian monsoon system.

Statistically significant centennial warming ($0.03^\circ\text{C}/\text{year}$) from the beginning of the 20th century till 1990 or 2000 also occurs over the marginal subtropic Northwest Pacific throughout a year, over subarctic coastal area in most months, and over arctic

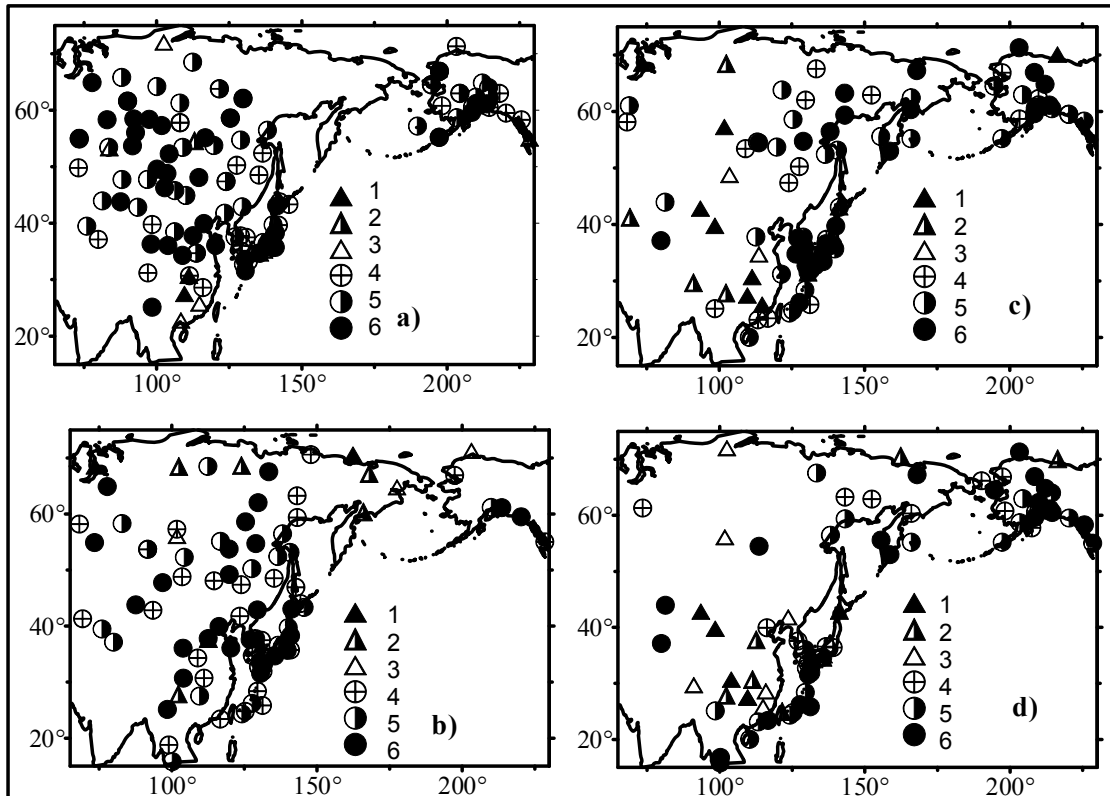


Figure 1. Negative (1, 2, 3) and positive (4, 5, 6) tendencies of surface air temperature with confidence probability: 90% (3, 4), 95% (2, 5) and 99% (1, 6) in December (a), January (b), June (c), and July (d) for the time series since 1945 till 2000

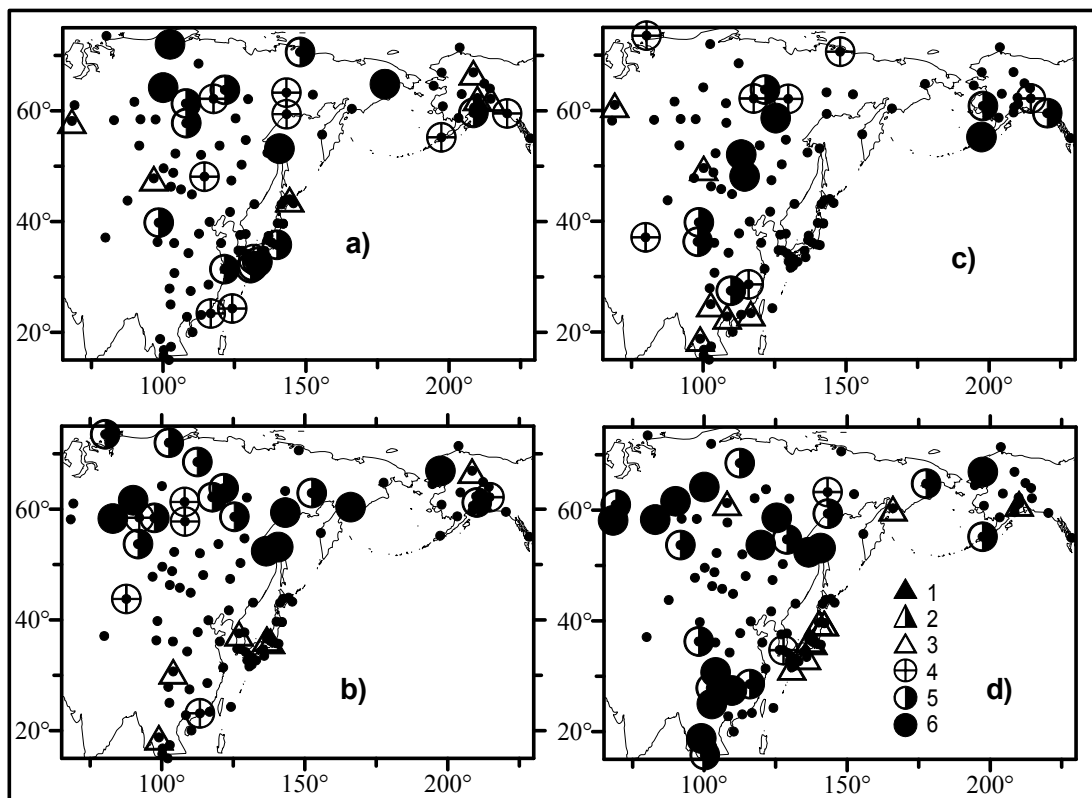


Figure 2. Negative (1, 2, 3) and positive (4, 5, 6) tendencies of precipitation sum with confidence probability: 90% (3, 4), 95% (2, 5) and 99% (1, 6) in March (a), October (b), June (c), and January (d) for the time series since 1945 till 2000

marginal zone only in a few months, particularly, in December, January, July and August. Centennial trend in offshore area of mid-latitude continental Asia also shows warming in winter and cooling in summer (Ponomarev *et al.*, 2001). So, centennial and semi-centennial trends of surface air temperature are similar and stable. At least, at the meteorological stations where the period of instrumental observations is more than 100 years (Japan, Korea, Russia), sign and significance of centennial trend do not substantially depend on a period of time series varying from 73 to 120 years. Similar patterns of linear trends in the area studied were found for the datasets of monthly mean air temperature since beginning of instrumental observations in late 19th century until 1990 or since 1917 until 1990 (Ponomarev *et al.*, 2001). It is also in agreement with tendencies of annual/seasonal mean surface air temperature and other climatic characteristics estimated for different countries, including Japan, Russia, China, Korea and so on (Arakawa, 1957; Rankova and Gruza, 1998; Varlamov *et al.*, 1998; Tyson *et al.*, 2002). On the whole, significant warming of both centennial and semi-centennial scale predominates in a cold period of a year in a broad mid-latitude continental zone north of 35–40°N (Figure 1a).

CLIMATIC TENDENCY IN PRECIPITATION

Statistically significant (with 95–99% confidence probability) trends of precipitation for the second half of the 20th century (1945–2000), as well as for the 20th century (1900–2000; 1916–2000) are revealed in large-scale areas of the Northeast Asia for each month of a year. This result is not in agreement with conclusion on statistical non-significance of precipitation trends estimated earlier by traditional least squares (LS) method in (Dashko *et al.*, 1997; Rankova and Gruza, 1998). A sign and confidence probability of semi-centennial trend of monthly precipitation estimated in by the nonparametric robust (NR) method are shown in Figure 2 (p. 127).

Increase of precipitation in the second half of the 20th century is found in large-scale continental areas of the Northeast Asia prevailing in October–May in the moderate and arctic latitude zones. Typical monthly precipitation rise of high confidence probability (99%) is 0.2–0.4 mm/year, and maximum values are in the range of 1.4–1.7 mm/year at some Russian meteorological stations in the continental area of the moderate latitudes. In October–February the positive semi-centennial trend of monthly precipitation sum occurs east of 55°E in the whole latitude band of 45–70°N, but in March, May and June it occurs in the area east of 100°E in the same latitude band. In February the positive precipitation trend of high confidence probability (99%) also occurs in the tropical and subtropical marginal area east of 95–100°E adjacent to the East China Sea,

where the air temperature trend is also positive. Negative precipitation trend (0.1–0.2 mm/year) in this subtropical area is found in May and October, and only at some meteorological stations it takes place from July to September. Bands of positive precipitation trend in summer months are stretched out from southwest to northeast, parallel to the Northwest Pacific marginal zone (Figure 2c). In June positive precipitation trend (0.2–0.5 mm/year) occupies the area along the Pacific and Bering Sea coast of Alaska and offshore band stretching out from continental area adjacent to the East China Sea to the arctic coast of the East Siberian Sea. So, positive patterns of precipitation and air temperature trends are very similar in the continental area of the Northeast Asia. Warming accompanies precipitation rise there. This result is close to conclusion on the accompanying centennial trends of global/hemisphere means air temperature and precipitations (Bradley *et al.*, 1986; Vinnikov *et al.*, 1990; Kondratiev and Demirchan, 2001; and others). Weak negative trend of precipitation is found in Japan south of Hokkaido and in Russian Primorye region adjacent to the Northwest Japan Sea. In this area of the NW Pacific marginal zone centennial and semi-centennial warming accompanies precipitation decrease. Relatively weak (with confidence probability of 90–94.9%) negative precipitation trends of both centennial and semi-centennial (Figure 2c, d) scales are found over Kyushu and Honshu Islands in September, October, December and January. Similar trends with low confidence probability (<90%) are found in Russian Primorye region in most months (Krokhin, 2001).

Significant positive precipitation trend occurs in Kyushu and Honshu Islands: centennial trend in May, and semi-centennial in March (Figure 2a). In the subarctic zone (Hokkaido, Sapporo) centennial increase of precipitation with high confidence probability (95–99%) occurs in January, February, March and August, and decrease of precipitation occurs in May, June, and July. Thus, seasonality of precipitation trend over Japanese Islands is significant and shows opposite patterns of trend in subtropic and subarctic zones. It is also controlled by storm track change like in low frequency anomalies (Branstator, 1995), including extratropical ENSO signal (Chan, 1985) and decadal oscillation (Nakamura *et al.*, 1997). In case of precipitation trends estimated by the Nonparametric Robust (NR) method are more objective and have greater reliability than LS method. About 50% of precipitation time series even for the whole period of instrumental observation have abnormal distribution function usually with substantial positive skewness and an abnormal kurtosis. Substantial difference for this case between statistical significance of the centennial precipitation trends in Japan estimated by NR and LS methods is demonstrated in Table 1 and Figure 3.

Table 1
Increment (Inc.) and confidence probability (CP) of precipitation trend in October estimated by LS and NR methods for some time series at Japanese meteorological stations since 1900 till 1998 (1) and since 1916 till 2000 (2) with abnormal skewness and kurtosis

Stations	Inc. LS (mm/year)		Inc. NR (mm/year)		CP LS, Fisher test (%)		CP NR, Kendal test (%)		Skewness		Kurtosis	
	1	2	1	2	1	2	1	2	1	2	1	2
Akita	-0.4	-0.6	-0.3	-0.6	89.4	96.9	92.7	99.3	0.6	0.3	1.3	0.2
Miyako	-0.8	-1.0	-0.8	-1.1	98.0	98.4	99.4	99.8	1.0	0.8	0.9	0.2
Osaka	-0.3	-0.4	-0.4	-0.4	87.6	83.2	97.9	92.4	0.8	0.9	0.4	0.4
Shionomisaki	–	-1.3	–	-1.2	–	96.6	–	97.6	–	0.9	–	0.5
Choshi	–	-1.0	–	-1.2	–	95.3	–	99.7	–	1.2	–	3.1
Kanazawa	–	-0.8	–	-0.6	–	96.3	–	98.6	–	1.4	–	3.2
Kagoshima	-0.5	-0.2	-0.7	-0.3	90.4	44.6	99.7	90.7	1.3	1.6	2.1	2.9
Matsumoto	-0.3	-0.6	-0.3	-0.5	83.3	95.3	95.5	98.0	1.9	2.1	6.6	7.2
Miyazaki	–	-1.2	–	-0.7	–	86.2	–	95.3	–	2.1	–	4.5

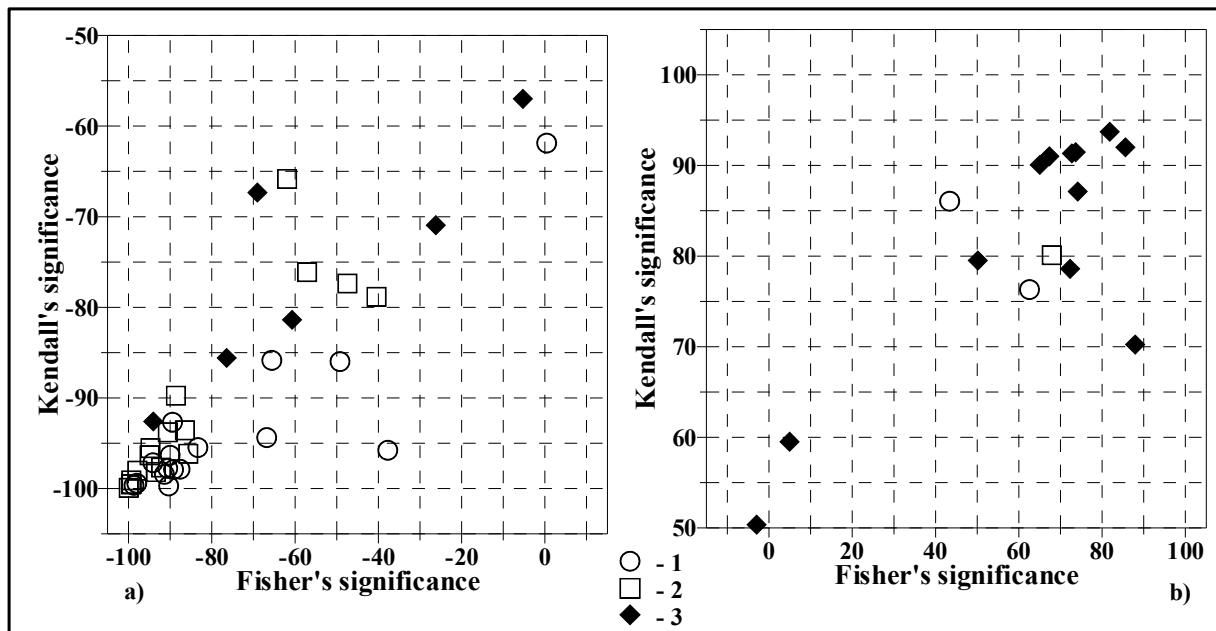


Figure 3. Confidence probability (%) of negative (a) and positive (b) centennial (1900–2000) trends of monthly precipitation in Japan for October (1), December (2), and May (3) estimated by LS method with Fisher's test and by NR method with Kendal's test for significance level. A negative value of in axis (a) means negative trend

The trends in precipitation estimated by both methods for the centennial time series in Honshu and Kyushu Islands are negative in October. It is shown in Table 1 and Figure 3 that confidence probability (CP) of precipitation trend estimated by NR method is higher than CP estimated by LS method in all cases with abnormal distribution functions for both time series: since 1900 until 1998 (1) and since 1916 until 2000 (2). Increment of the trend does not significantly depend on the method applied, and it depends more on the time period examined. Increment of the trend for the period 1916–2000 is higher than for the period 1900–1998.

Thus, the difference and similarity between the trend and its significance estimated by two methods

substantially depend on the distribution function, and mainly, on its skewness. NR method allows to get the most stable estimation of climatic trend in case of precipitation.

CLIMATIC TENDENCY IN THE NORTHWEST PACIFIC SST

The trend of annual mean SST of the World Ocean in 5° longitude-latitude bins was earlier analyzed by Casey and Cornillon (2001) for the period 1942–1993. In comparison with (Casey and Cornillon, 2001) we revealed regional details of high seasonality in SST tendency in the Northwest (NW) Pacific for the second half of the 20th century (1945–2000), estimating linear trend in a grid 2×2° for each month

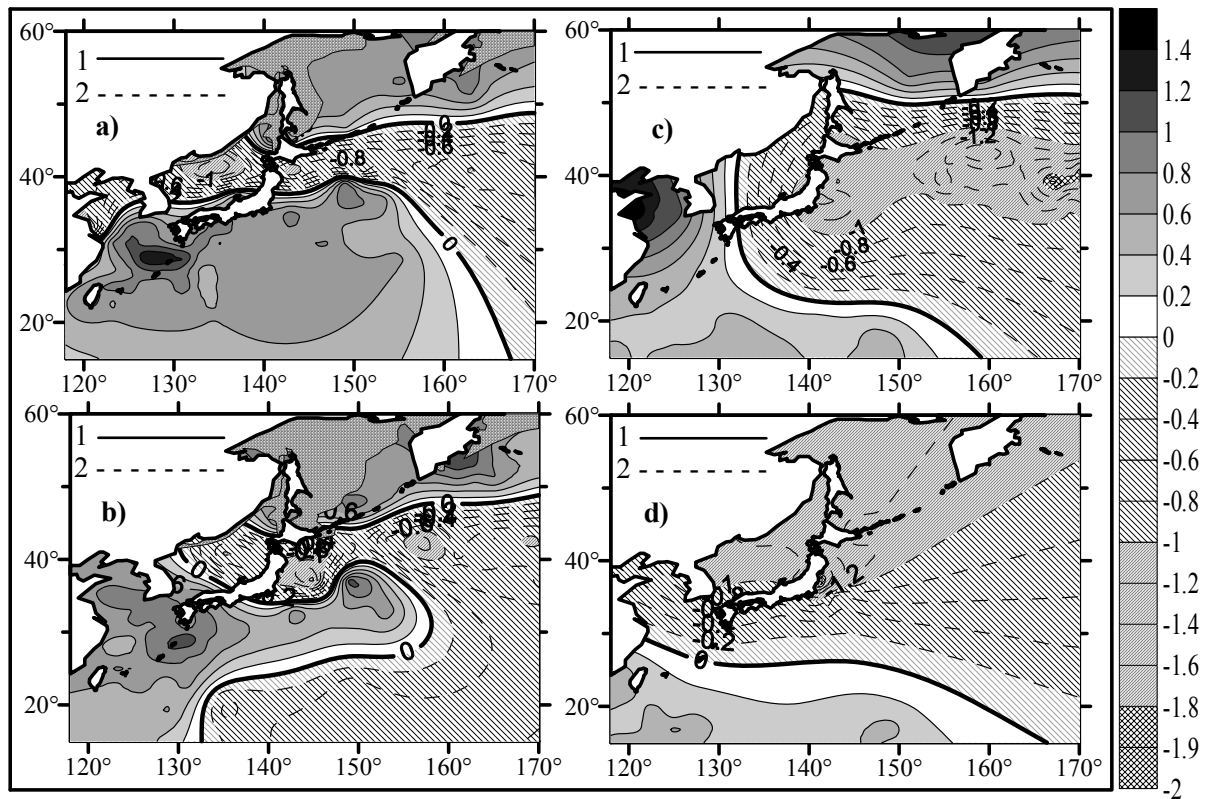


Figure 4. Positive (curve 1) and negative (curve 2) increment ($^{\circ}\text{C}$) of linear trend in SST (JMA) since 1946 until 2000 in January (a), February (b), July (c), and August (d). Ice coverage in marginal seas is filled by special pattern

of a year. The SST trends for two months of both winter and summer seasons are shown in Figure 4 demonstrating high seasonality.

Seasonality of SST trend is similar to that of surface air temperature trend over the Northeast Asia (Figure 1). Semi-centennial warming in SST dominates in November–January (Figure 4a), and cooling dominates in July–September (Figure 4c). It is important that warming tendency in November–December takes place, at first, in the western tropic and subtropic area including west Philippine Sea, East China Sea, Kuroshio region, and at second, it occurs in the northwestern subarctic Pacific. Warming in the cores of both pools is most significant (99%) and highest ($0.8\text{--}1.3^{\circ}\text{C}$ per 55 years) in December. The subarctic pool of warming in December occupies offshore Oyashio region, as well as areas adjacent to western Aleutian Islands and Kamchatka Peninsula. The most significant positive trend in the Northwest Pacific SST occupies indeed the largest area in December. In January subtropical warming pool expands northeastward to Kuroshio Extension and transition zone south of subarctic front (Figure 4a). In January–February the subarctic pool of warming also shifts northeastward to the southwest Bering Sea and ocean area adjacent to the north Kamchatka (Figure 4a, b).

At the same time, in January significant trend of cooling occurs in the latitude band of $39\text{--}45^{\circ}\text{N}$ east of Tsugaru Strait and Hokkaido Island, extending

eastward. This area of long-term cooling is associated with Oyashio, its intrusion and subarctic frontal zone. In February the pool of cooling occupies most of the western subarctic gyre, dominating in the Oyashio Intrusion and western core of the subarctic gyre. In March–May it expands substantially southward, occupying northeast area of the subtropic gyre. Pool of cooling also expands in subarctic gyre in spring, becomes deepest in July, and occupies NW Pacific north of 30°N in August with maximum negative SST trend in the Japan and Okhotsk Seas, being weak and insignificant in subtropical area and transitional zone.

Features of both SST trends and circulation change in the Japan Sea are very close to that in the Northwest Pacific. Warming in winter SST occurs in south subtropic region adjacent to Korean Strait and north subarctic area adjacent to Tatarskiy Strait, but the cooling pool occupies the central sea area associated with the subarctic gyre and subarctic frontal zone where intermediate low salinity water forms through the subduction mechanism in late fall and winter. Subtropic gyre in the Japan Sea spins up in the late 20th century, which follows from observation data analyses and modeling results presented in (Trusenkova *et al.*, 2003). Anomalously increased heat transport from the western subtropic Pacific and East China Sea to the Japan Sea accumulates in its intermediate and deep waters (Ponomarev and Salyuk, 1997; Ponomarev *et al.*, 2000a, 2001), but semi-

centennial trend in SST of subarctic gyre is negative. Physical mechanism of the SST cooling in the southwest area of the Northwest Pacific subarctic gyre, accompanying warming in the Kuroshio and Aleutian current systems seems to be similar to anatomy of climate change in the main pycnocline of the Japan Sea.

SEASONALITY OF LOW FREQUENCY CLIMATE OSCILLATION

Significant centennial regional climatic tendencies over the North Hemisphere Asian Pacific region in the 20th century may be caused both by anthropogenic factors and the natural secular oscillation with the period of a couple of centuries (Arakawa, 1957; Israel *et al.*, 2001). High regional semi-centennial winter warming in the Northeast Asia and subtropic Northwest Pacific in the second half of the 20th century can also depend on the warm phase of a 30–50 year period variation. A 50–70 year climatic oscillation over the North Pacific and North America are revealed in the winter–spring Sea Level Pressure (SLP) and the spring–summer SST (Minobe, 1997). The 50 year climate oscillations are examined by Minobe (1997) on the base of the Multi-Taper-Method applied to the analysis of the meteorological observation data over the North Pacific, North America and tropical ocean until 1990, as well as the reconstructed climate records of the surface air temperature for the North America from the tree-ring data since the 17th century.

We would compare seasonal features of the dominating oscillations in the surface air temperature and precipitation over the Northeast Asia with the seasonality of centennial/semi-centennial trends in the Northeast Asia and Northwest Pacific. Based on the wavelet technique (explained in details by Grossman (1988), Astafieva (1996), and Salomatin (2000)) we analyzed the time series of the monthly mean surface air temperature and precipitation only at the meteorological stations in the Northeast Asia for the period of instrumental observations including the time series since 1916 until 2000. Similar to trend analysis we consider, at first, the original time series at the basic meteorological stations with the minimum missing data. The time series are relatively short for the wavelet transform. Therefore, the units in a sample for the time series are artificially increased by the spline approximation. A “sombbrero” wavelet in the MATHLAB software is used to damp the biennial oscillation. In this case, wavelet transforms show the evolution of frequency, amplitude and phase of the dominating climate oscillation of the ENSO (3–7 years), decadal (8–13), and interdecadal (18–30 years) time scales. When the “sombbrero” wavelet is used, the anomalies of 35–40 years associated with the estimated trend are detected.

Typical wavelet transforms of the surface air temperature in January (a, c, e, g) and August (b, d, f, h) at four meteorological stations situated in different

climatic zones of the offshore continental area of moderate latitudes (Irkutsk 52.27°N, 104.32°E), as well as in the arctic transitional zone (Anadyr 64.78°N, 177.57°E) and subarctic region (Okhotsk 59.37°N, 143.2°E and Petropavlovsk-Kamchatskiy 52.98°N, 158.65°E) of the Northwest Pacific marginal area are presented in Figure 5. Only positive temperature anomalies of different time scale alternated with the periods from 3 to 42 years (axis of ordinates) are outlined by the shade of black and grey in this figure. Negative anomalies filled by white are invisible in the figure. Similar wavelet transforms of precipitation time series are shown in Figure 6 with exception of (g) and (h). The positive anomalies of precipitation in Vladivostok are demonstrated in Figure 6g, h.

The alternation of the positive temperature and precipitation anomalies related to the ENSO scale oscillation (3–7 years) is presented in the top part of Figures 5, 6. It is one of the prevailing oscillations both in subtropic (Hanawa *et al.*, 1988, 1989; Wang *et al.*, 1999) and subarctic regions of the Northwest Pacific (Oh and Park, 1999; Ponomarev *et al.*, 1999a, 1999b, 2002), its marginal seas and adjacent land area of the Northeast Asia (Fu and Teng, 1993; Volkov *et al.*, 1997; Ponomarev *et al.*, 1999a, 1999b, 2002; Oh and Park, 1999). Variability of ENSO scale in the area studied is associated with the unlagged and lagged extratropic El Niño/La Niña signals interacting with the internally generated oscillations due to the nonlinear atmosphere-ocean dynamics.

Winter El Niño accompanies the warming in the subtropic Northwest Pacific and the adjacent land, and the cooling in the subarctic ocean/land area during winter at a high confidence probability. The winter La Niña accompanies the cooling in the subtropics and the warming in the subarctic marginal area during winter, also at a high confidence probability. Similar winter anomalies occur after the preceding summer La Niña events, while the warming/cooling in summer is typical after the winter La Niña/El Niño both in subtropic and subarctic land and ocean areas (Ponomarev *et al.*, 1999a, 1999b, 2002). Coefficients of the cross-correlation between the SOI and the winter mean surface air temperature at the meteorological stations around the Sea of Okhotsk are shown in Table 2. The low-frequency thermal regime variations also manifest themselves in the Okhotsk Sea ice. Sea ice winter mean time series (1957–1989) were composed by averaging the 10-day ice cover in winter and early spring (21–28 of February, 1–10, 11–20 and 21–30 of March, and 1–10 of April). Both its unlagged and lagged (ice 6-month lagging SOI) cross-correlation with SOI is statistically significant and negative (Table 3). Thus, the ice cover in the Okhotsk Sea tends to increase during the winter El Niño events (when SOI reaches its highest negative values) and to decrease in the winters following the summer La Niña events (when SOI reaches its highest positive values).

Table 2

Cross-correlation of winter mean air temperature time series (1949–1990) at the coastal meteorological stations around the Sea of Okhotsk with each other and SOI averaged for the same winter, next summer (SOI, +6 m.) and previous summer (SOI, -6 m.)

	Okhotsk	Ajan	Icha	Nikolaevsk	Alexandrovsk	Poronaysk	Abashiry	Nemuro	SOI	SOI, +6 m.	SOI, -6 m.
Magadan	0.93	0.53	0.79	0.42	0.43	0.52	none	none	0.54	none	0.43
Okhotsk		0.66	0.71	0.58	0.52	0.59	none	none	0.58	none	0.38
Ajan			0.48	0.68	0.78	0.69	0.4	0.47	0.41	none	none
Icha				0.46	0.57	0.59	0.46	0.47	0.51	none	0.42
Nikolaevsk					0.73	0.66	0.50	0.52	0.38	none	0.32
Alexandrovsk						0.84	0.71	0.75	0.42	none	0.28
Poronaysk							0.49	0.57	0.56	none	0.43
Abashiry								0.97	none	none	none
Nemuro									none	none	none

Note:

Linear trend is subtracted.

95%-confidence level is equal to 0.308, according to the Fisher test.

Table 3

Unlagged and lagged cross-correlation with SOI of some oceanographic and meteorological characteristics in the Sea of Okhotsk calculated for the winter mean time series

Data	Unlagged SOI	SOI 6 months leading	95%-level
Ust-Hairuzovo air temperature, 1950–1990	0.55	0.34	0.312
Okhotsk sea ice, 1957–1990	-0.45	-0.46	0.349
North Pacific Index, 1940–1990	0.58	0.49	0.282

Note:

95%-confidence levels are calculated using the Fisher test

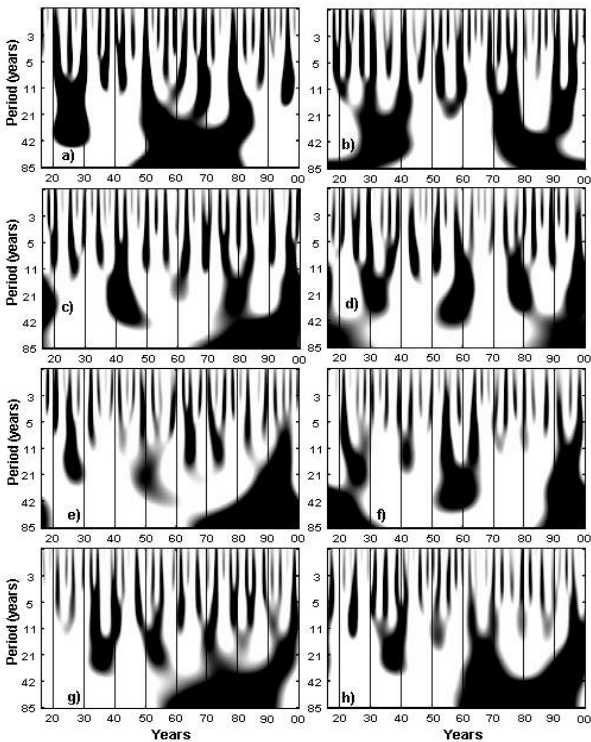


Figure 5. Wavelet transform of monthly mean surface air temperature in Anadyr (a, b), Okhotsk (c, d), Irkutsk (e, f), and Petropavlovsk-Kamchatskiy (g, h) for January (a, c, e, g) and August (b, d, f, h) since 1916 until 2000 year (abscissa axis)

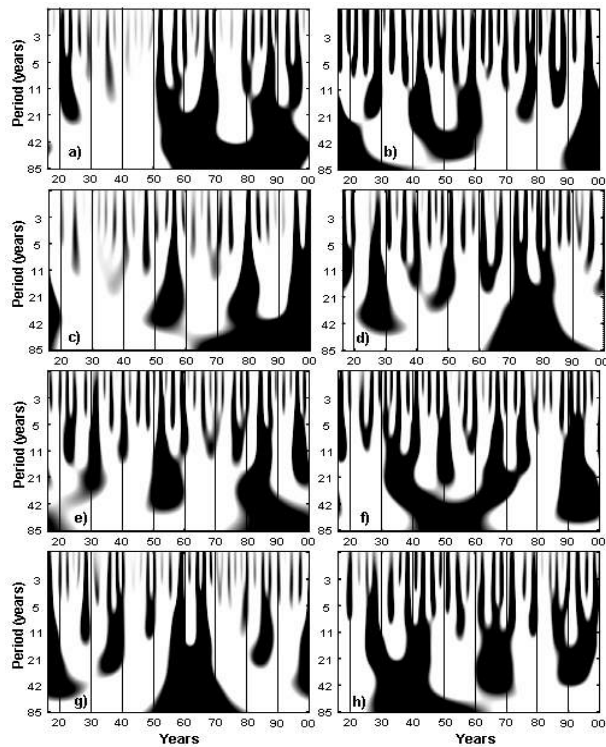


Figure 6. Wavelet transform of monthly precipitation sum in Anadyr (a, b), Okhotsk (c, d), Irkutsk (e, f), and Vladivostok (g, h) for January (a, c, e, g) and August (b, d, f, h) since 1916 until 2000 year (abscissa axis)

Unlagged monthly ENSO-scale anomalies in the extratropic Asian Pacific are due to El Niño/La Niña-accompanying anomalous circulation processes in the extratropic atmosphere and ocean. The relationship between heat displacement during ENSO cycle in tropics and the intensity of trade winds (Wyrski, 1975), location and intensity of the atmospheric circulation patterns (Horel and Wallace, 1981) and centers of action in the Asian Pacific, as well as Hadley circulation and westerly jet stream (Lau and Boyle, 1987; Yang and Webster, 1990; Oort and Yienger, 1996), South Asian, Indian and East Asian monsoons (Wu and Hastenrath, 1986; Webster and Yang, 1992; Tyson *et al.*, 2002) are actually considered as important physical devices of tropic-extratropic interaction, and the extratropic response to ENSO in the atmosphere. According to Sekine (1996), at least, La Niña event is effected by the anomaly of the winter snow coverage over the Asian continent and the summer monsoon wind. In this case the low frequency anomalies of the Northeast Asia monsoon system also have an impact on the anomalies of the tropical ENSO cycle.

Lagged and unlagged ENSO-scale remote linkages are actualized through the synoptic scale physical processes both in the atmosphere and ocean with the propagation of the faster, barotropic (Simmons *et al.*, 1983) and slower, baroclinic (Lau and Boyle, 1987) waves in the atmosphere, coastal Kelvin and Rossby waves in the North Pacific Ocean (Johnson and O'Brien, 1990), as well as the coupled atmospheric-oceanic waves in the global ocean-atmosphere (White and Cayan, 2000). The ENSO-scale variability in the Asian Pacific region is also considered as a response to the huge heat displacement in the tropics accompanying substantial seasonal anomalies in the tropical cyclone activity (Chan, 1985, Chen and Weng, 1998) in the Western Pacific and extratropical storm tracks change (Branstator, 1995). As for oceanic teleconnections, the poleward ENSO signal propagation in the North Pacific is explained by Johnson and O'Brien (1990). By the circulation model and observation data analysis, they show that the temperature and upper layer thickness anomalies propagate northward along the eastern coast of the North America due to the coastal Kelvin waves, and reach the 50°N latitude in about one year. Further in mid-latitude the westward temperature anomaly propagation to the central mid-latitude Pacific is due to the baroclinic Rossby waves excited by the coastal Kelvin waves. Formation of the temperature anomaly in the central Pacific accompanies the circulation change in the atmosphere and the North Pacific Ocean. Thus, one can suggest that both a northward fast ENSO signal in the atmosphere and a slow ENSO signal in the ocean exist. Propagation of both signals is controlled by synoptic-scale processes, atmospheric ones of an order of a week, and oceanic ones of an order of a few months, which, in turn, interact with the larger-scale processes.

A lot of meteorological and oceanographic data observed in tropics and extratropics during ENSO events were collected and analyzed particularly on the base of the TOGA project. As suggested, the irregularity of ENSO may be caused by the nonlinearity in the ocean-atmosphere system, particularly, by the nonlinear interactions between the heat displacement in tropics and the anomalies of annual cycle in the extratropics. At the same time, substantial anomalies of ENSO cycles and changes of El Niño and La Niña occurrence during the winters from 1950 to 1995 are shown by Zhang and Wallace (1996) and others. In particular, the La Niña occurrence in winter dramatically decreased since 1977. After the maximum interval between El Niño events from 1974 to 1982, La Niña events have become weaker and have taken place mostly in summer while El Niño have been dominating in winter, have become more frequent since 1987, and especially in 1990s.

The ENSO-like interdecadal variability is shown by Wang (1995) and Zhang *et al.* (1997), and interdecadal variability in the western Pacific and its amplification in global warming is manifested by Yamagata and Masumoto (1992). At the same time, the positive SST trend dominating during winter in the subtropic NW Pacific and the negative SST trend prevailing during summer in the subarctic NW Pacific (Figure 4) also look like accumulated El Niño impact. On a whole, the seasonality and regionality of the positive/negative anomalies of the El Niño signal in the extratropic Northwest Pacific are similar to the seasonality and regionality of positive/negative climatic trends in this large-scale area of the North Pacific (Figure 3). The questions arising from our study are why the anomalies of so different scales have a substantial similarity in the NW Pacific, and what forcing drives climate in the 20th century?

The alternation of positive/negative temperature anomalies with decadal (8–13) and interdecadal (18–30 years) time scales is shown in the mid part of Figures 5, 6. Similar oscillations of both scales were studied through the observation data analysis for the Northern Hemisphere (Trenberth, 1990) and the Pacific ocean-atmosphere system (Trenberth and Hurrell, 1994; Chen and Ghil, 1995; Yasuda and Hanawa, 1997; Nakamura *et al.*, 1997; Minobe and Mantua, 1999; Miller and Schneider, 2000; Tourre *et al.*, 2001), as well as by simulation with the circulation models of the North Pacific Ocean (Latif and Barnett, 1994; Miller *et al.*, 1994; Schneider *et al.*, 2002; Auad, 2003; Qiu, 2003), and the simulation with the coupled model showing a 30-year interdecadal mode (Robertson, 1996), also found in the Global Sea Ice Coverage and SST data set (Auad, 2003). Main features of decadal-interdecadal dynamics associated with the low frequency variations of the Aleutian Low, wind stress curl, subduction in the central NW Pacific, SST anomaly in the Kuroshio-

Oyashio Extension area, as well as positive feedback from the SST anomaly to the Aleutian Low are described in (Miller and Schneider, 2000; Schneider *et al.*, 2002).

By the data analysis, Tourre *et al.* (2001) found that the oscillations of decadal (8–13) and interdecadal (longer than 13 years) time scales are quite different and statistically independent. The substantial differences between the decadal (8–13) and interdecadal (18–26 years, bi-decadal scale) bands in the North Pacific Ocean were shown and explained by Auad (2003) based on numerical experiments with the isopycnal ocean model forced by the NCEP-NCAR reanalysis wind stress and heat fluxes for the period since 1958 until 1997. According to the simulation results, the decadal band is mostly driven by the wind stress curl, unlike the interdecadal band, which is mostly driven by the atmospheric heat fluxes exciting a high baroclinic mode and counterclockwise pycnocline anomaly moving around the basin (Auad, 2003). This pycnocline anomaly of interdecadal time scale moves across the Gulf of Alaska toward the Aleutian Island up to about Kamchatka Peninsula, continuing to the southwest down to about 28°N. Auad (2003) has also shown that the maximum SST variability takes place west of the date line at 45°N and along the eastern boundary in the interdecadal band and in the central North Pacific and Kuroshio-Oyashio Extension areas in the decadal band. According to Qiu (2003), the Kuroshio Extension jet is weakening and strengthening with a prevailing period of about 12 years that is caused by the wind stress curl anomalies.

At the same time, the SST anomaly of joint ENSO-decadal band can also propagate from the Aleutian Low area to the central region of the subarctic gyre, as well as from the Kuroshio-Oyashio Extension and central subtropic Pacific areas to the western tropical region (Ponomarev *et al.*, 1999b; 2000b). The frequency of the SST anomalies can drift in some areas from ENSO to decadal scale within the observational records.

The decadal and interdecadal variability in terms of the wavelet transforms of the air temperature and precipitation in some regions of the Northeast Asia are shown in the mid parts of Figures 5, 6. The bi-decadal (18–26 years) oscillation both in the air temperature and precipitation is indeed most evident in the subarctic marginal Northwest Pacific zone, particularly, in the Kamchatka Peninsula and Okhotsk Sea area: Petropavlovsk-Kamchatski (Figure 5g, h), Okhotsk (Figure 5c, d). The decadal (8–13 years) oscillations are most evident in the arctic marginal zone, including western Bering Sea (Figure 5a, b; Figure 6a, b) all the year round, as well as over land in the latitude band of Kuroshio-Oyashio Extension area mainly in months of the cold period of a year. The period of interdecadal variability in most of these regions shifts to the red spectrum and comes to about

a 30–40 years band (Figure 5e, f; Figure 6e, f). In a transitional zone between the subarctic and subtropic regions, continental and marginal areas of the Northeast Asia the frequency of the prevailing variability in the joint decadal-interdecadal band is drifting from the decadal to interdecadal scale up to 30–40 years or from the interdecadal to decadal scale within the period of observations (Figure 5c; Figure 6d, g). It seems to be due to the nonlinear dynamics in the ocean-atmosphere system.

Figures 5, 6 also show seasonality of the positive 20–30 year anomalies associated with the long-term oscillations with a period of 40–60 years (Minobe, 1997). The winter anomalies of this scale both in the air temperature and precipitation in Chukotka Peninsula have an opposite sign in comparison with the summer one. Positive interdecadal anomaly of the air temperature in Anadyr occurs from 1950s to 1970s in January (Figure 5a) and from the late 1970s to early 1990s in August (Figure 5b). It is in agreement with the negative winter temperature trend and the positive summer temperature trend estimated for the second half of the 20th century. In most subarctic area the positive long-term anomaly of the winter air temperature occurs in late 1970s–1990s (Figure 5c, e, d), and the negative anomaly takes place in 1930s–1940s. A positive long-term anomaly of the winter precipitation in the subarctic area is also revealed in late 1970s–early 1990s or in 1980s–1990s for the most subarctic marginal and continental areas (Figure 6c, e). On the contrary, a negative 35–40 year anomaly of the summer precipitation in a subarctic marginal zone (Figure 6d) and the winter precipitation in subtropics are found for the last two decades of the 20th century.

The long-term anomalies are similar and more evident in the wavelet transforms for the air temperature/precipitation time series since the late 19th century until 2003 (not shown in the figures). In this paper we demonstrate only a historical period of the observations, which is the same for the most of the time series analyzed. The boundary artificial effect of the wavelet transforms (Astafieva, 1996; Salomatin, 2000) at the lower left and right edges (bottom left and right edges of Figures 5, 6) is not high. We compared the wavelet transforms for two samples of the air temperature in Vladivostok: 1872–2003 and 1916–2000. The characteristic time-scale of the artificial negative/positive anomaly at the edge does not exceed 5 years for the band with the periods of 30–40 years.

CONCLUSION

Climatic tendencies in the Northeast Asia in the 20th century are characterized by the significant warming in winter and the cooling in summer over the offshore continental area west of 120–110°E in mid and moderate latitudes. Difference between the summer and winter surface air temperature is significantly decreasing in this continental area during the 20th

century and its second half. The warming tendency being characteristic throughout a year for the area east of 110–120°E accompanies the precipitation increase in this area of moderate latitudes. Thus, the continental climate in moderate latitudes of the Northeast Asia becomes closer to marine climate. The positive air temperature trend occupies the marginal land area adjacent to the Northwest Pacific practically all the year round, with the exception of the subtropic continental area adjacent to the East China Sea. The warming tendency in fall and winter accompanies the precipitation decrease in Japan and Russian Primorye Region adjacent to the Northwest Japan Sea. Significant precipitation reduction in Japan takes place in October, December and January, with the exception of the subarctic area (Hokkaido Island) where the precipitation slightly increases in December–March and in August, but decreases in May–July.

Statistically significant positive SST trend in the Kuroshio region and in the northwest area of the Pacific subarctic gyre dominates from November to February, accompanying the warming in the continental and marginal areas of the Northeast Asia. The semi-centennial negative SST trend occurs in the Oyashio region and occupies the southwestern area of the subarctic Pacific gyre. As a whole, temperature contrasts between the Asian continent area of moderate latitudes and subarctic Northwest Pacific, as well as the contrast in the SST between the western boundaries and the offshore areas of the Northwest Pacific increases, while the air temperature contrast over the offshore area in the East Asia decreases during the second half of the 20th century. Seasonality of the semi-centennial linear trend in the Northwest Pacific and some areas of the Northeast Asia for the second half of the 20th century is similar to the seasonality of the El Niño signal in the Northwest Pacific SST.

REFERENCES

- Arakawa H. 1957.** Climatic change as revealed by the data from the Far East. *Weather* 12 (2), pp. 46–51.
- Astafieva N.M. 1996.** Wavelet analyses: theory and applications. *Uspekhi fizicheskikh nauk* 166 (11), pp. 1145–1170.
- Aud G. 2003.** Interdecadal dynamics of the North Pacific ocean. *Journal of Physical Oceanography* 33 (12), pp. 2483–2503.
- Bendat J.S., Piersol A.G. 1986.** Random data: analysis and measurement procedures. New York: John Wiley & Sons Publications, 540 p.
- Bradley R.S., Diaz H.F., Eischeid J.K., Jones P.D., Kelly P.M., Goodess C.M., 1986.** Precipitation fluctuations over Northern Hemisphere land areas since the mid-19th century. *Science* 237, pp. 171–175.
- Branstator G.W. 1995.** Organization of stormtrack anomalies by recurring low frequency circulation anomalies. *Journal Atmospheric Science*, Vol. 52, pp. 207–226.
- Casey K.S., Cornillon P. 2001.** Global and regional Sea surface temperature trends. *Journal of Climate*, Vol. 14, pp. 3801–3818.
- Chan J.L. 1985.** Tropical cyclone activity in west Pacific in relation to the El Niño-Southern Oscillation phenomenon. *Monthly Weather Review*, Vol. 113, pp. 599–606.
- Chen F., Ghil M. 1995.** Interdecadal variability of the thermohaline circulation and high-latitude surface fluxes. *Journal of Physical Oceanography* 25 (11), pp. 2547–2568.
- Chen T.C., Weng S.P. 1998.** Interannual variation in the tropical cyclone formation over the western north Pacific. *Monthly Weather Review*, Vol 126, pp. 1080–1090.
- Dashko N.A., Varlamov S.M., Khan E.X., Kim E.S. 1997.** Variability of precipitation above coast of the Japan Sea. *Meteorology and hydrology*, 12, pp. 12–24.
- Folland C.K., Rayner N.A., Brown S.J., Smith T.M., Shen S.S., Parker D.E., Macadam I., Jones P.D., Jones R. N., Nicholls N., Sexton D.M.H. 2001.** Global temperature change and its uncertainties since 1861. *Geophysical Research Letters* 28 (13), pp. 2621–2624.
- Fu C.B., Teng H.L. 1993.** Relationship between summer climate in China and the El Niño/Southern Oscillation phenomenon. *Frontiers in Atmospheric Sciences*, Allerton Press, pp. 166–178.
- Gan Th. 1995.** Trends in air temperature and precipitation for Canada and north-eastern USA. *Int. Journal Climatology* 15 (10), pp. 1115–1134.
- Grossman A. 1988.** Wavelet transform and edge detection. *Stochastic processes in physics and engineering*. New York: Reidel, pp. 149–157.
- Hanawa K., Watanabe T., Iwasaka N., Suga T., Toba Y. 1988.** Surface thermal conditions in the Western North Pacific during the ENSO events. *Journal Meteorological Society of Japan* 66 (3), pp. 445–456.
- Hanawa K., Yoshikawa Y., Watanabe T. 1989.** Composite Analyses of wintertime wind stress vector fields with respect to SST anomalies in the Western North Pacific and the ENSO events. Part I: SST composite. *Journal Meteorological Society of Japan* 67 (3), pp. 385–400.
- Hettmansperger Th.P. 1984.** Statistical inference based on ranks. New: John Wiley and Sons Inc. Publications, 334 p.
- Holander M., Wolfe D. 1973.** Nonparametric statistical methods. New York: John Wiley and Sons Inc. Publications, 407 p.
- Horel J.D., Wallace J.M. 1981.** Planetary-scale atmospheric phenomena associated with the Southern Oscillation. *Monthly Weather Review*, Vol. 109, pp. 813–829.
- Izrael Yu.A., Gruza G.V., Kattsov V.M., Meleshko V.P. 2001.** Global climate change: the role of anthropogenic impact. *Meteorology and hydrology*, 12, pp. 12–24.
- Johnson M.A., O'Brien J.J. 1990.** The Northeast Pacific Ocean response to the 1982–1983 El Niño. *Journal Geophysical Research* 95 (C5), pp. 7155–7166.

- Kondratiev K.Ya., Demirchan K.S. 2001.** Earth climate and "Kyoto Protocol". *Vestnik Rossiyskoy Akademii Nauk* 71 (11), pp. 1002–1009.
- Krokhin V.V. 1997.** About some methods of statistical data processing of the monthly sums of precipitation. FERHRI Proceedings. St. Petersburg: Hydrometeorological Press, Vol. 148, pp. 116–127. (In Russian).
- Krokhin V.V. 2001.** On the precipitation trends over the Russian Far East in a warm season. Reports of International Workshop on the Global Change Studies in the Far East, Sept. 7–9, 1999. Vladivostok: Dalnauka. TEACOM Publication 7(1), pp. 111–122.
- Latif M., Barnett T.P. 1994.** Causes of decadal climate variability over the North Pacific and North America. *Science* 266, pp. 634–637.
- Lau K.M., Boyle J.S. 1987.** Tropical and extratropical forcing of the large-scale circulation: a diagnostic study. *Monthly Weather Review*, Vol. 11, pp. 400–428.
- Matsumoto J., Yanagimachi H. 1991.** Long-term variations of precipitation and snow depth in Japan. Proceedings of Environment Change and Gis. Intern. Symp., Asahikawa, Japan, Aug. 28, 1991, pp. 431–444.
- Miller A.J., Cayan D.R., Barnett T.P., Graham N.E., Oberhuber J.M. 1994.** Interdecadal variability of the Pacific Ocean: model response to observed heat flux and wind stress anomalies. *Climate Dynamics*, Vol. 9, pp. 287–302.
- Miller A.J., Schneider N. 2000.** Interdecadal climate regime dynamics in the North Pacific Ocean: Theories, observations and ecosystem impacts. *Progress in Oceanography*, Vol. 47, pp. 355–379.
- Minobe S. 1997.** A 50–70 year climatic oscillation over the North Pacific and North America. *Geophysical Research Letters*, Vol. 24, pp. 683–686.
- Minobe S., Mantua N. 1999.** Interdecadal modulation of interannual atmospheric and oceanic variability over the North Pacific. *Progress in Oceanography*, Vol. 43, pp. 163–192.
- Nakamura H., Lin G., Yamagata T. 1997.** Decadal climate variability in the North Pacific during the recent decades. *Bull. American Meteorological Society* 78(10), pp. 2215–2225.
- Oh I.S., Park W. 1999.** Variability of SST and Atmospheric Variables related to ENSO in the North Pacific and in the East Asian Marginal Seas. Proceedings CREAMS'99 International Symposium, Fukuoka, Japan, 26–28 Jan. 1999, pp. 104–107.
- Oort A.H., Yienger J.J. 1996.** Observed interannual variability in the Hadley circulation and its connection to ENSO. *Journal of Climate* 9 (11), pp. 2751–2767.
- Ponomarev V., Kaplunenko D., Ishida H. 2001.** Centennial and semi-centennial climatic tendencies in the Asian continental and Pacific marginal areas. *Bulletin of Japan Sea Research Institution. Kanazawa University. Japan* 32, pp. 77–90.
- Ponomarev V.I., Salyuk A.N. 1997.** The climate regime shifts and heat accumulation in the Sea of Japan. Proceedings of CREAMS Symposium, Jan. 26–31, 1997. Fukuoka, pp. 157–161.
- Ponomarev V.I., Trusenkova O.O., Kaplunenko D.D., Ustinova E.I. 1999a.** Interannual Variations of Oceanographic and Meteorological Characteristics in the Sea of Okhotsk. Proceedings of The Second PICES Workshop on the Okhotsk Sea and Adjacent Areas, 9–12 Nov., 1998, Nemuro, Japan, pp. 31–40.
- Ponomarev V.I., Trusenkova O.O., Trousenkov S.T. 2002.** Relationship between surface temperature anomalies in the mid-latitude North Pacific region and ENSO. Reports of the Int. Workshop on Global Change Studies in the Far East, September 7–9, 1999, Vladivostok, Russia, TEACOM Publication 7 (2), pp. 34–65.
- Ponomarev V.I., Trusenkova O.O., Trusenkov S.T. 2000.** Propagation of low frequency sea surface temperature anomalies in the North Pacific. *Russian Meteorology and Hydrology* 6, New York: Allerton Press, Inc., pp. 41–48.
- Ponomarev V.I., Trusenkova O.O., Trousenkov S.T., Ustinova E.I., Kaplunenko D.D., Polyakova A.M. 1999.** The ENSO signal in the Northwest Pacific. Proceedings of the Science Board 98 Symposium on the 1997/98 El Niño event, 14–25 Oct., 1998, Fairbanks, PICES Scientific Report 10, pp. 9–31.
- Ponomarev V.I., Ustinova E.I., Salyuk A.N., Kaplunenko D.D. 2000.** Climate variation in the Japan Sea and adjacent area in the 20th century. *Izvestiya TINRO (Collection of papers Trans. Pacific Res. Fish. Center)* 127 (2), pp. 20–36. (In Russian).
- Qiu B. 2003.** Kuroshio extension variability and forcing of the Pacific decadal oscillations: responses and potential feedback. *Journal of Physical Oceanography* 33 (12), pp. 2465–2482.
- Rankova E.Ya., Gruza G.V. 1998.** Indicators of climate change for Russia. *Meteorologiya i Gidrologiya* 1, pp. 5–18.
- Robertson A.W. 1996.** Interdecadal variability in the multicentury climate integration. *Climate Dynamics*, Vol. 12, pp. 227–241.
- Salomatin A.S., Yusupov V.I., Savelieva N.I., Semiletov I.P. 2000.** Wavelet analyses: examples of processing in acoustic and hydrometeorological data (North Pacific-North Asian region). *Hydrometeorological and biochemical research in Arctic. Proceedings of the Arctic Regional Center*, Vol. 2, part 1, Vladivostok: Dalnauka, pp. 202–211. (In Russian).
- Schafer J.L. 1997.** Analysis of incomplete Multivariate data. London: Chapman & Hall Publications, 430 p.
- Schneider N., Miller A.J., Pierce D.W. 2002.** Anatomy of North Pacific decadal variability. *Journal of Climate*, Vol. 15, pp. 586–605.
- Sekine Y. 1996.** Anomalous Oyashio intrusion and its teleconnection with subarctic North Pacific circulation, sea ice of the Okhotsk Sea and air temperature of the Northern Asian continent. Proceedings of PICES Workshop on the Okhotsk Sea and Adjacent Areas, Vladivostok, June 19–24, 1995. Canada, 1996, pp. 177–187.
- Simmons A.J., Wallace J.M., Branstator G.W. 1983.** Barotropic wave propagation and instability, and atmospheric teleconnection patterns. *Journal Atmospheric Science*, Vol. 40, pp. 1363–1392.
- Tase N., Nakagawa S. 1990.** Spatial and temporal characteristics of precipitation in Japan. Long-term trends of annual precipitation. *Annual Report Institution Geosciences Univ. Tsukuba* 16, pp. 553–572.
- Tourre Y.M., Rajagopalan B., Kushnir Y., Barlow M., White W.B. 2001.** Patterns of coherent decadal and interdecadal climate signals in the Pacific basin during the 20th century. *Geophysical Research Letters*, Vol. 28, pp. 2069–2072.

- Trenberth K.E. 1990.** Recent observed interdecadal climate change in the Northern Hemisphere. *Bull. Amer. Meteor. Society*, Vol. 71, pp. 988–993.
- Trenberth K.E., Hurrell J.W. 1994.** Decadal atmosphere - ocean variations in the Pacific. *Climate Dynamics*, Vol. 9, pp. 303–319.
- Trusenkova O., Ponomarev V., Ishida H. 2003.** Impact of climate change on circulation patterns in the Japan Sea. *Journal Hydraulic Coastal Environment Engineering* 733/II-63, pp. 131–150.
- Tyson P., Fu C., Fuchs R., Lebel L., Mitra A.P., Odada E., Perry J., Steffen W., Virji H. (Eds.) 2002.** Global-regional linkages in the Earth system. *Global Change, START, IGBP Series*: Springer, 186 p.
- Varlamov S.M., Kim Y.S., Han E.Kh. 1998.** Recent variations of temperature in East Siberia and in the Russian Far East. *Meteorology and hydrology*, 1, pp. 19–28.
- Vinnikov K.Ya., Groisman P.Ya., Lugina K.M. 1990.** Empirical Data on Contemporary Global Climate Changes (Temperature and Precipitation). *Journal of Climate* 3(6), pp. 662–677.
- Volkov Yu., Kalashnikov B., Zhukov A., Abramich A., Anzhina G. 1997.** Anomalies of the atmospheric processes and possibility of prediction of extreme air temperature in the El Niño year. *Trudi DVNIGMI (Collection of papers of the Far East Regional Hydrometeorological Institute)* 147, pp. 120–133. (In Russian).
- Wang B. 1995.** Interdecadal change in El Niño onset in the last four decades. *Journal of Climate*, Vol. 8, pp. 267–285.
- Wang C., Weisberg R.H., Virmani J.I. 1999.** Western Pacific interannual variability associated with El Niño-Southern Oscillation. *Journal Geophysical Research* 104 (C3), pp. 5131–5149.
- Webster P.J., Yang S. 1992.** Monsoon and ENSO: Selectively interactive systems. *Quart. J. Roy. Meteorological Society*, Vol. 118, pp. 877–926.
- White W.B., Cayan D.R. 2000.** A global El Niño - Southern Oscillation wave in surface temperature and pressure and its interdecadal modulation from 1900 to 1997. *Journal Geophysical Research*, 105 (C5), pp. 11232–11242.
- Wu M.C., Hastenrath S. 1986.** On the interannual variability of the Indian monsoon and the Southern oscillation. *Arch. Meteor. Geophys. Biocl.*, Vol. B39, pp. 239–261.
- Wyrtki K. 1975.** El Niño – The dynamic response of the equatorial Pacific Ocean to atmospheric forcing. *Journal Physical Oceanography* 5, pp. 572–584.
- Yamagata T., Masumoto Y. 1992.** Interdecadal natural climate variability in the western Pacific and its implications in global warming. *Journal Meteorological Society of Japan*. Vol. 70, pp. 167–175.
- Yang S., Webster P.J. 1990.** The effect of summer tropical heating on the location and intensity of the extratropical westerly jet streams. *Journal Geophysical Research*, 95 (D11), pp. 18705–18721.
- Yasuda T., Hanawa K. 1997.** Decadal changes in the mode waters in the mid-latitude North Pacific. *Journal Physical Oceanography*, Vol. 27, pp. 858–870.
- Zhang Y., Wallace J.M. 1996.** Is climate variability over the North Pacific a linear response to ENSO? *Journal of Climate*, Vol. 9, pp. 1468–1478.
- Zhang Y., Wallace J.M., Battisty D.S. 1997.** ENSO-like interdecadal variability: 1900–93. *Journal of Climate*, Vol. 10, pp. 1004–1020.

MULTIYEAR VARIABILITY OF NORTH PACIFIC HIGH AND ALEUTIAN LOW

T.V. Bogdanovskaya, N.S. Kupera

Far Eastern Regional Hydrometeorological Research Institute (FERHRI), Russia

Email: tbogdanovskaya@hydromet.com

Variability of certain features (pressure, coordinates, area) of North Pacific High and Aleutian Low over the last 56 years is analyzed. Analysis is based on the monthly average sea level pressure from NCEP/NCAR Reanalysis in the points of $2.5 \times 2.5^\circ$ grid from January 1948 to September 2003. Dependency of the area of the center of action (COA) on its parameters, as well as on the El Niño/Southern Oscillation indices, is revealed. It is shown that Aleutian Low was deepening during the last 56 years and its area was increasing in winter–spring. North Pacific High is characterized by weakening and shifting southward. 1970s are considered to be the critical moment for the North Hemisphere atmospheric circulation and affect variability of almost all parameters of two North Pacific centers of action.

INTRODUCTION

Investigation of the Earth's climate change has recently become one of the promising fields of meteorology. Centers of action (COA), which result from the prevalence of baric systems of the same sign in a certain region, are the climate indicators. Centers of action interact with other global circulation systems and external factors and their dynamics affects weather patterns all over the world in a certain way.

Investigation of long-term changes in the COA parameters with the use of the new reliable data is critical for understanding a mechanism of climate oscillations.

During the last century several turning points have been identified in the multiyear variability of the North Hemisphere atmospheric circulation. Many scientists mention the atmospheric circulation change in 1970s and predict a new turning point in 2010s (Baydal, 1986; Minobe, 1999; Trenberth *et al.*, 2002). How much are these turning points reflected in the behavior of the centers of action? What COA parameters do they primarily affect? How have centers of action changed recently? The present research is going to answer the questions above.

The present research is focused on variability of some features of two main North Pacific pressure centers (North Pacific High and Aleutian Low) during the last 56 years. The area covered by COA is a newly studied parameter that allows assessing the magnitude of COA influence on the climatic features of the Pacific and continental Asian regions. So far, the areas covered by the Atlantic subtropical highs (Balashova, 1986) and winter Asian High (The manual..., 1965; Vasilevskaya *et al.*, 2000) have been studied only. Therefore, investigation of the area of other centers of action, in particular of two North Pacific pressure centers, is of a great interest.

DATA AND METHODS

The average monthly NCEP/NCAR Reanalysis sea level pressure data in the points of a $2.5 \times 2.5^\circ$ grid for the period from January 1948 to September 2003 (<http://www.cdc.noaa.gov/cgi-bin/Composites/>) have been used as initial data. Before 1948 the sea level pressure data are isolated and missing to a certain extent.

The area of COA localization has been specified for each of the analyzed centers of action, and coordinates of points with maximum (North Pacific High) or minimum (Aleutian Low) pressure and corresponding pressure values have been indicated.

The area of North Pacific High was assumed to be the area limited by the 1020 hPa isobar in the vicinity of COA ($20\text{--}50^\circ\text{N}$, $150^\circ\text{E}\text{--}120^\circ\text{W}$). The area of Aleutian Low was assumed to be the area limited by the 1010 hPa isobar in the vicinity of $30\text{--}70^\circ\text{N}$, $160^\circ\text{E}\text{--}130^\circ\text{W}$. Location of the areas and magnitude of defining isobars have been assumed basing on the mean long-term pressure charts and results of the previous studies (Apasova, 1979; Dashko and Varlamov, 2003; and others). The areas of the analyzed COA for winter and summer seasons are schematically shown in Figure 1.

Linear trends have been studied to reveal specific features of the multiyear variability of the COA parameters. Significance of linear trends has been assessed by a Student criterion (Korn and Korn, 1984), significant trends being the ones with the 0.05 confidence level.

In order to calculate the area of COA, coordinates of pressure zones have been converted into the metric Lambert's cylindrical equal area projection. The area of COA has been calculated over the polygon area formula based on its coordinates (Korn and Korn, 1984; Map projections, 1994):

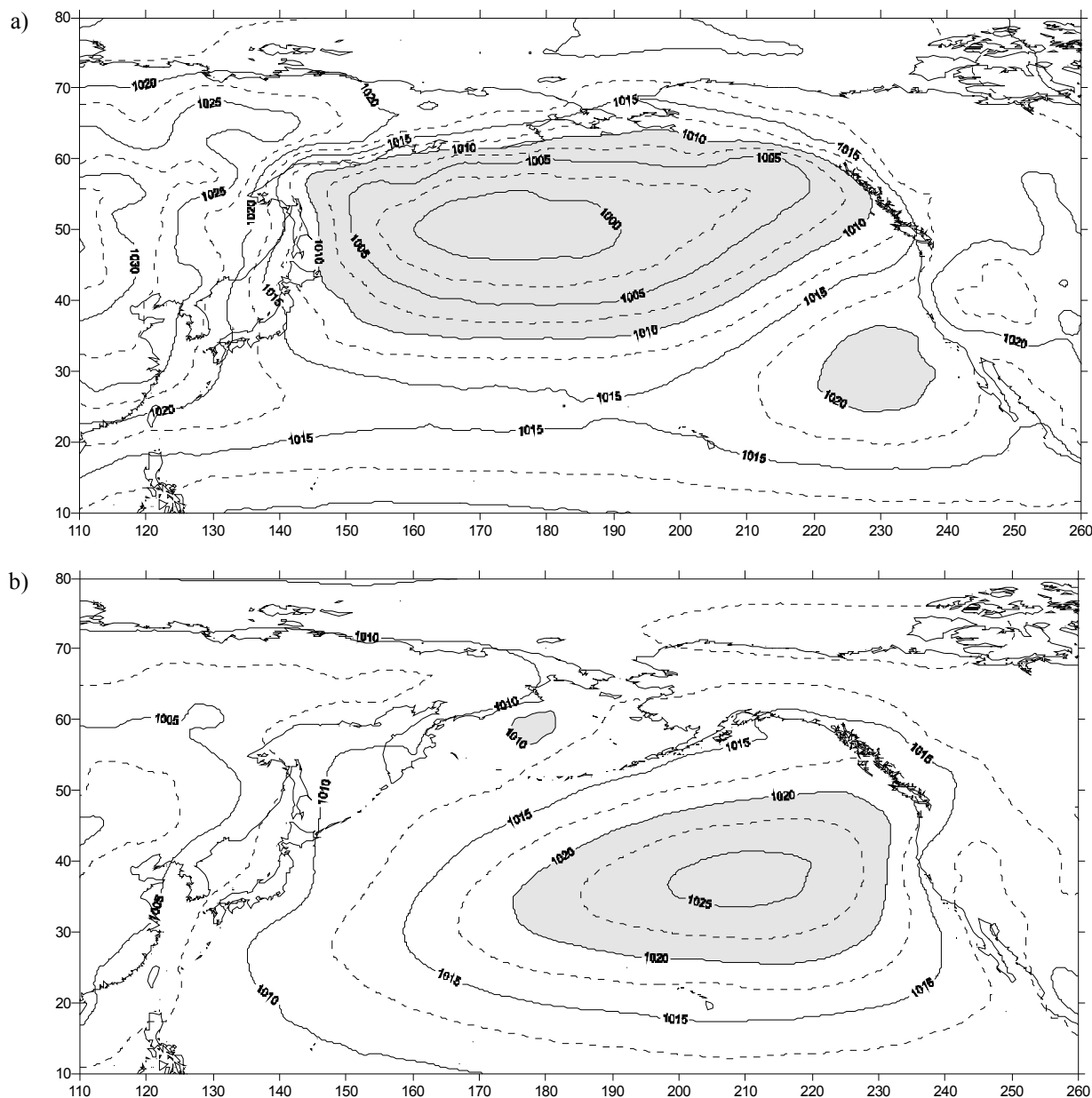


Figure 1. Schematic map of the analyzed COA areas in winter (a) and summer (b)

$$S = \frac{1}{2} \left(\begin{matrix} x_1 & y_1 \\ x_2 & y_2 \end{matrix} + \begin{matrix} x_2 & y_2 \\ x_3 & y_3 \end{matrix} + \dots + \begin{matrix} x_n & y_n \\ x_1 & y_1 \end{matrix} \right), \quad (1)$$

where:

- $x = 6378137 * \lambda;$
- $y = 6363876.615 * \sin \varphi;$
- λ – is a point longitude;
- φ – is a point latitude.

WGS84 ellipsoid has been taken as a geoid.

Multiyear variability of the COA parameters has been analyzed by the average COA data of the calendar seasons (winter, spring, summer, and fall). Average multiyear values have been calculated for the whole studied period.

MULTIYEAR VARIABILITY OF THE COA PARAMETERS

Since on climatological charts the centers of action show the real prevalence of baric systems of the same sign, they allow estimating weather patterns that are specific for a given region. The shift of the centers and the change of their intensity influence the spread of planetary air currents and result in the change of climate of both the whole North Hemisphere and its specific regions.

Pressure and coordinates. Winter and spring are two remarkable seasons in the multiyear variability of the COA parameters (pressure, latitude, longitude). Over the last 56 years these seasons were characterized by the pressure drop in both centers (Figure 2, hereinafter only statistically significant trends are discussed), the shift of North Pacific High

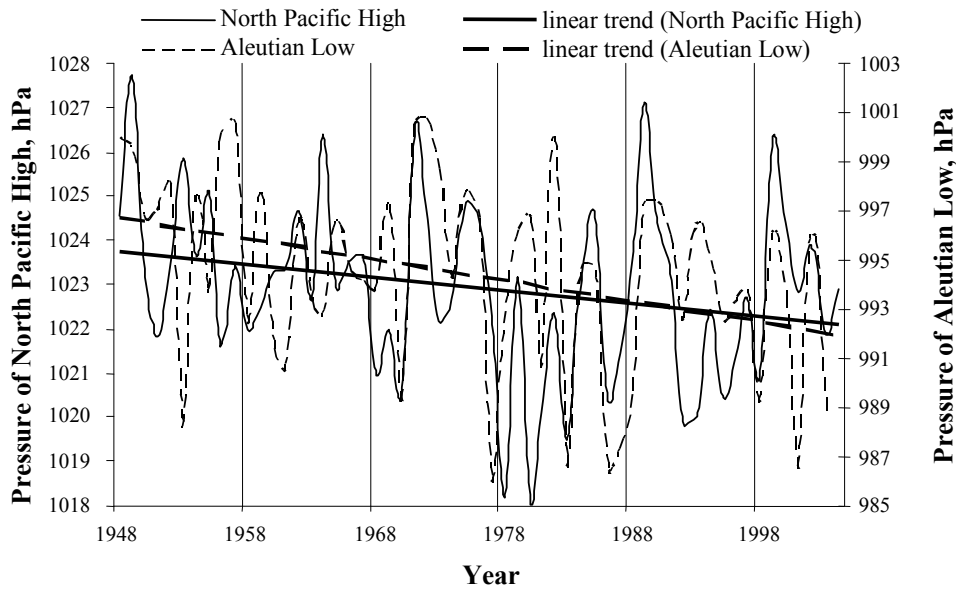


Figure 2. Multiyear variability of pressure in two main North Pacific centers of action in winter

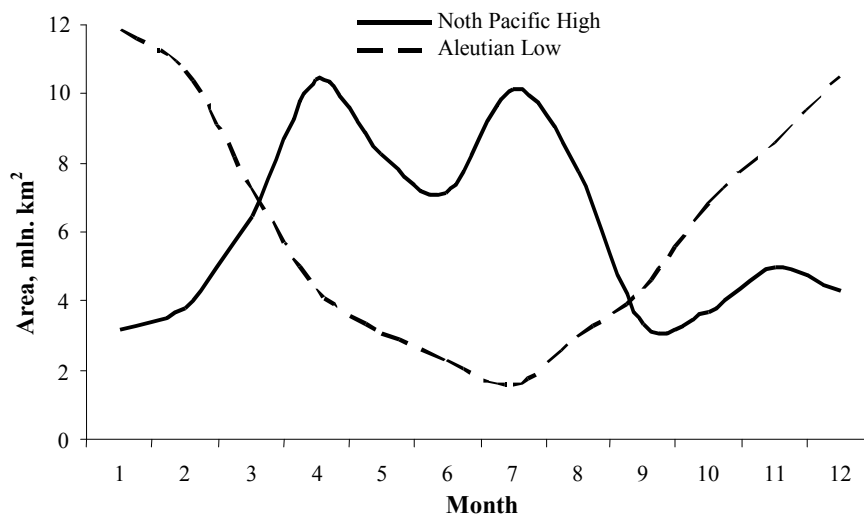


Figure 3. Variability of average multiyear area of two main North Pacific centers of action during the course of the year

southward, and the shift of both centers westward. The most abrupt changes in the multiyear variability of the COA parameters were registered in 1970s.

As was shown before, subtropical highs were driven away to the south at the intensive zonal circulation (Baydal and Neushkin, 1990). Southward shift of North Pacific High is probably related to the strengthening zonal circulation observed in the moderate latitudes of the North Hemisphere recently (Gillett *et al.*, 2000; and others).

It is remarkable that multiyear pressure patterns in Aleutian Low in winter–spring and summer–fall periods are opposite.

Area of COA. North Pacific High. During the course of the year the average monthly area of North Pacific High changes from 3.2 to 10.4 mln. km² (Figure 3).

The largest areas are observed in April (primary maximum) and July (secondary maximum) and the third small maximum is marked in November. On average, the area limited by the 1020 hPa isobar covers about 30% of the analyzed area. In some years in summer the area of North Pacific High may amount to 20 mln. km², covering more than 70% of the analyzed area. There are some winters, however, when North Pacific High is not seen within the 1020 hPa isobar at all.

In order to have comparable areas of both centers of action, we used normalized values of the COA area, hereinafter referred to as “relative area”. Multiyear variability of the COA areas was described as a deviation from a mean multiyear area of the center.

Multiyear variability of the relative area of North Pacific High is not the same in different seasons. The

COA area exceeding the average multiyear one was observed in winter – in 1950s, 1960s, late 1980s and in the beginning of the present millennium (Figure 4); in spring – in middle 1960s and 1970–80s; in summer – in 1950s and in the beginning of the present millennium; and in fall – in 1960s, 1970s and late 1980s.

The COA area smaller than the average multiyear one was observed in winter and fall in early 1980s and in winter and spring – in middle 1990s. Reduction of the area of North Pacific High was also marked in all the seasons in late 1960s, however, in spring this reduction was not significant (Figure 4).

Statistically significant trends have not been revealed in the multiyear variability of the relative area of North Pacific High. Small reduction in the area of the center was observed in winter and spring only (except for March, when the trend is statistically significant). Almost no changes have been observed in the area of the center in summer and fall during the last 56 years.

The last decade has been characterized by an abrupt shift of the center of action northward in early 1990s and then back southward, as well as by the growing area of the center.

Aleutian Low. During the course of the year the average monthly area of Aleutian Low changes from 1.3 to 11.8 mln. km². Maximum area of the center is observed in January, whereas minimum one – in July (Figure 3). In some years in winter the area of Aleutian Low may amount to 20 mln. km². In January it may cover more than 90% of the analyzed area. There are some years, however, when the 1010 hPa isobar is not seen at all during the warm season.

Multiyear variability of the relative area of Aleutian Low is not the same in different seasons. During the last 56 years (1948–2003) the area of the center was increasing in winter and spring, especially starting from 1970s, and decreasing in summer and fall, especially during the last 30 years (Figure 5).

Since both centers are two main pressure zones in the northern Pacific, the periods with similar changes in the areas of both centers appear to be of great interest. Pressure gradients between the centers grow when the areas of both centers increase, and drop – when the areas of both centers decrease. Increasing areas of both centers were observed in winter – in early 1960s; in spring and summer – in early 1970s–early 1980s; and in fall – in late 1950s–early 1960s and in late 1990s. Decreasing areas of two centers were marked in spring in early 1970s.

DEPENDENCE OF THE AREA OF COA ON OTHER COA PARAMETERS

Dependence of the COA area on its intensity and location seems rather interesting. Analysis of correlation of the COA area and other COA

parameters (coordinates, index of COA anomaly (Smolyankina, 1999)) has revealed that the areas of North Pacific High and Aleutian Low are largely dependent on the pressure inside. As a rule, the higher is intensity of the pressure zone, the bigger is its area (The manual..., 1965; Vasilevskaya *et al.*, 2000). At the same time, the areas of North Pacific High and Aleutian Low increase when the centers shift westward of their mean multiyear position, which is especially evident in winter and spring, and less evident – in summer. Moreover, the area of North Pacific High increases when the center shifts northward. Synchronous significant correlation coefficients are marked between the area of the center and its index ($|r| = 0.5–0.8$), North Pacific High having a higher correlation than Aleutian Low.

DEPENDENCE OF THE AREA OF COA ON ENSO INDICES

Climate researchers pay much attention to the large-scale changes in atmosphere-ocean circulation. El Niño/Southern Oscillation (ENSO) is one of such phenomena, which influences weather conditions in many parts of the world. When the ENSO influence on the North Hemisphere atmosphere is studied, centers of actions are used as indicators. We studied dependencies of the relative areas of two North Pacific centers of action on some ENSO indices: SOI (Southern Oscillation Index – pressure difference between Haiti Island and Darwin Port) and Niño3 (sea surface temperature anomaly (SSTA) in the area of 5°N–5°S, 90–150°W). Data have been kindly provided by Trusenkova O.O. (POI FEBRAS).

We paid most attention to winter, as this is the ENSO-typical season. Correlation analysis has revealed a synchronous direct relation of the area of North Pacific High and SOI ($|r| = 0.4–0.6$), and a synchronous inverse relation of the area of the center and Niño3 ($|r| = 0.4–0.6$). Aleutian Low has been characterized by weaker and opposite correlations (an inverse relation with SOI and a direct relation with Niño3).

As was shown before (Wyrтки, 1982; and others), high SOI values correspond to the intensification of South Pacific High (growing intensity and area), strengthening of trade winds and the cold Peruvian current, strong equatorial upwelling, and formation of the negative sea surface temperature anomalies in the eastern equatorial Pacific. When South Pacific High diminishes (low SOI values), ENSO phenomenon develops. These dependencies show that intensity and area of North Pacific High fall at the moments of ENSO. As a result, Californian current weakens (Kort, 1970), and sea surface temperature anomalies in the equatorial-tropical part of eastern Pacific become positive. Thus, the fact that ENSO causes a synchronous atmospheric circulation breakdown going far beyond the South Hemisphere is confirmed once again.

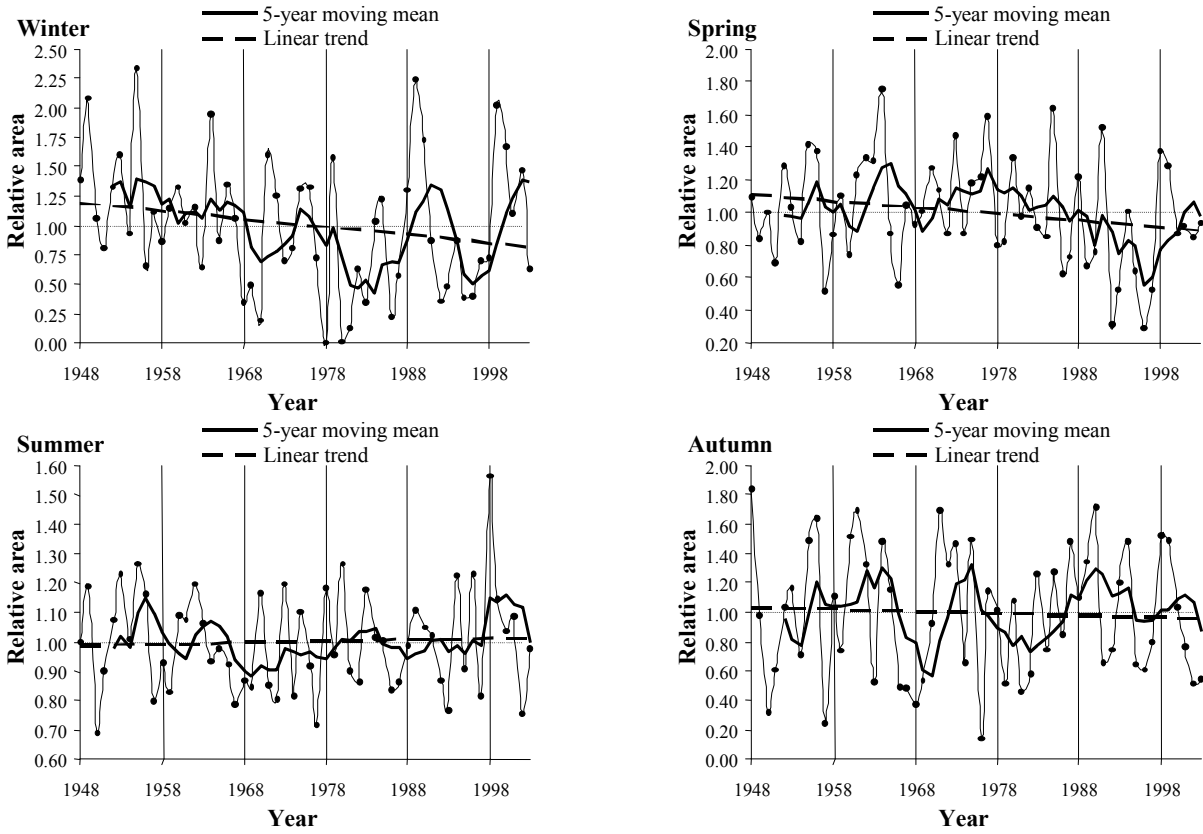


Figure 4. Multiyear variability of the relative area of North Pacific High

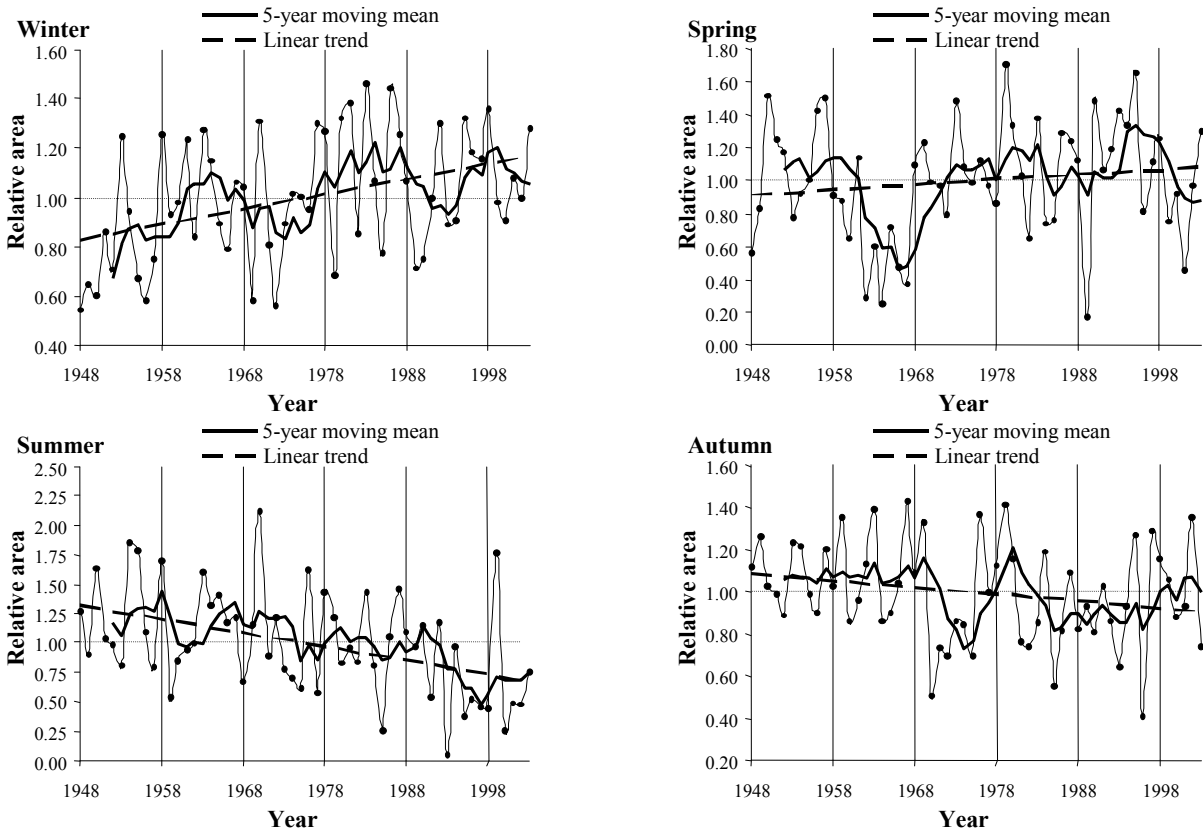


Figure 5. Multiyear variability of the relative area of Aleutian Low

CONCLUSIONS

The study of pressure and coordinates of two main North Pacific centers of action has revealed the deepening of Aleutian Low and increase in its area in winter and spring during the last 56 years. This testifies to the strengthening of cyclonic activity in the moderate latitudes of the northern Pacific. North Pacific High has been weakening and shifting southward. The patterns revealed for both centers are in a good accord with the strengthening zonal circulation observed in recent years (Gillett *et al.*, 2000; and others).

The highest variability of the COA parameters is observed in winter and spring, Aleutian Low being more variable than North Pacific High at that.

The turning point of 1970s, which is typical for the North Hemisphere atmospheric circulation, showed the gradual pressure drop in both centers, shift of North Pacific High southward, shift of both centers westward, and simultaneous increase in the area of both centers of action.

ACKNOWLEDGEMENTS

The authors express their sincere gratitude to Professor Dashko N.A. and Professor Tunegolovets V.P. for their valuable comments and suggestions.

REFERENCES

- Apasova E.G. 1979.** About location of centers of action. Proceedings of RIHMI-WDC. Issue 58, pp. 89–98. (In Russian).
- Balashova E.V. 1986.** Interannual variability and patterns of centers of action in the tropical and subtropical latitudes of the Atlantic Ocean. Proceedings of RIHMI-WDC. Issue 122, pp. 56–70. (In Russian).
- Baydal M.H. 1986.** Circulation parameters of climate before and after 1930s. Proceedings of RIHMI-WDC. Issue 129, pp. 107–111. (In Russian).
- Baydal M.H., Neushkin A.I. 1990.** Multiyear variability and conjugation of oceanic centers of action. Proceedings of RIHMI-WDC. Issue 153, pp. 60–64. (In Russian).
- Dashko N.A., Varlamov S.M. 2003.** Hydrometeorology and hydrochemistry of seas. Vol. 8. The Japan Sea, Part 2: Meteorology and climatology. St.P.: Hydrometeoizdat, pp. 18–102. (In Russian).
- Gillett N.P., Hegerl G.C., Allen M.R., Stott P.A. 2000.** Implications of changes in the Northern Hemisphere circulation for the detection of anthropogenic climate change. *Geophys. Res. Lett.*, 27, № 7, pp. 993–996.
- Korn G., Korn T. 1984.** Mathematics guide. Moscow: Nauka. 832 p. (In Russian).
- Kort V.G. 1970.** On the large-scale interaction between the ocean and the atmosphere. *Oceanology*. Vol. X, Issue 2, pp. 222–239. (In Russian).
- Map projections. 1994.** Moscow: Date+, ltd. (In Russian).
- Minobe S. 1999.** Resonance in bidecadal and pentadecadal climate oscillation over the North Pacific: Role in climatic regime shifts. *Geophys. Res. Lett.* 26, № 7, pp. 855–858.
- Smolyankina T. 1999.** Multi-year variability of pressure, latitude and longitude anomalies of atmospheric action centers in Asian-Pacific region. FERHRI Special Issue. Vladivostok: Dalnauka, № 2, pp. 10–16. (In Russian).
- The manual on short-term weather forecasts. 1965.** Leningrad: Hydrometeoizdat, Part 3, Vol. 4, pp. 18–25. (In Russian).
- Trenberth K., Caron J., Stepaniak D.P., Worley S. 2002.** Evolution of ENSO and global atmospheric surface temperatures. *J. Geophys. Res. D.*, 2002, 107, № 7–8, pp. AAC/1–AAC/19.
- Vasilevskaya L.N., Zhuravleva T.M., Man'ko A.N. 2000.** Long-term changes of parameters of the Siberian anticyclone and their connection with varieties of the forms of atmospheric circulation. Abstracts of Workshop “Global change studies in the Far East”, Vladivostok, September 11–15, pp. 50–51.
- Wyrtki K. 1982.** The southern oscillation, ocean-atmosphere interaction and El Niño. *J. Mar. Technology Soc.* Vol. 16, №1, pp. 3–10.

INTRA-ANNUAL BUNDLES OF CLIMATIC PARAMETERS

V.A. Svyatukha¹, G.Sh. Tsitsiashvili¹, T.A. Shatilina², A.A. Goryainov²

¹ Institute of Applied Mathematics, Far Eastern Branch of Russian Academy of Sciences (IAM FEBRAS), Russia

² Pacific Fisheries Research Centre (TINRO-Centre), Russia

Email: tinro@tinro.ru

A new approach to the choice of information indicators of climate (atmospheric pressure near the earth surface, in the middle troposphere and near-ground air temperature) that is based on visual estimation of intra-annual bundle fluctuations of climatic parameter trajectories is proposed. Disclosure of intra-annual bundles of climatic parameters provided the opportunity to develop a unique algorithm for the extreme conditions recognition.

The possibility to forecast dramatic events has been studied over dynamics of the attendant feature. Operation of the proposed algorithm is described on the example of recognition of "critical" levels of the Asian pink salmon catch in different fishery regions in the Far Eastern seas.

It is concluded that the suggested method can be used for the forecast of extreme conditions in the natural processes.

INTRODUCTION

Regressive models describing mainly the averaged dynamics, and not the skips (the term of random process theory) over a high level, are the general mathematical methods that are used to forecast hydrometeorological phenomena in the Russia Far East. Statistic processing of temporal series is fulfilled by the standard techniques that have a few defects. They are not capable of revealing critical moments (anomalies) and natural cycles clearly enough (possibly, wrong). Almost all the forecasts based on the correlation between environment parameters are of low reliability (not more than 50–60%). Especially it concerns the forecast of anomalous (disastrous) hydrometeorological processes that produce great economic damage.

As a result, the necessity to use other mathematical methods for the forecast of extreme climatic events is in urgent demand.

The present work offers a new approach to the choice of climatic indicators (atmospheric pressure near the Earth surface and in the middle troposphere and surface air temperature) that is based on visual estimation of fluctuations in the intra-annual bundles of climatic parameter trajectories.

DATA

Average monthly data on the surface atmospheric pressure in the points of regular 5° grid for 1960–2000 placed at the web page of NOAA-CIRES Climate Diagnostic Center <http://www.cdc.noaa.gov/PublicData> and geopotential H_{500} at 19 aerological stations of the Russia Far East located along the perimeter of the Japan and Okhotsk Seas and the Kuril islands during 1950–1989 have been used as initial data. Additionally, data on the surface air temperature in Vladivostok and Terney provided by Primorsky Hydromet office for 1942–1992 and data on the catch

of Asian hunchback salmon during 1950–1989 have been attracted (Yanovskaya *et al.*, 1989; Summary on salmon fishery catch..., 1995, 1998, 2000).

Analysis of interannual dynamics of climatic parameters testifies to their chaotic character that is hardly subject to the correct statistic analysis (since the temporal series is very short). The average annual change of surface pressure in Vladivostok is shown in Figure 1 as an example.

Analysis of intra-annual change of climatic parameters turned out to be more interesting and significant for their mathematic interpretation and development of extreme phenomena forecasting techniques.

Thus, Figure 2 shows variability of H_{500} geopotential above Vladivostok and Okhotsk during the course of the year for the long period (1950–1989). It is clear that intra-annual H_{500} change for the long-term period forms a distinct bundle of trajectories, *i.e.* has a small scatter of magnitudes (about 5 dkm). Intra-annual change of H_{500} geopotential at all the aerological stations, including offshore ones, has the same features. It is evident that intra-annual dynamics of average monthly values of geopotential H_{500} has a clearly defined trend at the background of small fluctuations (their amplitude is one order less than the

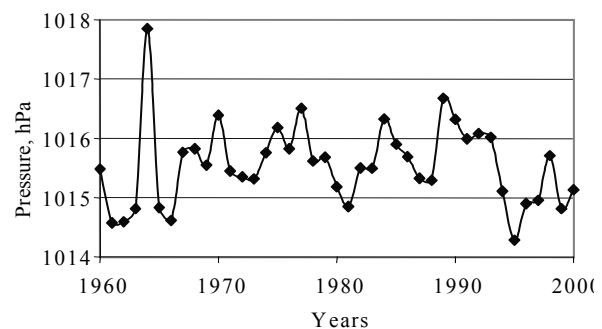


Figure 1. Average annual run of near-ground pressure in Vladivostok during 1960–2000

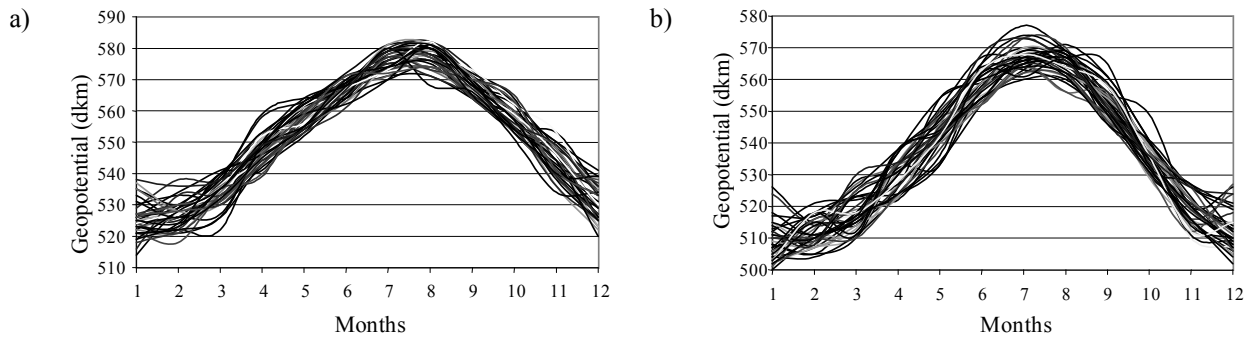


Figure 2. Intra-annual dynamics of H_{500} geopotential during 1950–1989 in: (a) Vladivostok, (b) Okhotsk

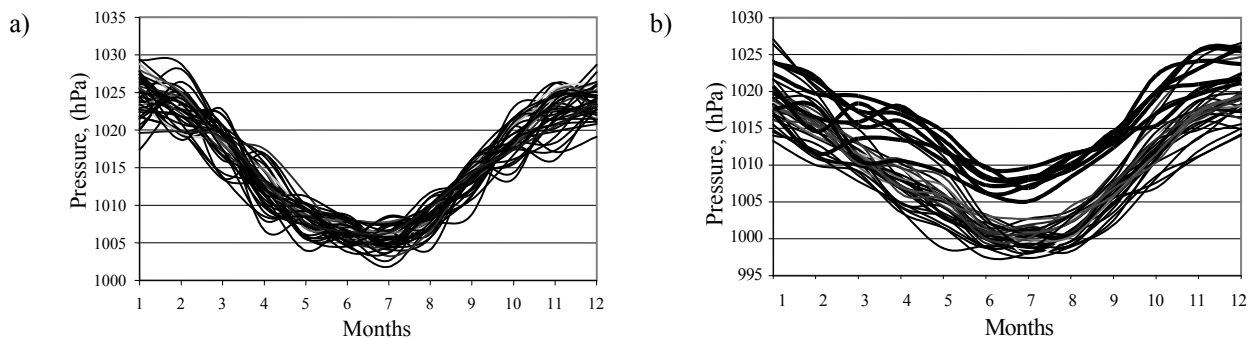


Figure 3. Intra-annual run of near-ground pressure during 1960–2000 in: (a) Vladivostok, (b) center of South-Asian depression (30°N, 90°E)

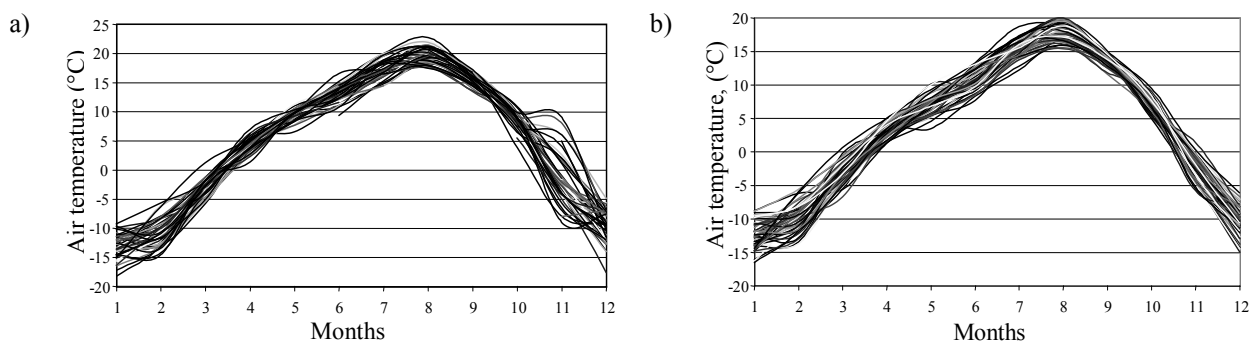


Figure 4. Intra-annual run of air temperature during 1942–1990 in: (a) Vladivostok, (b) Terney

trend amplitude). It can be concluded for sure that intra-annual dynamics of average monthly H_{500} values is repeated every year and produces rather a distinct bundle as a result. Statistical data samples increase from 40 (interannual dynamics) to 480 (for all months of a year).

Intra-annual dynamics of the near-ground pressure field has the same type only above the continental regions of Asia and coast of the Sea of Japan, *i.e.* above the regions of clear exposure of the Far East monsoon. It should be noted also that intra-annual run of atmospheric pressure near the surface and in the middle troposphere (at a 5000 m height) is in anti-phase, which is explained by widely known regularities of the synoptic processes evolution near the surface and at a certain height. Unlike the intra-annual change of H_{500} geopotential, the intra-annual run of near-ground

pressure above the seawater areas varies significantly and does not form a distinct resultant bundle.

Figure 3a shows an example of intra-annual run of near-ground pressure above Vladivostok during 1960–2000. It is evident that the width of this bundle is within 5 hPa (the feature, which has a small scatter). Figure 3b shows the intra-annual run of near-ground pressure in the center of Asian depression (30°N, 90°E) during the same period. Two periods are distinguished that produce different levels of near-ground pressure, namely, 1960–1993 with low pressure and 1994–2000 (bold lines) with high pressure. It also should be marked that two different bundles are distinctly distinguished in the center of Asian depression (center of action in atmosphere) only. It possibly means that at the edge of 1993–1994 the epoch climatic changes occurred.

The distinct bundles of intra-annual run of near-ground air temperature, which is a thermal indicator of climatic changes, have been found. Figure 4 shows an example of intra-annual run of near-ground air temperature in Vladivostok and Terney (North Primorye) during 1942–1992. It is remarkable that intra-annual change of near-ground air temperature coincides with intra-annual change of H_{500} geopotential that is a dynamic parameter of atmosphere. It is also known that the middle troposphere is an energetic level of atmosphere.

METHODS OF INVESTIGATION

Revealing intra-annual bundles in the climatic parameters (H_{500} geopotential, near-ground pressure, air temperature) gave a chance to develop the algorithm for the extreme situations recognition. The possibility to forecast dramatic events has been investigated according to the dynamics of indicators of a coupled feature. Figure 5 shows the algorithm of the decisive rule development for recognition of dramatic events. Upper diagram demonstrates dynamics of the main feature that is subject to a high intra-annual variability (ice cover of seas, catch of Asian hunchback salmon in the local areas, precipitation, *etc.*) When choosing the critical level that is specific for the main feature, we mark with “x” sign those moments of time, when dynamics trajectory of the main feature exceeds the established level (*i.e.* the anomaly moments of deviation). In our calculations the frequency of the exceeded criterion level was no more than 10%. The rest of moments of time are marked by “0” sign. Then we analyze dynamics of the attendant

feature that is characterized by the small scatter of intra-annual variations (pressure on isobaric surface 500 hPa, near ground pressure and air temperature, *etc.*) Then the magnitudes of the attendant feature during “dramatic” moments of time (marked by “x”) are projected to the axis of ordinates and minimum B and maximum A values of the attendant feature are found. The next step is to develop a rule of recognition of a certain moment of time belonging to the critical level according to the belonging of the attendant feature to a section [A, B]. If during a non-dramatic moment of time the attendant feature is found in the section [A, B], then the given moment will be mistakenly attributed to the critical one. This procedure is generalized by finding a separate critical section for each attendant feature. Thus, belonging of a certain moment of time to the critical one will be identified according to the belonging of each of attendant features to their own critical sections.

This task satisfactorily meets demands for decision within the following model on the images recognition.

The algorithm of recognition of extreme events was applied to forecast extreme ice cover in the Okhotsk Sea (Tsitsiashvili *et al.*, 2002).

May the curves $X(t) = (X_j(t-1), j = 1, \dots, 12)$ of average monthly dynamics of H_{500} geopotential during a year $t-1$ that is preceding to the year t from a set of observed years T be the objects and the expression $\{X(t), t \in T_1\}, \{X(t), t \in T_2\}$, where T_1 is the combination of years with maximum (minimum) ice cover $T_2 = T - \text{addition } T_1 \text{ to } T$, be the classes of those objects.

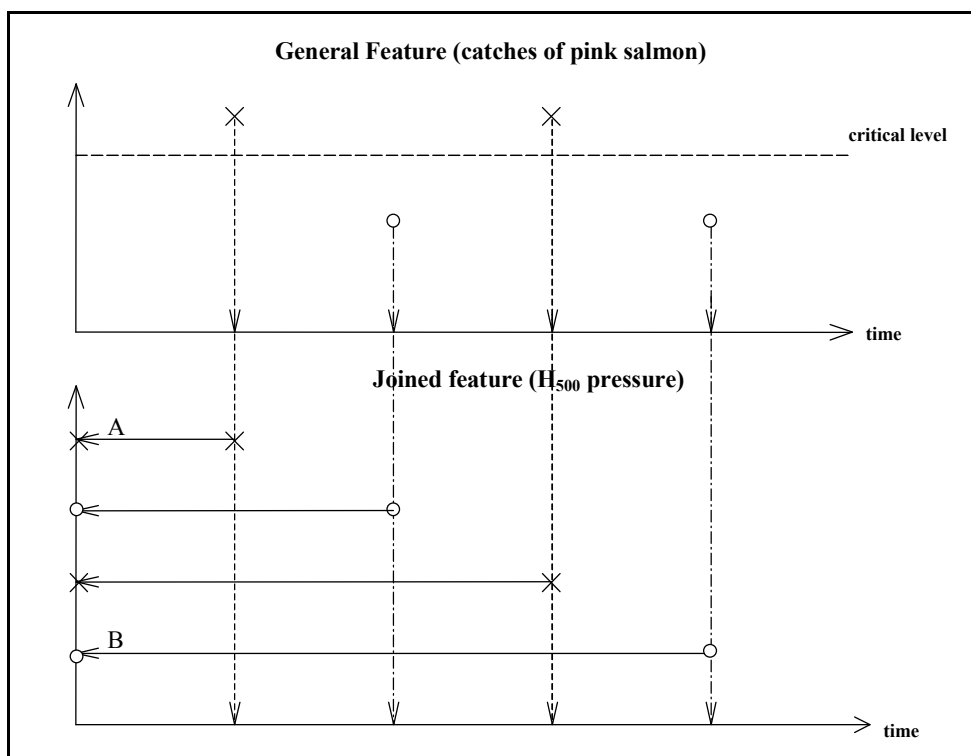


Figure 5. Construction of lines [A, B] recognizing excess by general feature of critical level

At a first glance, such a formulation of task looks traditional for the images recognition, however, a new element is introduced here consisting of the class of extreme (maximum or minimum ice area) years.

The peculiarity of a new method is the choice of the following condition as the simplest decision rule for attribution of an object ($y_j, j = 1, \dots, 12$) to class T_1 :

$$a_j \leq y_j \leq b_j, j = 1, \dots, 12, \quad (1)$$

where:

$$a_j = \min(x_j(t-1), t \in T_1);$$

$$b_j = \max(x_j(t-1), t \in T_1).$$

In other terms, the object ($y_j, j = 1, \dots, 12$) is attributed to T_1 class, if the corresponding trajectory of average monthly dynamics during the course of the year gets within the bundle of trajectories corresponding to pre-extreme years. This version of the decision rule is unique for recognition of extreme environmental conditions by the data available.

The given decision rule is based on the ideas of interval mathematics and can be very quickly calculated by a computer. The quality of the proposed decision rule will be characterized by the rate of mistakes of the first and second type within the initial data sample $\{X(t), t \in T\}$.

A mistake of the first (second) type means a wrong identification of extreme (non-extreme) year in the initial data sample. Proposed decision rule provides the estimation of frequency of mistaken identification guaranteed from data omission (Bolotin and Tsitsiashvili, 2003).

DISCUSSION OF RESULTS

Our calculations based on the 40-year data on H_{500} geopotential with 4 years of anomalously high ice cover in the Okhotsk Sea as observed at 5 stations, namely, Okhotsk, Petropavlosk-Kamchatsky, Blagoveshensk, Kharbin, Tateno (Japan), have shown that this frequency at every station equals zero. It means that it is possible to introduce a summarized decision rule for the identification of years of maximum ice formation that would consist of the observance of inequality (1) by data obtained from at least one of 5 chosen stations. Here, the rate of mistakes of the first and second type will again be equal to zero.

So, if the average monthly climatic parameters (near ground pressure and air temperature, geopotential) during one year (two years) belong to the trajectory bundles shown in Figures 2–4, then the same features will belong to the narrower bundles during the critical years. The fact of belonging of the curve of intra-annual run of average monthly parameters to the narrow bundles is just a condition for the forecast of dramatic events.

The main entity of salmon fishery in the Russia Far

East is pink salmon, which share takes no less than 40% of the total catch (Shuntov, 1994). This species has been thoroughly studied for a long time, however, accurate forecasting of salmon catch faces a regular failure in practice every year. One of the reasons of poor fishery forecasts (and not for salmon only) is linked to the fact that dynamics of pink salmon catch is characterized by a strong or chaotic variability, namely, it is greatly different from the intra-annual run of the above-mentioned climatic parameters (being a feature undergoing significant scatter in intra-annual variability). For example, pink salmon catch near western Kamchatka can fluctuate from several hundreds to tens of thousand tons.

Let us consider the operation of our proposed unique algorithm for recognition of a “critical” level in the Asian salmon catch in different fishery regions of the Far Eastern seas according to the H_{500} geopotential data (other climatic parameters were not considered in the work).

Figure 6 shows results of the quality of the “critical” level recognition in the catch of Asian pink salmon in the fishery regions of the Far Eastern seas (North-Okhotsk, Amur, Primorye, East Kamchatka, West Kamchatka, East Sakhalin, South Kurils) according to the H_{500} geopotential data from 19 aerological stations of the Russia Far East placed along the perimeter of the Japan and Okhotsk Seas (which characterize climate above the fishery regions) during January–December of 1950–1989. Each station of a separate year is characterized by the set of average monthly values of H_{500} . Y axis shows the number of stations, where 100% correct recognition of excess of the assigned level of pink salmon catch according to data on H_{500} geopotential during two previous years is found.

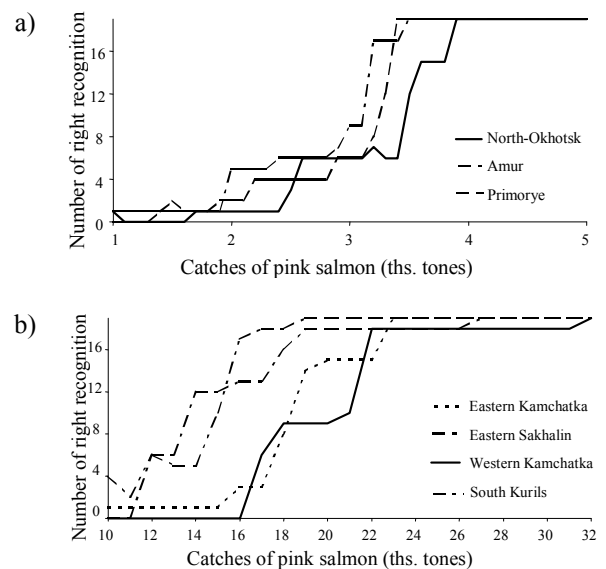


Figure 6. Quality of recognition of a critical level in the pink salmon catches over different Far Eastern fishery regions dependence on the number of right recognition aerological stations of H_{500}

For example, in West Kamchatka the number of stations with 100% correct recognition of the salmon catch exceeding 22,000 tons amounts to 18 (almost all stations), the number of critical years is equal to 8. In case of the pink salmon catch exceeding 32,000 tons, all 19 stations produce 100% correct recognition (Figure 6b), the number of critical years is 5.

CONCLUSION

Disclosure of intra-annual bundles of some climatic parameters gave the opportunity to develop a unique algorithm for recognition of extreme natural phenomena. The possibility to forecast disastrous

phenomena (a feature possessing the great scatter of intra-annual variations) by the dynamics of the attendant feature with a small scatter of values was shown to be possible.

Application of the proposed algorithm for recognition of “critical” levels in the Asian pink salmon catch (during two precedent years) and ice cover in the Okhotsk Sea has shown that the method proposed can be used to forecast extreme hydrometeorological processes and anomalous catch of the Asian pink salmon.

REFERENCES

- Bolotin E.I., Tsitsiashvili G.Sh. 2003.** Spatial-temporal prognostication in functioning of center of mite encephalitis infection. News of FEBRAS. 2003. N 1. pp. 5–19. (In Russian).
- Shuntov V.P. 1994.** New data on marine stage of life of Asian pink salmon. News of TINRO. Vol. 116, pp. 3–41. (In Russian).
- Summary on salmon fishery catch (Russian Federation) 1995.** Fish industry. No. 6. 31 p. (In Russian).
- Summary on salmon fishery catch (Russian Federation) 1998.** Fish industry. No. 6. 28 p. (In Russian).
- Summary on salmon fishery catch (Russian Federation) 2000.** Fish industry. No. 6. 27 p. (In Russian).
- Tsitsiashvili G.Sh., Shatilina T.A., Kulik V.V., Nikitina M.A., Golycheva I.V. 2002.** Modification of method of interval mathematics applicable to the forecast of extreme ice cover in the Okhotsk Sea. News of FEBRAS, No. 4. pp. 111–118. (In Russian).
- Yanovskaya N.V., Sergeeva N.N., Bogdan E.A. et al. 1989.** Catch of Pacific salmon, 1900–1986. Moscow: VNIRO. 213 p. (In Russian).

FLUXES AND BALANCE OF ^{210}Pb IN THE NORTHWESTERN JAPAN SEA

S. Otosaka¹, M. Baba², O. Togawa¹, E.V. Karasev³

¹ Marine Research Laboratory, Japan Atomic Energy Research Institute (JAERI), Japan
Email: otosaka@popsvr.tokai.jaeri.go.jp

² Mutsu Marine Laboratory, Japan Marine Science Foundation (JMSF), Japan

³ Far Eastern Regional Hydrometeorological Research Institute (FERHRI), Russia

A sediment trap experiment was carried out in the western Sea of Japan (Station MS: 41°16'N, 132°21'E, water depth 3424 m). Lead-210 (^{210}Pb) and major components (biogenic opal, biogenic carbonate, organic matter and aluminum) in settling particles were measured. Large (>1000 mg/m²day) mass fluxes derived from the production of diatoms were observed in spring (March–April). Although fluxes of ^{210}Pb were also large in spring, the pattern of seasonal variation of ^{210}Pb flux did not coincide with that of total mass flux. The flux/production (F/P) ratio of ^{210}Pb showed a positive correlation with aluminum flux. However, strong relationship between F/P ratio and biogenic (such as opal and carbonate) fluxes was not observed. At both depths, a strong correlation between F/P ratio and biogenic flux was observed during low-productive season (opal flux <100 mg/m²day). F/P ratio of ^{210}Pb decreased with depth and the vertical decrease of F/P ratio could be explained by 3 processes, (1) removal and vertical transport of ^{210}Pb from the surface layer by settling particles, (2) decomposition of particles in the deep layer, and (3) export by the deep current. F/P ratios of ^{210}Pb at 2746 m depth were large in winter and spring. The large F/P ratio in this season could be caused by the horizontal import of coastal seawater to the bottom layer of the Station MS. It was suggested that seasonal variation of particulate ^{210}Pb flux at the deep layer in the western Japan Basin indicated the formation of the deep water in this area.

INTRODUCTION

The Sea of Japan is a marginal sea, which is separated from the North Pacific by Japan Islands and Sakhalin. The exchange of seawater between the Sea of Japan and the Pacific Ocean is restricted by 4 shallow (<130 m) straits, the Tsushima, the Tsugaru, the Soya and the Mamiya straits. On the other hand, the Japan Sea has deep (>2000 m) basins and the deep part of the Japan Sea (>200 m) is occupied by remarkably uniform deep water, which is characterized by relatively low temperature (0.1–0.3°C) and low salinity (34.0–34.1‰). The deep water is called the Sea of Japan Proper Water (JSPW: Uda, 1934). It is suggested that the concentration of dissolved oxygen in the JSPW has decreased since 1960s because deep convection is weakened as a result of global warming (Gamo, 1999; Minami *et al.*, 1999). Recent studies revealed the renewal of the bottom water in the western Sea of Japan (Senjyu *et al.*, 2002; Tsunogai *et al.*, 2003).

Natural radionuclides such as lead-210 (^{210}Pb), thorium-230 (^{230}Th) and protoactinium-231 (^{231}Pa) are broadly used in order to investigate the scavenging processes of particle-reactive substances from the water column (Harada and Tsunogai, 1986a; Biscaye *et al.*, 1988; Heussner *et al.*, 1990; Biscaye and Anderson, 1994; Colley *et al.*, 1995). The main advantage of these tracers, as opposed to stable isotopes, is that their source is reasonably well defined. For example, ^{210}Pb ($t_{1/2} = 22.3$ year) is supplied to the water column by the radioactive decay of its great-grandparent radium-226 (^{226}Ra) in the water column and by deposition from the atmosphere.

Studies of ^{226}Ra – ^{210}Pb series in marine environment have revealed the short-term (decade to century time scale) removal of ^{210}Pb by particles and boundary scavenging in the deep sea (Moore and Dymond, 1988; Legeleux *et al.*, 1996; Borole, 2002; Yamada and Aono, 2003).

In this study, a sediment trap experiment was carried out in the western Sea of Japan, and concentrations of ^{210}Pb and major components (organic matter, biogenic opal, biogenic carbonate and aluminum) of settling particles were analyzed. The aims of this study are (1) to estimate the relative importance of vertical and horizontal transport by drawing up a ^{210}Pb mass balance, (2) to determine factors that control the removal of particle-reactive substances from the water column, and (3) to assess the influence of the bottom water formation on the particulate ^{210}Pb sink or source in the study area.

METHODS

Sampling. A mooring array with time-series sediment traps was deployed in the western Japan Basin (Station MS: Figure 1). Sediment traps were moored at 927 m and 2746 m depths. Each sediment trap (Nichiyu, SMD-26S) had a cone-shaped sampling aperture of 0.515 m² covered by a 2 cm meshed baffle and was equipped with 26 sample cups. Deployment and recovery of the mooring system were carried out by R/V “Professor Khromov” (FERHRI, Russia).

Samples of settling particles were collected for 52 periods between August 2000 and July 2002 at

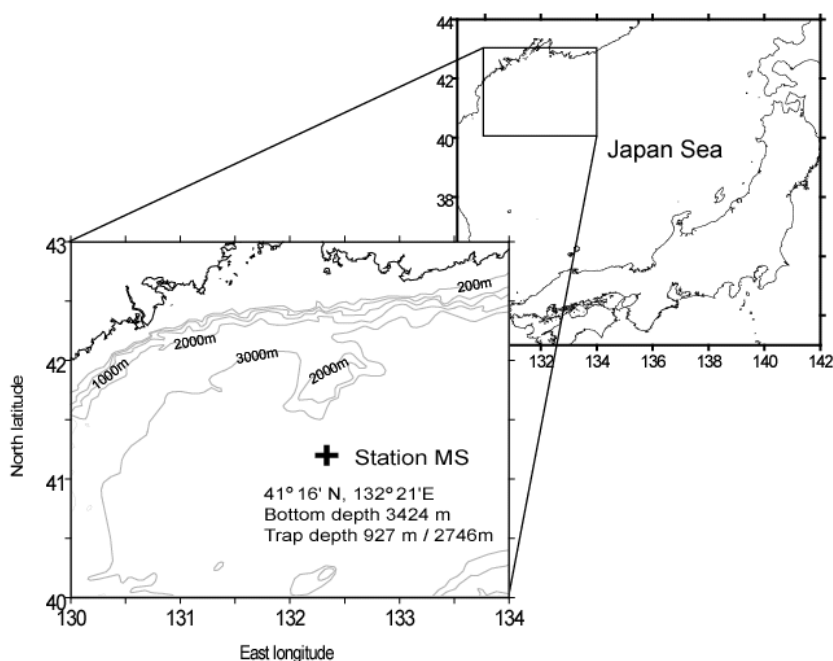


Figure 1. Sampling location

14–15 days intervals. Sampling cups were filled with 38 ppm salinity-controlled 5% formalin neutral buffer solution to prevent biological degradation. Samples were stored in a refrigerator at 5°C until filtration.

Chemical analysis. Settling particles in each sampling cup were filtered by a 0.6 µm membrane filter after picking out “swimmers”. Particles on the filter were dried at 60°C for 36 hours and weighed. Sediment samples were also dried at 60°C.

Activity of ^{210}Pb in the samples was measured by γ -ray spectrometry. Specific γ -ray emission of ^{210}Pb (46.5 keV) was measured by a low-energy photon detector (SEIKO EG&G ORTEC, LoAXTM-51370) with a multi-channel analyzer (SEIKO EG&G ORTEC, 7800). As a reference material, IAEA-368 was used.

Aliquot dried samples of 20–50 mg were ignited at 500°C for 24 hours. The loss of weight (CF: combustible fraction) was assumed to be equal to the content of organic matter. According to the method of Noriki *et al.* (1980), samples were decomposed in a Teflon[®] sealed vessel by mixed solution of nitric acid, perchloric acid and hydrofluoric acid. Solutions were used for determinations of aluminum (Al) and calcium (Ca).

Concentrations of Al and Ca were determined by an ICP-AES (SEIKO, SPS 7700). Contents of biogenic carbonate were calculated by the following equation.

Biogenic carbonate:

$$(\%) = [\text{Ca}(\%) - \text{Al}(\%) \times 0.5] \times 1.67 \quad (1)$$

Biogenic silicates (opal) in particles were extracted by a modified method of Mortlock and Froelich (1989). Concentration of silicates in extracted

solutions was determined by the molybdenum yellow spectrophotometry (Noriki *et al.*, 1980).

RESULTS

Total mass flux and major components. Seasonal variations of total mass flux are shown in Figure 2a. Total mass flux at 927 m depth at the Station MS varied between 64 and 2575 mg/m²/day and annual mean flux was 454 mg/m²/day. At 2746 m depth, mass flux varied between 0.1 and 2509 mg/m²/day and annual mean mass flux was 346 mg/m²/day. A pattern of seasonal variation of mass flux at 2746 m depth was similar to that at 927 m depth (Figure 2a). Mass fluxes were large in winter (December–January) and spring (March–May).

It has been known that settling particles consist of 4 major components, biogenic silicates (opal), biogenic carbonates, aluminosilicates and organic matter (Honjo, 1996; Noriki and Tsunogai, 1986). Flux-averaged annual mean opal content was 28% at 927 m and 34% at 2746 m depth. In spring, more than 40% of settling particles consisted of opal at each depth (Table 1 and 2). Average Al content at 927 m and 2746 m was 2.6% and 2.7%, respectively. Assuming that Al content in lithogenic aluminosilicates is 8.2% (average crust: Taylor, 1964), it is calculated that average content of aluminosilicates in settling particles was 31% at 927 m and 33% at 2746 m depth. In winter, more than 50% of settling particles consisted of lithogenic aluminosilicates. These results indicate that large mass fluxes in spring are derived from production and sinking of biogenic opal (*i.e.* diatoms), and large mass fluxes in winter are caused by transport of lithogenic aluminosilicates. Content of biogenic

Table 1

Total mass flux, ^{210}Pb activity and concentration of major components (biogenic opal, organic matter, carbonate and aluminium) in settling particles at 927 m depth

Open date	Interval (days)	Mass flux (mg/m ² day)	^{210}Pb activity (dpm/g)	Opal (%)	Org. M (%)	Carb. (%)	Al (%)
11.07.2001	14	259	73.9±3.2	13.2	27.8	21.5	1.69
25.07.2001	14	189	–	12.6	25.0	21.0	2.57
08.08.2001	14	107	61.5±1.7	16.5	23.6	17.7	2.33
22.08.2001	14	64	–	17.4	29.0	14.5	3.23
05.09.2001	14	65.8	100±6	19.3	28.2	14.5	3.02
19.09.2001	14	88.5	–	22.1	27.8	13.9	2.52
03.10.2001	14	103.5	102±3	24.4	30.2	10.1	3.17
17.10.2001	14	99.4	–	20.5	26.4	8.28	3.56
31.10.2001	14	177	105±3	22.9	23.0	7.34	3.94
14.11.2001	14	593	–	25.3	17.2	5.36	2.35
28.11.2001	14	536	62.2±1.3	27.8	18.8	13.4	2.03
12.12.2001	14	591	–	27.2	16.3	11.7	2.38
26.12.2001	14	434	79.7±1.2	19.9	14.6	7.7	4.17
09.01.2002	14	326	–	20.3	17.1	7.9	3.85
23.01.2002	14	275	88.0±2	15.8	14.8	9.8	4.00
06.02.2002	14	300	–	18.5	15.6	12.5	4.13
20.02.2002	14	480	118±2	18.7	18.8	12.4	3.80
06.03.2002	14	1455	–	40.9	16.8	5.46	1.70
20.03.2002	14	2575	41.8±0.7	25.8	12.2	0.74	3.50
03.04.2002	14	625	50.4±1.3	34.9	13.2	8.68	2.00
17.04.2002	14	843	42.2±1.2	40.4	16.3	7.00	1.20
01.05.2002	14	1158	25.8±0.8	33.1	17.3	3.64	1.18
15.05.2002	14	102	40.9±2.7	27.3	20.9	6.93	1.92
29.05.2002	14	88.5	–	24.4	22.5	15.4	2.50
12.06.2002	14	205	63.7±2.0	22.7	22.6	13.0	2.65
26.06.2002	14	80.1	63.3±5.6	22.2	20.1	11.9	2.71

carbonate in settling particles was less than 21% at 927 m depth and less than 13% at 2746 m depth.

^{210}Pb . Concentrations of ^{210}Pb in settling particles are shown in Figure 2b. Activities of ^{210}Pb varied between 26 and 118 dpm/g at 927 m depth and 5 and 181 dpm/g at 2746 m depth, respectively. Except during 2 periods in March and May 2002, activities of ^{210}Pb in settling particles at 2746 m depth were larger than those at 927 m depth. ^{210}Pb activities were relatively small in spring.

Fluxes of ^{210}Pb showed maxima in April 2001 and March–May 2002 (Figure 2c). Although the largest flux was observed in March 2002 at 927 m depth, remarkable increase of ^{210}Pb was not observed at 2746 m (Figure 2c). Annual mean ^{210}Pb flux was 0.99 dpm/cm²year at 927 m depth and 0.94 dpm/cm²year at 2746 m depth (Table 3). The result that particulate ^{210}Pb flux decreased with depth could indicate the export of particulate ^{210}Pb from the water column between 927 m and 2746 m depths.

DISCUSSION

Budget of ^{210}Pb in the water column. In order to understand the transport processes of ^{210}Pb at the Station MS, a balance of ^{210}Pb in the water column was estimated, consisting of ^{210}Pb production, radioactive decay and removal. There are two ways

for supplying ^{210}Pb to the water column; one is radioactive production from ^{226}Ra in seawater and the other is ^{210}Pb deposition from the atmosphere.

As mentioned above, it is known that deep part of the Sea of Japan is occupied by uniform seawater, called Sea of Japan Proper Water (JSPW). We observed that seawater temperature at 1000 m depth was about 0.2°C and salinity was 34.07‰ at the Station MS. Seawater in the deep layer of Station MS was considered as “typical” JSPW water. Harada and Tsunogai (1986b) measured ^{226}Ra concentrations in JSPW and reported that the ^{226}Ra concentration was 88 dpm/m³ at 0–200 m, 148 dpm/m³ at 200–2000 m and 157 dpm/m³ in bottom layer. Because ^{226}Ra in seawater was not measured in this study, we used the ^{226}Ra data in the JSPW as that of the Station MS. Inventories of ^{226}Ra in the western Sea of Japan were calculated to be 12.5 dpm/cm² at 0–927 m depth and 40.1 dpm/cm² at 0–2746 m, respectively. Radioactive production rate of ^{210}Pb was calculated by multiplying the inventory of ^{226}Ra by decay constant of ^{210}Pb (0.0311 year⁻¹). Therefore, production rates of ^{210}Pb were calculated to be 0.37, 1.24 and 1.57 dpm/cm²year at 927 m, 2746 m and 3424 m depth, respectively.

Atmospheric deposition of ^{210}Pb was reported to be 0.5 dpm/cm²year in the eastern Sea of Japan

Table 2

Total mass flux, ^{210}Pb activity and concentration of major components (biogenic opal, organic matter, carbonate and aluminium) in settling particles at 2746 m depth

Open date	Interval (days)	Mass flux (mg/m ² day)	^{210}Pb activity (dpm/g)	Opal (%)	Org. M (%)	Carb. (%)	Al (%)
06.08.2000	12	123	–	37.5	12.3	9.36	3.73
18.08.2000	12	135	103±2	38.3	14.0	5.92	4.55
30.08.2000	12	66.4	–	36.1	12.9	8.85	4.27
11.09.2000	12	92.3	109±3	38.9	12.6	7.36	4.15
23.09.2000	12	76.1	–	40.0	12.7	7.04	4.44
05.10.2000	12	82.5	117±3	37.2	13.3	5.95	4.54
17.10.2000	12	92.2	–	28.1	16.8	5.02	4.49
29.10.2000	12	71.2	129±2	31.8	14.3	3.55	4.41
10.11.2000	12	135	–	29.8	16.7	4.64	4.02
22.11.2000	12	72.8	133±3	27.3	15.7	5.67	4.18
04.12.2000	12	131	–	27.0	15.4	7.58	4.01
16.12.2000	12	138	118±2	23.4	14.6	13.8	4.20
28.12.2000	12	168	138±1	26.1	15.9	4.24	4.51
09.01.2001	12	180	140±2	22.3	16.0	2.35	4.69
21.01.2001	12	65.1	–	23.8	16.9	0.19	4.43
02.02.2001	12	122	141±2	20.7	18.7	3.23	4.36
14.02.2001	12	179	–	20.0	17.1	1.95	5.07
26.02.2001	12	50.3	127±5	19.0	16.4	13.0	4.80
10.03.2001	12	305	115±1	12.2	15.0	8.49	4.95
22.03.2001	12	266	119±1	12.1	15.4	8.04	4.81
03.04.2001	12	258	–	20.0	15.6	9.40	4.43
15.04.2001	12	1467	67.8±0.7	50.0	16.7	0.81	1.97
27.04.2001	12	980	–	52.6	18.4	1.58	1.27
09.05.2001	12	0.9	–	–	–	–	–
21.05.2001	12	0.1	–	–	–	–	–
02.06.2001	12	0.1	–	–	–	–	–
11.07.2001	14	176	104±2	16.0	13.3	15.3	3.50
25.07.2001	14	179	–	14.8	11.7	11.8	4.63
08.08.2001	14	153	134±3	15.8	11.8	10.4	4.75
22.08.2001	14	102	–	14.7	13.1	4.74	4.70
05.09.2001	14	112	160±4	13.3	11.8	6.16	3.83
19.09.2001	14	131	–	13.4	12.4	2.25	4.32
03.10.2001	14	132	168±4	13.5	14.3	0.91	5.00
17.10.2001	14	233	–	14.2	13.4	–	5.36
31.10.2001	14	148	181±4	12.6	14.1	–	4.90
14.11.2001	14	199	–	16.8	11.6	1.82	3.00
28.11.2001	14	216	133±2	19.7	12.2	11.0	2.50
12.12.2001	14	402	–	26.2	10.5	6.80	2.20
26.12.2001	14	292	141±2	19.2	13.5	6.47	3.45
09.01.2002	14	187	–	17.8	13.0	3.44	4.80
23.01.2002	14	141	162±4	16.7	12.9	5.35	2.83
06.02.2002	14	170	–	16.1	13.7	6.50	4.48
20.02.2002	14	183	145±5	17.7	15.3	6.52	4.21
06.03.2002	14	877	–	32.6	14.4	4.65	1.20
20.03.2002	14	2509	5.4±0.3	30.7	11.6	2.36	1.54
03.04.2002	14	699	82.5±1.4	30.6	11.8	8.14	0.74
17.04.2002	14	666	85.2±1.5	36.2	12.0	8.55	2.47
01.05.2002	14	1425	54.9±1.1	43.9	15.3	3.41	0.98
15.05.2002	14	922	13.7±0.4	36.0	18.0	5.64	0.90
29.05.2002	14	135	–	18.8	14.3	5.90	2.25
12.06.2002	14	233	136±3	18.1	16.6	0.72	4.32
26.06.2002	14	115	132±7	17.8	12.1	0.94	5.39

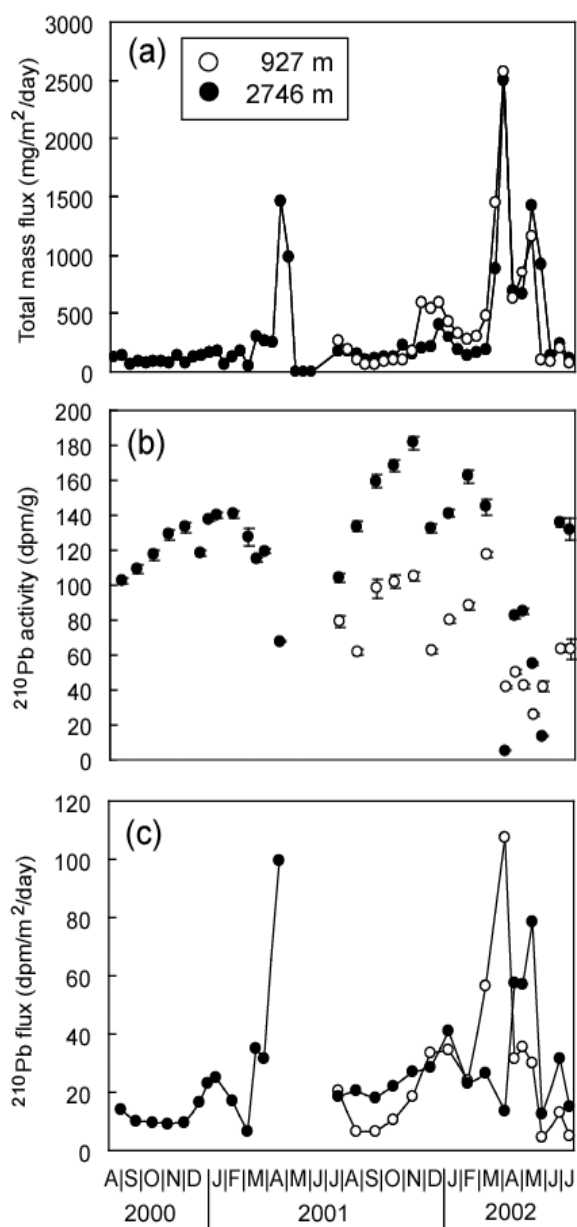


Figure 2. Seasonal variation of total mass flux (a), ^{210}Pb activity (b) and ^{210}Pb flux (c)

(Nozaki *et al.*, 1973). As sediment trap experiments in the eastern and western Sea of Japan estimated that the atmospheric ^{210}Pb flux at the Station MS was 2.7 times larger than that in the eastern Sea of Japan (Otosaka *et al.*, 2003), the atmospheric ^{210}Pb flux at the Station MS was calculated to be 1.35 dpm/cm²year (Table 3, Figure 3). Nozaki *et al.* (1973) measured ^{210}Pb concentration in seawater in the northern Sea of Japan, and reported that ^{210}Pb concentration was 167 dpm/m³ in the upper layer (0–500 m) and 57 dpm/m³ in JSPW (>500 m). Radioactive decay rate of ^{210}Pb was calculated by multiplying the inventory of ^{210}Pb by decay constant of ^{210}Pb . The decay rates of ^{210}Pb at 0–927 m and 0–2746 m water column were 0.19 and 0.51 dpm/cm²year, respectively (Table 3).

At the Station MS, activities of dissolved ^{210}Pb in seawater were in disequilibria to that of ^{226}Ra . Considering that ^{210}Pb in seawater is removed by settling particles, the difference between supply and decay rates of ^{210}Pb can be considered as expected particulate ^{210}Pb flux. It was estimated that the expected ^{210}Pb fluxes at 927 m and 2746 m depth were 1.55 and 2.09 dpm/cm²year, respectively (Table 3).

The ratio of observed/expected ^{210}Pb flux was 0.64 at 927 m depth and 0.45 at 2746 m depth, respectively (Table 3). At both depths, observed ^{210}Pb flux was smaller than expected ^{210}Pb flux. These results suggested that particulate ^{210}Pb was exported horizontally, and that Station MS could be defined as a “source” area of ^{210}Pb . At 2746 m depth, the ratio of observed/expected ^{210}Pb flux was smaller than that at 927 m, therefore, the ability to export particulate ^{210}Pb was higher in the deep layer.

A mass balance of ^{210}Pb at Station MS is summarized in Figure 3. Observed ^{210}Pb flux decreased vertically. This result would indicate the diffusion of particulate ^{210}Pb due to dissolution or decomposition of particles in the deep layer. On the other hand, horizontal flux of ^{210}Pb by lateral export increased with depth.

Table 3

^{210}Pb budget in the water column and comparison between expected and observed ^{210}Pb fluxes

Depth (m)	Production from ^{226}Ra (1)	Atmospheric input (2)	Total supply (3)	Radioactive decay (4)	Expected ^{210}Pb flux (5)	Observed ^{210}Pb flux (6)	Observed/expected
0–927	0.39	1.35	1.74	0.19	1.55	0.99	0.64
0–2746	1.25	1.35	2.60	0.51	2.09	0.94	0.45

Note:

(1) Calculated by the ^{226}Ra inventory (Harada and Tsunogai, 1986b).

(2) Calculated by multiplying the atmospheric input in the eastern Sea of Japan (0.5 dpm/cm²year: Nozaki *et al.*, 1973), by the ratio of atmospheric input between western/eastern Sea of Japan (2.7: Otosaka *et al.*, 2003).

(3) Sum of production and atmospheric input.

(4) Calculated by the ^{210}Pb inventory (Nozaki *et al.*, 1973).

(5) Difference between total supply rate and decay rate of ^{210}Pb .

(6) Annual mean flux observed in this study.

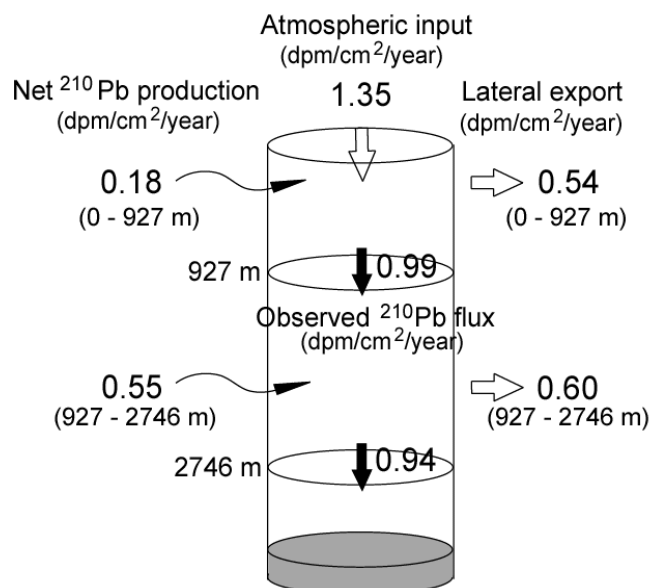


Figure 3. Schematic diagram of simple model to estimate rates of laterally transported ^{210}Pb in the water column. Net ^{210}Pb production rate was calculated by subtracting the ^{210}Pb decay rate from the ^{210}Pb production rate derived from decay rate of ^{226}Ra (Table 3)

Table 4

Correlation coefficients between F/P ratio of ^{210}Pb and fluxes of opal, carbonate, aluminium and organic matter

Trap depth	Number of samples	Opal	Carbonate	Al	Org. M
947 m	(n = 16)	0.83	0.31	0.93	0.88
2746 m	(n = 29)	0.59	0.37	0.47	0.54
All samples	(n = 45)	0.64	0.38	0.80	0.68

It is known that relatively strong (>3 cm/sec) deep currents were observed through the year at the Station MS (Takematsu *et al.*, 1999; Senju *et al.*, 2002). Considering that ^{210}Pb released in the deep layer is exported by the sea currents, it is reasonable that the deep current enhanced the horizontal export of ^{210}Pb in the water column.

Scavenging and transport processes of ^{210}Pb .

Recent studies have revealed that ^{210}Pb is a useful tracer to assess the removal of insoluble materials from the water column (*e.g.* Moore and Dymond, 1988). However, ^{210}Pb tracer is not valid in some cases (*e.g.* Legeleux *et al.*, 1996; Borole, 2002). Here we discuss the scavenging process of ^{210}Pb at the Station MS and factors that control scavenging of ^{210}Pb . Relationship between ^{210}Pb flux and fluxes of Al, organic matter and biogenic opal is shown in (Figure 4). In order to cancel the bias of ^{210}Pb flux by the change of water depth, ^{210}Pb flux recorded in sediment trap (F) is normalized by the production rate of ^{210}Pb in the water column (P) at each depth (Table 3). The production rate (P) is the sum of ^{210}Pb supply from the ^{226}Ra content in the overlying water column and the atmospheric deposition of ^{210}Pb to the surface ocean (Table 3).

At 927 m depth, there was a strong relationship between F/P ratio and Al flux. A correlation coefficient between Al flux and F/P ratio was 0.93 at 927 m depth (Table 4). There was no difference in correlation between Al flux and F/P ratio at different depths except March 2002 (Figure 4a). Correlation coefficient between F/P ratio and Al flux decreased with depth (Table 4). These results indicate that ^{210}Pb supplied to the shallow layer (<1 km depth) was efficiently removed from the water column by lithogenic particles, but the effect of ^{210}Pb scavenging was weakened in the deep layer.

Correlation coefficients between particulate organic matter (POM) flux and F/P ratio were 0.88 at 927 m depth and 0.54 at 2746 m depth (Table 4). At each depth, POM flux and F/P ratio showed a strong relationship in the low flux season (POM flux <60 mg/m²/day: Figure 4b). Large POM fluxes were observed in spring when extremely large opal fluxes were observed (Figure 5c and d). Therefore, it could be thought that the POM flux was controlled by biogenic opal. As for fluxes of biogenic opal, correlation coefficients toward F/P ratio were 0.83 and 0.59, respectively (Table 4). Similar to POM, relationship between opal flux and F/P ratio was

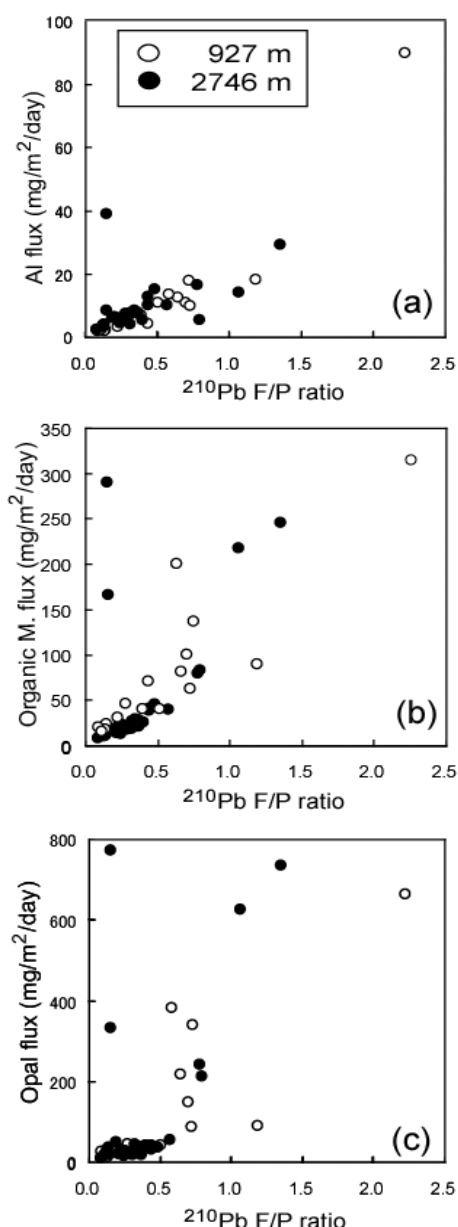


Figure 4. Relationship between flux/production (F/P) ratio of ^{210}Pb and fluxes of aluminum (a), organic matter (b) and biogenic opal (c)

weakened during high flux season (opal flux $>100 \text{ mg}/\text{m}^2/\text{day}$: Figure 4c).

During the high biogenic flux season, F/P ratio was smaller than expected F/P ratio (Figure 4b and c). This indicated that large biogenic flux lead to low efficiency to remove ^{210}Pb from the water column. On the other hand, the removal efficiency of ^{210}Pb did not change even during the high lithogenic flux season (Figure 4a). Taking into account that mass fluxes were not different between 927 and 2746 m during large flux season (March–May: Figure 2a), it could be thought that biogenic particles had large settling velocity in this season. Settling velocity of lithogenic particles in seawater is relatively small

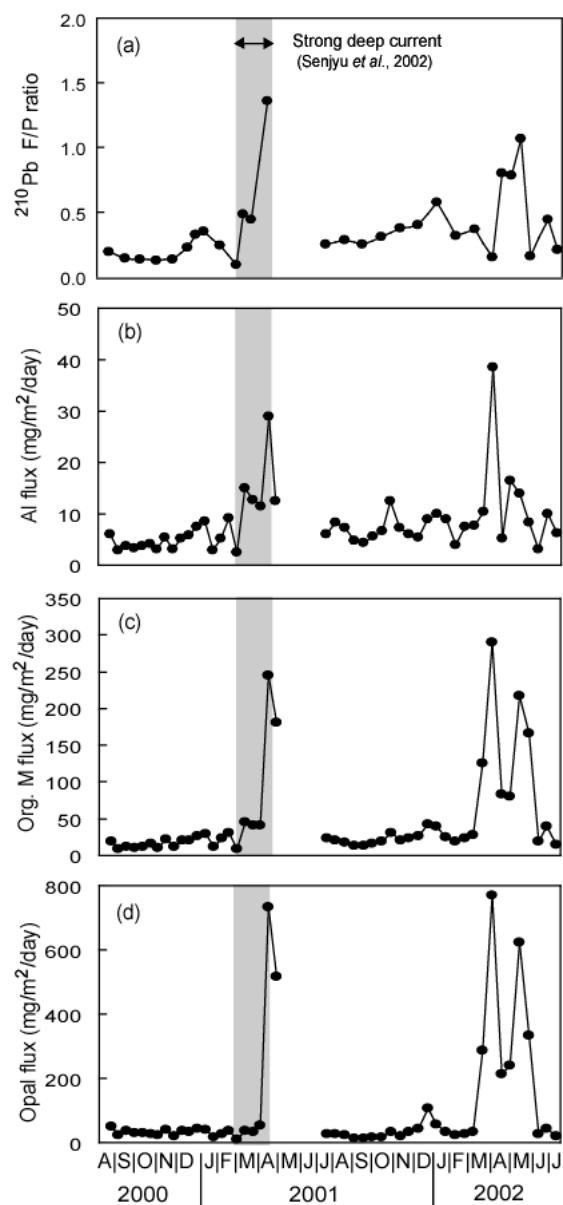


Figure 5. Seasonal variations of F/P ratio (a), Al flux (b), organic matter flux (c) and opal flux (d) at 2746 m at the station MS

because these particles are small in size (e.g. Hill, 1998). Considering that ^{210}Pb in seawater is adsorbed electrostatically onto the “small” lithogenic particles (e.g. Harada and Tsunogai, 1986a), it is reasonable to suggest that the removal efficiency of ^{210}Pb by lithogenic particles did not change through the year.

Temporal variations of ^{210}Pb flux and the deep water formation. Seasonal variation of F/P ratio at 2746 m depth at the Station MS is shown in Figure 5a. Four maxima of F/P ratio were observed (December 2000, April 2001, January 2002, and April 2002), and the largest F/P ratio was observed in spring. Although production and settling of biogenic particles brought large mass flux in spring, seasonal

variation of the ^{210}Pb F/P ratio did not coincide with that of biogenic flux. For example, an elevation of F/P ratio in 2001 was observed 2 months prior to that of opal flux (Figure 5a and d). In this season, the increment of F/P ratio coincided with that of Al flux (Figure 5a and b). This fact indicates that ^{210}Pb was “imported” with lithogenic particles to the deep layers of Station MS.

In the Sea of Japan, it was reported that lithogenic materials are transported from the arid area of the central Asia (*e.g.* Iwasaka *et al.*, 1983). However, analysis of satellite observations data revealed that there was no large-scale deposition of aerosols over the central Asia and the Japan Sea in March 2001 (NASA/GSFC, <http://toms.gsfc.nasa.gov/> aerosols). At the Station MS, it has been reported that strong deep currents occur in winter (Takematsu *et al.*, 1999; Senjyu *et al.*, 2002). It was mentioned that a severe winter in 2000–2001 stimulated the formation of bottom water in the coastal region of the western Sea of Japan, and the “fresh” bottom water was observed in the deep layer around the Station MS (Senjyu *et al.*, 2002; Tsunogai *et al.*, 2003). Remarkable strong deep current (>10 cm/sec) was also observed at the Station MS (Figure 5: Senjyu *et al.*, 2002). If coastal seawater is imported to the bottom layer of Station MS, it can be speculated that re-suspended lithogenic materials enhanced lithogenic flux and the F/P ratio in the bottom layer of Station MS. Seasonal variation of ^{210}Pb flux in the deep layers of Station MS could be an indicator of the renewal of the deep water in the western Sea of Japan.

CONCLUSIONS

In the western Sea of Japan, ^{210}Pb was efficiently scavenged by lithogenic particles. Although large biogenic fluxes were observed in spring (March–April), biogenic particles did not act as an efficient

REFERENCES

- Biscaye P.E., Anderson R.F. 1994.** Fluxes of particulate matter on the slope of the southern Middle Atlantic Bight: SEEP-II. *Deep-Sea Res.* II, 41, pp. 459–509.
- Biscaye P.E., Anderson R.F., Deck B.L. 1988.** Fluxes of particles and constituents to the eastern United States continental slope and rise: SEEP-I. *Continental Shelf Res.*, 8, pp. 855–904.
- Borole D.V. 2002.** Analysis of ^{210}Pb in sediment trap samples and sediments from the northern Arabian Sea: evidence for boundary scavenging. *Deep-Sea Res.* I, 49, pp. 1055–1069.
- Colley S., Thomson J., Newton P.P. 1995.** Detailed ^{230}Th , ^{232}Th and ^{210}Pb fluxes recorded by the 1989/90 BOFS sediment trap time-series at 48 °N, 20 °W. *Deep-Sea Res.* I, 42, pp. 833–848.
- Craig H., Krishnaswami S., Somayajulu B.L.K. 1973.** ^{210}Pb - ^{226}Ra : radioactive disequilibrium in the deep sea. *Earth Planet. Sci. Lett.*, 17, pp. 295–305.
- Gamo T. 1999.** Global warming may have slowed down the deep conveyor belt of a marginal sea of the northwestern Pacific: Japan Sea. *Geophys. Res. Lett.*, 26, pp. 3137–3140.
- Gardner W.D., Biscaye P.E., Richardson M.J. 1995.** A sediment trap experiment in the Vema Channel to evaluate the effect of horizontal particle fluxes on measured vertical fluxes. *J. Mar. Res.*, 55, pp. 995–1028.
- Harada K., Tsunogai S. 1986a.** Fluxes of ^{234}Th , ^{210}Po and ^{210}Pb determined by sediment trap experiments in pelagic oceans. *J. Oceanogr. Soc. Japan*, 42, pp. 92–200.
- Harada K., Tsunogai S. 1986b.** ^{226}Ra in the Japan Sea and the residence time of the Japan Sea water. *Earth Planet. Sci. Lett.*

“scavenger” of ^{210}Pb in this season. Only during the low biogenic flux season (opal flux <100 mg/m²day), ^{210}Pb was efficiently scavenged by the sinking of biogenic particles. By drawing up a mass balance of ^{210}Pb , the Station MS was revealed to be a source area of ^{210}Pb , and it was estimated that the horizontal export of ^{210}Pb was large in deep layer. The deep current in the western Sea of Japan could play a role to export ^{210}Pb from the water column. On the other hand, it was suggested that the renewal of bottom water in the western Sea of Japan enhanced the “import” of particulate ^{210}Pb to the Station MS. Seasonal variation of particulate ^{210}Pb flux in the western Sea of Japan could act as an indicator of the deep water circulation in this area.

ACKNOWLEDGMENTS

This study was conducted under the Partner Project Agreement between the International Science and Technology Center (ISTC), the Far Eastern Regional Hydrometeorological Research Institute (FERHRI), and the Japan Atomic Energy Research Institute (JAERI). We would like to thank captains and crew of R/V “Professor Khromov” (FERHRI). We are also grateful to Dr. A. Tkalin (FERHRI), Dr. T. Senjyu (Kyusyu Univ.), Dr. H. Amano (JAERI) and staff of Marine Research Laboratory, JAERI, for valuable discussions. We also appreciate Messrs. A. Scherbinin and S. Yarosh (FERHRI), Dr. T. Aramaki (National Institute of Environmental Sciences) and Messrs. T. Kobayashi and T. Suzuki (JAERI) for their assistance at the sea. We express special thanks to the two anonymous reviewers for their constructive reviews of the manuscript.

- Heussner S., Cherry R.D., Heyraud M. 1990.** ^{210}Po , ^{210}Pb in sediment trap particles on a Mediterranean continental margin. *Continental Shelf Res.*, 10, pp. 989–1004.
- Hill 1998.** Controls on floc size in the sea. *Oceanogr.*, 11, pp. 13–18.
- Honjo S. 1996.** Fluxes of particles to the interior of the open ocean. In: V. Ittekkot, P. Schafer, S. Honjo, P.J. Depetries (Eds.), *Particulate flux in the Ocean*, Scope 57. John Wiley & Sons, New York, pp. 91–154.
- Iwasaka Y., Minoura H., Nagaya K. 1983.** The transport and spacial scale of Asian dust-storm clouds: a case study of the dust-storm event of April 1979. *Tellus*, 35B, pp. 189–196.
- Legelux F., Reyss J.-L., Etcheber H., Khripounoff A. 1996.** Fluxes and balance of ^{210}Pb in the tropical northeast Atlantic. *Deep-Sea Res.*, I, 43, pp. 1321–1341.
- Minami H., Kano Y., Ogawa K. 1999.** Long-term variations of potential temperature and dissolved oxygen of the Japan Sea Proper Water. *J. Oceanogr.*, 55, pp. 197–205.
- Moore W.S., Dymond J. 1988.** Correlation of ^{210}Pb removal with organic carbon fluxes in the Pacific Ocean. *Nature*, 331, pp. 339–341.
- Mortlock R.A., Froelich P.N. 1989.** A simple method for the rapid determination of biogenic opal in pelagic marine sediments. *Deep-Sea Res.*, 36, pp. 1415–1426.
- NASA/GSFC 2003.** Data product of Total Ozone Mapping Spectrometer: Aerosol Index. WWW page: <http://www.toms.gsfc.nasa.gov/aerosols>
- Noriki S., Nakanishi K., Fukawa T., Uematsu M., Uchida T., Tsunogai S. 1980.** Use of a sealed Teflon vessel for the decomposition followed by determination of chemical constituents of various marine samples. *Bull. Fac. Fish. Hokkaido Univ.*, 31, pp. 354–361.
- Noriki S., Tsunogai S. 1986.** Particulate fluxes and major components of settling particles from sediment trap experiments in the Pacific Ocean. *Deep-Sea Res.*, 33, pp. 903–912.
- Nozaki Y., Tsunogai S., Nishimura M. 1973.** Lead-210 in the Japan Sea. *J. Oceanogr. Soc. Japan*, 29, pp. 251–256.
- Otosaka S., Aramaki T., Suzuki T., Togawa O., Baba M., Senju T., Noriki S., Karasev E.V., Scherbinin A.F., Volkov Y.N. 2003.** Particulate flux and biogeochemical cycle in the Japan Sea. Abstracts of 17th biennial conference of the Estuarine Research Federation, 99 p.
- Senju T., Aramaki T., Otosaka S., Togawa O., Danchenkov M., Karasev E., Volkov Y. 2002.** Renewal of the bottom water after the winter 2000–2001 may spin-up the thermohaline circulation in the Japan Sea. *Geophys. Res. Lett.*, 29, doi: 10.1029/2001GL010493.
- Takematsu M., Nagano Z., Ostrovski A.G., Kim K., Volkov Y. 1999.** Direct measurement of deep currents in the northern Japan Sea. *J. Oceanogr.*, 55, pp. 207–216.
- Taylor S.R. 1964.** Abundance of chemical elements in the continental crust: a new table. *Geochim. Cosmochim. Acta*, 58, pp. 1567–1579.
- Tsunogai S., Kawada K., Watanabe S., Aramaki T. 2003.** CFC indicating renewal of the Japan Sea Deep Water in winter 2000–2001. *J. Oceanogr.*, 59, pp. 685–694.
- Uda M. 1934.** The results of simultaneous oceanographical investigations in the Japan Sea and its adjacent waters in May and June, 1932. *J. Imp. Fish. Exp. Sta.*, 5, pp. 57–190.
- Yamada M., Aono T. 2003.** ^{210}Pb and ^{234}Th in settling particles collected by time-series sediment traps in the Okinawa Trough. *Deep-Sea Res. II*, 50, pp. 487–501.

THE PRESENT STATUS OF BOTTOM ECOSYSTEMS OF PETER THE GREAT BAY (THE SEA OF JAPAN)

T.A. Belan^{1,2}, A.V. Tkalin¹, T.S. Lishavskaya¹

¹ Far Eastern Regional Hydrometeorological Research Institute (FERHRI), Russia
Email: tbelan@hydromet.com

² Institute of Marine Biology, Far Eastern Branch of the Russian Academy of Sciences (IMB FEBRAS), Russia

Pollution characteristics and the state of benthic communities in the coastal zone of Peter the Great Bay are discussed. According to the data obtained in August 2001, highest concentrations of petroleum hydrocarbons (PHCs), trace metals (TM), DDT and its metabolites were observed in bottom sediments of Golden Horn Inlet. Contents of Pb, Cu and Zn exceeded the threshold concentrations when serious negative alterations in benthic organisms and their communities were beginning. Relatively low values of pollutants were detected in Ussuriysky Bay. Though bottom sediments of Amursky Bay are characterized by intermediate pollutant concentrations, local zones with elevated pollutant contents were identified (located near industrial and municipal wastewater outfalls and city landfill).

Benthos in Golden Horn Inlet was characterized by poor species composition, low total biomass (10.8 g/m²), and high density of opportunistic polychaete species (*Tharyx pacifica* up to 4090 ind/m², *Schistomeringos japonica* 1636 ind/m², *Capitella capitata* 909 ind/m²). The highest values of benthos biomass (253.7 g/m²), species richness and diversity were detected in Ussuriysky Bay. The total benthos biomass in Amursky Bay was 157.5 g/m². Two non-tolerant species (polychaetes *Sigambra bassi* and *Scalibregma inflatum*) became more numerous again in Amursky Bay (as in 1970s), while abundance of some positive pollution indicator species declined. Data on chemicals in bottom sediments in the study areas demonstrated statistically significant decrease in recent years. Possible reason of this trend might be a decreasing pollution load entering the bay.

INTRODUCTION

The aim of this report is to review the state of bottom sediment pollution and benthic communities in the coastal zone of Peter the Great Bay in August 2001, and to compare these results with similar data for 1980s and 1990s. Amursky Bay, Ussuriysky Bay and Golden Horn Inlet were the study areas. The following basic parameters will be discussed: 1) concentrations of trace metals, petroleum and chlorinated hydrocarbons in bottom sediments; 2) benthos quantitative characteristics and species composition.

MATERIALS AND METHODS

Sediment samples were taken in the coastal zone of Peter the Great Bay in August 2001 (Figure 1). The sampling design in 2001 was the same as in 1986–1989 and 1994. Four replicate sediment samples at each site were taken (with the exception of Golden Horn Inlet where 2 samples were collected per site) with van-Veen grab (0.11 m²). Only surface sediments (1–2 cm) were collected for chemical analysis (trace metals, chlorinated hydrocarbons and total non-polar petroleum hydrocarbons). For TM analysis, sediments were digested by a mixture of HNO₃ and HClO₄, concentrations of trace metals were determined using a flame atomic absorption spectrophotometer. Detection limits (ppm) were as follows: Zn 0.5, Pb 0.1, Cu 0.02, and Cd 0.002. PHCs were measured by IR spectrophotometry after extraction with acetone and methylene chloride and column chromatography on Al₂O₃. The detection limit was 0.05 ppt (parts per thousand). Chlorinated

hydrocarbon concentrations were determined using a Russian gas chromatograph LCM-80 with glass packed column (1 m length, 3 mm inner diameter, SE stationary phase) and electron capture detector. Detection limits for DDT, DDD and DDE were 0.3–0.5 ppb.

For biological analysis, sediments were washed by seawater through 1.0 mm sieve, and residues including macrobenthos were preserved by 4% buffered formaldehyde. In the laboratory, benthic organisms were sorted to major taxa. All individuals were identified to species level, but some organisms could only be identified to higher taxa. Wet weight of macrofauna was determined: organisms were blotted and air-dried for approximately one minute prior to weighting. Benthos parameters were calculated using four replicate samples and included the following: total biomass (*B*), abundance (*A*), Shannon-Wiener diversity index (*H*), Pielou evenness index (*e*), Margalef richness index (*R*), and Simpson domination index (*Si*). Ecological indices were calculated as:

$$H = \sum p_i \times (\log_2 p_i), e = H/\log_2 S,$$

$$R = (S-1)/\log_2 A; Si = \sum (p_i)^2,$$

where:

p_i – is the proportion of abundance *i*th species from total benthos abundance (*A*).

For determination of species structure of benthic communities SIMPER-analysis (PRIMER Program) was used (UNEP, 1995).

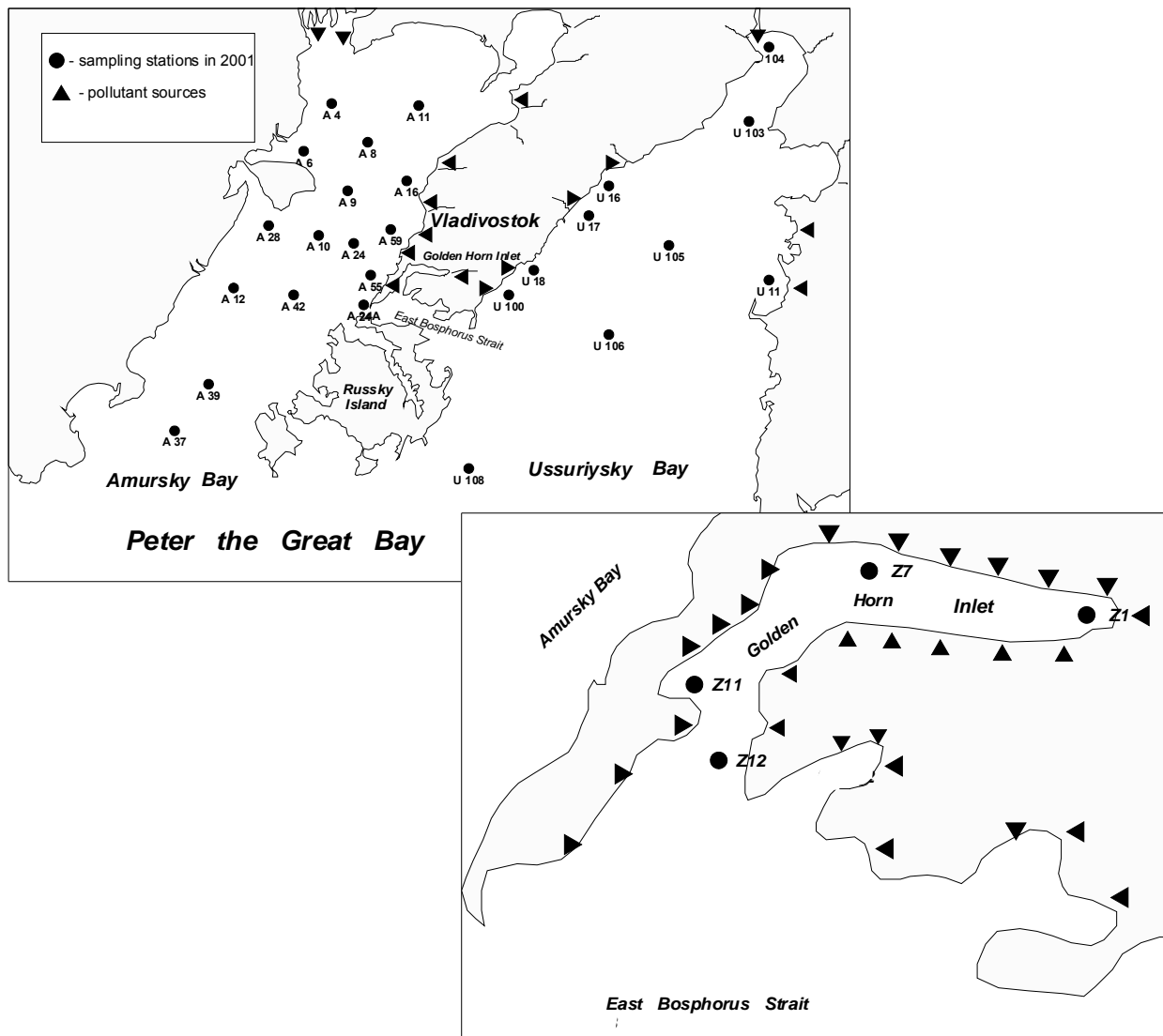


Figure 1. Sampling stations in August 2001

STUDY AREAS

Amursky Bay is located in the northwestern portion of Peter the Great Bay (Figure 1). The highest depth is 53 m, and the mean depth is about 20 m. Bottom sediments are characterized by the prevalence of silt, but in the southern part of the bay fine sands are present. Salinity ranges from 26.5PSU in shallow waters to 33.5PSU in the deepest areas. Dissolved oxygen (DO) saturation in the bottom layer usually exceeds 90%. In the shallow part of the bay DO saturation is sometimes decreased dramatically (down to 30%). The highest nutrient levels are observed in the inner part of the bay because of river runoff. Eastern part of the bay is polluted due to influence of municipal and industrial wastewater discharges, urban runoff (stations A16, A24, A55, A59) and former dredged material dumping (A24A). As a result of high load of pollutants (including nutrients and dissolved organic matter), Amursky Bay is under chronic anthropogenic impact

(Shapovalov *et al.*, 1989; Tkalin *et al.*, 1993; Belan, 2003). The data on contaminant levels in bottom sediments of the bay in 1986–1989, evaluated by principal component analysis (PCA), have shown three distinctive areas (Belan, 2003), namely less polluted (northern and southern parts of the bay), moderately polluted (eastern part) and severely polluted (dumping site).

Ussuriysky Bay is larger in size with predominantly sandy sediments. The highest depth is 75 m, water salinity varies from 21.0 to 34.5PSU, DO content in bottom layers is about 93% of saturation. Ussuriysky Bay is characterized by moderate pollution level (Table 1), mainly due to municipal wastewater discharge (station U100), river runoff (U104), city landfill (U18), and zones of recreation (U16, U17).

Golden Horn Inlet is the inner harbour of Vladivostok, where numerous industrial enterprises and ship terminals are situated. Average depth is 8 m, while the greatest depth is 25 m. Bottom sediments

are represented by silts with extremely high content of pollutants. DO saturation in bottom layers varies from 67 to 98%, the lowest levels (down to 10–20%) are usually registered in summer in the inner part of the inlet. Waters of Golden Horn Inlet contain very high amount of pollutants due to influence of numerous industrial and municipal sewage outfalls, urban runoff and discharges from ships.

RESULTS AND DISCUSSION

The results of ecological investigations in the coastal zone near Vladivostok in 1980s and 1990s demonstrated that the most polluted areas were Golden Horn Inlet and eastern part of Amursky Bay, where anomalously high concentrations of TM, PHCs and total DDT (sum of DDT, DDD and DDE) in bottom sediments were detected. For example, contents of pollutants at the former dumping site exceeded background level by a factor of 7–10 (Shapovalov *et al.*, 1989). The associated negative changes in ecosystems of Golden Horn Inlet and Amursky Bay have been explained by anthropogenic factors: chronic pollution and progressive eutrophication (Tkalin *et al.*, 1993; Belan, 2003). Anthropogenic load in Ussuriysky Bay was considerably less than in Amursky Bay, and bottom communities were characterized by higher richness of species composition and other quantitative parameters (Belan, 2001).

Joint ecological expedition carried out by FERHRI and the Institute of Marine Biology in Peter the Great Bay in August 2001 obtained new data on bottom sediment pollution and the status of benthic fauna. In total, 16 stations were sampled in Amursky Bay (mostly silt) with depths ranging from 6 to 35 m, 10 stations were taken in Ussuriysky Bay (sand/silt, 6–48 m), and 4 stations in Golden Horn Inlet (silt, 9–24 m). Location of sampling stations is shown on Figure 1.

Amursky Bay. The data on average pollutant contents in surficial bottom sediments of the study areas are given in Table 1. The distributions of petroleum hydrocarbons, total DDT, and Zn in Amursky and Ussuriysky bays and Golden Horn Inlet in August 2001 are shown on Figures 2 and 3. In case of PHCs, discharge of Razdolnaya River flowing into Amursky bay is clearly seen (in addition to discharges from industrial enterprises). Maximum concentrations of TM and DDTs were also found near industrial wastewater outfalls (near stations A16 and A59). Maximum concentrations of Cu, Pb and DDTs in Amursky Bay sediments exceed the minimum threshold concentrations (ERL) causing negative biological effects (Long *et al.*, 1995). The pollutant contents at the former dumping site (A24A) are no longer different from the surrounding areas (the dumping site has been closed for about 15 years). More detailed information on spatial distribution of trace metals in bottom sediments around Vladivostok

is given in the short correspondence of A.V. Tkalin and B.J. Presley published in this issue of “*Pacific Oceanography*” (see p. 185).

Figure 4 shows the temporal trends of some pollutants (PHCs, DDTs and Cd as an example) in bottom sediments of Amursky Bay from 1990 to 2001. The data for summer (sum.), fall (f.) and spring (sp.) surveys were used for trend analysis. The trends are statistically significant for Cd and PHCs, but not for DDTs. The possible reason of these decreasing trends is the decline of the Russian Far East economy after the Soviet Union breakdown.

The first hydrobiological expeditions in Peter the Great Bay have been carried out in 1925–1933, when initial data on benthos distribution patterns, species composition and benthic quantitative characteristics were obtained. Average benthos biomass in Amursky Bay at that time was more than 150 g/m² (wet weight), the most abundant and wide-spread species in silty and silty-sand sediments (with depth ranging from 14 to 40 m) were polychaetes *Maldane sarsi*, *Scoloplos armiger*, *Lumbrineris minuta*, *Sigambra bassi*, *Anobothrus gracilis*, bivalve mollusc *Nucula tenuis*, ophiuroid *Ophiura sarsi*, hydroid *Obelia longissima* (Deruygin and Somova, 1941).

The expeditions carried out in 1970s, 40 years later, have demonstrated the following alterations in benthos communities of Amursky Bay (Klimova, 1971):

- Composition and distribution of widespread assemblages were changed.
- The abundance of dominant species (*M. sarsi*, *S. armiger*, *O. longissima*) was declined.

In 1986–1989, the following significant changes, in comparison with 1970s, have been recorded (Table 2, 3) (Klimova, 1988; Belan 2001, 2003):

- The average benthos biomass decreased by a factor of 2.
- Reduction of the habitat areas and disappearance of Echinodermata (starfish *Luidia quinaria*, ophiuroids *O. sarsi*) as well as decreasing of abundance of some polychaete species (*Scalibregma inflatum*, *S. armiger* and *M. sarsi*) took place.
- Pollution-tolerant species became widespread with anomalously high density in the most polluted areas (polychaetes *Tharyx pacifica* up to 8100 ind/m²; *Dipolydora cardalia* up to 2100 ind/m²; phoronids *Phoronopsis harmeri* up to 2000 ind/m²).

The average benthos biomass in Amursky Bay in 2001 was 157.5 g/m², and it was formed mainly (64.5%) by large bivalves *Arca boucardi*, *Macoma tokoyensis*, *M. orientalis*, *Scapharca broughtoni* and polychaetes (21.3%) *Cirratulus cirratus*, *Potamilla reniformis*, *Th. pacifica*. In 1986–1989 (Belan, 1992, 2001) the average biomass (73.9 g/m²) was created

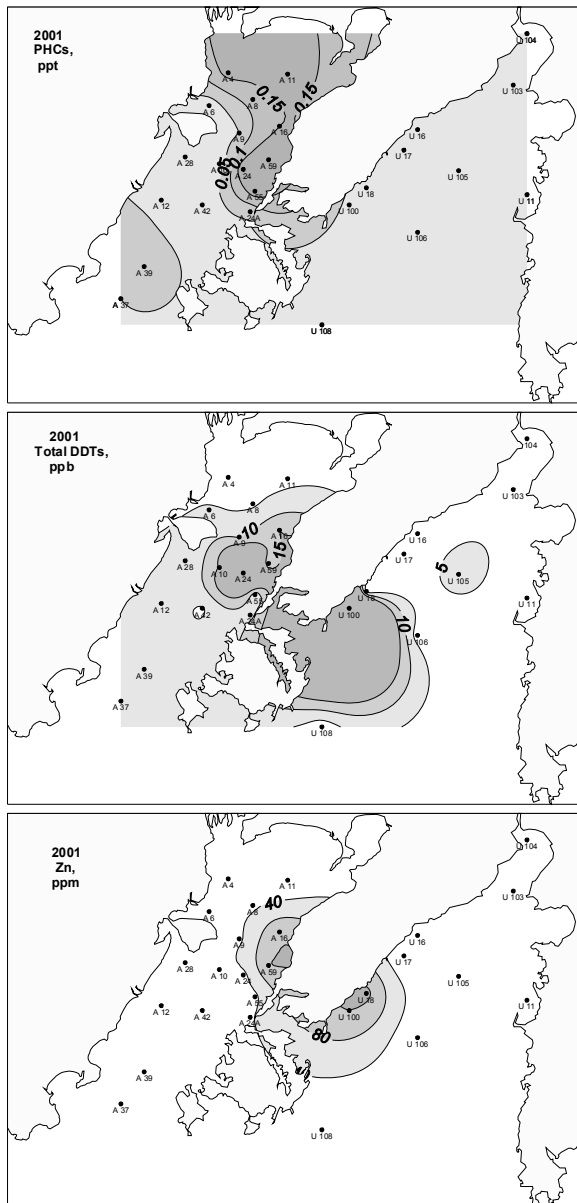


Figure 2. Distribution of PHCs, DDTs and Zn in surficial bottom sediments of Amursky and Ussuriysky bays, August 2001

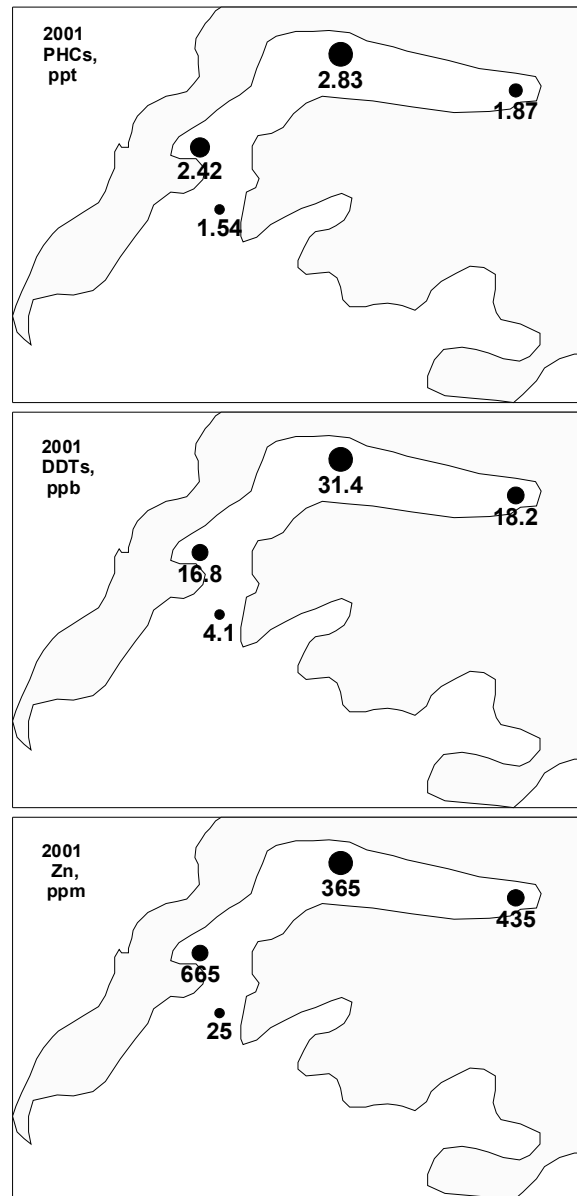


Figure 3. Distribution of PHCs, DDTs and Zn in surficial bottom sediments of Golden Horn Inlet, August 2001

Table 1

Content of some pollutants (mean ± SD) in bottom sediments in 2001 (numerator) and in 1980–1990s (denominator)

Environmental variables	Ussuriysky Bay	Amursky Bay	Golden Horn Inlet
PHCs (ppt)	<u>0.02±0.02</u>	<u>0.10±0.07</u>	<u>2.17±0.57</u>
	0.28±0.23	0.62±0.72	16.42±16.32
DDTs (ppb)	<u>3.0±2.5</u>	<u>7.9±4.0</u>	<u>17.6±11.2</u>
	12.3±16.8	10.7±4.6	42.5±20.5
Pb (ppm)	<u>30.30±36.94</u>	<u>31.25±16.00</u>	<u>153.50±84.82</u>
	11.00±15.97	32.27±33.59	175.00±102.47
Cu (ppm)	<u>24.70±40.77</u>	<u>21.31±7.70</u>	<u>155.25±101.82</u>
	9.00±5.45	27.39±28.08	111.25±76.39
Cd (ppm)	<u>0.00±0.00</u>	<u>0.16±0.63</u>	<u>1.60±1.35</u>
	1.30±1.79	1.08±0.89	4.25±2.02

Note:

DDTs – the sum of DDT and its metabolites (DDE and DDD), statistically significant differences ($p < 0.05$) are shown in bold

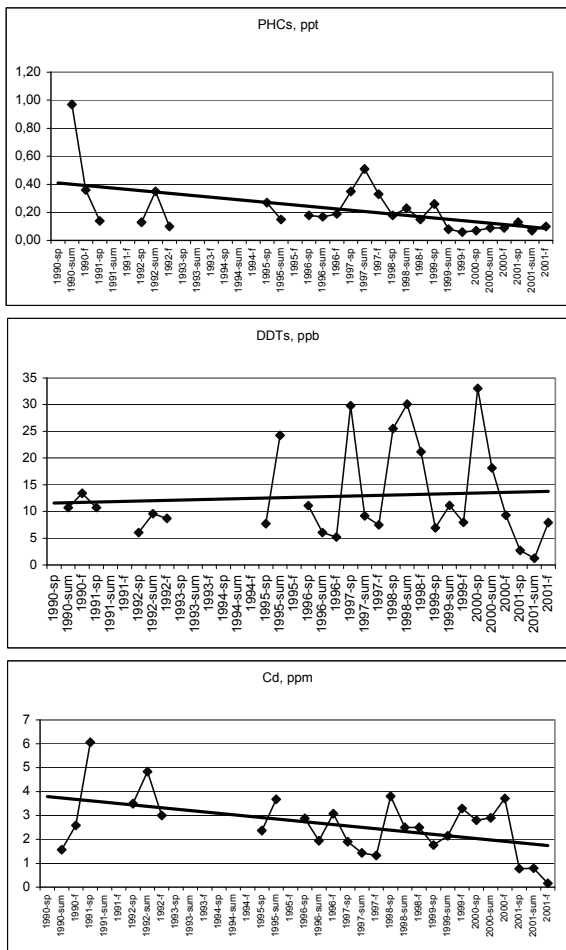


Figure 4. Temporal trends of PHCs, DDTs and Cd in Amursky Bay

by polychaetes (65.0%) *Th. pacifica*, *Maldane sarsi*, *P. reniformis* and bivalves (19.0%) *Yoldia* sp. and *Alveinus oijanus* (Table 2). The dominant and widespread species in 2001 were different in comparison with 1986–1989: non-tolerant species (in order of their importance in community structure: polychaetes *Lumbrineris* sp., *Sigambra bassi*, *M. sarsi* and *S. inflatum*) were responsible for community structure in Amursky Bay. Some of them (*S. bassi* and *S. inflatum*) became more numerous again, as in 1930s and 1970s (Deryugin and Somova, 1941; Klimova, 1971; Volova, 1975), while abundance of some positive pollution indicator species (polychaetes *Th. pacifica*, *Sch. japonica*, *Dipolydora cardalia* and phoronid *Ph. harmeri*) decreased (Figure 5, Table 2). While the mean benthos biomass in 2001 has been increased, the average abundance decreased comparing with 1986–1989, when anomalously high density of tolerant polychaete species was observed (Klimova, 1988; Tkalin *et al.*, 1993; Belan, 2003). The contribution of benthic group to the total biomass in Amursky Bay in 1970s, 1980s, and in 2001 is presented in Table 3. The diversity index was not significantly different in 1986–1989 and in 2001 (Table 2). Perhaps, decline of pollution-tolerant polychaete species might be

explained by decreasing pollutant load entering the bay. However, it must be noted that the mean number of species and index of richness in 2001 decreased considerably (Table 2).

Ussuriysky Bay. Comparing to Amursky Bay, the pollutant contents in sediments of Ussuriysky Bay are generally lower, mainly due to predominance of sandy sediments (Table 1, Figure 2). Nevertheless, in local areas near wastewater outfalls and city landfill (stations U18 and U100), concentrations of DDTs, Cu and Pb exceed the minimum threshold levels (Long *et al.*, 1995). The spatial distributions of Cu and Pb in Ussuriysky and Amursky bays in 2001 were similar to those of Zn shown on Figure 2 as an example. The temporal trends of PHCs, DDTs and Cd in bottom sediments of Ussuriysky Bay (Figure 6) are statistically significant and might be explained by the same reason (economic decline).

Long-term changes of benthos characteristics in Ussuriysky Bay are not as serious as in Amursky Bay. The total biomass in 1930s was 170–200 g/m² (Table 2). Dominant species at the depths 25–35 m in silty-sand sediments were represented by polychaetes *Magelona longicornis*, *Chone cincta*, *Anobothrus gracilis*, *M. sarsi*, *S. armiger*, ophiuroids *O. sarsi vadicola* and *Amphiodia craterodmeta*, snail *Turitella fortilirata*, bivalves *N. tenuis*, *Yoldia johanni*, *Axinopsida subquadrata* (Deryugin and Somova, 1941). In 1970s, the total benthos biomass (218 g/m²) was very close to those obtained in 1930s. However, according to the data of V.L. Klimova (1971), decreasing of biomass and density of some species (*T. fortilirata*, *M. sarsi*, *S. armiger*) took place in Ussuriysky Bay too.

In 1994, the total benthos biomass was 264.7 g/m². Cluster analysis allowed to distinguish two bottom communities located at different parts of the bay. The first community occupied the east and west shallow parts of the bay (12–18 m) and was represented by echinoderm *E. cordatum*, bivalves *Callithaca adamsi*, *Acila insignis* and polychaete *M. sarsi*. The second community was located in the deep part of the bay (45–55 m). Echiurid *Echiurus echiurus*, bivalve *Macoma orientalis* and polychaete *Asychis* sp. dominated there. Species composition in 1994 was very similar in comparison with those found in 1930s and 1970s. The anthropogenic pressure in Ussuriysky Bay in 1990s was considerably lower than in Amursky Bay.

The total average benthos biomass in Ussuriysky Bay in August 2001 was comparable with those registered in 1930s, 1970s and 1994: 170–200 g/m², 218 g/m², and 264.7 g/m², respectively (Deryugin and Somova, 1941; Klimova, 1971; Belan, 2001). The contribution of different faunal groups to the total biomass was almost the same too (Table 4). Only average abundance of benthos in 2001 has been significantly (5 times) higher than in 1994. In 2001, as well as in

Table 2

Benthic community parameters in study areas in 2001 and in 1980–1990s

Amursky Bay		
Year	1986–1989	2001
<i>n</i>	25	55
Dominant species (ind/m ²)	<i>Tharyx pacifica</i> (1872.0), <i>Lumbrineris</i> sp. (339.6), <i>Phoronopsis harmeri</i> (335.2), <i>Schistomeringos japonica</i> (132.0), <i>Maldane sarsi</i> (333.6)	<i>Lumbrineris</i> sp. (190.2), <i>Sigambra bassi</i> (85.9), <i>Tharyx pacifica</i> (604.6), <i>Maldane sarsi</i> (82.9), <i>Scalibregma inflatum</i> (80.2)
<i>B</i>	73.9±41.4	157.5±427.6
<i>A</i>	5104.6±4106.9	1556.1±1751.6
<i>N</i>	21.6±9.9	13.0±8.1
<i>R</i>	1.7±0.8	1.2±0.7
<i>H</i>	2.3±0.9	2.1±1.2
<i>e</i>	0.5±0.1	0.6±0.3
Ussuriysky Bay		
Year	1994	2001
<i>n</i>	13	40
Dominant species (ind/m ²)	<i>Scoloplos armiger</i> (22.5), <i>Maldane sarsi</i> (80.3), <i>Acila insignis</i> (70.2), <i>Ophiura kinbergi</i> (18.2), <i>Echinocardium cordatum</i> (23.7)	<i>Lumbrineris</i> sp. (216.3), <i>Scoloplos armiger</i> (100.1), <i>Goniada maculata</i> (34.8), <i>Maldane sarsi</i> (207.0)
<i>B</i>	264.7±252.7	253.7±256.9
<i>A</i>	443.4±262.3	2106.1±2057.2
<i>N</i>	16.0±5.5	20.9±9.2
<i>R</i>	1.7±0.5	1.9±0.8
<i>H</i>	2.7±0.9	3.1±1.0
<i>e</i>	0.7±0.2	0.7±0.2
Golden Horn Inlet		
Year	1986–1989	2001
<i>n</i>	15	6
Dominant species (ind/m ²)	<i>Capitella capitata</i> (35.4), <i>Nereis vexillosa</i> (53.2), <i>Schistomeringos japonica</i> (14.8)	<i>Tharyx pacifica</i> (1016.3), <i>Capitella capitata</i> (289.1), <i>Schistomeringos japonica</i> (419.9)
<i>B</i>	17.7±24.0	10.8±18.6
<i>A</i>	221.8±291.9	1483.2±2356.9
<i>N</i>	4.2±2.2	4.0±2.5
<i>R</i>	0.4±0.2	0.3±0.2
<i>H</i>	1.4±0.6	1.2±0.6
<i>e</i>	0.7±0.3	0.6±0.4
Note: <i>n</i> – number of samples; <i>B</i> – biomass, <i>A</i> – abundance, <i>N</i> – number of species, <i>R</i> – Margalef richness index, <i>H</i> – Shannon-Wiener diversity index, <i>e</i> – Pielou evenness index; average abundance (ind/m ²) of dominant species are presented in bracket, the statistically significant values (<i>p</i> <0.05) are bolded		

1994, non-tolerant species were responsible for benthos community structure. However, some differences in benthic community structure in Ussuriysky Bay were detected between 1994 and 2001. Polychaetes *S. armiger*, *M. sarsi*, bivalve *A. insignis*, ophiuroid *O. kinbergii* and sea urchin *E. cordatum* were the most abundant and widespread species in Ussuriysky Bay in 1994. In 2001, only polychaetes *Lumbrineris* sp., *S. armiger*, *Goniada maculata* and *M. sarsi* had the high frequency of occurrence and density. Abundance of bivalve *A. insignis*, ophiuroid *O. kinbergii* and sea urchin *E. cordatum* has declined in 2001.

Golden Horn Inlet. The pollutant concentrations in bottom sediments of Golden Horn Inlet are a few times higher than in Amursky and Ussuriysky bays (Table 1, Figures 2 and 3) due to more intensive anthropogenic pressure. The concentrations of Cu, Pb and Zn exceed not only minimum threshold levels (ERL) but also medium ones (ERM, see Long *et al.*, 1995). Nevertheless, during 1990–2001, the same decreasing temporal trends (statistically significant) were observed (Figure 7).

The regular hydrobiological observations in Golden Horn Inlet began since 1970s. The data obtained at 5 stations from 1979 to 1981 seasonally have shown

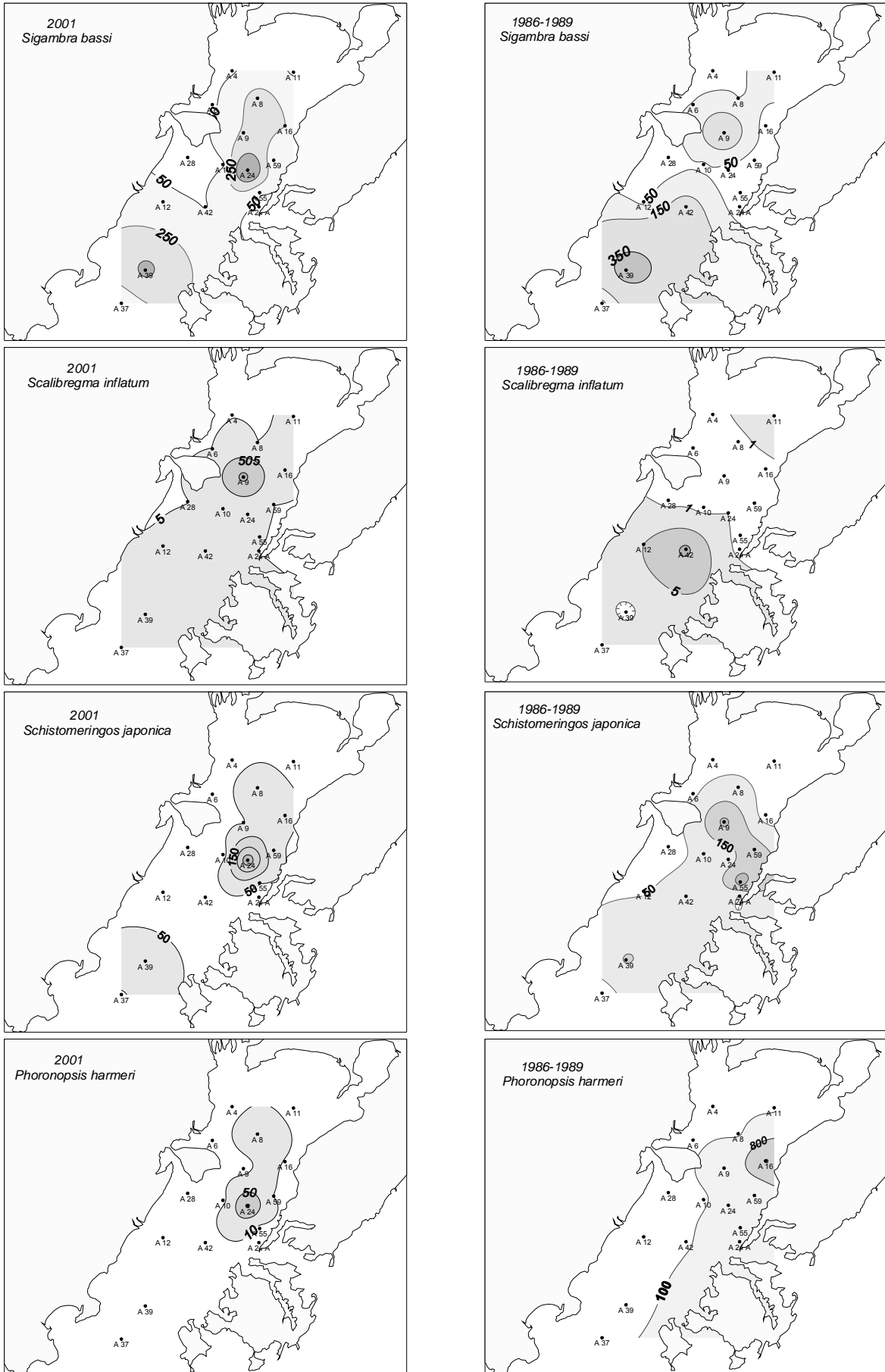


Figure 5. Distribution of species-indicators (g/m^2) in Amursky Bay in 1986–1989 and in 2001

Table 3

Temporary changes of benthos in Amursky Bay

Benthic group	Biomass		
	1970	1986–1989	2001
Polychaeta	<u>85.8</u>	<u>48.1</u>	<u>33.6</u>
	57.2	65.0	21.3
Bivalvia	<u>25.4</u>	<u>14.0</u>	<u>101.7</u>
	16.9	19.0	64.5
Crustacea	<u>0.9</u>	<u>1.8</u>	<u>6.1</u>
	0.6	2.4	3.9
Echinodermata	<u>17.8</u>	<u>2.9</u>	<u>8.8</u>
	11.9	4.0	5.6
Ascidia	<u>7.0</u>	<u>1.0</u>	<u>0.3</u>
	4.6	1.3	0.2
Others	<u>12.2</u>	<u>6.1</u>	<u>7.1</u>
	8.3	8.3	4.5

Note:
 Numerator – g/m², and denominator – %.
 V.L. Klimova (1971) obtained the data of 1970.

Table 4

Temporary changes of benthos in Ussuriysky Bay

Benthic group	Biomass		
	1970	1994	2001
Bivalvia	<u>23.2</u>	<u>122.6</u>	<u>112.8</u>
	10.6	46.3	44.4
Crustacea	<u>0.7</u>	<u>0.3</u>	<u>3.9</u>
	0.3	0.1	1.5
Echinodermata	<u>14.0</u>	<u>59.7</u>	<u>94.4</u>
	6.4	22.5	37.3
Echiurida	<u>111.0</u>	<u>33.3</u>	<u>0.96</u>
	51.0	12.6	<1
Others	<u>11.7</u>	<u>12.8</u>	<u>12.2</u>
	5.3	4.9	4.8

Note:
 Numerator – g/m², and denominator – %.
 V.L. Klimova (1971) obtained the data of 1970.

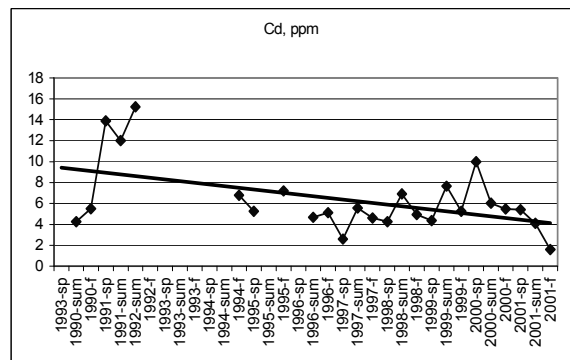
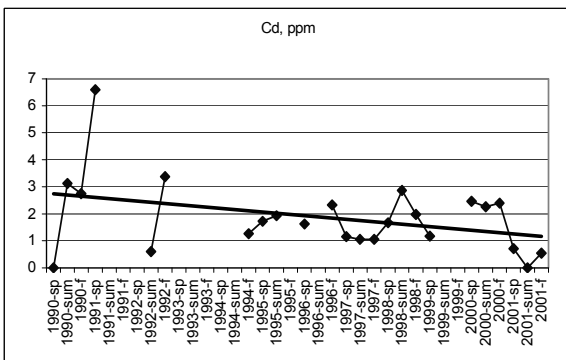
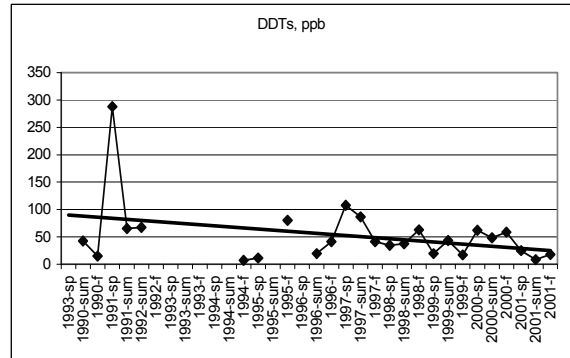
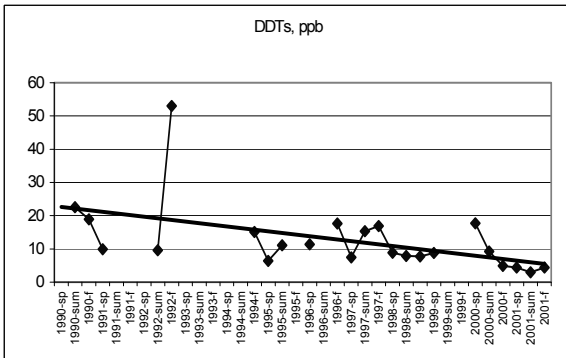
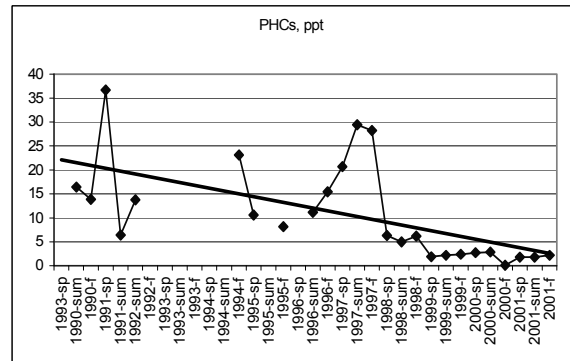
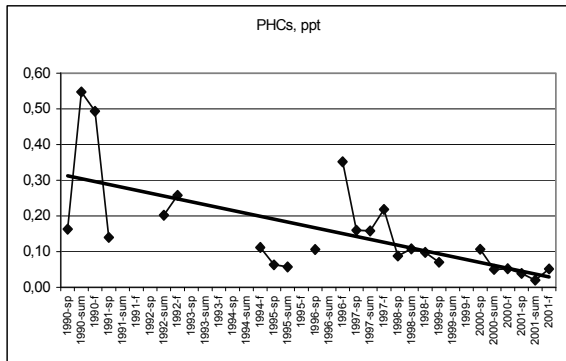


Figure 6. Temporal trends of PHCs, DDTs and Cd in Ussuriysky Bay

Figure 7. Temporal trends of PHCs, DDTs and Cd in Golden Horn Inlet

that macrozoobenthos in the inlet was represented mainly by polychaetes. Some of them formed strong agglomerations: *Capitella capitata* (up to 920 ind/m²), *Schistomeringos japonica*, 1770 ind/m², and *Cirratulus cirratus*, 1080 ind/m² (Bagaveeva, 1992).

The average benthos biomass and abundance in 1986–1989 were 17.7 g/m² and 221.8 ind/m², respectively (Table 2; Belan, 2001). Dominant species were represented by pollution-tolerant polychaete species, *C. capitata*, *Sch. japonica* and *Nereis vexillosa*. In the inner part of the inlet the “dead” areas were registered where living macrobenthos organisms were not found. The biological data have been confirmed by the data on pollutants in bottom sediments, which gave evidence about extremely high anthropogenic load in Golden Horn Inlet (Table 1; Belan, 2001).

Table 2 demonstrates that only density of benthos in 2001 was significantly different from those in 1986–1989: average abundance in 2001 was 6 times higher. Average values of biomass and diversity index are not significantly different in 2001 and in 1986–1989 and these parameters in Golden Horn Inlet are the lowest among other study areas. The pollution tolerant species were dominant both in 1986–1989 (Bagaveeva, 1992) and in 2001 (Table 2). “Dead area” at station Z1 (where no living macrobenthos organisms were found) was observed in the inlet in 2001 again.

CONCLUSIONS

The results of August 2001 expedition in Peter the Great Bay allowed to estimate the current status of coastal bottom ecosystems. Among the study areas, the most polluted and ecologically stressed area is the Golden Horn Inlet. In spite of decreasing pollution load, bottom communities there are still degraded and characterized by a low diversity and biomass as well as an exclusive domination of opportunistic species. The average values of biomass, number of species and ecological indices have not changed significantly in Golden Horn Inlet and were the lowest among other study areas in 2001 as well as in 1986–1989.

Ussuriysky Bay is the relatively “clean” area. Bottom communities there are characterized by much more stable quantitative parameters. In 2001, as well as in

1994, non-tolerant species were responsible for benthos community structure. Changes of benthos community structure might be a revelation of natural ecosystem variability. Ecological conditions and the status of benthic communities in Ussuriysky Bay from 1930s to 2001 as whole are considered to be well being.

Amursky Bay is moderately polluted, however maximum concentrations of Cu, Pb and DDTs in sediments exceed the threshold concentrations causing negative biological effects. In 2001, some non-tolerant species (*S. bassi*, *S. inflatum*) became more numerous again in Amursky Bay (as in 1970s), while abundance of a few positive pollution indicator species (*Th. pacifica*, *Sch. japonica*, *D. cardalia*, *Ph. harmeri*) decreased. Increasing of bivalve abundance and decline of pollution-tolerant polychaete species might be explained by decreasing pollutants’ load entering the bay.

Available biological data for the period from 1930s to 2001 showed that the most significant alterations of benthos were observed in Golden Horn Inlet, and in Amursky Bay. The most dramatic ecological situations occurred in 1975–1980, when industrialization and urbanization growth was very intensive. Total pollution load in ecosystems has caused serious negative change of benthic communities’ structure of these areas – many pollution sensitive species have been replaced by tolerant organisms. In 2001, non-tolerant species became more numerous again in Amursky Bay (as in 1970s), while abundance of some species-positive indicator of pollution decreased.

ACKNOWLEDGEMENT

Authors are grateful to the following specialists of FERHRI, IMB FEBRAS and TINRO-center (in alphabetical order): E.V. Bagaveeva, B.M. Borisov, L.L. Budnikova, A.V. Chernyshov, S.Sh. Dautov, E.E. Kostina, K.A. Lutaenko, M.V. Malutina, E.V. Oleynik, and T.G. Sobolevskaya for identification of the basic benthic taxa (crustaceans, mollusks, echinoderms and others). Special thanks to A.V. Moschenko for statistical analysis of environmental and biological data.

REFERENCES

- Bagaveeva E.V. 1992. Ecology of Polychaeta in Golden Horn Bay (Peter the Great Bay, the Sea of Japan). Studies of marine fauna 43. pp. 115–129. (In Russian).
- Belan T.A. 1992. Polychaetes as pollution indicators in Amursky Bay (the Sea of Japan). Studies of marine fauna 43. pp. 120–125. (In Russian).

- Belan T.A. 2001. Benthos abundance pattern and species composition in conditions of pollution. Ph.D. thesis. Vladivostok. 141 p. (unpublished, in Russian).
- Belan T.A. 2003. Benthos abundance pattern and species composition in conditions of pollution in Amursky Bay (Peter the Great Bay, the Sea of Japan). Marine Pollution Bulletin 49. pp. 1111–1119.

Deryugin K.M., Somova N.M. 1941. Contributions to quantitative estimate of the benthonic population of Peter the Great Bay (Japan Sea). Studies of Far Eastern Seas of USSR. Moscow-Leningrad. pp. 13–36. (In Russian).

Klimova V.L. 1971. The quantitative distribution of benthos from Peter the Great Bay (the Sea of Japan) in summer of 1970. Proceedings of VNIRO 87/7. pp. 97–104. (In Russian).

Klimova V.L. 1988. Biological effects of dredged material disposal in the Japan Sea. Results of investigations of dredged-material disposal in the sea. M.: Hydrometeoizdat. pp. 137–141. (In Russian).

Long E.R., MacDonald D.D., Smith S.L., Calder F.D. 1995. Incidence of adverse biological effects within ranges of chemical concentrations in marine and estuarine sediments. Environmental Management 19. pp. 81–97.

Shapovalov E.N., Tkalin A.V., Klimova V.L. 1989. Effect of dredged material dumping on the marine environment quality and biota. Meteorology and Hydrology, No. 6. pp. 82–88. (In Russian).

Tkalin A.V., Belan T.A., Shapovalov E.N. 1993. The state of the marine environment near Vladivostok, Russia. Marine Pollution Bulletin 26. pp. 418–422.

UNEP 1995: Statistical analysis and interpretation of marine community data. Reference Methods for Marine Pollution Studies. UNEP. 1995. No 64.

Volova G.N. 1975. Bottom biocenosis of Amursky Bay (the Sea of Japan) Proceedings of TINRO 110. pp. 111–120. (In Russian).

SEASONAL AND SPATIAL VARIABILITY OF SEA CURRENTS ON THE SAKHALIN NORTHEASTERN SHELF (BY INSTRUMENTAL DATA)

S.I. Rybalko¹, G.V. Shevchenko²

¹ Far Eastern Regional Hydrometeorological Research Institute (FERHRI), Russia
Email: srybalko@hydromet.com

² Sakhalin Scientific Research Institute of Fisheries & Oceanography (SakhNIRO), Russia

Mooring of current meters on the shelf and continental slope of northeastern Sakhalin Island by University of Hokkaido (Japan) and FERHRI (Russia) allowed obtaining instrumental data to analyze the seasonal and spatial variability of tidal and residual currents.

The most intensive tidal currents are observed in the shelf zone. Along the shelf slope and farther offshore velocity of tidal currents is low. The shelf break is a transition zone from a cyclonically rotating tidal vector in the open sea to an anticyclonically rotating vector on the shelf.

East Sakhalin Current is observed year round, being most intensive in autumn–winter. The current line is at the shelf edge. High velocity of East Sakhalin Current in winter corresponds to the zonal sea level gradients with high sea level near the shore and low sea level in the deep waters.

INTRODUCTION

The detailed study of hydromet parameters is critical for the safe design and construction of offshore oil and gas producing facilities on the Sakhalin northeastern shelf that is currently one of the most promising oil and gas regions. Sea currents are an important environmental parameter.

Instrumental series of current vectors measured by self-contained instruments during hydro-meteorological surveys appear to be very important for analysis of seawaters dynamics. Near the northeastern coast of Sakhalin Island current meters have been deployed in the shelf zone in the vicinity of offshore oil and gas fields; thus, most of instrumental data are confined to the coastal shallow waters. There are almost no instrumental observations at the shelf edge and its slope.

The joint deployment of deep-water current meters on the shelf and continental slope of northeastern Sakhalin by the Hokkaido University and FERHRI made it possible to get instrumental data for almost a two-year period (July 1998–June 2000). The length and high quality of available instrumental series open up new possibilities for investigating the seawater dynamics in the region.

In July–October 1998, sea currents near the shore were measured at Piltun–Astokh and Arkutun–Dagi offshore oil and gas fields within engineering surveys (Kochergin *et al.*, 1999). Available synchronous vectors of sea current velocities at a different distance from the shore and at various depths allowed studying the spatial structure of cross-shelf currents in detail. The present research is focused on variability of tidal and nonperiodic sea currents depending on a season and distance from the shore.

INITIAL DATA

Temporal and spatial variability of sea currents on the Sakhalin northeastern shelf have been analyzed basing on instrumental data obtained during the Russia–Japan joint research cruise aboard R/V “Professor Khromov” (FERHRI) (Figure 1, Table 1, stations M1–M4). Variability of sea currents in the coastal zone has been analyzed basing on the synchronous current series measured during engineering surveys at Piltun–Astokh offshore field in June–October 1998 (Figure 1, Table 1, station PA98). All measurements were made almost at one and the same latitude; therefore, data available are regarded as the ones describing the cross section of the shelf zone from the shoreline to the shelf break. Besides, observations of the sea currents at Arkutun–Dagi offshore field that is somewhat southward of the stations above have been used (Figure 1, Table 1, station AD98).

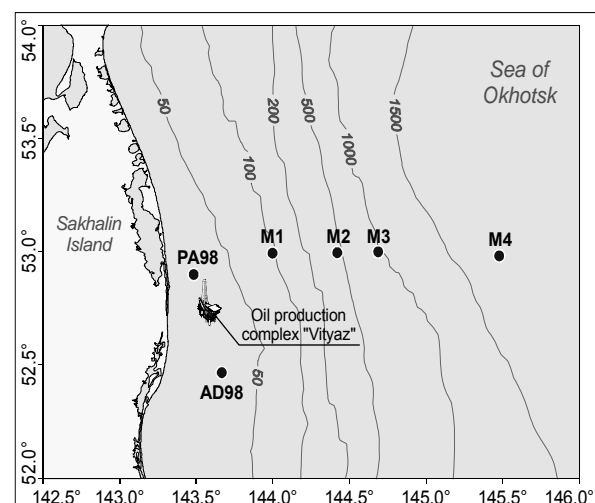


Figure 1. Studied area and location of moored current meters

Table 1

Description of instrumental current series

Station	Depth, m	Measurement level, m	Period	Length, days	Measuring instrument
M1	100	20, 50, 90	Jul/98 – Jul/99	349	WH-ADCP
M2	480	200, 430	Jul/98 – Jun/00	688	CM
M3	970	20, 100, 170	Jul/98 – Sep/99	406	BB-ADCP
		460, 870	Jul/98 – Sep/99	405	CM
M4	1720	30, 90, 140	Oct/99 – Jun/00	284	BB-ADCP
		200	Jul/98 – Sep/99	403	CM
		470	Jul/98 – Jun/00	684	CM
PA98	30	10, 20, 25	Jun/98 – Oct/98	109	S-4 (Inter Ocean)
AD98	40	3, 10, 25	Jul/98 – Oct/98	81	AANDERAA RCM-4
Note: <i>WH-ADCP: RDI Workhorse ADCP (300 kHz);</i> <i>BB-ADCP: RDI Broadband ADCP SC (150 kHz)</i> <i>CM: Union current meter RU-Inotes text</i>					

All data series used were tested for quality by means of estimating a tidal constituent. Stability of tidal currents on the Sakhalin northeastern shelf, which are mainly of barotropic character, testified to reliability of instrumental measurements. Measured data series had a few errors that were easily identified in the residual current series (result of extraction of a precomputed tide from initial current series) and accordingly corrected in the initial series. However, some of the errors failed to be corrected and several observation series or their fragments were excluded from analysis. On the whole, the quality of initial data is rather high and testifies to the reliability of the results obtained.

Sakhalin northeastern shelf is characterized by very dynamic sea currents conditioned on the tides, wind, and permanent East Sakhalin Current. Tidal and nontidal currents are described separately below.

TIDAL CURRENTS

Tidal currents on the Sakhalin northeastern shelf have a well-defined diurnal character (the ratio of the sums of two major diurnal and semidiurnal harmonics for the study area is as follows $R = (H_{O1} + H_{K1}) / (H_{M2} + H_{S2}) \sim 4$). Diurnal tidal harmonics Q_1 , O_1 , K_1 , P_1 and semidiurnal harmonics M_2 , S_2 make the largest contribution to the generation of tidal currents, whereas other tidal waves are not very significant (Putov and Shevchenko, 1998). However, we increased the quantity of tidal waves that are used for the tidal currents analysis to 9 by adding two more diurnal ($2Q_1$, HI_1) constituents and one more semidiurnal (N_2) component. It allowed higher reduction of the tidal oscillation energy and avoidance of distorting influence of tides on the calculation of a nontidal current component.

We compared ellipses of different tidal waves that have been drawn over the harmonic constant data calculated for each station. Harmonic constants have been extracted from instrumental data series using the least square method. Since the tidal wave P_1 , which is very important in the study area, failed to be extracted directly due to the similarity of its period to the period of diurnal wave K_1 , its parameters have been calculated using a specific correction factor.

Tidal currents in the study area are characterized by a high velocity and significant dynamics. Calculated harmonic constants of diurnal tidal waves O_1 and K_1 appear to be highly stable and allow identifying regularities of their spatial and temporal variability.

Analogous calculation revealed unstable harmonic constants for the major semidiurnal wave M_2 . Instability of harmonic constants is usually attributed to baroclinic effects and used to estimate the correlation of barotropic and baroclinic components of a tide (for the Okhotsk Sea described in (Bashmachnikov, 2000; Bashmachnikov and May, 2001)). A certain impact of internal waves on semidiurnal tidal currents has also been revealed during three-component sea current measurements at Piltun-Astokh field (Shevchenko and Kantakov, 2002). At the same time, calculated features allow distinguishing basic tendencies in the spatial variability of M_2 wave, thus testifying to rather a big role of a barotropic component.

Spatial variability. The most specific feature of tidal currents in the study area is a rapid decrease of the amplitude of diurnal tidal waves from the shore to the shelf edge. In the coastal zone, 30–40 m deep, the amplitude of major diurnal tidal waves amounts to 35–45 cm/sec (stations PA98 and AD98). Similar results have been obtained by Rabinovich and Zhukov (1984), Popudribko *et al.* (1998) Putov and

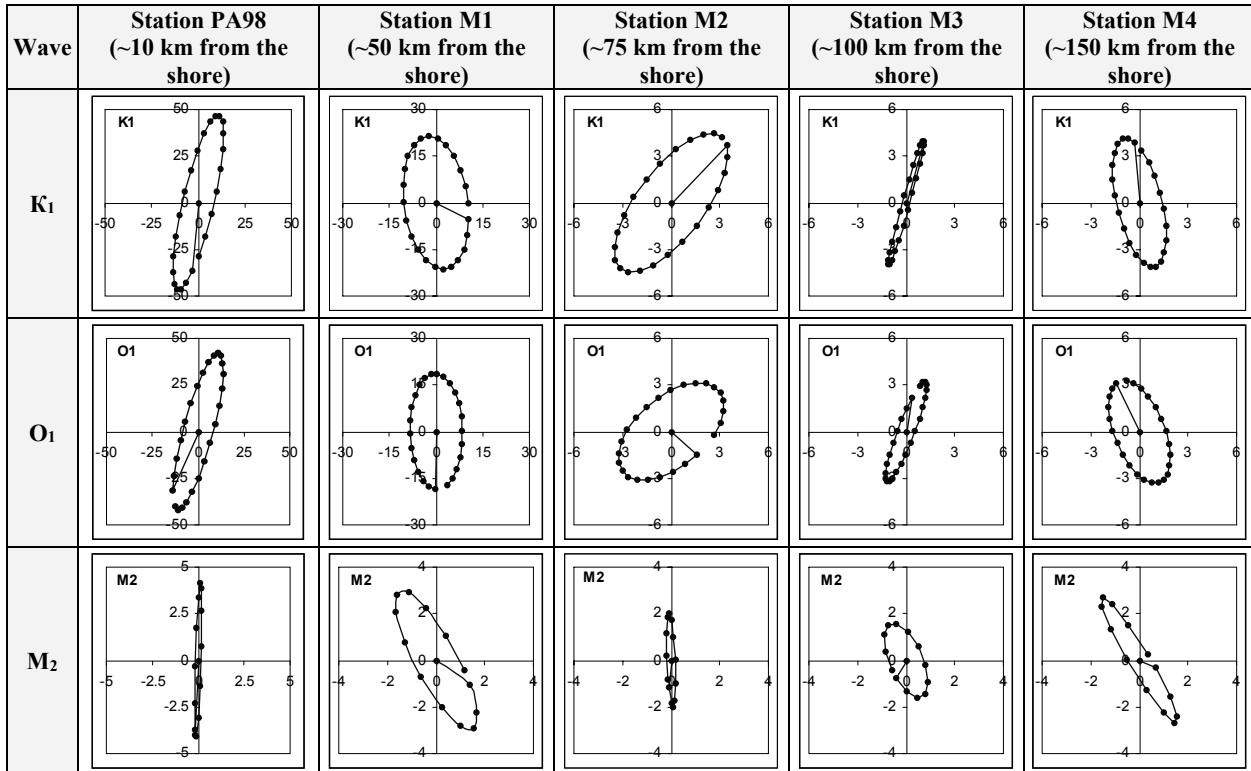


Figure 2. Ellipses of tidal waves K_1 , O_1 and M_2 (cm/sec) for stations PA98, M1–M4

Shevchenko (1998). At the depth of 100 m the amplitude of tidal waves decreases twice to 15–25 cm/sec (Figure 2, station M1). Along the shelf slope and farther offshore the amplitude of tidal waves O_1 and K_1 does not exceed 5 cm/sec (Figure 2, stations M2–M4) and tidal waves become incorrectly diurnal.

Decreasing amplitude of tidal waves from the shore to the shelf edge is in a good accord with theoretical estimates of the shelf wave features: a high current velocity near the shore and a rapidly decreasing current velocity towards the open ocean waters (Rabinovich and Zhukov, 1984).

Velocities of semidiurnal tidal currents are low. M_2 wave has the highest velocity amounting to 2–5 cm/sec, that is about 10 times less than velocity of diurnal waves. Along the shelf slope and farther offshore velocities of semidiurnal currents do not change almost, but semidiurnal harmonics become much more significant for generation of the tidal currents.

In the shelf zone (stations PA98, AD98, M1) and along the shelf slope (station M2) tidal currents look like the barotropic tidal flow, vertical variability of which is dependent on a bottom friction. The major semiaxis of the tidal wave ellipses shortens and turns anticlockwise, whereas rotation of the current velocity vector remains clockwise at all the horizons.

At the shelf slope base (station M3) the tidal currents are almost reverse and rotation of the current velocity vector becomes cyclonic. It should be noted, however, that O_1 velocity vector rotates cyclonically year round,

whereas K_1 velocity vector rotates cyclonically during the ice-free period only. In the open ocean waters (station M4) velocity vectors of both tidal waves are anticlockwise year round. Station M3 is probably located at the boundary of the effect of diurnal shelf waters, which cause the change of velocity vector rotation from cyclonic in the open sea to anticyclonic near the shore.

Harmonic constants of major diurnal tidal waves are characterized by a cyclonic turn of the initial phase (direction of the tidal current vector at 0 GMT) (reduction factor and astronomic phase are not taken into account when drawing tidal waves ellipses, only harmonic constants are accounted for). Initial phase of tidal wave K_1 in the coastal zone is southward directed. Farther offshore it turns smoothly anticlockwise and at the depth of 100 m it is east-southeastward directed, at the depth of 500 m – northeastward directed, and at the depth of 1000–1700 m – northward directed. A similar change of initial phase location is typical for the tidal wave O_1 as well: an anticlockwise turn from southwest to north-northwest. In the open sea waters the steady north-northwest position of initial phase of diurnal tidal waves K_1 and O_1 is observed.

Different positions of initial phase show that directions of diurnal tidal waves in the open sea and on shelf (near Piltun-Astokh field) are quite different. This is not surprising, since at a distance of a half of shelf wave (about 150 km) its phase changes 180 degrees and the current becomes reverse, whereas there are no significant changes in the open sea.

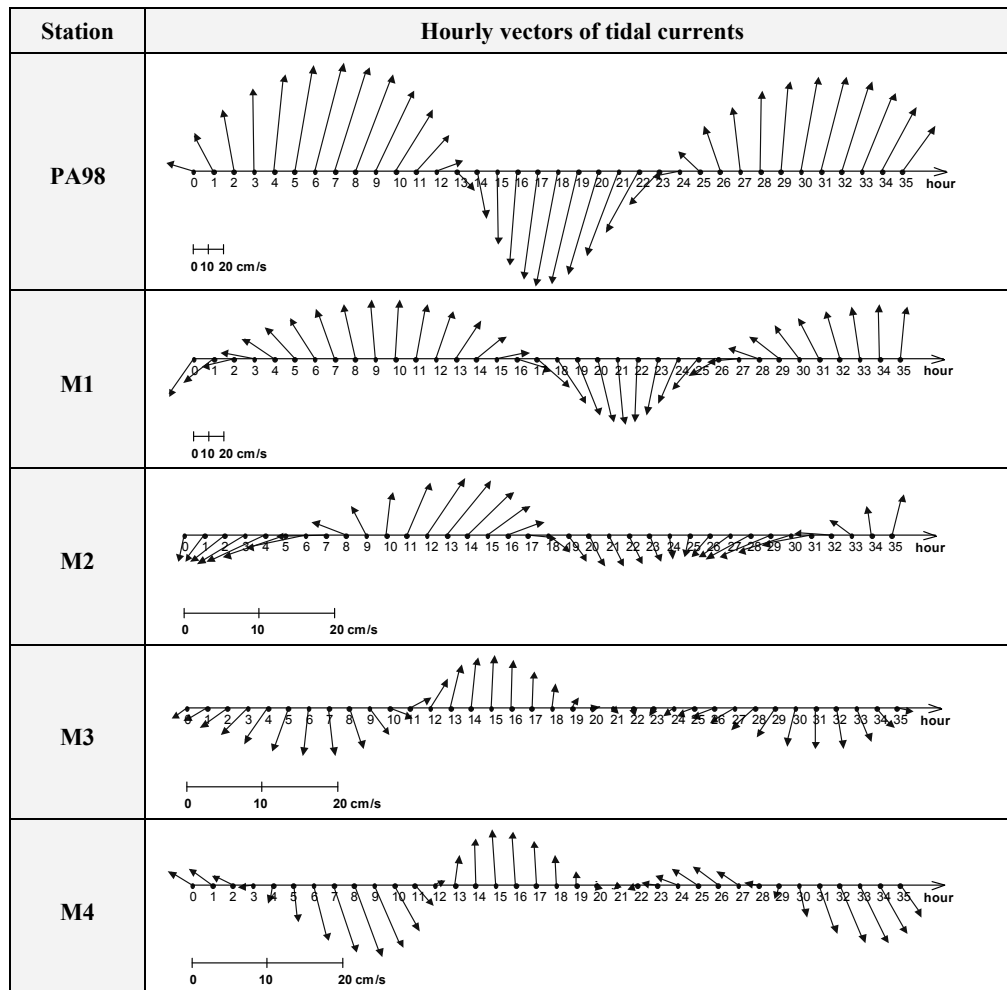


Figure 3. Synchronous vectors of tidal currents for stations PA98, M1–M4

As a result, tidal currents in the shelf zone and open sea are in-phase at the shelf edge and anti-phase at a distance of a half of shelf wave. See hourly synchronous vectors of tidal currents calculated for stations PA98, M1–M4 for summer conditions for 36 hours (Figure 3).

Anticyclonic rotation of current velocity vectors is typical for the major semidiurnal harmonic M_2 as well, though calculated ellipses are less stable if compared with diurnal tidal waves. As was mentioned before, variability of harmonic constants of semidiurnal waves is most probably caused by baroclinic effects and confirmed by a sufficiently high stability of ellipses of harmonic M_2 at different stations in winter and especially in spring, when water stratification is weak. Along the shelf slope (Figure 2, station M2) the amplitudes of semidiurnal waves are minimum and ellipses are very compressed, being probably caused by an abrupt change of water depth.

Seasonal variability. The change of harmonic constants of diurnal tidal currents during the course of the year is not significant almost over the whole seawater area studied, however, seasonal variability

is observed (Shevchenko, 1996) and characterized by the following features:

- high seasonal stability of harmonic constants of diurnal tidal waves K_1 and O_1
- highly stable position of initial phase of tidal waves in the open sea waters year round
- smooth variation of harmonic constants of tidal waves from season to season
- winter compression of tidal wave ellipses (probably caused by ice conditions)
- decreasing amplitudes of tidal waves in winter in the shelf zone and increasing amplitudes of tidal waves in the open sea by 10–50%.

Varying position of K_1 initial phase is observed in the shelf zone. In spring and summer the initial phase of the wave is directed eastward and in autumn and winter – southeastward, phase turn amounting to about 40° . Wave O_1 on the shelf slope (station M2) is characterized by the similar anticyclonic turn of the wave phase. In spring the initial phase of O_1 wave is directed eastward, in summer and autumn – southeastward and in winter – southward, the turn of the wave phase during the course of the year amounting to about 90° .

EAST SAKHALIN CURRENT

Available comprehensive instrumental measurements allow studying the seasonal variability of East Sakhalin Current, which is one of the most complicated and least studied issues, especially concerning the cold season when there are almost no oceanological investigations in the area.

However, there are some variances related to the warm season as well. Available charts of sea currents of the Okhotsk Sea reviewed by Verkhunov (1997) show the southward flow on the Sakhalin eastern shelf. This fact is confirmed by numerous instrumental measurements of a current velocity on the Sakhalin northeastern shelf in the vicinity of oil and gas producing areas (Kochergin *et al.*, 1999; Krasavtsev *et al.*, 2001).

On the other hand, numerical modeling of sea currents based on a typical distribution of oceanographic parameters and a wind speed (Budaeva and Makarov, 1999; Pishchalnik and Arkhipkin, 1999; Zalesniy and Kontorovskiy, 2002) testifies to a northward reverse flow. This flow is conditioned on the so called summer monsoon with permanent southward and southeastward winds registered in summer at all meteorological stations along the coast of Sakhalin Island (Kato *et al.*, 2001).

Thus, we aimed at studying the character of sea currents in summer at a different distance from the shore – in the shallow shelf waters, on the continental slope and adjacent areas.

The second aim was to study a spatial variability of East Sakhalin Current and analyze oceanographic parameters that cause the current variability. Besides, available data allow specification of winter strengthening of southward flow at the shelf break described by Japanese scientists (Mizuta *et al.*, 2001; Mizuta *et al.*, 2003).

Reconstruction of the current field from summer to autumn. Figure 4 shows vectors of current velocity registered at coastal and open sea stations during August–September 1998 and averaged over a 5-day period. In August, a relatively low current velocity (general southward direction) is observed at all stations, varying with the periods of about 10 days and being caused probably by wind. Starting from the second 10-day period of September, velocity of the southward flow at coastal stations (PA98, AD98) increases abruptly through the whole water column. At Arkutun-Dagi field the 5-day averaged velocities of southward and southwestward flows amount to 35–40 cm/sec at surface and 25–30 cm/sec in intermediate waters and near the bottom. At the shallower station PA98 sea currents are highly variable conditioned probably on wind and distorting autumn intensification of East Sakhalin Current to a certain extent. Intensification of East Sakhalin Current (Figure 4, station M1) is well seen at the shelf edge,

vectors of current velocity being turned towards the open sea as compared to coastal stations. However, in autumn when moving farther offshore, intensified flow is not observed.

In order to explain the nature of intensified flow in the coastal zone, see Figure 5. It shows long-term monthly average values of oceanological parameters measured at the standard section №11 Piltun Bay – sea according to (Pishchalnik and Klimov, 1991; Pishchalnik and Bobkov, 2000) and kindly provided by V.M. Pishchalnik. This standard section is zonally oriented and runs at the latitude of 52°51', just in the vicinity of stations PA98, M1–M4 mooring. The section is about 200 km long and covered by 10 stations with water depth varying from 11 m to 1550 m. Coastal stations 40–37 (enumerated starting from the farthest offshore point of the section) are located in the shelf zone, station 37 – at the shelf edge, two next stations – at the shelf break, and three last stations – on the continental slope.

In summer considerable vertical gradients of water temperature (up to 10°C) and salinity (up to 4 psu) are observed in the upper 20-m layer almost over the whole section. Vertical gradients (typical for water salinity to a greater extent) decrease at deep-water stations. However, in autumn vertical gradients of oceanological parameters decrease significantly, and water temperature in the upper 20 m layer is almost of the same magnitude over the whole section. In October water salinity at coastal stations is considerably lower than at open sea stations, being caused by Amur River runoff that is maximum during the first half of September. River runoff is probably one of major factors that cause autumn intensification of East Sakhalin Current. Dominating northward winds, leaving the shore on the right, result in the formation of downwelling: concentration of fresh waters in the coastal zone and their deepening (Bouden, 1988).

Current intensification on the shelf slope in winter. Vectors of non-periodic (residual) currents in the shelf zone, shelf slope and offshore area adjacent to northeastern Sakhalin averaged over a 15-day period have been used to study the seasonal variability of East Sakhalin Current during the course of the year (Figures 6–7).

In summer (June–September) East Sakhalin Current is weak with average current velocity amounting to 4–5 cm/sec in the shelf zone (Figure 6, station M1) and 7–8 cm/sec on the shelf slope (Figure 6, stations M2 and Figure 7 – M3). At the most distant point (Figure 7, station M4) current velocity decreases and does not exceed 4 cm/sec. Nonetheless, at all stations and at different depths southward flow is registered, that is the flow opposite to the direction of wind flow, most probably caused by seasonal gradients of water level of the Okhotsk Sea. In summer maximum sea level is observed at tide-gauges Okhotsk and Ayan, whereas at

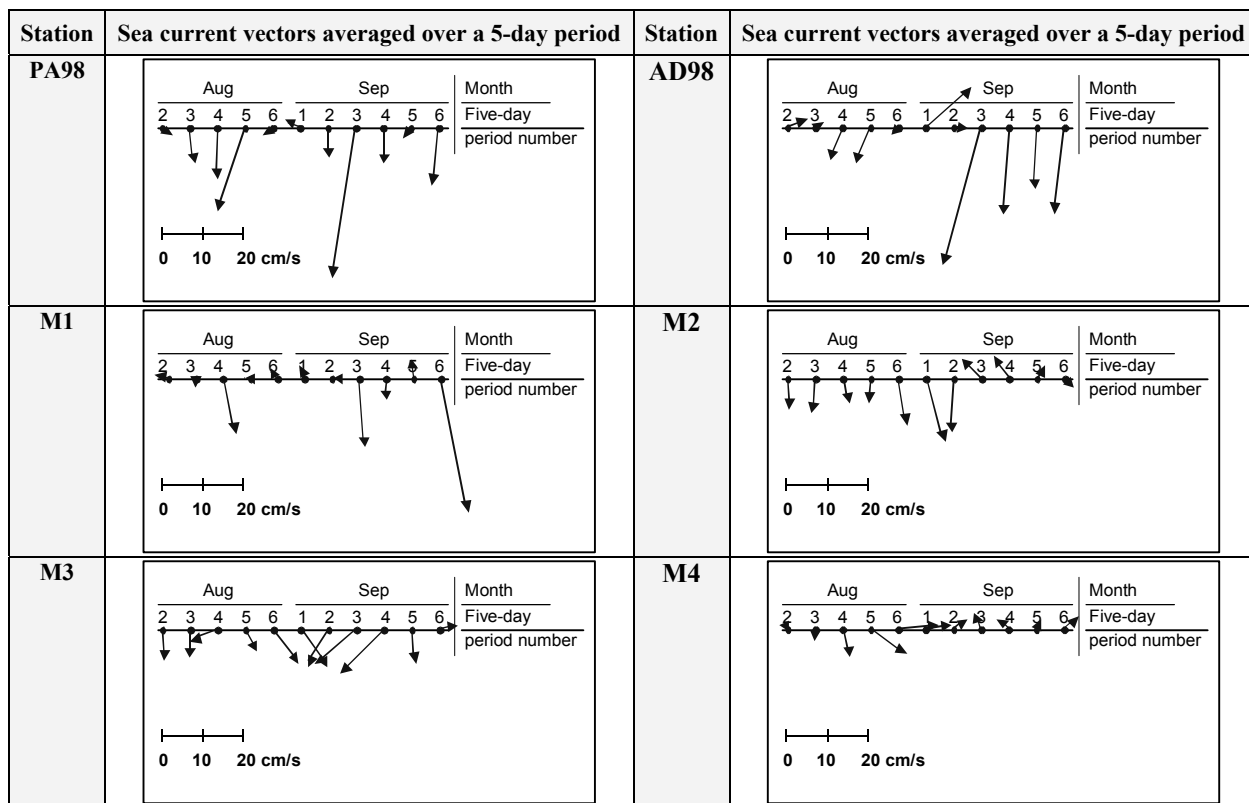


Figure 4. Synchronous current vectors averaged over a 5-day period (August–September 1998)

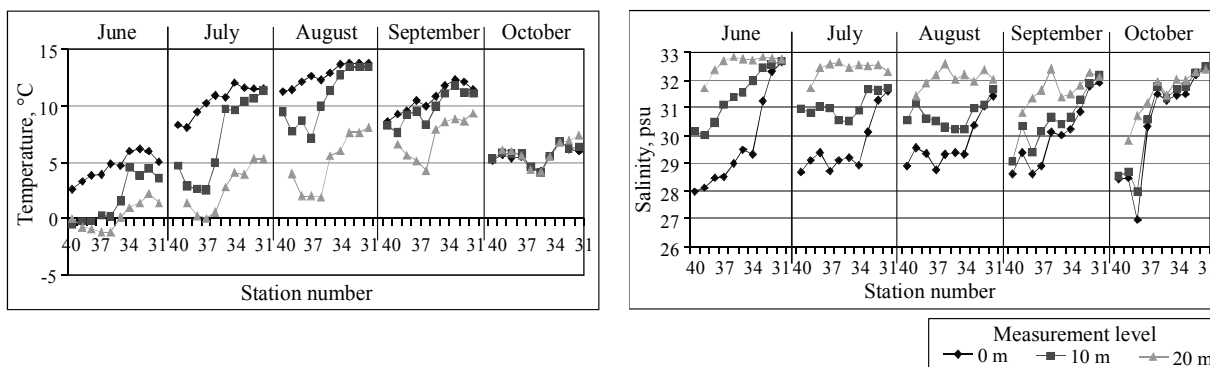


Figure 5. Long-term average water temperature and salinity at the depth of 0, 10 and 20 m during June–October at the standard section Piltun Bay – sea

the northeastern Sakhalin coast (Nabil Bay) sea level is minimum (Poezzhalova and Shevchenko, 1997). Maximum sea level near northwestern coast of the Okhotsk Sea is most probably caused by water warming-up in summer and dominating southward and southeastward surge winds.

During October–March average water transport velocity in the shelf zone amounts to 30 cm/sec. Maximum current velocity averaged over 15 days comes to 45 cm/sec. The current intensification on the shelf slope is registered a little bit later: the current velocity increases in early November and amounts to its maximum value in January (up to 35 cm/sec). Current velocity at the most remote station M4 in autumn and winter increases insignificantly; average

current velocity is 6 cm/sec and maximum current velocity averaged over a 15-day period amounts to 12 cm/sec. Low water transport velocity at station M4 testifies to the weakening East Sakhalin Current at the distance of 150 km from the shore.

Spatial and temporal distribution of sea current velocities at the shelf cross-section along 53°N (Figure 8) shows the change of sea current velocities in time depending on the distance from the shore.

Observations over the ice drift from the coastal radar stations installed on the northeastern coast of Sakhalin Island do not reveal a high velocity of the southward flow at the distance of 15–20 km from the shore as well (Tambovsky and Shevchenko, 1999).

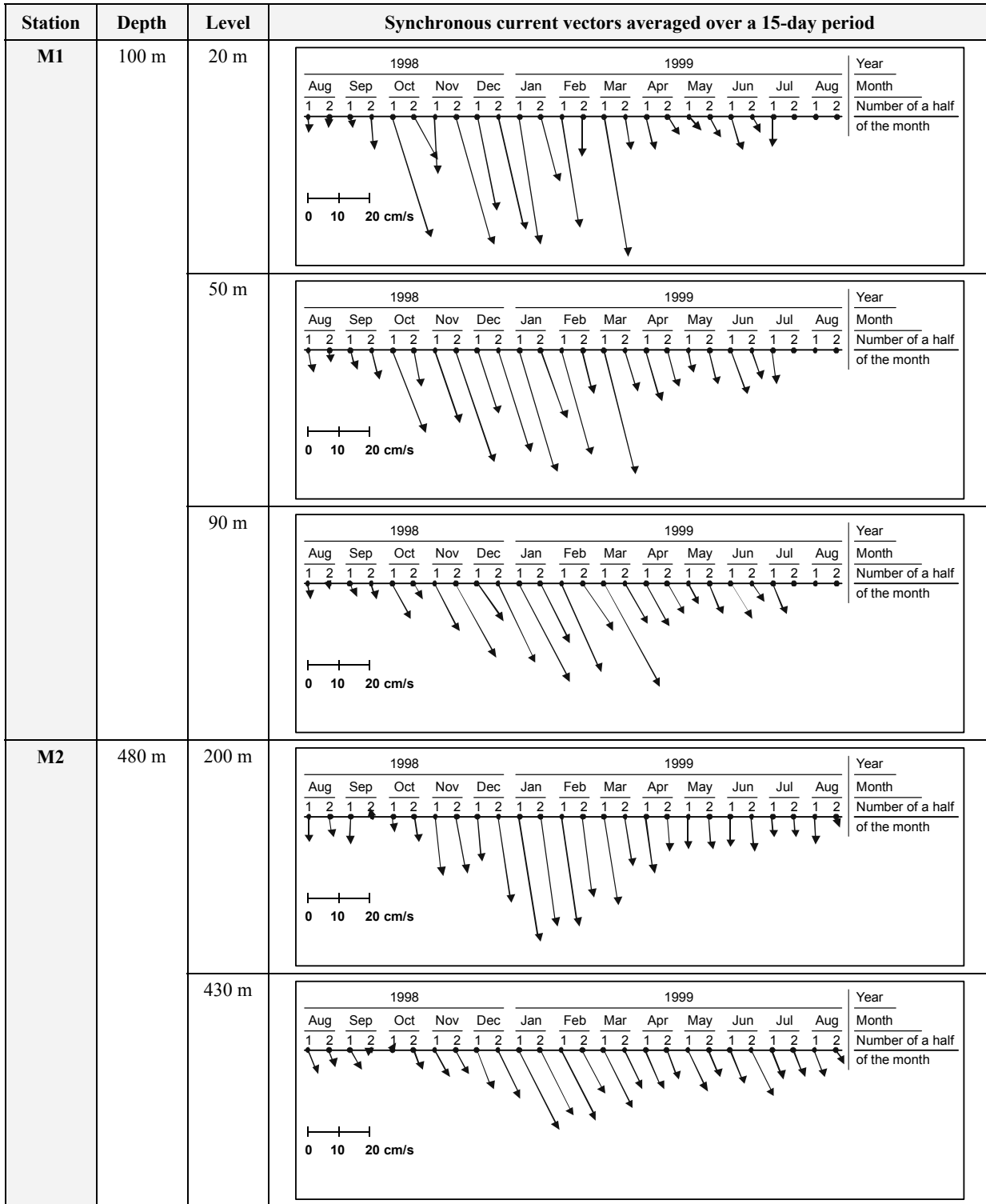


Figure 6. Synchronous current vectors averaged over a 15-day period for M1–M2 stations

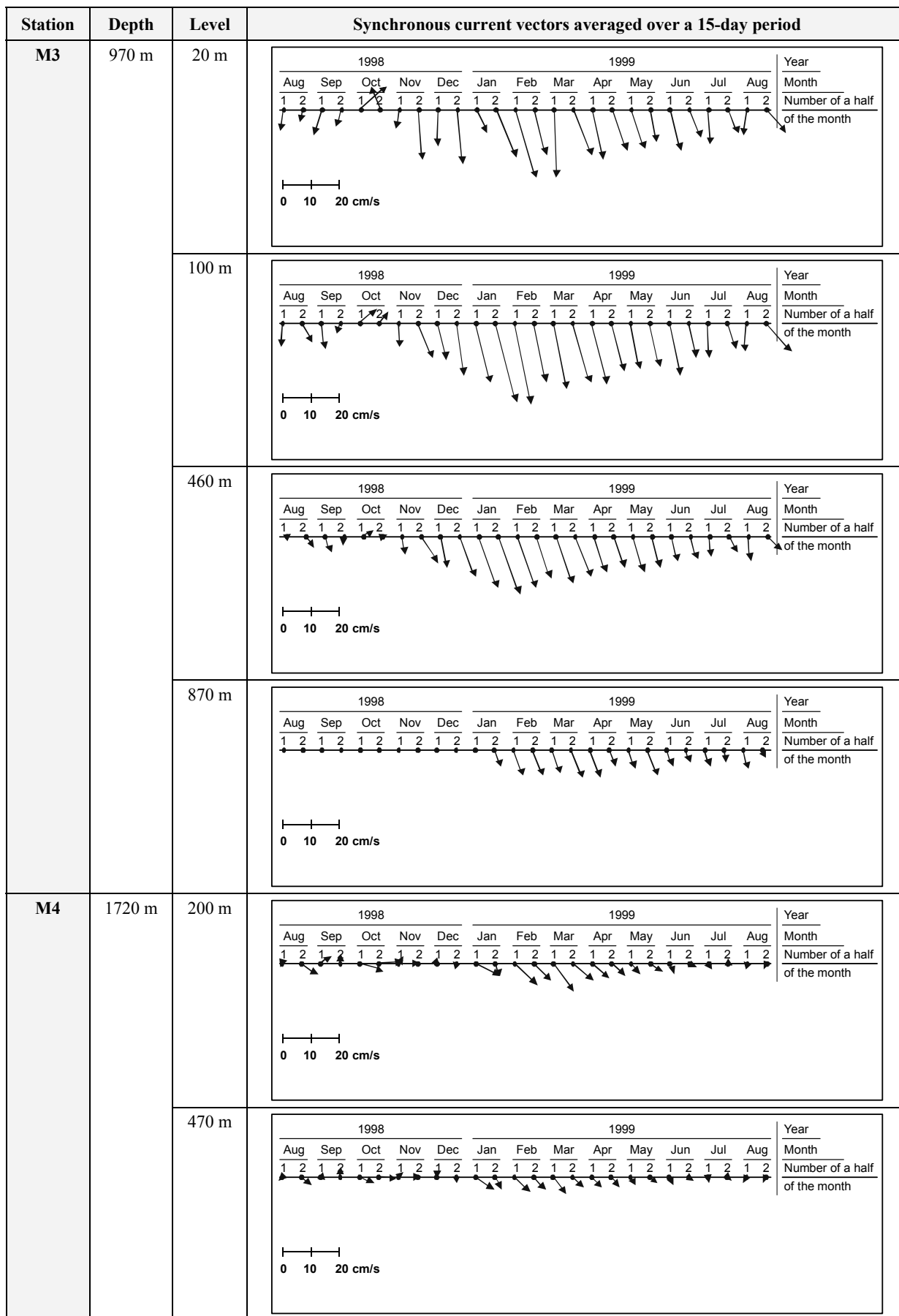


Figure 7. Synchronous current vectors averaged over a 15-day period for M3–M4 stations

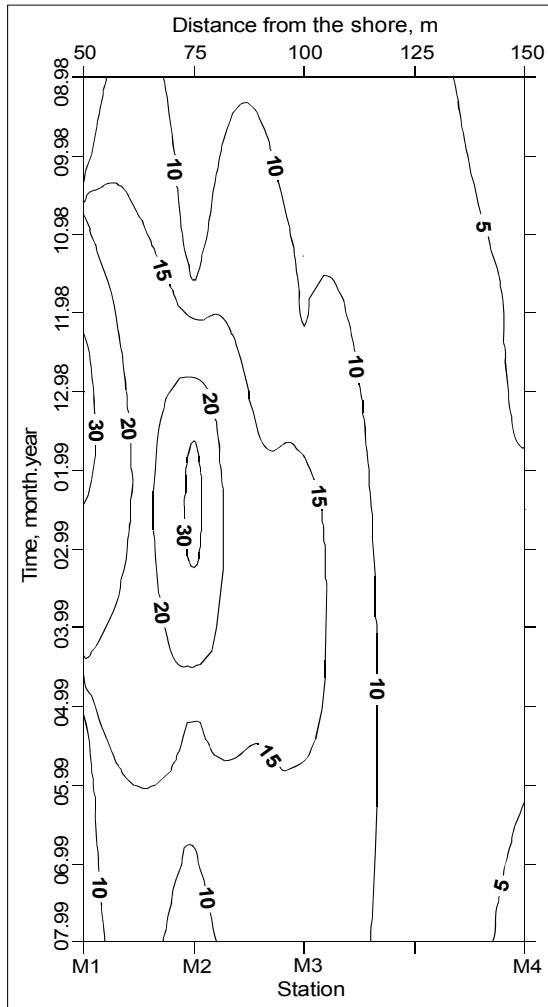


Figure 8. Spatial and temporal distribution of sea current velocities (cm/sec) at the shelf cross-section along 53°N

Average velocity of non-periodic ice drift registered at radar station Odoptu in February amounts to about 35 cm/sec and notably falls in March–April, being largely dependent on the strong permanent northward and northwestward winds related to the so called winter monsoon. Thus, it can be affirmed that intensification of the southward flow spreading over the most part of water column is mainly found on the shelf slope and weakens both towards the shore and the open sea.

Satellite altimetry data have been used to explain the features of seasonal variability of East Sakhalin Current. We have used the series of satellite measurements of sea level in the centers of 1° squares for 1993–2002 period that have preliminarily been treated of tidal component (Shevchenko and Romanov, 2004). We have chosen 3 points along 53° parallel (a point that is closest to the shore is on the upward track, the next one is on the downward track, and the most remote point is near the intersection of two tracks and, as a result, has a data series two times longer than series in other points). Two points have been chosen along the parallels of 52° and 54°. Monthly data have been averaged over the whole period of observations and calculated results are shown in Table 2. During ice cover development period altimetric data are rejected and there are almost no data for February–March. Data for January and April should be treated carefully as well. Nonetheless, analysis of data series has allowed revealing significant differences in the seasonal variations of sea level depending on the distance from the shore.

Winter maximum and summer minimum sea levels are well defined near the shore near Piltun and Niyskiy Bays, being in accord with sea level measurements by the tide gauge in Nabil Bay.

Table 2

Nonperiodic component of sea level (precomputed tidal component being extracted) for different months of the year averaged over 1993–2002 (the number in brackets shows the total quantity of data used)

Coordinates	52 N, 144 E	52 N, 145 E	53 N, 144 E	53 N, 145 E	53 N, 146 E	54 N, 144 E	54 N, 145 E
January	17.0 (2)	1.6 (4)	13.2 (3)	-1.9 (8)	-2.8 (26)	2.6 (8)	-5.7 (14)
February	–	1.1 (1)	–	–	-2.7 (2)	-18.0 (1)	-7.4 (4)
March	–	–	–	–	-4.3 (3)	–	-1.7 (3)
April	-1.1 (5)	-6.0 (7)	-6.6 (5)	-6.8 (13)	-8.8 (23)	6.0 (5)	-6.8 (13)
May	-0.9 (20)	-1.2 (21)	-1.6 (17)	-0.7 (21)	-2.8 (54)	-4.8 (19)	-1.6 (30)
June	-0.7 (26)	1.8 (26)	-0.2 (22)	1.6 (29)	0 (51)	1.5 (23)	-0.2 (26)
July	-1.7 (21)	3.6 (25)	1.3 (24)	2.0 (24)	1.7 (49)	5.7 (26)	4.4 (23)
August	-1.5 (23)	4.7 (26)	-0.1 (23)	5.1 (27)	4.9 (55)	2.7 (27)	6.3 (27)
September	-2.5 (25)	2.2 (27)	-0.8 (27)	2.5 (25)	3.8 (51)	-1.5 (29)	3.6 (26)
October	2.5 (27)	-2.6 (25)	-1.5 (25)	0.6 (28)	1.6 (53)	-1.2 (23)	0.1 (26)
November	0.5 (27)	-3.0 (28)	0.4 (26)	-4.6 (28)	-0.7 (54)	-2.9 (25)	-1.6 (27)
December	6.0 (10)	-5.5 (20)	4.0 (11)	-3.1 (22)	-2.8 (53)	-2.4 (22)	-2.6 (25)
Average	3.9	3.6	7.3	4.7	4.1	4.5	2.1

Northward and farther offshore the character of seasonal variations of the sea level changes for the opposite: maximum sea level is observed in August, whereas minimum sea level – in winter. Significant sea level gradient marked across the shoreline in winter is undoubtedly the reason for the high-velocity flow on the shelf slope. Sea level increase towards the shore is more probably a result of intensified water circulation in the Okhotsk Sea due to the strong inflow through the straits of the northern Kuril ridge as a result of the ocean response to the passage of Aleutian Low (Sedaeva and Shevchenko, 2001). Almost all tidal gauges show maximum sea level in winter (Poezzhalova and Shevchenko, 1997).

High sea level registered near Schmidt peninsula in summer, as compared to the rest of Sakhalin northeastern shelf, confirms the above assumption that sea level gradients cause the general water transport opposite to the wind direction. Low sea level in the studied area is probably caused by the coastal upwelling that is formed in the coastal zone in summer under the influence of southward winds, leaving the shore on the left, (Krasavtsev *et al.*, 2000) and results in a low air temperature.

Thus, analysis of sea level data allowed revealing the character of seasonal variability of East Sakhalin Current. In summer the current velocity is not high and the current is directed southward against prevailing southward winds, being probably caused by meridional sea level gradients.

In autumn, most often during the second half of September when the summer monsoon begins changing for the winter one, the narrow flow with a relatively low salinity and velocity of 30–40 cm/sec is formed near the coast under the influence of Amur river runoff and northward winds.

In winter southward current near the shelf slope intensifies as a result of general intensification of water circulation in the Okhotsk Sea (Mizuta *et al.*, 2001; Mizuta *et al.*, 2003). Intensification of East Sakhalin Current results in the formation of zonal sea level gradient with higher sea level values near the shore.

CONCLUSION

The present study is based on the data of instrumental sea current observations in the Okhotsk Sea aboard R/V “Professor Khromov” in 1998–2000. Researchers from Hokkaido University (Japan) have studied the structure and seasonal variability of East Sakhalin Current and published their results in (Mizuta *et al.*, 2003).

Results of the present study confirm conclusions made by Japanese researches and contain new ideas:

- Use of the data of synchronous current observation in the coastal zone (stations PA98, AD98) allowed analyzing the spatial variability of nontidal currents. Southward-directed East Sakhalin Current flows through the shelf zone cross-section from the shore to the shelf break and farther offshore. In summer the current velocity is low (5–10 cm/sec), in autumn the current intensifies in the shelf zone (up to 35–40 cm/sec) not affecting the shelf slope and offshore part.
- Use of the synchronous satellite altimetry data allowed explaining intensification of East Sakhalin Current at the shelf break in winter. Current intensification appeared to be caused by the zonal gradients of sea level with high sea level near the shore and low sea level in deep waters.

Besides, results obtained confirm, partially or fully, conclusions made before by other authors (Putov and Shevchenko, 1998; Mizuta *et al.*, 2001; Mizuta *et al.*, 2003; Pishchalnik and Bobkov, 2000; Bouden, 1988):

- The most intensive tidal currents are observed in the shallow shelf zone (up to 160 cm/sec). Along the shelf slope and farther offshore velocity of tidal currents is considerably lower (not more than 12 cm/sec).
- The shelf break is a transition zone from a cyclonically rotating tidal vector in the open sea to an anticyclonically rotating vector on the shelf. As a result, the tidal currents observed on the shelf and in the open sea are oppositely directed.
- Intensification of East Sakhalin Current is observed in autumn–winter (up to 45 cm/sec). East Sakhalin Current is not almost seen at the distance of 150 km from the shore.
- In autumn, most often during the second half of September when the summer monsoon begins changing for the winter one, the narrow flow with a relatively low salinity and velocity of 30–40 cm/sec is formed near the coast under the influence of Amur river runoff and northern winds.

ACKNOWLEDGEMENTS

Authors are sincerely grateful to Professor M. Wakatsuchi and his colleagues (University of Hokkaido) for arrangement of instrumental observations over the sea currents within the Russia-Japan marine expedition in the Okhotsk Sea aboard R/V “Professor Khromov” (FERHRI) in 1998–2000.

REFERENCES

- Bashmachnikov I.L.** 2000. Diurnal inertial tides in the Okhotsk Sea and their influence on the environment. The 15th International Symposium on Okhotsk Sea & Sea Ice, 6–10 February 2000, Mombetsu, Hokkaido, Japan: Abstracts. pp. 359–365.
- Bashmachnikov I.L., May R.I.** 2001. K1 inertial tidal wave energy distribution in the Okhotsk sea. The 16th International Symposium on Okhotsk Sea & Sea Ice, 4–8 February 2001, Mombetsu, Hokkaido, Japan: Abstracts. pp. 348–355.
- Bouden K.** 1988. Physical oceanography of the coastal waters. Moscow: Mir. 322 p. (In Russian).
- Budaeva V.D., Makarov V.G.** 1999. A peculiar water regime of currents in the area of eastern shelf of Sakhalin. PICES Sci. Reports. – Sidney; Canada. No 12. pp. 131–138.
- Kato E., Saveliev V.Yu., Shevchenko G.V.** 2001. Sakhalin Island wind characteristics by instrumental data. Dynamic processes on Sakhalin shelf and Kuril Islands. IMGG FEBRAS. Yuzhno-Sakhalinsk. pp. 177–194. (In Russian).
- Kochergin I.E., Rybalko S.I., Putov V.F., Shevchenko G.V.** 1999. Processing of the instrumental current data collected in the Piltun-Astokh and Arkutun-Dagi oil fields, North East Sakhalin shelf: some results. FERHRI Special Issue №2. pp. 96–113. (In Russian).
- Krasavtsev V.B., Popudribko K.K., Shevchenko G.V.** 2001. Spatial structure of nonperiodic sea currents on the Sakhalin northeastern shelf by measurements of 1990. Dynamic processes on Sakhalin shelf and Kuril Islands. IMGG FEBRAS. Yuzhno-Sakhalinsk. pp. 48–61. (In Russian).
- Krasavtsev V.B., Puzankov K.L., Shevchenko G.V.** 2000. Wind-induced upwelling in the area of the northeastern Sakhalin shelf. FERHRI Special Issue №3. pp. 106–120. (In Russian).
- Mizuta G., Fukamachi Y., Ohshima K.I., Wakatsuchi M.** 2001. Southward current off the east coast of Sakhalin in the Sea of Okhotsk observed from 1998 to 2000. The 16th International Symposium on Okhotsk Sea & Sea Ice, 4–8 February 2001, Mombetsu, Hokkaido, Japan: Abstracts. pp. 198–205.
- Mizuta G., Fukamachi Y., Ohshima K.I., Wakatsuchi M.** 2003. Structure and seasonal variability of the East Sakhalin Current. Journal of Physical Oceanography, 2003. Vol. 33, pp. 2430–2445.
- Pishchalnik V.M., Arkhipkin V.S.** 1999. Seasonal variations of water circulation in the Okhotsk sea area of Sakhalin shelf. FERHRI Special Issue №2. pp. 84–95. (In Russian).
- Pishchalnik V.M., Bobkov A.O.** 2000. Oceanography atlas of Sakhalin Island shelf. Part II. Yuzhno-Sakhalinsk: SakhGU. 108 p. (In Russian).
- Pishchalnik V.M., Klimov S.M.** 1991. Data of deep-water observations on the Sakhalin Island shelf in 1948–1987. Yuzhno-Sakhalinsk: IMGG FEBRAS. 166 p. (In Russian).
- Poezhalova O.S., Shevchenko G.V.** 1997. Variations in the mean water level of the Okhotsk Sea. Tsunami and attendant phenomena. Yuzhno-Sakhalinsk, pp. 131–144. (In Russian).
- Popudribko K.K., Putov V.F., Shevchenko G.V.,** 1998. Estimation of features of sea currents at Piltun-Astokh oil-gas field (Sakhalin northeastern shelf). Meteorology and hydrology, 4, pp. 82–95. (In Russian).
- Putov V.F., Shevchenko G.V.** 1998. Features of tidal conditions on the Sakhalin northeastern shelf. FERHRI Special Issue. pp. 61–82. (In Russian).
- Rabinovich A.B., Zhukov A.E.** 1984. Tidal currents on Sakhalin shelf. Oceanology. Vol. 24, pp. 238–244. (In Russian).
- Sedaeva O.S., Shevchenko G.V.** 2001. On relation of seasonal variations of sea level and atmospheric pressure near the Kuril ridge. Dynamic processes on Sakhalin shelf and Kuril Islands. IMGG FEBRAS. Yuzhno-Sakhalinsk. pp. 81–93. (In Russian).
- Shevchenko G.V.** 1996. About quasi-periodic seasonal variability of tidal harmonic constants in northwestern Okhotsk Sea. Meteorology and hydrology, 8, pp. 90–99. (In Russian).
- Shevchenko G.V., Kantakov G.A.** 2002. Recent measurements of physical and chemical parameters of water environment for monitoring purposes (August–September 2000). TINRO Proceedings, Vol. 130, pp. 95–102. (In Russian).
- Shevchenko G.V., Romanov A.A.** 2004. Determination of tidal features of the Okhotsk Sea by satellite altimetry data. Earth research from space, No. 1. (In Russian).
- Tambovsky V.S., Shevchenko G.V.** 1999. Velocity characteristics of wind- and tide-dependent ice drift in the coastal area of North East Sakhalin. FERHRI Special Issue №2. pp. 114–137. (In Russian).
- Verkhunov A.V.** 1997. Large-scale water circulation in the Okhotsk Sea. Complex researches of the Okhotsk Sea ecosystem. Moscow: VNIRO. pp. 8–19. (In Russian).
- Zalesniy V.B., Kontorovskiy S.E.** 2002. Numerical modeling of wind-driven, thermohaline and tidal currents in the Okhotsk Sea. Oceanology. Vol. 42, pp. 659–667. (In Russian).

SEAWATER DENSITY DISTRIBUTION IN PETER THE GREAT BAY

M.A. Danchenkov

Far Eastern Regional Hydrometeorological Research Institute (FERHRI), Russia
Email: danchenk@vladivostok.ru

In order to clarify the features of spatial water density distribution in Peter the Great Bay both in summer and winter, the data of unique oceanographic surveys of 1999–2003 have been used. Surface fronts of density – along the coast and 47°N – and steady near-bottom eastward current were revealed. Known Liman current was not traced within the limits of the bay.

INTRODUCTION

Peter the Great Bay (PGB), located in the northwestern part of the Japan Sea (Figure 1), is a unique sea area because of subarctic and subtropical waters combination.

During winter, about 10% of total sea ice cover is formed here (Bulgakov, 1968). Monthly average winter air temperature in Vladivostok is less than at the station Belkin located far to the north (46.5°N) of Vladivostok (Danchenkov *et al.*, 1996).

In August–September, the mola-mola, anchovy, barracuda, tuna, *i.e.* fish species typical for subtropics are caught here (Ivankov and Ivankova, 1998). Warm waters penetrating into this area by a chain of eddies (Danchenkov *et al.*, 1997; Nikitin *et al.*, 2002) promote long and warm autumn.

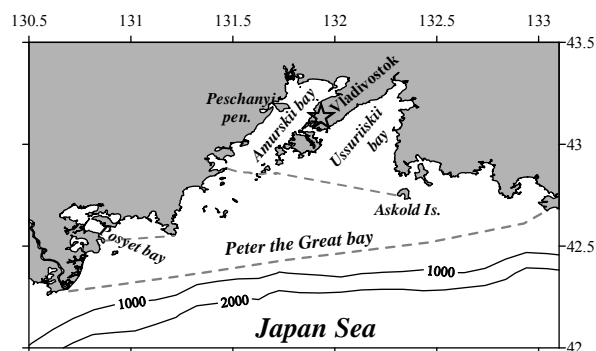


Figure 1. Peter the Great Bay

The waters of PGB are investigated rather poorly in comparison with waters of the whole Japan Sea (Bibliography, 2000). It is usually considered (Yarichin, 1982; Sailing directions, 1996) that Liman current with cold and fresh waters crosses this area. Spatial distribution of water density is poorly known in particular.

The knowledge of spatial distribution of density is necessary for study of currents. On the base of density data it is possible to calculate the direction and speed of currents in offshore areas. Even in coastal areas the horizontal distribution of density allows (Uda *et al.*, 1977) to show the approximate direction of gradient currents. Thus, for example, the frequently cited map of surface currents of the Japan Sea (Uda, 1934) was constructed. From the analysis of vertical distribution of density it is possible to get information about direction of vertical water movement.

The present work is a follow-up of previous research of PGB waters published earlier (Danchenkov *et al.*, 2003a; Danchenkov *et al.*, 2003c).

DATA

For analysis of water density distribution in PGB, the data of 5 oceanographic surveys in different seasons were used (Table 1).

The distribution of stations is shown on the maps below. It is important to note that accuracy of measurements of temperature and salinity, on which

Oceanographic surveys, which CTD-data were used in this work

R/V	Period	Latitude (N), Longitude (E)	Z, m	T, °C	S, psu	Nst
Lugovoye	23.11–3.12.1999	42.3–43.3, 130.7–133.0	235	0.5–11.1	32.0–34.18	104
Lugovoye	4–12.03.2000	42.3–43.3, 130.7–133.0	221	-1.9–01.0	33.3–34.70	84
Gordienko	15–18.8.2001	42.6–43.2, 131.2–132.3	85	0.9–25.3	12.3–34.26	67
Gidrobiolog	15–16.8.2001	42.8–43.2, 131.6–132.3	68	1.1–24.4	25.6–34.05	46
Gordienko	14–17.11.2001	42.6–43.2, 131.2–132.3	84	0.7–10.8	32.1–34.19	75
Gidrobiolog	14–15.11.2001	42.8–43.2, 131.7–132.3	54	1.6–10.2	33.2–34.05	36
Gordienko	9–11.08.2003	42.6–43.2, 131.2–132.3	85	0.9–25.3	13.7–34.23	67

Note:
R/V – research vessel; Z – lowest level of measurements; T – water temperature; S – water salinity; Nst – number of CTD stations

density was calculated, in these expeditions were different (but not less than 0.01°C and 0.02 psu, respectively).

Density of sea water ($\sigma\text{-}t_0$) was calculated from the measured values of temperature and salinity using standard formulas (UNESCO, 1983).

RESULTS AND DISCUSSION

In winter, surface waters of PGB have low (from -1.7°C up to 0°C) temperature and low (less than 34.00 psu) salinity. In this period, the density of PGB surface waters is about 27.25–27.35 (Vanin *et al.*, 2001). Waters with high (more than 27.38) density were found usually near the bottom or in shallow bays (Koryakova, 1987). Near-bottom waters of high density in PGB usually do not reach the continental slope (located approximately at 42.2°N).

In winter, two local areas of PGB had specific features. One of them was located to the south of Posyet bay, and another one in the area near Askold island. For the first area warm and fresh waters were typical. The origin of warm waters is probably connected with the penetration of warm subtropical waters from the south. Due to comparatively warm waters, the surface pycnocline was located to the south of Posyet. Waters of high salinity were characteristic for the second area. They were probably resulting from seasonal upwelling (Goncharenko *et al.*, 1993) and westward current (Aubrey *et al.*, 2001). Waters of these two areas had low and high density, respectively.

November–December of 1999 and November of 2001. In November–October of 1999, area of the upwelling to the south of Askold island was the basic feature of spatial distribution of density. Inside it, homogeneous waters of high density (more than 27.15) occupied almost the whole water column with the exception of near-bottom layer. Water density below near-bottom pycnocline was more than 27.33. From the west, area of the upwelling was limited by the strong front of density (approximately along 132°E). Surface southward current (picked out by gradients of density) corresponded to it. Waters from Golden Horn Bay distributed both into Amurskiy Bay and into Ussuriyskiy Bay.

In 1999 light waters existed in two areas – in Amurskiy Bay and to the south of Posyet bay (area of warm salty water).

Zonal heterogeneity in the density distribution and front of density along meridian testify to the absence of Liman current in limits of PGB.

In November 14–17, 2001 surface water density was essentially less than it was two years before. The upwelling was absent. Basic features of surface density distributions were two fronts of density – zonal front in Amurskiy bay and coastal one – in Ussuriyskiy bay. Light (warm and salty) water

distributed by two fingers to the west and to the north from Askold island. Comparatively high density (more than 26.4) corresponded to the coastal waters of Ussuriyskiy bay only. Water density of near-bottom layer in its south-eastern part was unusually high – more than 27.3.

March of 2000. During winter the surface pycnocline disappeared in most part of the bay – waters of PGB in winter were mixed up well. And near-bottom pycnocline, limiting the newly formed waters of high salinity, appeared. The density of near-bottom waters reached very high values (more than 27.8) – Figure 2. In winter of 2000 high values of density were characteristic not only for the shallow bays, but also for the whole shelf of eastern part of PGB. By values of density (Figure 2) and area engaged in waters of high density (Figure 3), the winter of 2000 has to be considered as unusually cold. Dense (more than 27.40) waters were found above the slope. Newly formed waters of high salinity were found later, in summer of 2000, in bottom layer of deep Japan Basin. The measurements in winter of the next year also have shown the occurrence of newly formed dense waters at the continental slope and near the bottom of deep Japan Basin (Senjyu *et al.*, 2002).

To the south of Askold island, rather warm (1–27°C higher than it was in surrounding areas) waters were traced during the whole winter. It is known (Moiseev, 1937), there is a congestion of flounders of PGB on winter stay. The origin of warm waters is connected to a westward current along 42°N (Aubrey *et al.*, 2001; Danchenkov *et al.*, 2003b). These waters are peculiar due to rather high (more than 27.3) density and low contents of the dissolved oxygen.

However the limits of these waters are allocated better by high salinity: from the south they border interfrontal (between Subarctic and Northwest fronts) waters of low salinity, and from the north – fresh coastal waters (Danchenkov *et al.*, 2000).

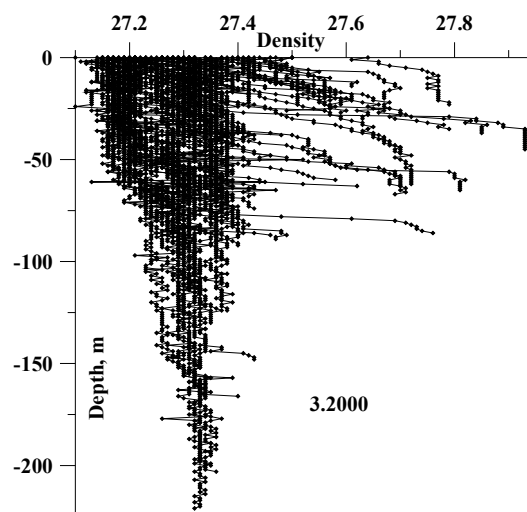


Figure 2. Vertical distribution of water density in PGB in winter (March of 2000)

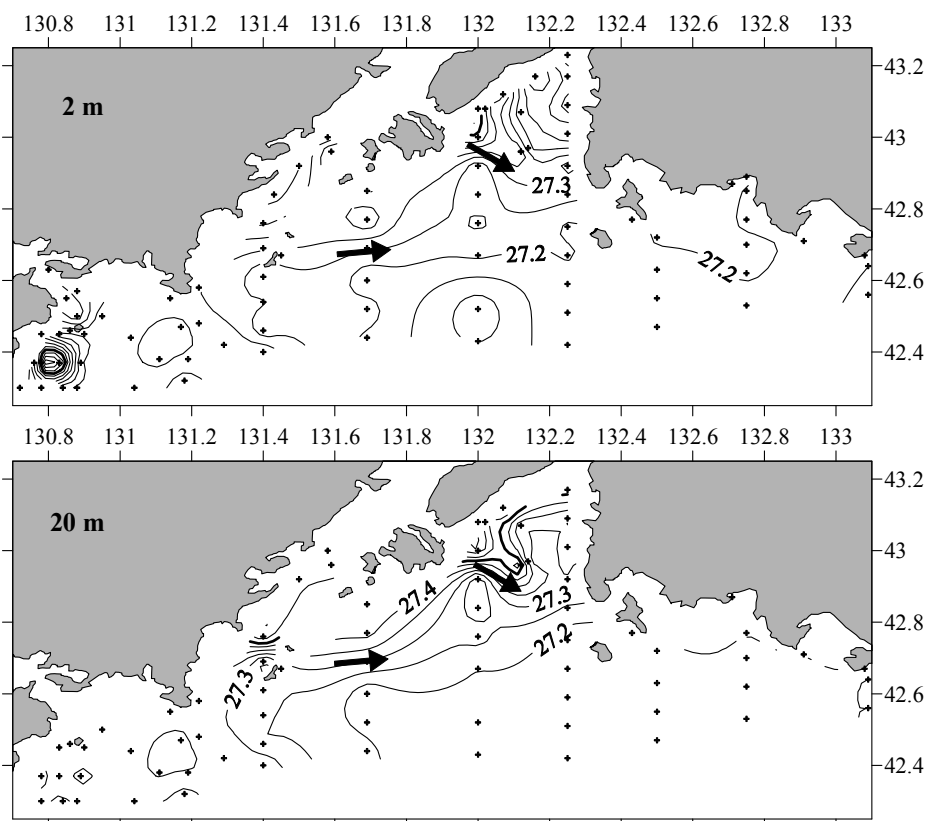


Figure 3. Distribution of PGB water density at the surface and 20 m level in winter (March of 2000)

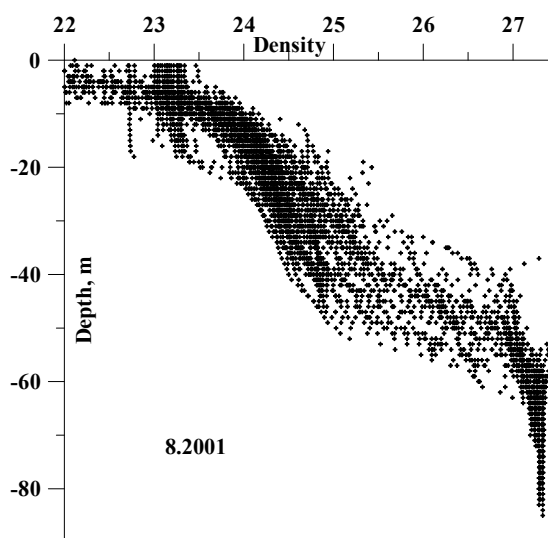


Figure 4. Vertical distribution of PGB water density in summer (August of 2001). The lowest value of salinity scale is restricted

Summer of 2001. Basic feature of PGB waters in summer is a strong (down to 5 psu) decrease of water salinity in Amurskiy Bay.

Fresh waters are distributed within the limits of a thin surface layer (Figure 4) and along the western coast of the bay only. Due to it, the strongest water stratification was characteristic to the north-western part of PGB (Figure 4).

Vertically, the PGB waters are possible to be divided into three parts: the surface layer, pycnostad and near-bottom layer. Between them two pycnoclines are located: surface and near-bottom ones.

The thickness of homogeneous surface layer was various in different parts of PGB. The lowest thickness was characteristic for the Amurskiy Bay (in its northern part thickness was less than 1 m), and the greatest (to 20 m) – for waters south of Askold is. (the south-eastern part of PGB).

In pycnostad (intermediate layer) the water temperature, salinity and density changed in small limits (16–18°C, 32.8–33.5 psu, 23–25, accordingly). The thickness of pycnostad was various also. To the north of Peschanyi peninsula its thickness decreased. And in the northern part of the bay it disappears at all – both pycnoclines (surface and near-bottom) merged.

Density of near-bottom layer in Amurskiy and Ussuriyskiy bays was different (it was higher in the latter bay). The value of near-bottom water density in Ussuriyskiy Bay, in summer of 2001 was close to the characteristic for Japan Sea Proper water (more than 27.32). Near-bottom water in summer of 2001 was colder and saltier than in September of 1981 or in November of 1999.

At the surface of PGB some seasonal fronts of density were allocated (Figure 5): across Amurskiy Bay at 43.15°N, along the Amurskiy Bay, along the coast of Ussuriyskiy Bay and at 42.7°N.

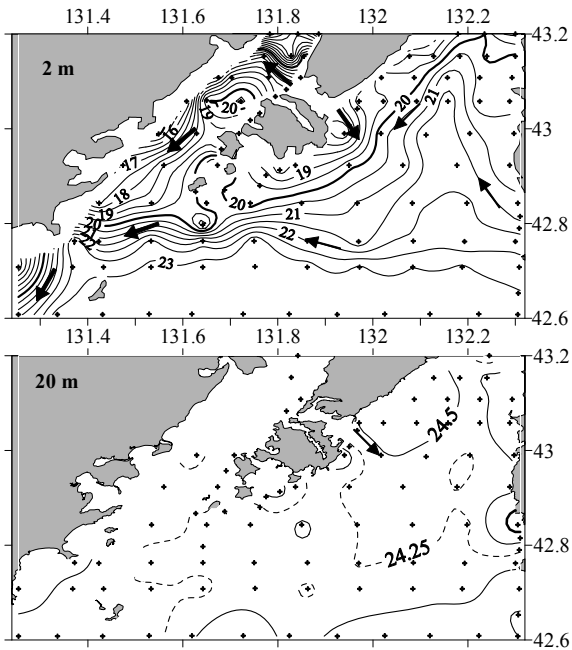


Figure 5. Distribution of density in August of 2001 at the surface and 20 m level

Front of density crossing Amurskiy Bay is the barrier for coastal current. The existence of this front explains the known (Gomoyunov, 1927) difference of water circulation to the south and north of 43.15°N. The continuous coastal current begins to the south of this front only.

At such distribution of density in summer, two contrary directed currents (as pointed in Sailing directions, 1996) could not exist.

Weak gradients of density along 42.7°N show that surface waters have to be transported there from the east to the west. Such a weak current could be identified with the known Liman current. However these gradients are limited to a thin surface layer. Usually (Yarichin, 1982) the position of Liman current is shown to the south – “along continental slope” – and “below surface thermocline”. The thickness of Liman current is considered more than 10 m (core of current was shown at 100 m level). Therefore, surface current along 42.7°N is possible to consider as local, distinctive one from Liman current.

Summer of 2003. Does Liman current pass to the south of areas of these expeditions? The data of the measurements in area situated south of them (in summer of 2003) allows us to answer this question.

In this summer in eastern part of PGB water gradients along 42.4°N at the surface and at 20 m level showed currents of opposed directions (Figure 6). Below the tongue of warm and salt waters was found. Let us notice, that Liman current is considered as the flow of cold and fresh waters (Yarichin, 1982). This tongue was revealed in winter (between PGB and 137°E) also (Danchenkov *et al.*, 2000).

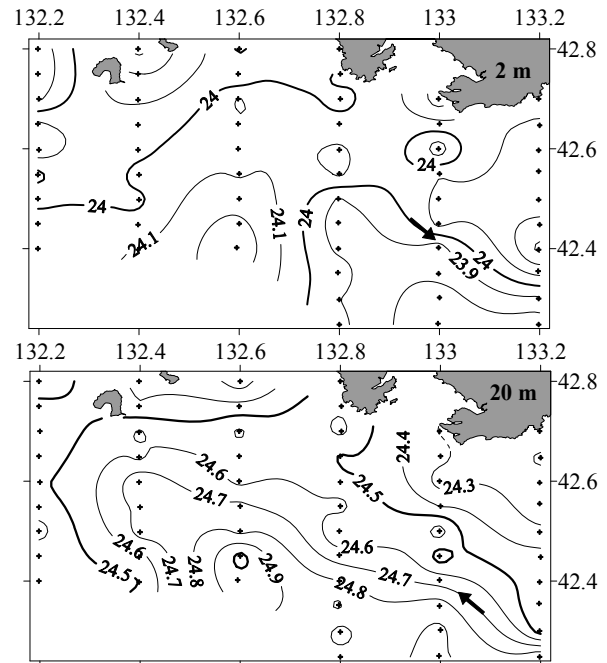


Figure 6. Distribution of density in August of 2003 at the surface and 20 m level

Density gradients to the north and to the south of the tongue correspond to two currents of different directions: eastward one along 42.6°N and westward – along 42.4°N. However, westward current (like it was at the surface) was limited to the longitude of 132.6°E. Therefore it is possible to conclude: no westward flow of cold waters (Liman current) was traced along the coast neither in summer nor in winter.

ON VERTICAL WATER MOVEMENT

Areas where the isolines of density come out from intermediate layer to the surface are probable areas of upwelling. Therefore, areas of pointed fronts in summer as well as in winter could be considered as areas of strong vertical movements. In summer of 2001 strong upwelling was traced just to the south of the density front near Peschaniy peninsula. Water temperature inside the isolated area was 2.5°C lower and salinity 4.5 psu higher than in surrounding waters.

During summer, any vertical water movement in the northern Amurskiy Bay is impossible due to strong stratification. Therefore, the penetration of nutrients from the bottom layer into the surface layer is possible during storms only.

In November (1999, 2001), the upwelling was characteristic for the southeastern part of Ussuriyskiy Bay close to Askold island. There the output on the surface of comparatively cold and salty waters was traced.

In winter, waters of PGB in general are well mixed owing to strong winds. In spite of that, it is possible to separate the area of strongest vertical movements: along the slope.

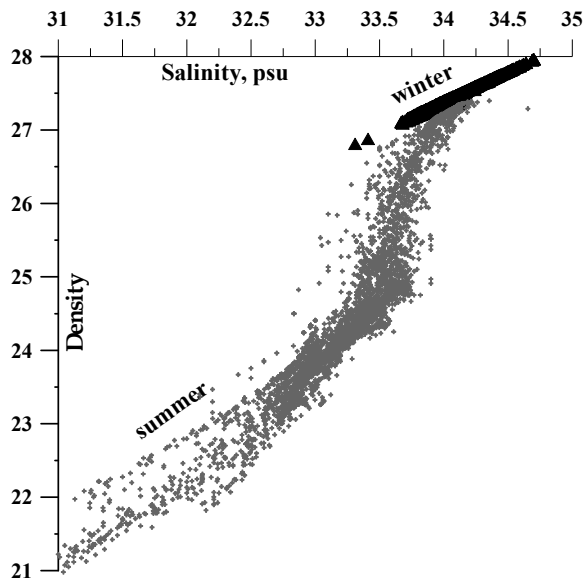


Figure 7. Dependence of density on salinity. Winter (2000) values are designated by black triangles, summer (2001) ones – by grey points. Salinity scale is limited by 33.5 psu

ON LINEAR DEPENDENCE OF DENSITY ON SALINITY

In winter, the dependence of density on salinity (except for a range 33.9–34.3 psu) can be described by a linear function (Figure 7).

In summer, density/salinity ratio submits to this simple function in some intervals (0–17°C and 20–25°C of temperature and 15–33 psu of salinity).

The dependence of temperature on salinity – T(S)-diagram – for two seasons is shown in Figure 8. Salinity scale is restricted by 32.5 psu. It can be seen that PGB is the source of two different types of waters: fresh (salinity is less than 33.6 psu) water in summer and high salinity (more than 34.06 psu) water in winter.

REFERENCES

- Aubrey D.G., Danchenkov M.A., Riser S.C. **2001**. Belt of salt water in the north-western Japan Sea. "Oceanography of the Japan Sea" (Ed. M.A.Danchenkov), Vladivostok, Dalnauka, pp. 11–20.
- Bibliography** of the oceanography of the Japan/ East Sea. PICES Sci.Rep., **2000**, N13, 99 p.
- Bulgakov N.P. **1968**. Sea ice. Hydrology of the Pacific ocean. Moscow, Nauka, pp. 434–468. (In Russian).
- Danchenkov M.A., Kim K., Goncharenko I.A. **1996**. Extremal winters in the NW part of the East/Japan Sea by monthly air temperature. Proc. 4-th CREAMS Workshop, Vladivostok, pp. 7–16.

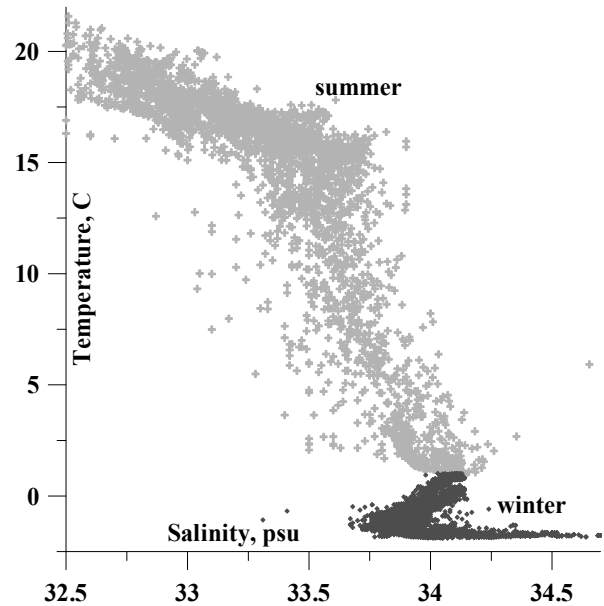


Figure 8. Dependence of temperature on salinity. Winter (2000) values are designated by black and summer – by grey colour. Scale salinity is limited

CONCLUSIONS

Two pycnoclines in summer and one in winter were revealed in Peter the Great Bay.

Liman Current was not traced in summer and in winter.

The following features of PGB waters are characteristic in summer:

- three surface fronts
- tongue of dense water to the south of Askold island
- eastward near-bottom current.

Danchenkov M.A., Aubrey D.G., Feldman K.L. **2003a**. Oceanography of area close to the Tumannaya river mouth (the Japan Sea). Pacific oceanography, v.1, N1, pp. 61–69.

Danchenkov M.A., Aubrey D.G., Lobanov V.B. **2000**. Spatial water structure in the north-western Japan Sea. "Hydrometeorology and ecology of the Russian Far East seas" (Ed. Kochergin I.E.). Vladivostok, Dalnauka, pp. 92–105. (In Russian).

Danchenkov M.A., Feldman K.L., Fayman P.A. **2003c**. Water temperature and salinity of the Peter the Great bay. "Hydrometeorology and ecology of the Russian Far East area" (Ed. Kochergin I.E.). Vladivostok, Dalnauka, pp. 10–25. (In Russian).

- Danchenkov M.A.**, Riser S.C., Yoon J.-H. **2003b**. Deep currents of the central Sea of Japan. *Pacific oceanography*, v.1, N1, pp. 6–11.
- Danchenkov M.A.**, Lobanov B., Nikitin A.A. **1997**. Mesoscale eddies in the Japan Sea, their role in circulation and heat transport. *Proc. CREAMS Int. Symposium*. Fukuoka, pp. 81–84.
- Fayman P.A.** **2003**. The currents modeling for the Peter the Great bay on the base of FERHRI survey, 2001. *Pacific oceanography*, v.1, N1, pp. 79–81.
- Gomoyunov K.A.** **1927**. Hydrological description of the Amurskii bay and Suifun river. “Productive opportunities of Russian Far East area”. Vladivostok, Knizhnoye delo, N2, pp. 73–91. (In Russian).
- Goncharenko I.A.**, Federyakov V.G., Lazaryuk A.Yu., Ponomarev V.I. **1993**. The processing of AVHRR data on an example of coastal upwelling. *Issledovanie Zemli Iz Kosmosa*, N 2, pp. 97–107. (In Russian).
- Ivankov V.N.**, **Ivankova Z.G.** **1998**. Tropical and subtropical species of fishes in the north-western Japan Sea. *Izvestiya TINRO*, v.123, pp. 291–298. (In Russian).
- Koryakova M.D.** **1987**. Hydrochemical and hydrological characteristics of Peter the Great Bay waters. *FERHRI Proc.*, N 36, pp. 59–67. (In Russian).
- Moiseev P.A.** **1937**. Fishery of flounders by small-sizes vessels in Ussuri Bay in spring of 1935. *Izvestiya TINRO*, v.12, pp. 125–158. (In Russian).
- Nikitin A.A.**, Lobanov V.B., Danchenkov M.A. **2002**. Possible routes of warm subtropical water transport to the area of Far Eastern Marine Reserve. *Izvestiya TINRO*, v.131, pp. 41–53. (In Russian).
- Sailing directions** of north-western Japan Sea. **1996**. Saint-Petersburg, 354 p. (In Russian).
- Senjyu T.**, Aramaki T., Otsuka S., Togawa O., Danchenkov M., Karasev E., Volkov Yu. **2002**. Renewal of the bottom water after the winter 2000–2001 may spin-up the thermohaline circulation in the Japan Sea. *Geophys.Res.Letters*, v.29, N7, pp. 53-1–53-4.
- Uda M.** **1934**. Results of simultaneous oceanographical investigations in the Japan Sea and its adjacent waters during October and November 1933. *J.Imp.Fish.Exp.Station*, v.7, pp. 91–151.
- Uda M.**, Kishi A., Nakao T. **1977**. Cyclonic eddies along the edge of the Kuroshio. *J. Fac.Mar.Sci., Tokai Univ.*, N 10, pp. 19–30.
- UNESCO**, **1983**. Algorithms for computation of fundamental properties of seawater, by N.P.Fofonoff and R.C.Millard Jr. *Tech.Pap.Mar.Sci.*, N44, 53 p.
- Vanin N.S.**, Yurasov G.I., Zuenko Y.I., Nedashkovskiy A.P., Ermolenko S.S. **2001**. Monitoring of the update state of Peter the Great bay waters based on observations of November 1999–April 2000. “Oceanography of the Japan Sea” (Ed. M.A. Danchenkov), Vladivostok, Dalnauka, pp. 150–157.
- Yarichin V.G.** **1982**. Some peculiarities of horizontal movement of water of the Japan Sea northward of 40 N. *FERHRI Proc.*, N 96, pp. 111–120.

TRACE METALS IN BOTTOM SEDIMENTS NEAR VLADIVOSTOK, RUSSIA

A.V. Tkalin¹, B.J. Presley²

¹ Far Eastern Regional Hydrometeorological Research Institute (FERHRI), Russia
Email: atkalin@hydromet.com

² Texas A&M University, College Station, USA

Vladivostok city is situated on a peninsula between Amursky Bay to the west and Ussuriysky Bay to the east, Vladivostok harbor is located in Golden Horn Bay and East Bosphorus Strait (Figure 1). The main pollution sources are as follows: 1) industrial wastewaters and municipal sewage; 2) river runoff; 3) atmospheric deposition; 4) dredged material dumping; 5) discharges from ships. The total discharge of industrial and domestic wastewaters from Vladivostok to Amursky, Ussuriysky and Golden Horn Bays is estimated as $483 \times 10^6 \text{ m}^3$ (Gavrilevsky *et al.*, 1998). Some of these discharges, such as trace metals supplied by river runoff usually are deposited to the bottom sediments within the estuarine area. Therefore, for the coastal waters around Vladivostok, trace metals are introduced to the marine environment mainly with industrial wastewaters and polluted dredged material. Estimated annual inputs of trace metals to Amursky Bay from these two sources are,

for example, about 60 t for Ni and 90 t for Cu (Tkalin, 1990). An additional source of trace metals for Ussuriysky Bay is the coastal landfill which is sliding into the sea.

The trace metal content in bottom sediments around Vladivostok has been studied by several groups of researchers (*e.g.*, Anikiev *et al.*, 1993; Khristoforova *et al.*, 1993; Shulkin, 1991). As a result, distribution of trace metals in bottom sediments of Peter the Great Bay is quite well documented. Unfortunately, most of these works were published in Russian and therefore are not accessible to the wider scientific community. This short contribution is intended to supplement the data published earlier (Tkalin *et al.*, 1996) and to demonstrate the spatial distribution of different metals in surficial bottom sediments of Amursky and Ussuriysky bays and the East Bosphorus Strait.

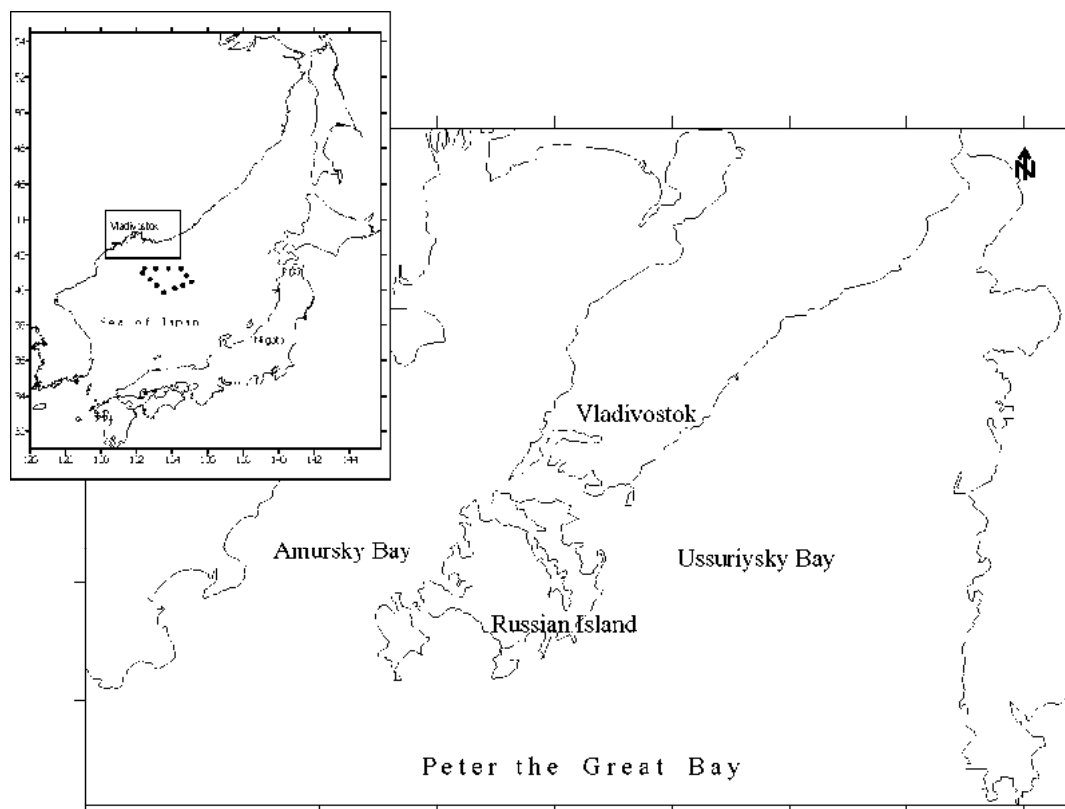


Figure 1. Peter the Great Bay

The methods of trace metal analysis were described in detail in the earlier publication (Tkalin *et al.*, 1996). Bottom sediments were collected by a Petersen grab in September–October 1994. Only the surface layer (0–2 cm) was used for analysis. Sediments were dried at 105°C and ground to a fine powder. 200 mg of the powdered sediments were weighed into Teflon “bombs” and completely dissolved in a mixture of nitric, hydrofluoric and boric acids by a prolonged exposure of the closed bombs to a temperature of 130°C. Concentrations of metals were measured in the clear digests (diluted if necessary) by atomic absorption spectrophotometry (AAS) as described in the US National Status and Trends methods (Leuenstein and Cantillo, 1993). A Perkin-Elmer Corp. Model 306 flame AAS was used for Fe, Mn and Zn analysis. Other elements were determined using a Perkin-Elmer 3030Z equipped with a HGA-600 graphite furnace and an auto sampler. Details of furnace programs, matrix modifiers, blanks, spikes, reference materials and other QA/QC information can be found in (Leuenstein and Cantillo, 1993). Matrix spike recovery was almost always >90% as were recoveries of certified values of reference materials.

The distributions of Zn, Pb, Cu, Cd, Hg and Ag in bottom sediments are shown in Figure 2. Elevated concentrations of trace metals in bottom sediments were found near their sources: industrial wastewater outfalls in Amursky and Ussuriysky bays; Vladivostok harbor (Golden Horn Bay and East Bosphorus Strait); city landfill on the shore of Ussuriysky Bay. Maximum concentrations of Zn, Pb, Cu and Hg (and

Cd at two most polluted stations) in bottom sediments around Vladivostok were higher than those which might cause negative biological effects (Long *et al.*, 1995).

Sediment grain size and organic carbon content also affect trace metal distribution. In general, bottom sediments have higher sand content in Ussuriysky Bay than in Amursky. Therefore, average concentrations of trace metals in Amursky Bay are higher than in Ussuriysky. The content of organic carbon (C_{org}) in bottom sediments in 2001 is shown in Figure 3. There is a strong similarity in distributions of trace metals and C_{org} in bottom sediments (Figure 2 and Figure 3). The effect of river discharge (Razdolnaya river discharge to Amursky Bay and Artemovka river discharge to Ussuriysky Bay respectively) on trace metal distribution in bottom sediments is quite limited. Similar effect of city landfill on trace metal distribution in bottom sediments was noted by Anikiev *et al.* (1993), in mussels by Shulkin *et al.* (2003) and Tkalin *et al.* (1998). The slight difference in distributions of Hg and Ag and those of other metals might be explained by mineralogical composition of bottom sediments.

This work became possible due to a Fulbright Program grant to A.V. Tkalin and the generosity of the Trace Element Research Lab (B.J. Presley) at Texas A&M University. Thanks also to Tatiana Belan for providing organic carbon data. The help of all specialists who participated in sample collection is greatly appreciated.

REFERENCES

- Anikiev V.V., Perepelitsa S.A., Shumilin E.N. 1993. Estimation of influence of anthropogenic and natural sources on spatial distribution of heavy metals in bottom sediments of the Peter the Great Bay (the Sea of Japan). *Geokhimiya*, No. 9, pp. 1328–1340. (In Russian).
- Gavrilevsky A.V., Gavrilo T.A., Kochergin I.E. 1998. Comprehensive quantitative assessment of pollution sources adjacent to Vladivostok. In: *Hydrometeorological Processes at the Sea Shelf, Marine Environmental Impact Assessment*. Dalnauka, Vladivostok, pp. 102–113. (In Russian).
- Khristoforova N.K., Shul'kin V.M., Kavun V.Ya., Chernova E.N. 1993. Heavy Metals in Fished and Cultured Species of Marine Molluscs in Peter the Great Bay. Vladivostok, Dalnauka. 296 p. (In Russian).
- Leuenstein G., Cantillo A., editors. 1993. Sampling and Analytical Methods of the National Status and Trends Program, National Benthic Surveillance and Mussel Watch Projects, 1984–1992. Vol. III, Comprehensive Descriptions of Elemental Analytical Methods. NOAA Technical Memorandum NOS ORCA 71. Silver Spring, MD, USA. 219 p.
- Long E.R., MacDonald D.D., Smith S.L., Calder F.D. 1995. Incidence of adverse biological effects within ranges of chemical concentrations in marine and estuarine sediments. *Environment and Management*, vol. 19, pp. 81–97.
- Shulkin V.M. 1991. Heavy metals in modern bottom sediments of Amursky Bay (Japan Sea). Vladivostok, PGI FEBRAS. Deposited in VINITI, No. 4017-B91, 25 p.
- Shulkin V.M., Presley B.J., Kavun V.Ia. 2003. Metal concentrations in mussel *Crenomytilus grayanus* and oyster *Crassostrea gigas* in relation to contamination of ambient sediments. *Environment International*, vol. 29, pp. 493–502.
- Tkalin A.V., editor. 1990. Some Regional Consequences of Anthropogenic Impact on the Marine Environment. Leningrad, Hydrometeoizdat. 163 p. (In Russian).
- Tkalin A.V., Lishavskaya T.S., Shulkin V.M. 1998. Radionuclides and trace metals in mussels and bottom sediments around Vladivostok, Russia. *Marine Pollution Bulletin*, vol. 26, pp. 551–554.
- Tkalin A.V., Presley B.J., Boothe P.N. 1996. Spatial and temporal variations of trace metals in bottom sediments of Peter the Great Bay, the Sea of Japan. *Environmental Pollution*, vol. 92, pp. 73–78.

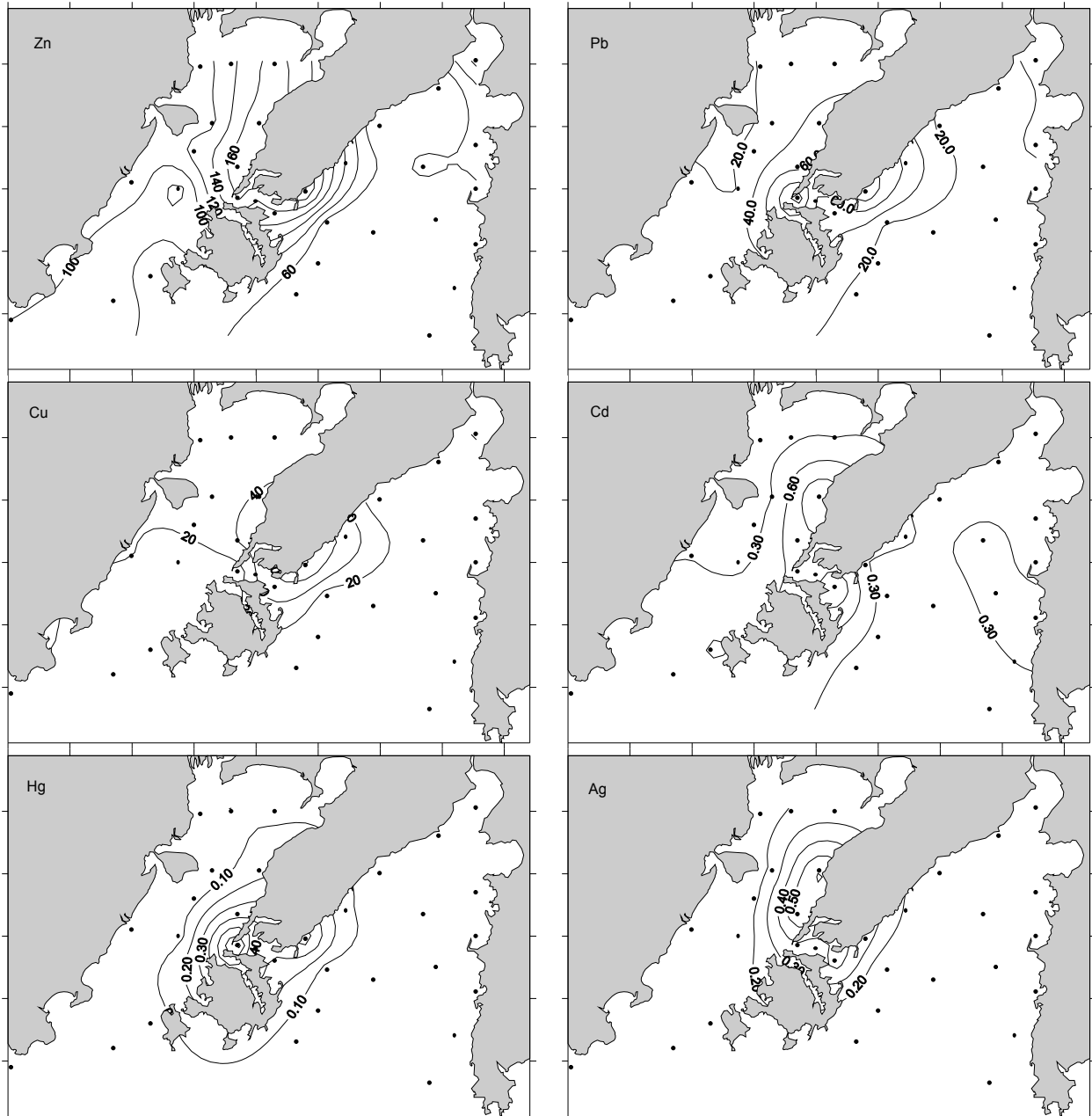


Figure 2. Distribution of Zn, Pb, Cu and Cd (ppm, dry weight) in bottom sediments, 1994

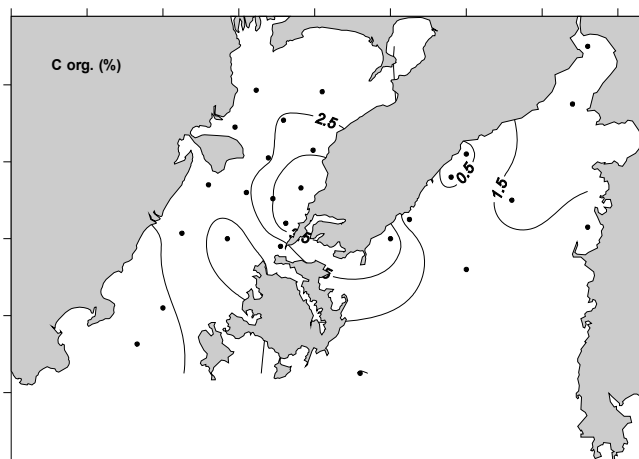


Figure 3. Distribution of C_{org} (% dry weight) in bottom sediments, 2001

ARSENIC CONTENT IN THE WATERS OF AMURSKY BAY (THE SEA OF JAPAN) IN NOVEMBER 2001

E.A. Grebenyuk

Far Eastern Regional Hydrometeorological Research Institute (FERHRI), Russia
Email: hydromet@online.ru

INTRODUCTION

Amursky Bay is situated in the northwestern part of Peter the Great Bay (the Sea of Japan) (Figure 1a). Amursky Bay runs inland to the northeast for 35 miles, its width is about 8 miles. Water depth in the bay changes from 2 m (in the north) to 30–35 m (in the south). By thermal conditions Amursky Bay can be divided into the shallow, medium and open parts. In summer shallow waters of the bay warm up to 23°C and in winter they cool down intensively to -1.9°C. Maximum water temperature is registered in middle August. Ice growth starts in late November. Razdolnaya River flows into the bay in its northern shallow part (Biryulin *et al.*, 1970).

Water salinity at surface increases from the north to the south, varying from 26.5 psu near the mouth of Razdolnaya River to 33.5 psu in the southern part of the bay (Tkalin, 1990). Minimum water salinity is observed in May–June and August–September (up to 9 psu) due to the river runoff variations and intensive atmospheric precipitation. Maximum water salinity (up to 34 psu) is observed in January–February, when the ice cover is most developed. Deep waters are characterized by the similar water salinity distribution, but salinity gradients become lower. Water salinity increases with depth (Biryulin *et al.*, 1970).

In environment free arsenic (As) occurs very seldom, mainly it is in the form of sulphides and sulfoarsenides, and more rare in the form of arsenates and arsenides. Under the damp climate arsenic is easily washed out from the soil. Arsenic content in the earth's crust amounts to 5×10⁻⁴% (Bokris, 1982). Average arsenic concentration in the World Ocean amounts to 3 µg/l (Zenin and Belousova, 1988).

Arsenic gets into the coastal waters from soil, mineral springs, and arsenious mineralization sites pertaining to the sedimentary sandy-argillaceous deposits, and with wastewaters from galvanic plants, coloring agent manufacturers, pesticide producers, and agricultural households using pesticides and herbicides. Arsenic compounds are widely applied in glass and porcelain production, medicine, electronic engineering, and dressing. High arsenic concentrations are harmful for animals and people, hampering oxidation and suppressing oxygen supply

to the organs and tissues (Zenin and Belousova, 1988). Maximum allowable concentration (MAC) of arsenic in water bodies used for drinking and domestic purposes amounts to 0.05 mg/l (Maximum allowable..., 1998).

In Primorsky region there are geochemical implications of high arsenic content in the water bodies conditioned on the existing facilities for production and processing of sulphide ores of non-ferrous metals. At the same time, there are several industrial enterprises located on the shore, from which arsenic may enter the coastal seawaters with industrial effluents (Kovekovdova *et al.*, 2002).

Data on arsenic content in the coastal seawaters of Primorsky region are available for the bottom sediments and commercial hydrobionts only (Kovekovdova *et al.*, 2001, 2002; Ivanenko, 2002). No investigations have been carried out before to study the content of arsenic in waters of Amursky Bay.

MATERIALS AND METHODS

Arsenic measurements in Amursky Bay in November 2001 (Figure 1b) served the basis for research. Seawater samples were taken from FERHRI R/V "Pavel Gordienko", on the whole 90 water samples at 30 stations being taken and treated.

Arsenic content was defined by a spectrophotometric method specifically intended to determine arsenate, arsenite and phosphate content in natural waters and developed by Johnson and Pilson (Johnson and Pilson, 1972). Like phosphates, arsenates react with molybdate-ion and form a complex compound that is easily reduced to heteropolyblue, whereas arsenites do not react with molybdate-ion. If reduce quinquevalent arsenic to trivalent arsenic, phosphate compound produces a color and optical density is proportional to the phosphorus content in water. If oxidize arsenite to arsenate, both arsenate and phosphate produce colored compounds. The difference between two values of the optical density is proportional to a concentration of inorganic arsenic in water. Average relative error of measurement amounts to 5–7% (Instruction..., 1977).

The author of the paper and M.I. Gorelkin determined arsenic content in the seawater samples using a photocolormeter KFK-3 with dishes 100 mm long and wave length of 870 nm.

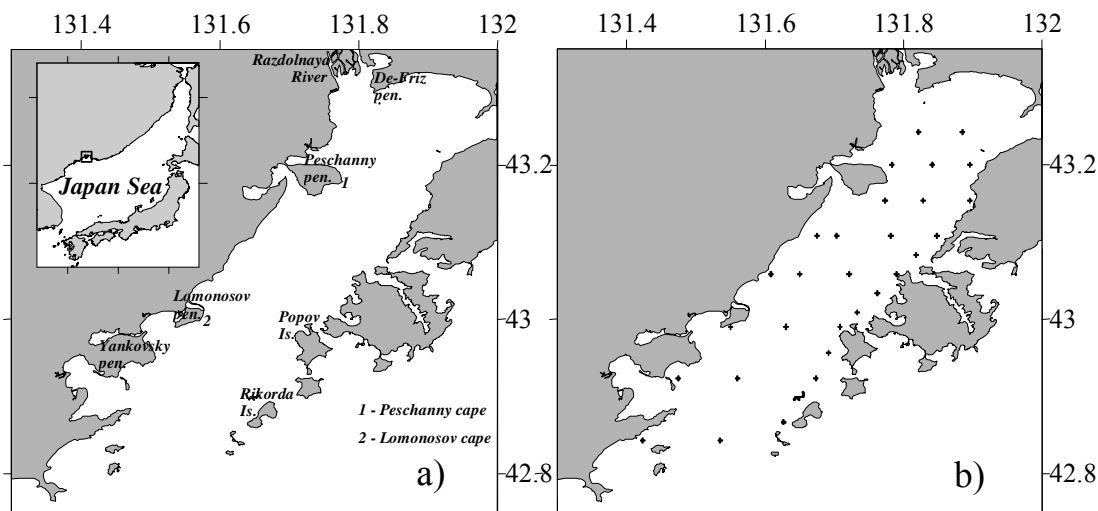


Figure 1. Map of Amursky Bay (a) and location of stations (b)

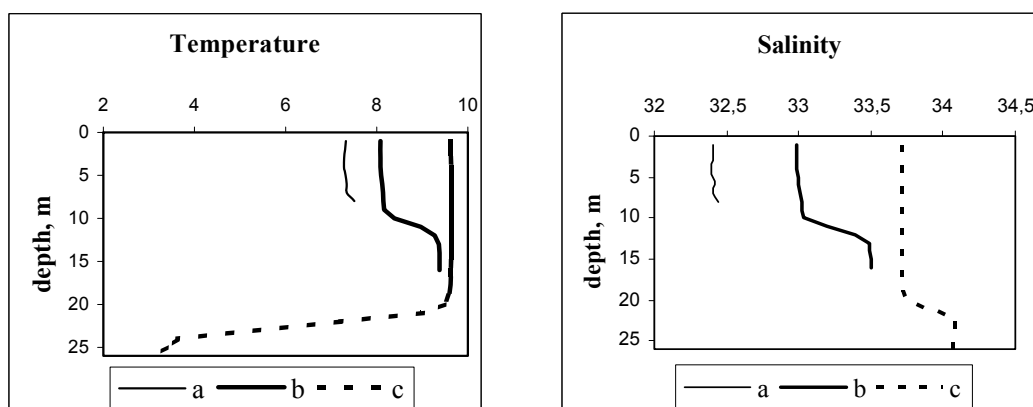


Figure 2. Vertical distribution of water temperature ($^{\circ}\text{C}$) and salinity (psu) in the water of Amursky Bay (a – northern part; b – central part; c – southern part)

RESULTS AND DISCUSSION

Distribution of water temperature and salinity.

Water temperature in Amursky Bay was varying from 5.33°C (in the northeastern part of the bay) to 9.65°C (near Rikorda Island) at surface, and from 1.40°C (at the bay entrance in the south) to 9.50°C (in the central part of the bay) near the bottom. Water salinity was changing from 32.10 psu (in the northern part of the bay) to 33.73 psu (in the southern part of the bay) at surface, and from 32.38 psu (in the northeastern part of the bay) to 34.07 psu (in the southern part of the bay) near the bottom.

Basing on the vertical distribution of water temperature and salinity, Amursky Bay can be divided (Tkalin, 1990) into the following three parts (Figure 2):

- northern shallow part bounded with Peschaniy Cape in the south, with upper quasi-homogeneous layer spreading up to 4–8 m deep and water temperature and salinity slightly increasing to the bottom

- medium part, from Peschaniy Cape to Lomonosova Cape, with upper quasi-homogeneous layer spreading to 4–16 m deep. Then water temperature and salinity increase smoothly, keeping permanent starting from 6–22 m deep
- southern, relatively open part, with upper quasi-homogeneous layer spreading to 13–22 m deep. Then water temperature falls abruptly, while water salinity keeps on growing. Near the bottom (2–5 m to the bottom) water temperature gradients decrease considerably, whereas water salinity keeps permanent.

Analysis of vertical profiles of water temperature and salinity of November 2001 suggests existence of three water layers in Amursky Bay: upper quasi-homogeneous layer, subsurface layer with maximum vertical gradients, and near-bottom layer.

Distribution of arsenic. Arsenic distribution in the water of Amursky Bay is not homogeneous. Values measured do not exceed MAC standards (Maximum allowable..., 1998). The range of arsenic concentrations in different parts of Amursky Bay is shown in Table 1.

Table 1

Arsenic content in different parts of Amursky Bay, $\mu\text{g/l}$

Parts of Amursky Bay	Range	
	at surface	at surface
Northern (from the top of the bay to Peschaniy Cape)	2.4–26.0	4.8–28.4
Medium (from Peschaniy Cape to Lomonosova Cape)	2.0–13.6	2.0–19.2
Southern (open)	0.0*–18.4	0.0–12.4

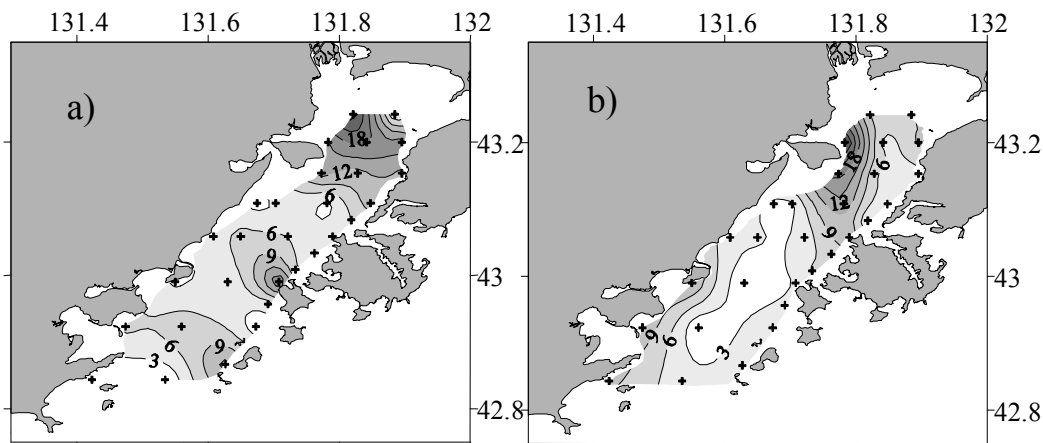
Note:
* – hereinafter “0.0” implies arsenic concentration lower than a detection limit

Table 2

Statistic measures of arsenic at different water depths

Depth	n	min	max	$x_{av.}$	σ_{n-1}
0	28	0.0*	26.0	8.1	6.4
10	28	2.0	28.4	8.5	6.2
20	18	0.0	22.0	8.4	5.8
Bottom	28	0.0	28.4	7.1	6.1

Note:
* – hereinafter “0.0” implies arsenic concentration lower than a detection limit
n – is the quantity of water samples, $x_{av.}$ – is an average arsenic content, σ_{n-1} – is a standard deviation

Figure 3. Distribution of arsenic ($\mu\text{g/l}$) at surface (a) and near the bottom (b)

A station located in the open part of Peter the Great Bay and showing arsenic content changing from 2.0 $\mu\text{g/l}$ at surface to 2.8 $\mu\text{g/l}$ near the bottom was assumed to reflect conditional background.

Table 2 shows statistic measures of arsenic at different water depths. As is seen, arsenic content at surface and near the bottom is, on average, 3 and 3.5 times higher than arsenic background content, thus, testifying to an anthropogenic impact produced on waters of Amursky Bay.

Arsenic concentration at surface was changing from “not found” to 26.0 $\mu\text{g/l}$ (Figure 3a). Maximum arsenic content was observed in the northern part of Amursky Bay (9 times excess of background values), being caused by the Razdolnaya River runoff and wastewaters discharged from onshore facilities. Most of local industrial facilities discharge their effluents into municipal sewage system. There are several

outlets from municipal sewage system located in the northeastern part of Amursky Bay, including in the vicinity of Verkhneportovaya St., Pervaya Rechka, Vtoraya Rechka, and De-Friz peninsula (according to a questioning by Primorsky Committee on environment protection and natural resources, 1994).

Besides, exceeded arsenic concentrations were observed near Popov and Rikkorda Islands (6 and 4 times, correspondingly). As the data are not sufficient, it is not possible to conclude for sure whether increased arsenic content is caused by anthropogenic activities on these islands, or related to the water advection by the sea currents from other parts of the bay. When moving offshore, arsenic content in water was decreasing everywhere.

Before, high mercury concentrations were observed in the components of ecosystem of Alekseev Bay (Luchsheva, 1995). Three-time exceeded arsenic

concentrations were observed in the soils in Zapadnaya Bay near Popov Island. Observed values are in accord with estimated content of other chemical elements in marine environment in this area and are obviously caused by geochemical processes (Kovekovdova *et al.*, 2002).

Arsenic concentration near the bottom was changing from “not found” to 28.4 µg/l (Figure 3b). Maximum arsenic content was observed at the stations near Peschaniy, Lomonosov, and Yankovsky peninsulas (background arsenic concentration exceeded 9, 4, and 4 times, correspondingly). It could be explained by the fact that arsenic brought to the waters of the bay by rivers settles down rather quickly and accumulates on the bottom.

According to 1998–2001 data (Kovekovdova *et al.*, 2002; Ivanenko, 2002), arsenic concentration in the bottom sediments of Amursky Bay was varying in the range of 0.22–6.4 µg/g dry weight. A station near Reyneke Island showing arsenic content in bottom sediments changing from 1.98 to 2.20 2.0 µg/g dry weight was assumed to reflect conditional background. Arsenic content in Golden Horn Bay was measured to be 10 times higher than a background concentration and change from 23.0 to 25.4 µg/g dry

weight. The author believes that Golden Horn Bay is polluted by the production plants situated onshore and household and domestic facilities of Vladivostok city. Arsenic content in the soils at the entrance to Golden Horn Bay near Tokarevsky Cape was measured to be 3 times higher than a background concentration.

CONCLUSIONS

1. Distribution of water temperature and salinity is analyzed and arsenic content in the waters of Amursky Bay is assessed.
2. Areas with high arsenic content have been identified (mouth areas of the rivers, locations of wastewater discharges from different onshore facilities). High arsenic concentrations have been found to be close to the areas of contaminant inflow from Razdolnaya River.
3. Existence of areas with high arsenic content suggests the necessity of further investigations in the given field.

ACKNOWLEDGEMENTS

Author expresses gratitude to M.I. Gorelkin for assistance in data management and highly appreciates valuable advice of V.A. Luchin, T.A. Belan and A.V. Gavrilovsky.

REFERENCES

- Biryulin G.M., Biryulina M.G., Mikulich L.V., Yakunin L.P. 1970.** Summer modifications of Peter the Great Bay waters / FERHRI Proceedings, № 30, pp. 286–299. (In Russian).
- Bokris J.O.M. 1982.** Chemistry of the environment. Edited by Bokris J.O.M. M.: Chemistry. 404 p. (In Russian).
- Instruction** on the methods of chemical analysis of seawaters. 1977. Edited by Oradovsky S.G. L.: Hydrometeoizdat, pp. 115–118. (In Russian).
- Ivanenko N.V. 2002.** Chemical and ecological assessment of selenium and arsenic content in the components of ecosystem of the coastal waters of northwestern part of the Sea of Japan / Abstract. Vladivostok. 25 p. (In Russian).
- Johnson D., Pilson M. 1972.** Spectrophotometric determination of arsenite, arsenate and phosphate in natural water. Anal. Chim. Acta, Vol. 58, №2. pp. 289–299.
- Kovekovdova L.T., Ivanenko N.V., Simokon M.V. 2002.** Features of arsenic distribution in the components of marine coastal ecosystems of Primorsky region. Electronic edition “Studied in Russia”, 127, pp. 1437–1445. <http://zhurnal.ape.relarn.ru/articles/2002/127.pdf>. (In Russian).
- Kovekovdova L.T., Ivanenko N.V., Simokon M.V., Shcheglov V.V. 2001.** Arsenic and selenium content in the commercial hydrobionts inhabiting coastal waters of Primorsky region. TINRO News, Vol. 129, pp. 3–8. (In Russian).
- Luchsheva L.N. 1995.** Mercury content in the components of ecosystem of Alekseev Bay (Peter the Great Bay of the Sea of Japan) / Marine biology, Vol. 21, №6, pp. 412–415. (In Russian).
- Maximum allowable** concentration (MAC) of chemicals in water of the water bodies used for drinking and domestic purposes. Hygienic standards. 1998. M.: Russian register of potentially dangerous chemical and biological substances by Ministry of Health of the Russian Federation. 126 p. (In Russian).
- Tkalin A.V. 1990.** Some regional consequences of anthropogenic impact produced on marine environment. Edited by Tkalin A.V. FERHRI Proceedings, № 144, pp. 7–11. (In Russian).
- Zenin A.A., Belousova N.V. 1988.** Hydrochemical dictionary. L.: Hydrometeoizdat, pp. 134–135. (In Russian).

PROFILING FLOATS LOST AND CAUGHT IN THE JAPAN SEA

M.A. Danchenkov¹, S.C. Riser²

¹ Far Eastern Regional Hydrometeorological Research Institute (FERHRI),
Email: danchenk@vladivostok.ru

² School of Oceanography, University of Washington, USA

Argo project will saturate the World Ocean by floats-profilers. A big number of such floats (3000) means that part of them will be lost every year by different reasons.

Some parts of the World Ocean have depths less than the depth of the floats drift (parking depth). Floats could be lost there. The World Ocean is saturated not only with floats by fishing ships and their fishing nets also. So it is interesting to look at the destiny of 34 floats-profilers deployed in the Japan Sea in 1999–2000.

The Japan Sea has a vast deep basin (usually it is divided into 3 separate basins) where depth is more than 2000 m. The area with depth less than 1000 m covers more than 20% (Frolov, 1971).

The time interval between the appearance of floats at the surface of the Japan Sea was 7 days and parking depth – 800 m mainly. And most of floats were crossing such shallow areas.

In total the floats have produced more than 3000 CTD profiles of 7500 possible ones.

Every year about 25% of floats stopped their work by unknown reasons. So after 2 years only half of them had continued an operation and after 4 years – only 5.

Some of the floats sometimes disappeared (satellites did not get signal from them). Some of such floats after the long interval (0.5–12 months) have been appearing again in the areas located far from the point of previous stations (“made the jump”). Such cases are presented in Figure 1.

There are a few possible reasons why a float could stop operating:

- A float became heavier than it was planned and could not achieve the surface.
- A float could be captured by a fishery boat.

Most of “jumps” could be explained by the first reason. While contacting the bottom at the coastal stations (where the depth is less than the parking depth) the float could take some bottom sediments inside the pallet and covers of gauges. Similar dangerous area is situated in the center of the sea, around the Yamato Rise.

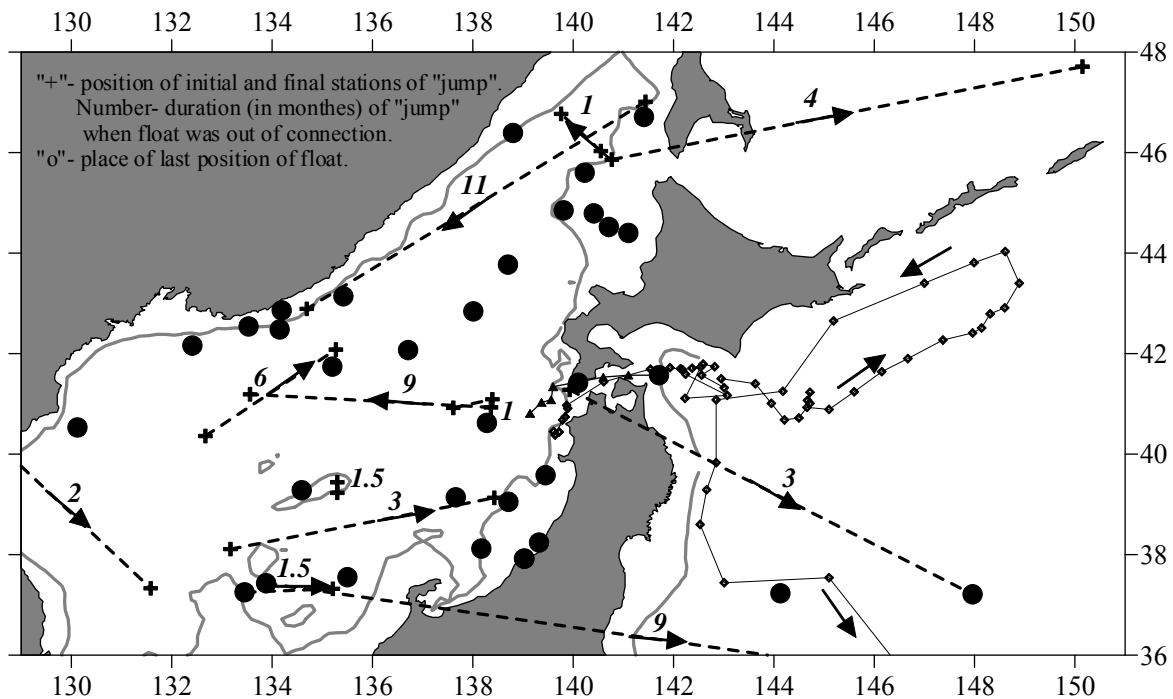


Figure 1. “Jumps” of floats (broken lines), final position of floats (circles) and trajectories of drift of floats that crossed the Tsugaru strait. Label indicates time (in months) of “jump”

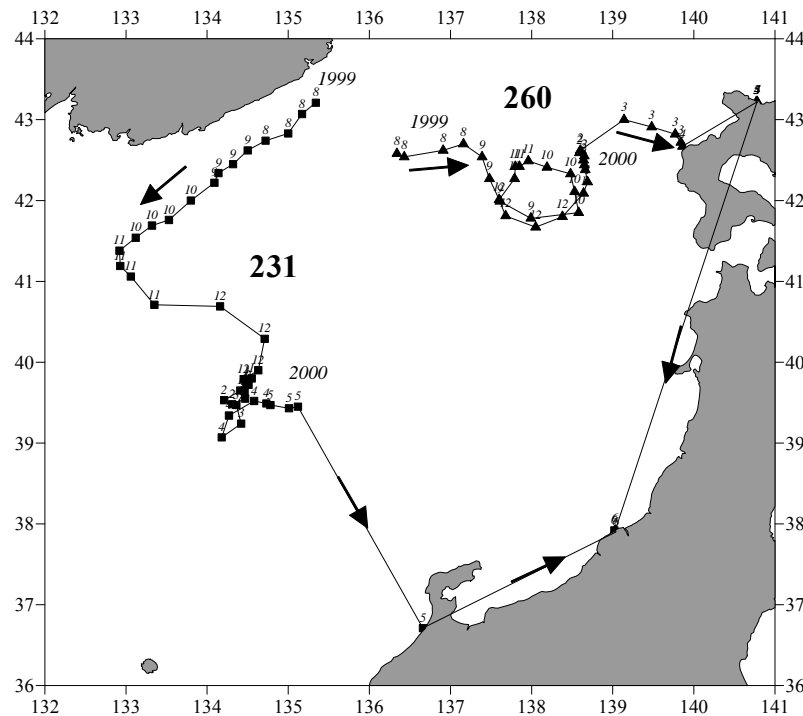


Figure 2. Trajectories of drift of 2 floats and their transportation after the capture

In spite of deep parking depth most of floats operated (produced CTD-measurements and transmitted data to satellites properly) on the shelf during several months. But all floats on the shelf finished their work at last. One float (229) even already crossed the shallow Tsugaru strait, but was lost very soon after it.

But some of the “jumps” on a very long distance (500–1100 nm) through the shallow straits of the Japan Sea are difficult to be explained by the first reason. Speed of their drift (mainly at parking depth at 800 dB) in such cases has to be 15–30 cm/s. In reality the speed has to be much more – floats move between the initial and final points not straight but by complicated trajectories.

The same high speed of floats has to be inside the sea also. For example, float 263 overcame the distance of 5° of longitude for about 2 months. Its averaged speed has to be much more than 20 cm/s.

Some floats (number 231 and 260) were captured by fishery boats and they were collected together later in one place (Figure 2). Float 259 was captured on August 8, 2001, near Otaru by a ship. But it was re-deployed again in the area west of it on September 18, 2001. Of course, it is a probabilistic explanation only (between two positions the float drifted from

Hokkaido to the west against a northward current). In any case, after this event the float worked for more than 1/5 year and made more than 60 CTD stations.

Stop of the floats was equal in open sea (16 cases) and on the shelf (16 cases). Most of losses occurred in Japanese EEZ of the Japan Sea and some of them – near the coast.

8 floats were lost in the area near the Russian coast and some of them in the area near Vladivostok.

Both Japanese and Russian vessels could catch some of such floats. Nevertheless, Russian agencies, connected with sea activity, did not reported about float recovery.

It is not easy to damage a float. In case of its recovery, float could be used again (after changing its batteries and software). Cost of every float is high enough and a reasonable award for its delivery to the nearest institute could be useful.

So, we think that instruction of fishermen, wide information about the use of floats-profilers and a special label on a float (with instructions for such cases and about the award for the delivery) could help to increase the life-time of the ARGO floats.

REFERENCE

Frolov Yu.S. 1971. New fundamental data on morphometry of World ocean. *Vestnik LGU*, No. 6, pp. 85–90. (In Russian).

ON-LINE OIL SPILL MODELING WITHIN NAVY EXERCISES IN THE NW PACIFIC MARGINAL SEAS IN AUGUST 2003

**I.E. Kochergin¹, A.A. Bogdanovsky¹, I.A. Arshinov¹, V.D. Budaeva¹,
N.S. Kupera¹, V.G. Makarov^{1,2}, S.I. Rybalko¹, P.A. Fayman¹**

¹ Far Eastern Regional Hydrometeorological Research Institute (FERHRI), Russia
Email: ikochergin@hydromet.com

² National Polytechnic Institute, Mexico

The Russian Pacific Navy exercises, "Vostok 2003", were held in the Far Eastern seas (Okhotsk Sea and Japan Sea) and northwestern Pacific (eastern Kamchatka peninsula) in August, 2003. Being the largest over the whole Russian history, navy exercises involved observers from Japan, South Korea, the USA, and China. The primary purpose of navy exercises was to perfect cooperation between the Pacific Navy and force and civil departments.

Russian Federal Service on Hydrometeorology and Monitoring of the Environment (Roshydromet) and its subordinate institution FERHRI participated in the navy exercises as well. For this purpose FERHRI arranged collection, processing and delivery of hydro-meteorological and oceanographic data to the users. Initial data were provided by:

- regional hydromet offices (Primorsky, Sakhalin, Kamchatka, Khabarovsk) – prognostic information;
- Russian central institutions of Roshydromet – archival, specific and satellite data (Hydrometcenter of RF, RIHMI-WDC, science and production center "Planeta");
- world hydrometeorological centers (JMA, NCEP) – available data on objective weather analyses and forecasts.

FERHRI was responsible for preparation of the sea-related prognostic and diagnostic data sets, among which there are 10-day SST (sea surface temperature) maps updated once every five days, construction of prognostic wave fields, forecasts of typhoon trajectories and features, and prognostic sea current schemes. All hydromet and oceanographic data were transmitted to the users without any delays.

On-line modeling of oil behaviour in the sea was the most science intensive task of FERHRI, oil fate forecasts being used to plan proper oil spill response activities, optimise operation of technical facilities eliminating the oil, and estimate probable shoreline pollution.

Input hydromet data included meteo data of the world hydromet data centers and oceanographic data of the Regional oceanographic data center (RODC FERHRI). Additional hydrologic data came from regional oceanographic surveys. Based on meteo and

sea current (tidal and nontidal) models, the oil trajectory and fate within 2.5 days (60 hours) were assessed.

FERHRI model (Bogdanovsky *et al.*, 2001; Kochergin *et al.*, 2000; Kochergin *et al.*, 1999) verified in the Far Eastern seas and adjusted to the area of navy exercises was applied to the oil spill modeling.

On-line oil spill modeling involves:

- automated selection of typical wind conditions and construction of the corresponding sea current fields;
- construction of nontidal current fields adjusted to the areas of potential oil spills based on verified Ekman-type linear and nonlinear diagnostic models;
- calculation of tidal harmonics and tidal current fields for the specified time intervals;
- trajectory modeling of oil behavior in the seawater;
- physical-chemical modeling of oil behavior in the seawater, including modeling of oil evaporation, emulsification, and dispersion;
- additional model features for specialized purposes, like oil stranding and shoreline pollution;
- automatic on-line simulation of oil fate in the seawater and production of oil fate tables and figures.

On the whole, oil spill model has been adjusted for four case studies of potential oil (oil products) spill in three areas of intensive economic activities (Figure 1).

1. Emergency oil spill in Peter the Great Bay (area 1 in Figure 1).

On August 20, 2003, at 14.40 (Vladivostok time) there was a mazut leakage from a tanker, 70 miles southward of Vladivostok. The spill lasted for 5 minutes and its volume amounted to 20 tons.

2. Emergency oil spill at the single-point mooring in Chikhacheva Bay (area 2 in Figure 1).

On August 24, 2003, there was a 2-hour late signal about 8-ton spill at the SMNG offshore mooring located in Chikhacheva Bay near De-Kastri at 09.00 (Vladivostok time).

3. Emergency oil spill from "Magadan" ice-breaker, 20 miles southward of Nakhodka Bay (area 1 in Figure 1).

On August 25, 2003, at 12.30 (Vladivostok time) there

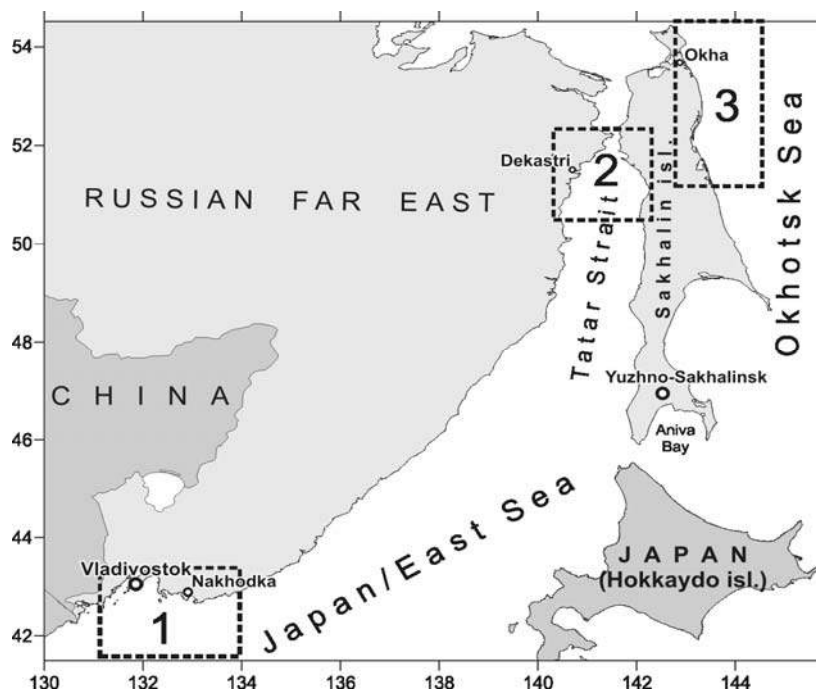


Figure 1. Areas of on-line oil spill modeling

was a signal about an emergency situation aboard “Magadan” ice-breaker with the fire, breach, and inflow of water. Volume of spilled mazut amounted to 50 tons.

At 12.50 (Vladivostok time) oil slick parameters and location were specified and oil spill volume was estimated at 10 tons. Oil fate within the first 0.5, 1, 2, and 4 hours needed to be simulated. The oil slick motion was simulated with the sawdust scattered onto the sea surface. Modeled oil fate was compared to *in situ* observations from ships involved in the oil spill response.

4. Emergency oil spill in the result of collision of a shuttle tanker on the Sakhalin northeastern shelf near Molikpaq platform (area 3 in Figure 1).

On August 27, 2003, a shuttle tanker was moving away from Okha oil storage and collided with another ship leading to a breach. Oil spill started at 11.00 (Sakhalin time) at 52.41 N, 143.30.5 E lasting for 30 minutes and amounting to 1500 tons in volume.

On-line modeling of oil fate in the seawater was implemented for each of four cases. Output results in the

form of figures and tables describing oil fate are delivered to the headquarters and operative departments of the navy exercises. The time from a notification signal to production of the modeling output results varied from 20 to 60 minutes. Probable oil trajectory was determined visually by the motion of special markers (sawdust) or by observable hydrometeorological conditions.

Example of the oil fate report under Case study 4 with all output tables and figures is given in Figures 2–4. The report describes parameters of the spill source, current weather conditions and forecasted ones, general simulation of oil behavior (Figure 3), and calculated oil slick parameters (Figure 4).

In conclusion it should be noted that the use of oil model in the navy exercises is just one of the model applications. On the whole, capabilities of the model enable up-to-date stochastic modeling of oil behavior in the Japan, Okhotsk, and Bering seas.

REFERENCES

- Bogdanovsky A.A.**, Kochergin I.E., Budaeva V.D., Makarov V.G., Mishukov V.F., Putov V.F., Rybalko S.I., Uraevsky E.P. **2001**. On-line modeling technique for the oil spill fate as applied to the northeastern Sakhalin shelf (the first internet version) // Proceedings of CREAMS’2000 “Oceanography of the Japan Sea”, Vladivostok: Dalnauka, pp. 86–93.
- Kochergin I.E.**, Bogdanovsky A.A., Budaeva V.D., Makarov V.G., Mishukov V.F., Ovsienko S.N., Putov V.F.,

- Reitsema L.A., Sciallabba J.W., Sergusheva O.O., Yarosh P.V. **1999**. Modeling of Oil Spills for the Shelf Conditions of North-Eastern Sakhalin // Proceeding of the Second PICES Workshop on the Okhotsk Sea and Adjacent Areas. No. 12. P. 123–130.

- Kochergin I.E.**, Bogdanovsky A.A., Mishukov V.F. & Putov V.F. **2000**. Oil spill scenario modeling for Sakhalin shelf // Proceedings of WITpress “Oil and Hydrocarbon Spills II”. 39-50 pp.

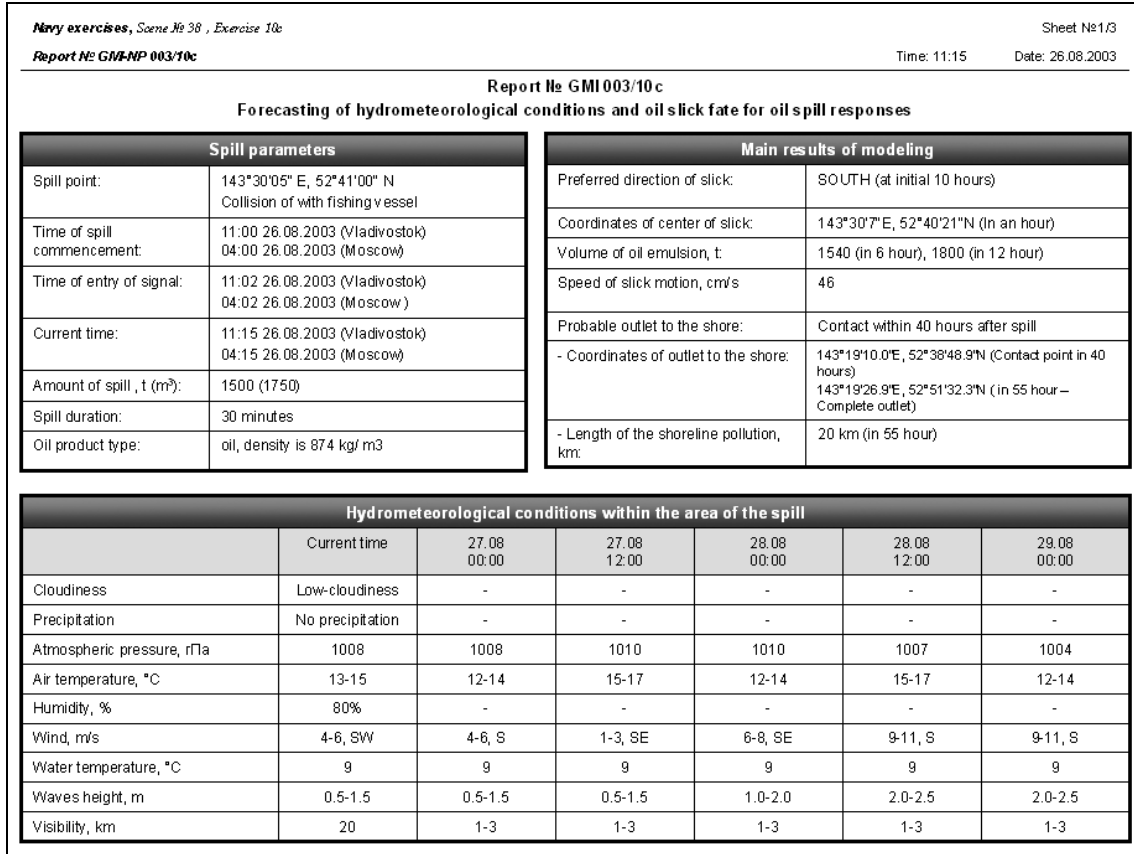


Figure 2. Example of oil fate report under Case study 4, page 1 of 3

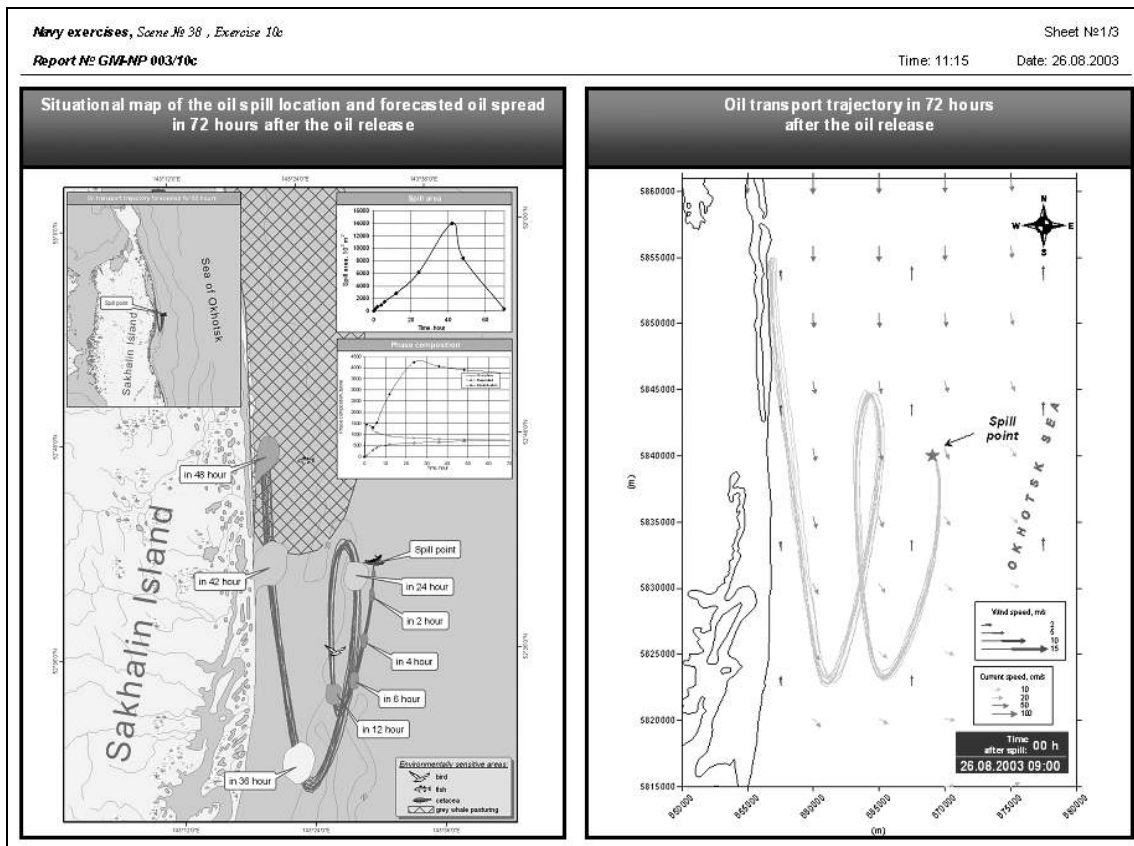


Figure 3. Example of oil fate report under Case study 4, page 2 of 3

Navy exercises, Soene № 38 , Exercise 10c									
Report № GANP 003/10c									
Sheet №1/3									
Time: 11:15 Date: 26.08.2003									
Spill characteristics									
Time after spill	Time	Coordinates of slick areal limits	Area, 10 ³ m ²	Perimeter, m	Density, kg/m ³	Speed, cm/s	Thickness, mm	Volume, t (m ³)	Damaged shores, km
1	26.08.03 12:00	143°29'57"E 52°40'32"N - 143°30'17"E 52°40'0"N	347	2602	879	46	3,71	at sea: 1464 (1666)	-
2	26.08.03 13:00	143°29'33"E 52°39'31"N - 143°30'6"E 52°38'50"N	662	3394	889	60	1,84	at sea: 1373 (1544)	-
4	26.08.03 15:00	143°29'26"E 52°37'21"N - 143°29'15"E 52°36'36"N	954	3884	916	65	1,28	at sea: 1330 (1452)	-
6	26.08.03 17:00	143°27'38"E 52°34'52"N - 143°28'16"E 52°34'2"N	1515	4818	945	60	0,96	at sea: 1541 (1631)	-
12	26.08.03 23:00	143°28'31"E 52°34'19"N - 143°26'32"E 52°33'12"N	2814	6298	993	48	0,99	at sea: 2819 (2838)	-
24	27.08.03 11:00	143°27'35"E 52°41'51"N - 143°29'4"E 52°39'40"N	6169	9016	1007	48	0,70	at sea: 4259 (4228)	-
48	28.08.03 11:00	143°19'17"E 52°48'22"N - 143°21'43"E 52°44'22"N	8421	29844	1009	13	0,47	at sea: 3011 (2985) на берегу: 900 (892)	8
60	28.08.03 23:00	143°18'58"E 52°45'31"N - 143°19'35"E 52°44'59"N	- (Complete outlet)	- (Complete outlet)	1009	-	0,47	on shore: 3809 (3774)	20

Figure 4. Example of oil fate report under Case study 4, page 3 of 3

BEGINNING OF HYDROMETEOROLOGICAL OBSERVATIONS IN VLADIVOSTOK

L.V. Kobylinsky

403th Hydrometeorological Center of Pacific Navy, Russia

Hydrometeorological support of the Siberian fleet ships, commercial trade and industrial vessels, as well as of Vladivostok port activities as a whole was started in 1873 before establishment of a meteorological agency by the Main Geophysical Observatory (MGO) of the Russian Federation.

After the main base of the Siberian navy was moved from Nikolaevsk-na-Amure to Vladivostok in 1873, regular meteorological observations were started at Vladivostok-port station managed by the Directorate of lighthouses and Eastern ocean sailing directions.

Observations over atmospheric pressure (inches), air temperature (Reaumur degrees), wind direction and force, cloudiness, air moisture, weather phenomena and precipitation (millimeters) were carried out three times per day – at 7.00, 13.00, and 21.00. “Note” column described weather conditions between observation hours, beginning or end of a certain weather phenomenon, and etc.

The first meteorological observation at Vladivostok-port station was carried out on January 20 (or February 1, by New Style), 1873, at 7.00 a.m. by Nikolay Shmidt (OIAK, D.1), who was the lieutenant of Naval College (Figure 1).

In January–October 1874 the lieutenant Badanin was responsible for meteorological observations. Following the direction of the Main Geophysical Observatory, he also carried out additional observations at 21.31 p.m. during February 18 – June 30, 1874.

In July 1874 the lieutenant baron E.V Maidell was appointed the chief of telegraph office and meteorological stations. He paid much attention to hydrometeorological observations in the Eastern Ocean. In 1875 he developed a complex hydrometeorological observation program that provided for the establishment of permanent meteorological stations, regular observations on ships, mutual exchange of telegraphic messages about weather conditions and forecasts “of storms between the Russian, Japanese and Chinese ports”, as well as the purchase of a building for the station allocation.

Maidell’s report and Vild-Rykachev’s proposals about establishment of the observatory in Vladivostok were discussed at the meeting of Academy of Sciences and Hydrographical department, though rejected because of heavy expenses (Bedritsky *et al.*, 1997).

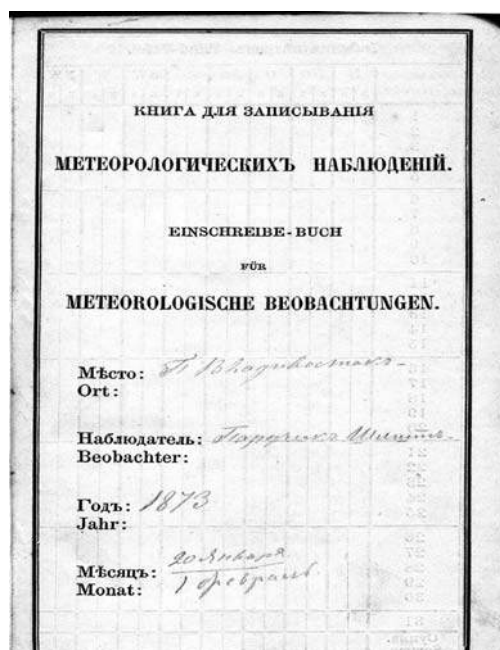
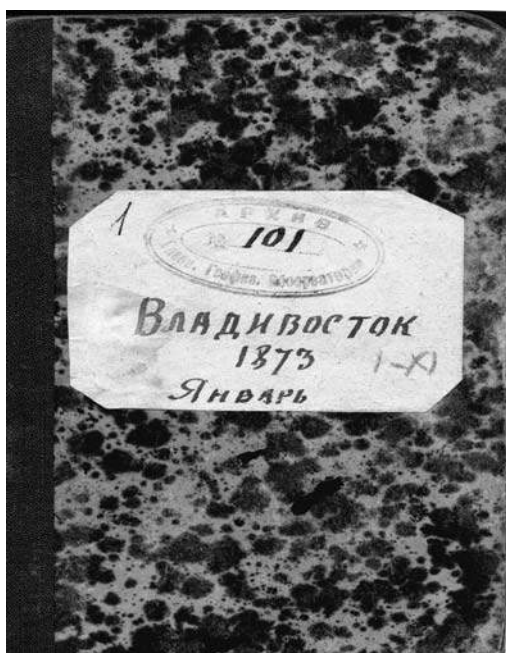


Figure 1. Book of meteorological observations, Vladivostok, 1873

In 1875–1878 Maidell studied hydrological conditions of the Japan Sea, Tatar Strait and La Perouse Strait and described sea current patterns in these water areas. Maidell also carried out hydrographic and hydrometeorological observations in Peter the Great Bay and studied the Suiphun river mouth (the largest river flowing into Amursky Bay and being navigable). On the basis of these researches the Main hydrographic department drew the map “Suiphun river mouth plan” (OIAK, D.8).

Maidell paid much attention to hydrometeorological observations at Vladivostok-port station and climate studies in the Russian Far East. From November 1874 to December 1878 observations at station were carried out by Valyasyn. At the same time Maidell himself entered some explanations in the books of meteorological observations related to the changes in observation conditions or the measuring instruments replacement.

According to M.E. Zhdanko’s report at the Society for Amur Region Studies (OIAK) meeting on March 26, 1899, “Maidell served in Vladivostok and managed hydrographic studies for many years. He was the first to prove the absence of the cold Liman current flowing from north to south along Primorsky region coast and mentioned by academician L.I. Shrenk. Maidell gave the right explanation of the regional climatic features: persistent summer fogs and extremely dry winter.” (Zhdanko, 1899).

The books of meteorological observations were sent to MGO for analysis and subsequent publication of research results in the “Chronicles of Nikolaevsky

Main physical observatory”, but they were always late.

All observations were carried out on schedule, making proper corrections for the measuring instruments. Changes in the location of the station or separate measuring instruments were described in the book, for example, “On April, 1 the station was moved to another room in the same building, but overlooking the west. Fuse barometer №73 was used, it was set on the internal wall, 11 feet away from the stove, 9 feet away from the window, the same height as before. All other instruments were not moved away.” (OIAK, D.84).

In May 1892 a merchant Yu.I. Brinner was appointed the station chief (the order of Vladivostok port admiral, No. 244, dated May 13, 1892) (Vladivostok, 1892). Brinner was responsible for meteorological observations at station from June 1892 to July 1896. Meteorological books were sent to MGO as before (Figure 2). From August 12, 1896, the captain P.N. Slavinsky continued the observations and started making observation tables for the station (OIAK, D.245).

In 1899–1908 and 1908–1909, hydrometeorological observations were carried out by the Naval College representatives: captain G.P. Smirnov and lieutenant colonel K.G. Gurin, respectively (Moshenichenko, 1970).

In 1879 the first commercial vessel “Nizhniy Novgorod” arrived in Vladivostok to start development of trade and industrial companies, commercial fleet, and trade relations along the whole coast of the Eastern Ocean.

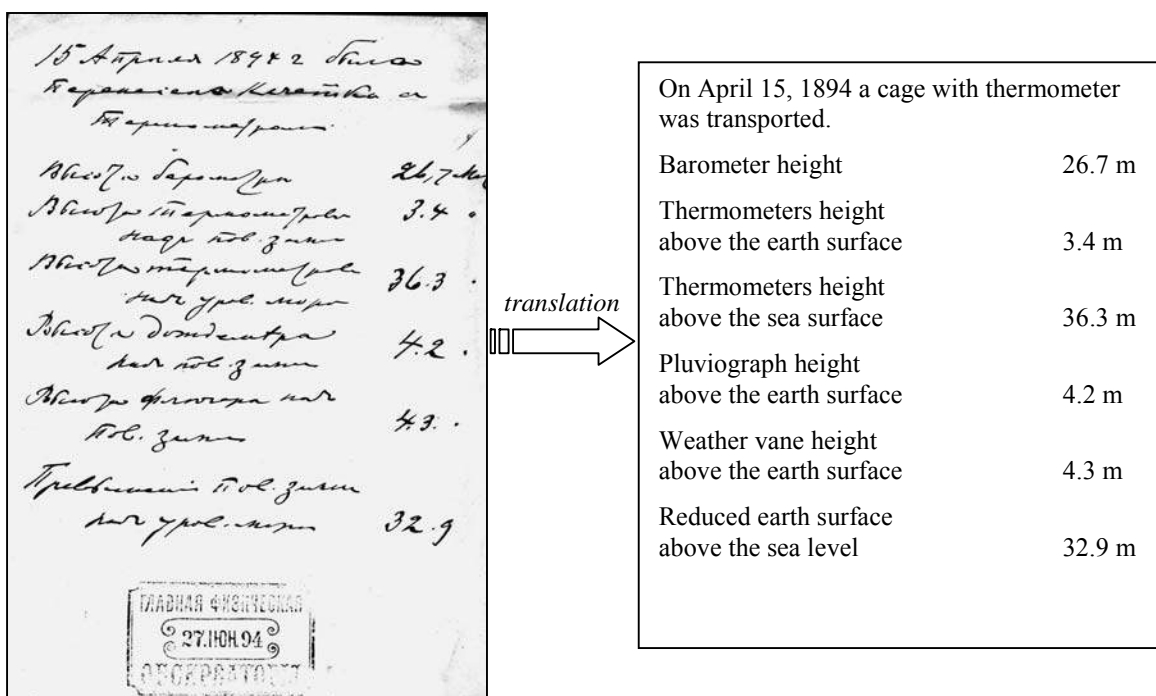


Figure 2. Explanations of Yu.I. Brinner, April 15, 1894

On April 17, 1883, the first issue of the new public and literary paper for seamen "Vladivostok" was published. The paper described activities of Vladivostok port and city, published the decrees of the Chief port admiral of the Eastern Ocean, and introduced the first bulletin of Vladivostok meteorological station. Development of the port, navigation in the Far Eastern seas, and agriculture in the coastal zone arouse much interest to meteorological observations, and starting from June 1887, meteorological bulletin published data for all observation periods (Vladivostok, 1887).

In the course of time Vladivostok-port station began to serve a Storm warning service to ensure safe navigation in the Far Eastern seas.

Tsikaveyskaya observatory in Shanghai sent warning messages of storm and typhoon emergence in the China Sea to Vladivostok-port station. The decree of the Chief port admiral of the Eastern Ocean No. 36 dated September 18, 1886, stated that in case of the typhoon originating in the China Sea, two cones at daytime and two lamps at nighttime should be lifted up at the guy end of gaff on the building of the Eastern Ocean ports department (Vladivostok, 1886). Since the meteorological station did not have necessary data, the above warning was only a kind of recommendation for the captains, who were allowed to act on their own.

Developing network of meteorological and alarm stations and appearance of the first synoptic charts in

China and Japan enabled Vladivostok-port station to receive meteorological telegrams from Shanghai, Hong Kong, Manila, Singapore, and Nagasaki. By that time the station had accumulated its own statistical meteorological data.

In 1896 the storm warning alarm appeared only in case there was a probability of typhoon passage to the Japan Sea (Vladivostok, 1896). Any interested person could read the warning message at the marine telegraph.

Starting from 1893, lighthouses were equipped with bells and guns to warn about fog. A bell was rung at Povorotniy lighthouse during all time of the fog. Guns were intended for the shots in answer to any signal from the sea heard during the time of the fog. On November 29, 1893, Petropavlovsk lighthouse was equipped with a steam siren with a sound tube revolving on its axis 90 degrees from SO to SW (Vladivostok, 1893).

In 1905–1912 meteorological observations were carried out at Vladivostok-port station and other departmental stations.

Starting from October 1909, the correspondent of MGO I.I. Zubritsky (first-class captain) was appointed the keeper of instrumental chamber and the chief of meteorological station. He was responsible for meteorological observations till July 1916 and participated in the publication of the first synoptic charts in Vladivostok.

REFERENCES

Bedritsky A.I., Borisenkov E.P., Korovchenko A.S., Pasetsky V.M. 1997. Historical essays of the Russian Hydrometeorological service. St.P.: Hydrometeoizdat. (In Russian)

Moshenichenko I.E. 1970. Development of meteorology in the Russian Far East. L.: Hydrometeoizdat. (In Russian)

OIAK Archives. Vladivostok, F. 28, Op. 0, D.8, L.607. (In Russian).

OIAK Archives. Vladivostok, F. 28, Op. 1, D.1. (In Russian).

OIAK Archives. Vladivostok, F. 28, Op. 1, D.245. (In Russian).

OIAK Archives. Vladivostok, F. 28, Op. 1, D.84. (In Russian).

OIAK Report. 1899. OIAK, Vladivostok. (In Russian).

Vladivostok. 1886. Weekly public paper for seamen. OIAK, Vladivostok, №38, 21.09.1886. (In Russian).

Vladivostok. 1887. Weekly public paper for seamen. OIAK, Vladivostok, №25, 21.06.1887. (In Russian).

Vladivostok. 1892. Weekly public paper for seamen. OIAK, Vladivostok, №20, 17.05.1892. (In Russian).

Vladivostok. 1893. Weekly public paper for seamen. OIAK, Vladivostok, №48, 28.11.1893. (In Russian).

Vladivostok. 1896. Weekly public paper for seamen. OIAK, Vladivostok, №29, 14.07.1896. (In Russian).

Zhdanko M.E. 1899. Review of hydrographic studies of the Russian seamen in the Pacific Ocean // Eastern News, pp. 27-28. (In Russian).

Notes from Editors:

In 2003 the Main department of navigation and oceanography of RF Ministry of Defence accepted the monograph "History of the Russian Hydrometeorological Service establishment and development in the Pacific region" by L.V. Kobylinsky for publication. It is devoted to hydromet observations in the Russian Far East and foundation of research institutions to support commercial, fishing, research, and navy ships and economy. For the first time materials of Society for Amur Region Studies, 403th hydrometeorological center of Pacific Navy, and Marine Observatory on establishment of the Russian Far East hydromet stations will be published.

FOR AUTHORS

GENERAL

- Papers submitted must not have been published previously and not be under consideration for publication elsewhere.
- Materials submitted must be in English only. The Editors have the right to reject the paper in case its level of English is poor.
- Publication is free of charge, but any financial support is welcome (to cover partially the costs on paper review, technical editing and publication).
- Authors should submit an electronic copy of their paper to the Editorial Office.
- The paper should start with Title and Authors and Abstract.
- The following information about authors should be attached: Name, Degree, Institution, Postal Address, Telephone Number (with Country and Region code), E-mail Address. The corresponding author should also be identified.
- Paper Length, including figures and tables, should be confined to no more than 10 pages. Papers, the length of which exceeds 10 pages, will be accepted for publication upon Editors' decision.
- References to unpublished results that are used for argumentation are not permitted.
- The Editors reserve the right to adjust style to certain standards of uniformity. The papers are reviewed and may be accepted for publication, recommended for revision, or rejected upon Editors' decision.

FORMAT INSTRUCTION

- Electronic copy of the paper should be provided on a 3.5" diskette, CD-R, CD-RW etc. or submitted by e-mail.
- Text and Tables – Text and tables should be provided in any of the following formats: Microsoft Word (.DOC), Rich-Text Format (.RTF), TeX Format (.TEX).
- Formulas and Equations – Formulas and equations should be provided as Microsoft Equation objects in Microsoft Word, RTF, or TeX Formats (with rare exception, formulas and equations are allowed to be written down on paper by hand but in distinct block letters).
- Illustrations – All figures, charts and photographs should be provided in electronic form and must be of a good quality, suitable for a high-resolution grayscale print.
- Units – International System of Units (SI System) should be used as far as possible. If other units are used, the metric equivalents must be given in parentheses, or the correct conversion factor must be presented in a footnote.
- Fractional part is separated from integer one with a dot.
- A list of references should be arranged alphabetically following the text of the paper. References should be given in the following form:

Boetius A., Lochte K. 1994. Regulation of microbial enzymatic degradation of organic matter in deep-sea sediments. *Marine Ecology Progress Series*, vol. 104, pp. 299–307.

Green A. 1991. Deformations in *Acanthaster planci* from the Coral Sea, observed during UEA Special Project 7, July 1978. *Journal of Pollution Research*, vol. 14, No. 7, pp. 114–125.

James Z. 1997. Ecological effects of sea wall construction during 1994 at Bridlington, UK. Listserv Message, Eco-list, 20 October 1995.

Jones P. 1996. Research activities at Smith Technology Institute. WWW Page, http://www.sti.com/about_us/research.

Leonov A.K. 1960. The Japan Sea. Regional oceanography. Moscow: Hydrometeoizdat. pp. 292–463. (In Russian).

Maxwell W.G.H. 1968. Atlas of the Great Barrier Reef. Elsevier, New York, 258 p.

Moustakas N. 1990. Relationships of morphological and physicochemical properties of Vertisols under Greek climate conditions. Ph.D. Thesis, Agricultural Univ., Athens, Greece.

- In the text refer to the author's name (without initials) and year of publication, for example: (Boetius and Lochte, 1994; Walker *et al.*, 1999; Jones, 1996a; Green, 1991b).

Secretariat contact:

**Elena Borozdinova, Pacific Oceanography, FERHRI,
24, Fontannaya Street, Vladivostok 690990, Russia**

Tel: +7 (4232) 267352 Fax: +7 (4232) 269281 Email: po@hydromet.com